1963

# A Study Ionic Permeability Changes Underlying Excitation in Myelinated Nerve Fibers of the Frog

Frederick Arthur Dodge

# A STUDY OF IONIC PERMEABILITY CHANGES UNDERLYING EXCITATION IN MYELINATED NERVE FIBERS OF THE FROG

A thesis submitted to the Faculty of The Rockefeller Institute
in partial fulfillment of the requirements
for the degree of Doctor of Philosophy

by

Frederick Arthur Dodge, Jr., A.B.

Acceptable for publication
Clarence M. Connelly
Associate Professor The Rockefeller Institute

May 15, 1963

The Rockefeller Institute
New York, New York

# PREFACE

I wish to express my gratitude to President D. W. Bronk for the opportunity to participate in the unique program of graduate education at the Rockefeller Institute.

The experimental investigations were carried out in the laboratory of Professors D. W. Bronk and F. Brink, Jr. I wish to especially thank Professor F. Brink, Jr. and Dr. C. M. Connelly for many valuable discussions and for their pertinent criticism, and constant help throughout this work.

I wish to thank Docent B. Frankenhaeuser of the Nobel Institute for Neurophysiology, Stockholm, for the hospitality of his laboratory, for training me in the experimental procedures, and for a stimulating and extensive correspondence that continued throughout the progress of this work.

I wish to express my appreciation to Mr. J. P. Hervey and to Dr. R. L. Schoenfeld for their advice and assistance in the construction of the electronic apparatus.

I gratefully acknowledge the use of the IBM 650 digital computer at the Watson Scientific Computing Laboratory, Columbia University.

I wish to thank Mrs. F. Brink, Jr. for her assistance in the preparation of the manuscript, Miss Sonia Wohl for checking and correcting the bibliography, Miss Ruth Mandlebaum and Mr. P. Rich for their assistance in preparation of the illustrations, and Miss Didi Bottemanne for typing the manuscript.

# ABSTRACT

Investigations by Huxley and Stämpfli (1) of the dependence of the resting potential and of the action potential at the node of Ranvier upon the ionic composition of the bathing medium provided evidence that the electrical activity resulted from a sequential alteration of the membrane permeability to sodium and to potassium ions. Their results suggested that the nodal membrane conformed in a general way to the ionic hypothesis developed in detail for the squid axon by Hodgkin and Huxley (2). This dissertation reports an investigation of the electrical characteristics of the nodal membrane aimed at developing a quantitative formulation of the ionic hypothesis applicable to the node.

Electronic control systems developed by Frankenhaeuser (3) were used to measure the electrical responses of the node under the condition that either the membrane current or the potential difference across the nodal membrane was the controlled variable. Constraint of the membrane current provided accurate measurement of the action potential and related phenomena typical of nerve excitation. Constraint of the membrane potential (the voltage clamp) provided direct measurement of the current carried by the movement of ions through the membrane. By applying operational procedures analogous to those used by Hodgkin and Huxley for the squid axon, the ionic current was resolved into components carried specifically by sodium and by potassium ions. Measurements of the relations between the specific ionic currents and their electrochemical driving forces were used to define appropriate quantitative measures of the specific sodium and potassium permeabilities. Critical examination of the kinetics of the permeability changes showed that the rate constants governing the variation of the permeabilities depend only upon the membrane potential and not upon the current or time. The kinetics are accurately described by empirical equations of the same form as those developed by

Hodgkin and Huxley for the squid axon (2). These empirical rate equations, together with the theoretical equations defining the specific ionic permeabilities and the theoretical equation for the distribution of current along the fiber, constitute an essentially complete mathematical model of the myelinated nerve fiber. Numerical solutions of these equations, under the appropriate boundary conditions, have established that the ionic hypothesis provides a sufficient and consistent interpretation of the action potential, subthreshold response, impedance change during an action potential, ionic exchanges during activity, refractoriness, and other phenomena associated with excitation and with conduction of the action potential.

Good agreement between the theoretical computations and the experimental observations has established the validity of the voltage-clamp analysis such that this may be confidently extended to characterize further the properties of the nodal membrane. In preliminary experiments aimed at elucidating the nature of the ionic selectivity of the membrane, it was found that during the state of high sodium permeability the membrane is only partially selective against ammonium ions.

(1) Huxley and Stämpfli (1951).

(2) Hodgkin and Huxley (1952d).

(3) Dodge and Frankenhaeuser (1958).

Table of Contents

Page

Page

Page

# INTRODUCTION

If a motor nerve is stimulated by a brief electric current of adequate strength, the muscle to which it is connected will twitch once. If the electrical stimulus to the nerve is repeated, the muscle responds again - one excitation of the nerve produces one response of the distant muscle. This unit of neural action propagated from the point of stimulation to the nerve endings on the muscle is called the nerve impulse. The physiologically significant property of an axon is the conduction of the nerve impulse.

The possibility of local electrical stimulation, well-known to physiologists of the last century, permitted Helmholz to devise an experiment that measured the velocity at which the effect spread along the nerve from the point of stimulation to the muscle. The time between the application of an electrical stimulus and the twitch of the muscle was measured. The stimulus was then applied at a more distant point of the nerve, and the time required until the muscle twitched was measured again. The average velocity was calculated as the ratio of the distance between the two points of stimulation to the difference between the two measured time intervals. Thus one physical property of the nerve impulse, a finite velocity of propagation along the axon, was demonstrated.

Also, in the middle of the last century, DuBois-Reymond developed a galvanometer sensitive enough to detect a transient variation of electric current generated by the nerve itself when it responded to an adequate stimulus. Subsequently, with refinement of the stimulating and recording apparatus, Bernstein, about 1866, was able to show that this wave-like variation of electric current traveled along the nerve with the same velocity as that of the physiological nerve impulse previously determined by Helmholz.

Such experiments firmly established two fundamental physical properties of nerve fibers. One, a nerve can be excited to physiological action by a brief electrical current imposed from an external source. Two, the axon has an

intrinsic electromotive force that can cause current flow, during activity, at points far removed from the site of the imposed stimulation. This electrical manifestation of the physiological nerve impulse focused attention on the physical origins of the intrinsic electromotive force and the physical description of the cycle of excitation, response, and recovery that characterized the participation of each region of the axon (or cell) in the conduction process.

Studies of the potential gradient between a normal and an injured region of a nerve or muscle, the demarcation potential, had revealed the longitudinal spread of current along the cells. Histological studies revealed the axons as long, thin tubes. These facts suggested an electrical description of the axon as a long tube with an inner core of conducting fluid and a wall of high electrical resistance that was immersed in an outer solution of low resistance. The mathematical formulation of the core-conduction model is now recognized as essentially that originally developed by Kelvin to describe the submarine telegraph cable. The properties of the core conductor model are embodied quantitatively in the cable equation:

$$\frac{1}{R_o + R_i} \frac{\partial^2 V}{\partial x^2} = I_m = C \frac{\partial V}{\partial t} + \frac{V}{R_m} \tag{0.1}$$

which relates the local circuit current in the external and internal conducting media (left hand terms) to the radial current density ($I_m$) which is the sum of the displacement current due to the charging of the membrane capacity and the current conducted by the finite resistance of the membrane (right hand terms); $V$ is the displacement of the potential difference across the membrane from its value in the resting state.

In the derivation of the cable equation (0.1) it is assumed that there are no intrinsic current sources in the region of the axon described by the equation. For this reason, it provides a valid description of the behavior of the axon only for the condition that the membrane parameters remain constant. This condition is well satisfied for experiments examining the spread of subthreshold extrinsic currents and the spread of current ahead

of a propagating action potential.

Subsequent experimental results have permitted a generalization of the cable equation so that it is applicable to active as well as passive regions of the axon. In this form, it has served to guide investigators into more precise analysis of the nerve as a physical system. Furthermore, the generalized cable equation is the basis for the quantitative description of propagation of the action potential.

Although the original formulations of the core-conductor models accounted well for the spread of current along the nerve cable, they begged the question of the nature of the intrinsic variable electromotive force sources in the membrane that are prerequisite to uniform propagation of the impulse. Bernstein (1902), building upon the new electrochemical theories of Nernst, proposed the first comprehensive hypothesis of nerve action that took into account the importance of the distribution of electrolytes in the nerve and related it to the cycle of excitation and response. He suggested that there existed an electrical polarization of nerve in the resting state which arose from the special permeability properties of the membrane. Specifically, in the resting nerve the membrane was supposed to be permeable only to potassium ions. Because the concentration of potassium was higher inside the membrane than outside, a potential difference was established. A further postulate was that the membrane lost its special permeability properties when stimulated by an electric current. As a consequence, the potential difference was decreased to that for the free flux of all ions.

This theory was important for it provided an explanation for the resting potential, for the generation of the action potential and for a mechanism whereby the action potential was propagated by local current distributed along the fiber according to the 'core-conductor' theory. Furthermore, the membrane theory identified the source of energy for the functioning of the nerve as the thermodynamic free energy available in the distribution of ions across the membrane. The quantitative properties of such an electrochemical system

were firmly based on thermodynamic relations between potentials and ion concentration. Perhaps because of this fundamental physical reasonableness, Bernstein's theory was accepted by many physiologists in spite of the fact that evidence in its favor was quite indirect, being derived chiefly from measurements of the changes of demarcation potential (which is only approximately proportional to the membrane potential) that occurred with changes of the concentration of potassium ion in contact with the intact membrane.

Critical experimental tests of the membrane theory were impossible on the vertebrate nerve due to its inherent structural complexity i. e., the large variation in fiber sizes, and the presence of non-neural structures, which made interpretation of both electrical and chemical measurements quite uncertain. Such difficulties are greatly reduced in the experiments on excised, isolated giant axons of the cephalopods, and the experiments on these nerves have led the way to our present understanding of the electrochemical properties of the nerve membrane.

The Bernstein theory focused attention on the surface membrane as the variable element in the cellular electro-chemical system. The membrane was considered to be the site of the cycle of excitation, response, and recovery that constituted the nerve impulse. In this sense his theory marks the beginning of the contemporary emphasis on measuring directly the properties of an isolated unit surface-area of the excitable cell.

The electrical nature of the nerve impulse was discovered over a century ago. Since then, each advance in techniques for stimulating and for recording the nerve response has permitted a clearer physical description of this process. Until the mid 1930's the most significant achievements were restricted to the phenomenological description of the excitation process (reviewed by Katz 1939). Although the exact physical nature of this process remained unknown, these investigations had firmly established that conduction of the nerve impulse is essentially an electrical process. The current flow

between active and inactive areas of an axon is distributed longitudinally described by the cable properties. These action currents excite the response of adjacent regions of the axon. Thus, a physical description of propagation of the nerve impulse emerged that has been substantiated and firmly established by all subsequent relevant experiments. Clearly, an explanation of conduction follows automatically from an adequate theory for the property of local electrical excitability.

The giant axon of the squid, described by J. Z. Young (1936), provided the ideal nerve preparation, which made possible the quantitative measurements necessary for the physical description of excitation and conduction. This axon approximates a uniform cylindrical structure - as much as 1 mm in diameter and up to 10 cm long. The rather uniform axoplasm surrounded by a typical cell membrane is covered by a cellular and connective tissue layer that is a few microns thick. This entire structure can be readily excised and experimentally manipulated in a variety of ways. Thus, electrodes can be inserted along the axis for direct measurement of the trans-membrane potential difference (Curtis and Cole, 1940; Hodgkin and Huxley, 1939). Such axial electrodes were also used to establish a constant membrane potential along the axon effectively isolating a constant area of membrane of known size (Marmont, 1949). Samples of axoplasm large enough for chemical analysis could be extruded. This permitted measurement of ion content and, by use of tracers, measurement of ionic movements across the membrane under controlled experimental conditions (Keynes and Lewis, 1951; Hodgkin and Keynes, 1955). Very recently, the axoplasm has been removed and replaced by solutions of known ionic content under conditions that preserved the electrical properties of the surface structures (Baker, Hodgkin and Shaw, 1962). Thus, the squid giant axon has provided extensive, experimental measurements permitting the electro-chemical description of excitation and conduction of the nerve impulse.

The first critical test of the membrane theory was the measurement

of the electrical impedance of the membrane during an action potential (Cole and Curtis, 1939). A squid axon was placed between two electrodes which formed one arm of a Wheatstone bridge, and the unbalance of the bridge was recorded as an action potential passed through the electrode region. Analysis of these measurements showed that during activity the electrical capacitance of the membrane remained approximately constant, and the conductance of the membrane increased rapidly to a maximum of forty times the initial conductance. This maximum change of conductance was coincident with the peak of the action potential, and the return toward the initial value was somewhat slower than the decline of the action potential. This increase in conductance was direct evidence for the increase in ionic permeability postulated by the Bernstein theory.

The introduction of an intracellular electrode into a giant axon permitted direct measurement of the potential difference across the cell membrane. With this technique the allocation of the processes of excitation response to the cell surface was substantiated, and the way was open for the contemporary emphasis on the measurement of properties of a unit area of cell surface. The definitive studies of this kind began with the observation that the membrane potential reversed its sign during the action potential (Hodgkin and Huxley, 1939). This unexpected result showed that the action potential was not simply a loss of the electrical polarization of a cell but actually a reversal of the membrane potential, which passed through zero and became about 40 millivolts positive with respect to the outside electrode at the peak of the action potential. Since the Bernstein theory postulated a simple loss of pre-existing polarization, this experiment required an important revision of the theory.

Further observations with the internal electrode showed that the steady-state membrane potential varied with the external potassium concentration in the expected manner (Curtis and Cole, 1942), confirming the original interpretation of the electrochemical basis of the polarization

of the resting axon. Thus, Bernstein's idea that the potential difference across the surface of an inactive axon arose from a selective potassium permeability of the cell membrane remained tenable, but some new state occurred in the membrane of active nerve.

An explanation of the reversal of the membrane potential and of the impedance change during excitation is provided by the hypothesis of Hodgkin and Katz (1949; Hodgkin, Huxley, and Katz, 1949) that, in response to depolarization by either an externally applied stimulus or by current flow ahead of a propagating action potential, the membrane goes through a transient state of high permeability to sodium ions, which later gives way to a state of enhanced potassium permeability. Since the electrochemical potential difference for sodium is opposite that for potassium, the membrane potential will reverse if the permeability of the membrane to sodium becomes greater than for potassium. The local change in the permeability properties of the membrane thus regulates the electromotive force for the local circuit current required to propagate the action potential. In an active region of high sodium permeability the net ionic current is inward, carried by sodium ions. To complete the local circuit, there is of necessity, a concomitant outward current in the inactive region ahead of the propagating action potential. This outward current acts to depolarize this region, triggering the sequence of changes in the permeability properties of the membrane and thereby propagating the associated potential and conductance changes along the axon.

This hypothesis was extensively tested by measurements of the action potential in external solutions of different ionic composition. The fundamental result was that the membrane potential at the peak of the action potential varied with the external sodium concentration, as would be expected if the membrane were nearly exclusively permeable to sodium at that time. This is in contrast to the membrane in the resting state where the potential varies with the external potassium concentration like a membrane almost exclusively permeable to potassium. Furthermore, during

the phase of hyperpolarization following the spike, the membrane behaves even more like a potassium electrode, reflecting an enhanced permeability to potassium associated with the falling phase of the action potential.

Thus the principal membrane processes underlying excitation and the propagation of the nerve impulse had been identified. The ionic hypothesis was shown to account for the generation of the local circuit current; it provided a consistent interpretation of the conductance change during the action potential; and it predicted an exchange of extracellular sodium for intracellular potassium during activity, which was consistent with experimental measurements (Hodgkin, 1951).

These experiments had established that the local electromotive force of the membrane was the consequence of the state of relative sodium and potassium permeability of the membrane and had indicated that the variation in the state of the membrane was under the control of the local electrical potential difference across the membrane. But additional information was still required before the ionic hypothesis could be formulated in quantitative terms. The exact nature of the coupling between the membrane potential and the permeability changes could not be elucidated from measurements of the potential changes because of the inherent complexity of the interaction between the various physical variables that describe the system. The degree of this complexity is well illustrated by the following equation (0. 2) in which the new information concerning the excitation process was used to generalize the cable equation in order that it be applied to active, as well as passive regions, of the axon. This is

$$\frac{1}{R_o + R_i} \frac{\partial^2 V}{\partial x^2} = I_m = C \frac{\partial V}{\partial t} + I_i (V, t) \qquad (0.2)$$

where the left-hand term, describing the local circuit current, is of the same form as for the passive cable (Equation 0. 1), since this current is dependent only on the conductivity of the intracellular and extracellular media; the capacity current is also of simple form, since the impedance

measurements (Cole and Curtis, 1939) had shown that the capacitance of the membrane remained essentially constant during excitation; but the term for the current carried by the movement of ions through the membrane, which was given simply as $V/R_m$ in the passive case, is now denoted $I_i(V, t)$, since this represents the sum of the specific sodium and potassium components which are each determined by the local permeability state of the membrane and the local value of the membrane potential, on which depends the electrochemical driving force for each ion species. In effect, knowledge of the functional dependence of $I_i$ on membrane potential and time was just that required to formulate the ionic hypothesis in quantitative terms. However, new and more powerful experimental techniques were required to obtain this knowledge.

At the same time that the Cambridge physiologists were working out the ionic dependence of the resting and action potentials, Cole and his collaborators were approaching the excitation process from an entirely different point of view, namely to experimentally isolate and control the electrical variables. A significant simplification of the system described by Equation 0.2 was achieved experimentally by eliminating the spatial variation of the membrane potential. This was accomplished by short-circuiting the interior of the squid axon with a low resistance axial electrode, and similarly short-circuiting the external solution by means of concentric external electrodes, with electrical guard rings to avoid end effects (Marmont, 1949). With this experimental arrangement, Equation 0.2 reduces to

$$I_m = C \frac{dV}{dt} + I_i \qquad (0.3)$$

and the membrane current ($I_m$) is now completely under experimental control.

Even under this constraint of the membrane current, however, the excitable properties of the nerve membrane remained essentially identical

to those of the unconstrained nerve (except, of course, excitation took place simultaneously at all points). Especially noteworthy was the observation that, in response to a brief stimulus, action potentials were elicited with the same waveform and the same characteristic threshold behavior as in the normal axon, notwithstanding the fact that under these experimental conditions there was no contribution of macroscopic longitudinal current.

Further simplification of the nerve system was achieved experimentally by eliminating the capacity current. This was accomplished by constraining the membrane potential to undergo only stepwise changes using an electronic servo-system to supply the necessary current to the axial electrode (Cole, 1949). Under this constraint of constant membrane potential $\frac{dV}{dt}$ is zero, and Equation 0.3 reduces to

$$I_m = I_i \tag{0.4}$$

where the ionic current is now equal to $I_m$, which flows in the external circuit where it is measured.

The concept and the experimental realization of constant membrane potential had profound implications for the ionic hypothesis (Hodgkin, Huxley, and Katz, 1952). When the membrane potential is constant, the electrochemical driving force on each ion species is constant. In effect, the observed changes in membrane current (Equation 0.4) become a measure of the change in the resistance of the membrane to current carried by the flow of ions through the membrane. In a series of experiments Hodgkin and Huxley (1952 a, b, c, d) were able to resolve the ionic current at fixed membrane potential into the specific sodium and potassium components. From these they deduced the kinetic laws governing the dependence of the specific sodium and potassium conductances of the membrane upon time and membrane potential. Expressed in analytical terms, these kinetic laws permitted a brilliant quantitative reformulation of the ionic hypothesis. Extensive computation with this quantitative theory (Hodgkin and Huxley, 1952 d; FitzHugh and Antosiewicz, 1959; Huxley, 1959; FitzHugh, 1960) has shown

that it provides a complete description of the electrical behavior of the normal squid axon under a variety of experimental conditions, including all the phenomena associated with excitation and conduction of the action potential.

It may be expected that similar membrane permeability changes occur during electrical activity in other excitable tissues which respond to changes in the external ionic environment in the same general manner as the squid axon. However, different cellular membranes may exhibit considerable differences in the precise relationships between the time courses of the permeability changes and their dependence upon membrane potential. Perhaps one might hope that if quantitative data are obtained on a wide variety of cells, the differences themselves might suggest something about the molecular mechanism underlying the permeability changes. In such a program of comparative electrophysiology, the myelinated fiber of vertebrates is an object of particular interest.

Myelination of vertebrate nerve fibers represents a very significant evolutionary advance in the cable structure of the nerve fiber. Basically, the myelinated fiber is a long thin cylindrical axon, covered over most of its surface by a thick layer of lipoprotein material, the myelin sheath. The myelin is interrupted periodically by narrow gaps, the nodes of Ranvier, where the membrane of the axon has essentially unimpeded access to the extracellular medium (Figure 0.1). For a large myelinated fiber of the frog, such as used in these experiments, the diameter of the axis cylinder is about 10 $\mu$, the myelin sheath is about 2 $\mu$ thick, the nodes are about 2 mm apart, and the length of the nodal gap is about 1 $\mu$. The present widely accepted theory of the formation of the myelin sheath is that Schwann cells, investing the embryonic fiber, migrate around the fiber. In this process the intracellular and extracellular material is squeezed out from between the successive layers of Schwann cell membrane, resulting in the spiral lamellar structure of the myelin (Geren, 1954; Robertson, 1960). If each of the lamellae had the passive electrical constants characteristic of most cellular membranes (transverse membrane resistance of 1000 ohm $cm^2$,

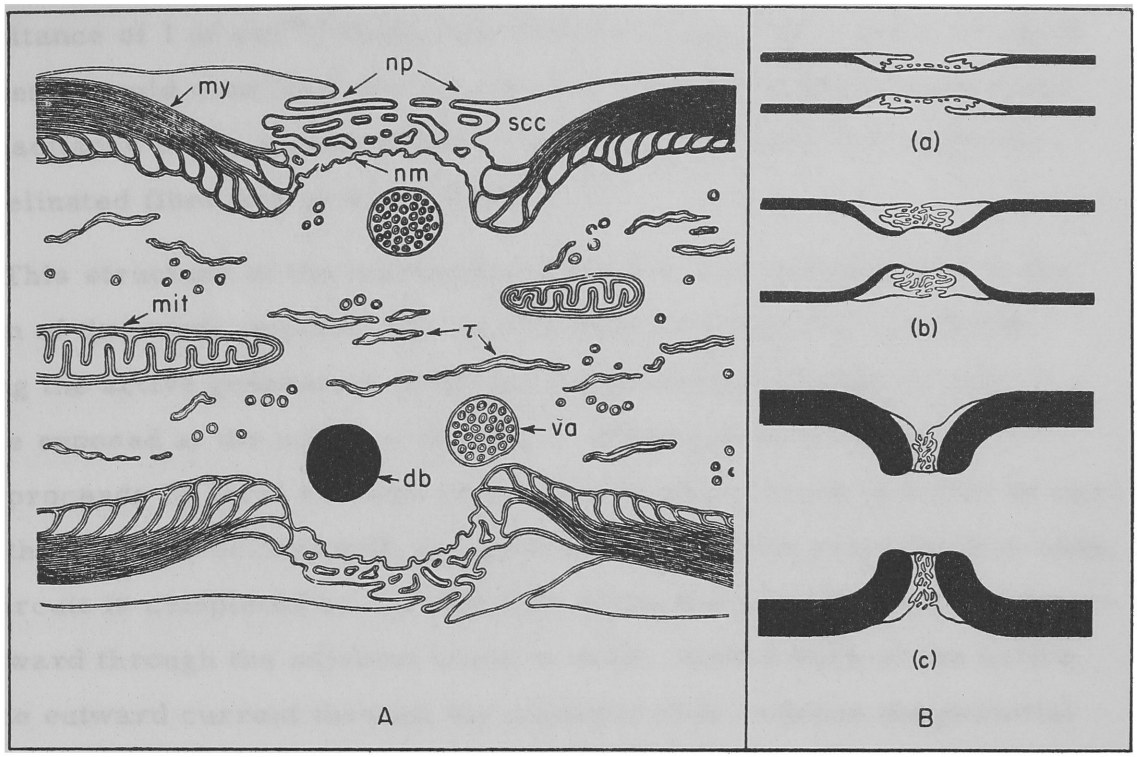


Figure 0.1: A: Diagram illustrating the structure of an amphibian myelinated fiber at a node of Ranvier as seen with the electron microscope. Away from the node the membrane of the nerve cell is enveloped by the many layers of Schwann cell membrane comprising the myelin sheath (my). At the node numerous finger-like processes (np) of Schwann cell cytoplasm (scc) project out over the nodal gap. The processes of adjacent Schwann cells are not fused, but are an open mesh through which the nodal membrane (nm) has more-or-less free access to the extracellular solution. Mitochondria (mit) are seen in the cytoplasm of both the Schwann cells and the axon. Densely stained bodies (db), tubular elements (t), and vesicular aggregates (va) are frequently seen in the axoplasm, but are of unknown physiological significance. B: Diagram illustrating the configuration of the myelin sheath at nodes in fibers of different size; (c) depicts a large fiber (14 μ outside diameter) such as were used in the present experiments; the diagram in Figure A corresponds to a medium-sized fiber (b). Both Figures are taken from Robertson (1960).

and capacitance of 1 $\mu f\ cm^{-2}$) then, the 200 or so layers forming a 2 $\mu$ thick myelin sheath would quantitatively account for the very high resistance and small capacitance of the myelin sheath. The passive electrical constants of the myelinated fiber are given in Table 0.1.

This structure of the myelinated fiber has a profound effect on the conduction of the nerve impulse; the myelin acts as electrical insulation, restricting the active generation of the action potential to areas of cell membrane exposed at the nodes of Ranvier. Propagation of the action potential proceeds by local circuits of current in which there is a flow of current into the fiber associated with the generation of action potential at a node, and the circuit is completed by current flow along the myelin-insulated internode, outward through the adjacent inactive node, thence back to the active node. The outward current through the adjacent node reduces the potential difference across the nodal membrane, triggering an active response in that node, resulting in a local circuit of current through the next node and so on. There are unavoidable electrical losses through the myelin, but the impulse is regenerated at each node: in the propagation of the impulse, the nodes play a role analogous to repeater stations along a submarine cable.

Myelination results in a very great gain in the efficiency of nerve fibers, for a 10 $\mu$ diameter frog fiber conducts the action potential about five times faster than a theoretical squid axon of the same size, and with only 1/200th the energy expenditure. ( the energy expenditure being measured by the exchange of intracellular potassium for extracellular sodium during the impulse. ).

The nature of the conduction process in myelinated nerve fiber was elucidated by the extensive investigations by Japanese physiologists, especially by Tasaki and his collaborators (reviewed by Tasaki, 1953), and was put on firm quantitative grounds by the investigations of Huxley and Stämpfli (1949). Their experimental analysis showed that the only sites where there was a phase of inward radial current were the nodes, whereas

TABLE 0.1.

Typical values of the electrical constants for an amphibian myelinated nerve fiber

Representative dimensions

| | |
|---|---|
| length of internode | 2 mm |
| diameter of axis cylinder | 10 μ |
| thickness of myelin | 2 μ |

| Electrical constants | Value | |
|---|---|---|
| longitudinal resistance of axis cylinder | 15 megohms/mm | (1) |
| specific resistance of axoplasm | 120 ohm cm | |
| capacity per unit length of myelin | 1.6 μμf/mm | (2) |
| capacity per unit area of myelin | 0.005 μf/cm$^2$ | (2) |
| transverse resistance times unit length of myelin | 290 megohm mm | (2) |
| specific resistance of myelin | 100,000 ohm cm | (2) |
| resistance of nodal membrane (resting state) | 40 megohms | (2) |
| capacity of nodal membrane | 1.5 μμf | (2) |

REFERENCES: (1) Tasaki and Frank (1955)

(2) Tasaki (1955)

the radial current was entirely outward through the myelin covered internode. For the quantitative description of this system, the internodes can be looked upon as short lengths of passive cable obeying the simple form of the cable equation (0. 1) connecting the areas of excitable nerve membrane at the nodes.

The demonstration that the action potential of a myelinated fiber is generated at the node focused attention on the electrical properties of the nodal membrane. The ionic dependence of the resting and action potentials was investigated by Huxley and Stämpfli (1951) and their results are shown in Figure 0. 2. They observed that the resting potential of the nodal membrane varied with the external potassium ion concentration. In particular, the change in resting potential with change of potassium ion concentration approached the theoretical limit for an ideal potassium electrode when the membrane was depolarized with high external potassium ion concentration. The amplitude of the action potential was observed to vary markedly with changes with sodium ion concentration. Thus, the curve relating the nodal action potential to the logarithm of the external sodium concentration was found to be linear with a slope of 25 mv per e-fold change. These experiments showed that the nodal membrane in the resting state is primarily permeable to the potassium ion and that, at the peak of the action potential, this membrane is primarily permeable to sodium ions. In a steady-state depolarization the node goes to a state of very high permeability to potassium ion. The foregoing results demonstrated that the excitable properties of the nodal membrane conformed to the ionic hypothesis so extensively developed for the squid axon.

From the experiments demonstrating saltatory conduction it is clear that the myelinated internode is a passive structure and that sites of generation of the action potential are restricted to the nodes of Ranvier. This result and the demonstration that the action potential at a single node has an ionic dependence similar to that of the squid axon suggested the experimental extension of the quantitative analysis to the myelinated fiber. There was, however, a very great obstacle to this program imposed by the

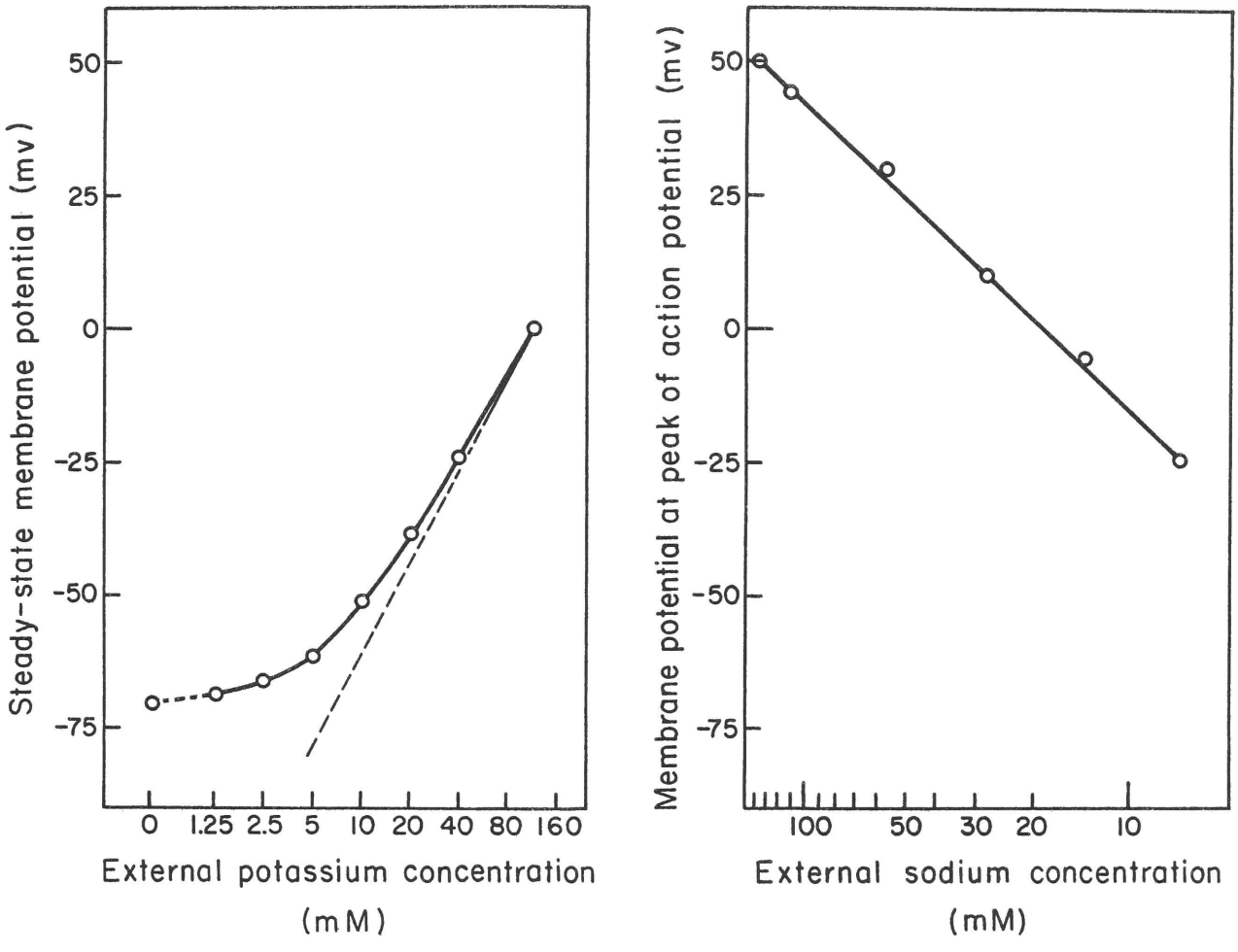


Figure 0.2: Dependence of the steady-state membrane potential on the external potassium concentration (left) and the dependence of the membrane potential at the peak of the action potential upon the external sodium concentration. Data of Huxley and Stämpfli (1951). Figures replotted from Hodgkin (1951). The dashed line in the left-hand figure is the theoretical curve expected if the membrane were exclusively permeable to potassium ions.

stringent condition under which the voltage-clamp measurements are valid. The criterion of an ideal voltage clamp has been stated succinctly by Cole and Moore (1960), "the potential difference across the membrane capacity shall have a known and constant value during the time and over the area of the membrane in which the current flow is measured". An adequate approach to realization of this ideal voltage clamp had been devised for the squid axon and, more recently, for the localized membrane at a node of Ranvier of a vertebrate myelinated nerve fiber by Frankenhaeuser. The experimental procedures for the study of the nodal membrane are very different from those used in experiments on giant axons. However, the interpretation of the data is patterned after that developed by Hodgkin and Huxley.

It is the purpose of this dissertation to report the use of the Frankenhaeuser voltage-clamp technique for the measurement of the current-voltage relations of the nodal membrane of a frog nerve, to analyze the data in terms of the quantitative model of Hodgkin and Huxley, and to achieve a complete quantitative description of the electrical behavior of the myelinated fiber that is associated with excitation and conduction of the nerve impulse.

Chapter I

# MEASUREMENT OF THE CURRENT-VOLTAGE RELATIONS OF THE NODAL MEMBRANE

## Theory

The fundamental assumption governing the design of these experiments is that the total current through the nerve membrane is the sum of the displacement current associated with the capacitance of the membrane and the current carried by the movement of ions through the membrane. This is expressed by the following relation for the current through each elementary area of membrane,*

$$I_m = C\dot{E} + I_i \qquad (1.1)$$

where $I_m$, the membrane current, is that current which flows in the local circuits required for propagation of the impulse, $E$ is the potential difference across the membrane, $C\dot{E}$ is the capacity current and $I_i$ is the ionic current.

In the experimental investigation of the nerve membrane using electrical methods, the measurable quantities are the membrane current ($I_m$) and the membrane potential ($E$). If an area of membrane is electrically isolated so that the membrane potential is uniform over that area, then Equation 1.1 is applicable to the experimental situation. Either of two simplifications of this relation is possible, using the appropriate experimental constraint.

If $I_m$ is constrained to zero, then all the ionic current serves only to charge and discharge the membrane capacitance. With this "current-clamp" constraint, the action potential is measured for the condition that

---

* Hereafter, dot notation will be used to denote differentiation with respect to time.

there is no longitudinal current flow into adjacent inactive regions of the fiber. However, the excitable behavior of the membrane remains qualitatively identical with that of the unconstrained nerve, and one obtains no new information which, in principle, could not be obtained from a simpler experimental arrangement.

On the other hand, if the membrane potential were constrained to undergo only step-wise changes, then, during the time that $E$ is constant, $\dot{E}$ is zero, and the ionic current ($I_i$) is equal to the total membrane current ($I_m$). With this "voltage-clamp" constraint, the ionic current is directly measured, providing the basic data for investigating the physical processes underlying generation of the action potential.

## Development of the Voltage-Clamp Technique for the Node

In order for voltage-clamp experiments to yield valid measurements, it is necessary that the membrane potential be uniform over the area of membrane for which the current is measured. For the vertebrate myelinated fiber, the myelin sheath effectively restricts the generation of current to the cell membrane at the node of Ranvier. The area of nodal membrane is so small that it is reasonable to assume from the cable theory that the membrane potential is sufficiently uniform, even when the membrane is maximally active (Appendix II).

Experimental control of the membrane potential is achieved by using an electronic servo-system to supply current to the membrane such that the measured membrane potential follows any desired time course. Accurate measurement of the membrane potential is thus prerequisite for an adequate voltage-clamp system. Because the minute size of the myelinated fibers precludes the use of internal electrodes, the only access, electrically, to the inside of the nodal membrane is along the axoplasmic core of the myelin-insulated internodes. The high series resistance of the internode, however, presents a formidable difficulty with respect to accurate measurement of the membrane potential.

The usual experimental arrangement for measuring the membrane potential involves measuring the longitudinal current through an internode when the external longitudinal resistance is made large with respect to the series resistance of the internode, as by the air-gap technique (Tasaki and Frank, 1955). Attempts to do voltage-clamp experiments have been made using such air-gaps (del Castillo, Letvin, McCulloch, and Pitts, 1957; Tasaki and Bak, 1958; Ooyama and Wright, 1962). Numerous technical difficulties made these measurements unreliable. The chief difficulty is that the effective high-frequency response of the air-gap system is so severely limited that there is considerable error in the control of the membrane potential. Often this error is so extreme as to cause wild oscillations of the membrane current (Appendix II).

Using a novel approach involving servo control of the internal longitudinal current, Frankenhaeuser (1957 ) developed an ingeneous method for measuring the membrane potential which had the necessary accuracy and high-frequency response. This was incorporated into a system for voltage-clamp experiments (Frankenhaeuser and Persson, 1957; Dodge and Frankenhaeuser, 1958).

Frankenhaeuser's method for measurement and control of the membrane potential was employed in the present experiments and will be described below in detail pertinent to assessing the reliability of these measurements. For specific details of design, the reader is referred to the published reports.

## Experimental Methods

### A. Single fiber preparation

From a 3 cm length of sciatic nerve of the frog (Rana pipiens), a single large fiber (12 to 15 μ diameter) was isolated by the standard technique (e.g. Tasaki, 1953) for a length of about 3 mm (including at least one node). The nerve was then transferred to a lucite chamber in which three partitions (about 0.2 mm wide) separated four pools of solution. The two pools (A and

B, in Figure 1.1) adjacent to the central partition were 0.2 and 0.3 mm wide, respectively (the critical nature of these dimensions is discussed in Dodge and Frankenhaeuser, 1958), whereas the end pools (C and E) were large enough to accommodate the undissected ends of the nerve trunk. The isolated fiber was positioned, as shown diagramatically in Figure 1.1, with the node under investigation in pool A. A thin layer of vaseline was applied to the fiber with a hypodermic syringe at each of the three partitions. These vaseline seals isolated the pools electrically by a resistance of about 2 megohms, which was the resistance of the thin layer of solution adhering to the fiber within the seals. Electrical contact to the pools was made with separate recording and current-carrying electrodes, consisting of calomel half cells and salt bridges made of short lengths of capillary tubing filled with 1% agar in 3 M KCl.

B. Electronic systems for measurement and control of the membrane potential

A block diagram of the experimental arrangement is shown in Figure 1.1. Through the operation of feedback Amplifier 1, a change in the membrane potential of the node was faithfully reproduced as a change in the potential difference between pool A and pool B, the latter being at ground potential. With the function switch in position I, constant-current stimuli were applied to the node under investigation upon application of constant-voltage pulse to pool E. Alternatively, when the function switch was in position V, the membrane potential was constrained to follow a predetermined sequence of reference pulses ($V_{ref}$) by the operation of feedback Amplifier 2. In this case, the nodal membrane current ($I_m$) was proportional to the potential difference between pool E and ground. As before, the membrane potential was very nearly equal to the potential difference between pool A and ground. These two signals were displayed simultaneously on an oscilloscope and recorded photographically.

1. Operation of the membrane potential measuring system: Amplifier 1 was employed in a negative feedback circuit to hold the longitudinal current

Figure 1.1 (opposite): Block diagram of the experimental arrangement for measurement and control of the membrane potential of a node of Ranvier. The node under investigation is in Pool A. Adjacent nodes in Pools E and C are rendered inactive by isotonic KCl. Vaseline seals are applied over the fiber at the lucite partitions. Electrical contact with the pools is made by separate potential-measuring (open circles) and current-carrying (filled circles) electrodes. Amplifiers 1 and 2 are high-gain, wide-band, direct-coupled, feedback amplifiers. Amplifier 1 operates to measure the membrane potential; amplifier 2 operates to clamp the membrane potential to a preselected sequence of changes determined by the pulse generator. The potential difference between Pool A and ground, the measure of the membrane potential (E), is displayed on one channel of an oscilloscope (Tektronix Type 532 with Type 53/54 C chopped-beam preamplifier), and the potential difference between Pool E and ground, the measure of the membrane current, is displayed simultaneously on the second channel, the oscilloscope traces being recorded photographically.

Figure 1.2 (opposite): Equivalent circuit for electronic measurement and control of the nodal membrane potential. D designates a point inside the fiber at the node under investigation. The series resistance of the current path from point D to Pool C, i.e. through the left-hand internode and the inactive nodes in Pool C, is represented by $R_{CD}$; similarly, the resistance of the current path from point D to pool E is represented by $R_{ED}$. For further description see text.

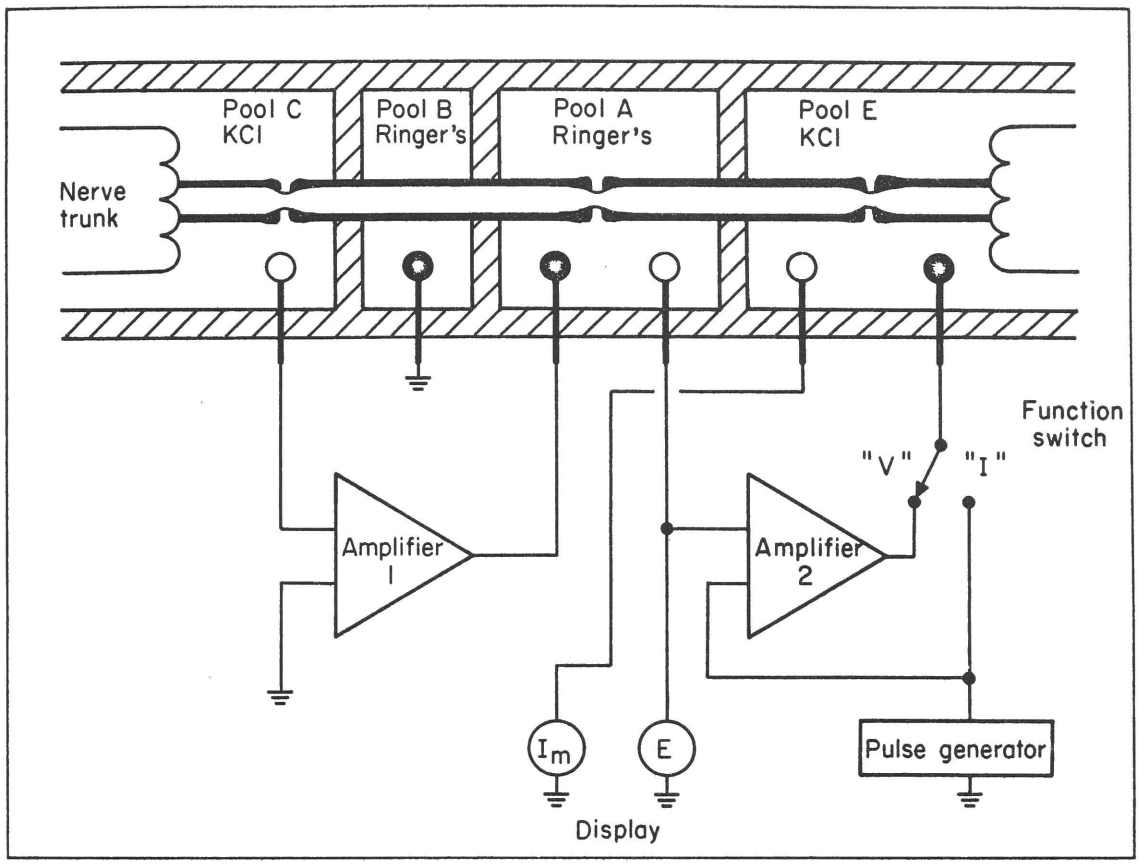
Pool C
KCl
Pool B
Ringer's
Pool A
Ringer's
Pool E
KCl
Nerve
trunk
Function
switch
"V"
"I"
Amplifier
1
Amplifier
2
$I_m$
E
Pulse generator
Display

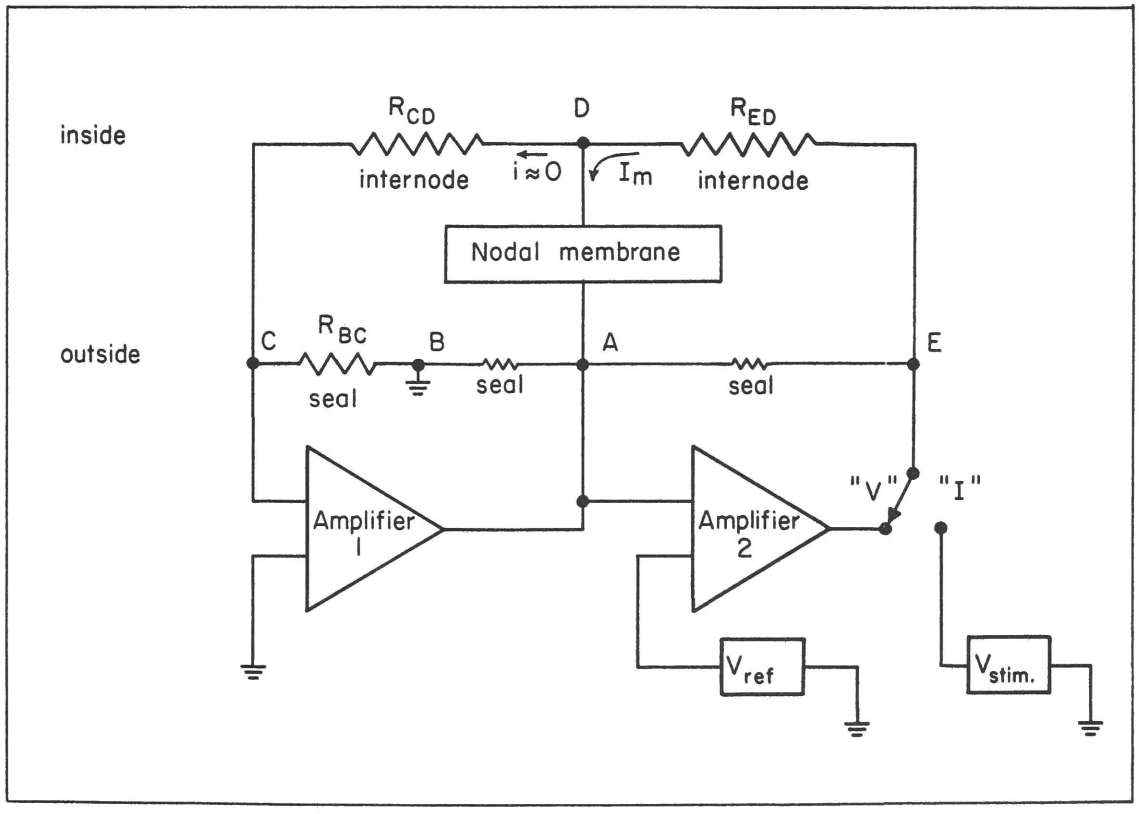
inside
outside
$R_{CD}$
D
$R_{ED}$
internode
i ≈ 0
$I_m$
internode
Nodal membrane
C
$R_{BC}$
B
A
E
seal
seal
seal
Amplifier
1
Amplifier
2
"V"
"I"
$V_{ref}$
$V_{stim.}$

in the left-hand internode to a negligibly small value by causing the potential difference between pools A and B (the latter being at ground potential) to undergo the inverse of changes in the potential difference across the nodal membrane (Frankenhaeuser, 1957). This is more easily seen from analysis of the equivalent circuit of the system, Figure 1.2. Considering a point in the axis cylinder at the node (point D), the total impedance of the current path from this point to pool C through the left-hand internode and adjacent node, represented by the resistance* $R_{CD}$ was approximately 40 megohms when pool C contained isotonic KCl. The resistance of the external current path through the seal BC, represented by $R_{BC}$, was approximately 2 megohms. Current flow through the other seals AB and EA, which were shunted by low impedances to ground, could be neglected. A change in the potential difference across the node ($V_{AD}$) caused a variation of the longitudinal current (i) in the left-hand internode. The only return path for this current is across the seal BC, where it develops a potential drop $V_{BC} = iR_{BC}$. This potential drop is amplified and inverted by Amplifier 1 which had a voltage gain ($a_1$) of 3000. The output was applied across seal AB. Applying Kirchoff's laws to this circuit shows that

$$V_{AD} = V_{AB}\left[1 + \frac{1}{a_1}\left(1 + \frac{R_{CD}}{R_{BC}}\right)\right]$$

Inserting the appropriate values for the quantities in the brackets, this

---

* The electrical structure of the myelin-covered internode is in fact more complicated than is assumed here. Associated with the myelin there is a finite, but very high, transverse resistance and some capacitance. The very small leakage of current through the resistance of the myelin has a negligible effect on the operation of this system, and the effect of the distributed capacitance is to limit the response of the amplifier at very high frequencies (Dodge and Frankenhaeuser, 1958). However, with respect to the operation of this system over the useful frequency range, the electrical properties of the internode were not sensibly different from that of an ohmic resistance, as indicated in model experiments.

equation predicts that, theoretically, changes in the membrane potential ($V_{AD}$) are measured by the potential difference $V_{AB}$ with less than 1 percent attenuation.

In practice, however, it was discovered that non-ideal current flow within pool B caused some additional attenuation (Dodge and Frankenhaeuser, 1958). Under the conditions of the present experiments, this attenuation was judged to be less than 5 percent, and no correction was applied to the measured values of membrane potential.

Analysis of this circuit shows that the potential at point D is held virtually constant relative to the ground by the operation of Amplifier 1. When the nodes in pool E were rendered inactive, the impedance of the current path between pool E and the point D could be approximated by a constant resistance ($R_{ED}$). Hence, when the function switch was in position I, a constant voltage applied to pool E injected a constant current through the nodal membrane of a magnitude given by

$$I_m = \frac{V_{ED}}{R_{CD}} \approx \frac{V_{EB}}{R_{CD}}$$

2. Operation of the voltage-clamp system: Amplifier 2 was employed in a negative feedback circuit to control the membrane potential. The measured membrane potential ($V_{AB}$) was compared with a reference pulse ($V_{ref}$) at the input of Amplifier 2, the difference was amplified, and the output was applied to pool E when the function switch is in position V. Denoting the gain of the amplifier by $a_2$, it follows that

$$a_2(V_{AB} - V_{ref}) = V_{EB}.$$

The potential difference $V_{EB}$ injected a current through the right hand internode of magnitude $V_{EB}/R_{ED}$, which was also the current through the node $I_m$, since the operation of Amplifier 1 prevented current flow in the left-hand internode. Thus the membrane potential potential should have been

stabilized to the reference potential within an error given by $V_{EB}/a_2$. The maximum variation of $V_{EB}$ during a voltage clamp was about a volt, and the gain of Amplifier 2 was about 1000; so theoretically, the maximum error should have been about one millivolt.

However, other sources of error affecting the speed of stabilization and the control of the membrane potential have been identified and analyzed (Appendix II). The analysis indicated that, in response to a step change of the reference pulse, the nodal membrane potential was stabilized to its new value in less than 50 μsec, and then held within a maximum deviation of about 3 mv.

The ultimate limit in resolution of the membrane current in the voltage-clamp experiment was set by noise, principally that generated within the feedback amplifiers, but also including some radio interference. This noise was particularly rich in high-frequency components which were not acted upon by the feedback loops involving the nerve fiber. This high-frequency noise, which should have had no significant effect on the nodal membrane, was partially suppressed by recording the membrane current through a low-pass filter (single time constant of 10 μsec). The remaining noise appeared on the photographic records as a broadening of the trace equivalent to from 0.2 to 0.4 x $10^{-9}$ amp per node, in different experiments.

C. Calibration of the membrane current

According to relations derived above $I_m = V_{EB}/R_{ED}$. With this apparatus, there was no direct method for determining the value of $R_{ED}$. Using a different method, Tasaki (1955) has determined that the average resting resistance of nodes of similar fibers is about 40 megohms. Accordingly, in this work, the membrane currents were calculated assuming this value for the resistance of the node in the resting condition.

For these frog fibers, estimates of the area of the nodal membrane are subject to considerable uncertainty. Therefore, the membrane currents

were not normalized to unit area but are reported in terms of the total current through the node. The convenient unit of current is the nanoamp (na) which is $10^{-9}$ amp.

D. Nomenclature

Conforming to recent practice, the membrane potential (E) is reported as the potential difference across the membrane taken in the sense of internal potential minus external potential, outward current through the membrane is therefore positive. The zero of the potential scale was taken as that obtained when the nerve was depolarized by isotonic KCl (Stämpfli and Willi, 1957). Consequently, with isotonic KCl in pools E and C, the nodal membrane potential (E) is given directly as $-V_{AB}$.

Conforming to the traditional usage of the terms, depolarization of the membrane refers to any positive going variation of the internal potential, even when this is sufficiently large to polarize the membrane in the sense opposite to that of the resting state; hyperpolarization of the membrane refers to a change in the membrane potential which makes the internal potential more negative than it is at the resting potential.

E. Resting membrane potential

In these experiments, the Ringer's solution in pools E and C was replaced by isotonic KCl in order to make the nodes in these pools inexcitable and also to reduce the resistance of the current paths to the node under investigation. Amplifier 1 was then balanced so that in the resting state $V_{AB}$ was equivalent to a membrane potential $E_R \doteq -75$ mv, at which value the amplitude of the action potential and threshold were essentially the same as that observed before KCl was put in the end pools This value of resting potential agrees satisfactorily with previous measurements (Huxley and Stämpfli, 1951; Frankenhaeuser, 1957).

F. Temperature

The preparation was cooled a few degrees below ambient room temperature by flowing tap water through a brass shield enclosing the recording chamber and electrode assembly. During any experiment the temperature did not vary more than $1^0$ C. The range of temperatures in different experiments was $18^0$ C to $22^0$ C.

G. Ringer's solution

The standard Ringer's solution used in these experiments had the following composition: 113 mM NaCl, 2.5 mM $NaHCO_3$, 2.5 mM KCl, and 2.0 mM $CaCl_2$; pH = 7.5.

## Preliminary Results

A. Measurement of the action potential under the current-clamp constraint

As a consequence of the operation of the membrane potential measuring system, the membrane current ($I_m$) is constrained to be proportional to the potential difference between pool E and the ground. Thus, when a rectangular stimulating pulse is applied, the current is effectively clamped to a constant value.

When the resting node is perturbed by small constant currents in either direction, the time course of the change in membrane potential is a simple exponential approach to a steady value which is proportional to the applied stimulus (Frankenhaeuser, 1957). Thus, the resting membrane behaves simply as a constant resistance shunted by a capacitor. From the observed time constant of the resting membrane ($\tau$) and the assumed value for the resting resistance ($R_m$ = 40 megohms), the capacitance of the node (including the short length of the two internodes in pool A) was estimated from the relation: $\tau = R_m C$. In these experiments, the observed time constant ranged from 84 to 120 μsec, yielding values of 2.2 to 3.0 μμf for the effective capacitance of the node, in agreement with Tasaki's (1955)

measurements.

The response of a node to somewhat larger, constant currents is illustrated in Figure 1.3. When the applied current was inward through the node hyperpolarizing the membrane, the time course of the change in membrane potential was simply that predicted by the passive (constant) resistance and capcitance of the resting membrane. However, when the applied current was outward, depolarizing the membrane, the response was very different - for a short time at the beginning of the stimulus, the membrane potential change was that expected of a passive RC network, but soon thereafter the node gave the "all-or-none" regenerative response or action potential. Typically, the action potential of a node in its normal ionic environment is a positive going variation of the membrane potential, about 110 mv in amplitude and about 1 msec in duration at room temperature.

The electrical behavior of a node under current-clamp constraint is virtually identical with the behavior of an unconstrained fiber. It demonstrates all the typical phenomena associated with excitation of nerve, such as a critical threshold for the action potential, graded subthreshold responses, refractoriness, impedance change during the action potential, accommodation, and the like. There is, of course, the fundamental difference that, due to the constraint on the longitudinal current, the active response of the node under investigation is not propagated to adjacent nodes.

In the case of the myelinated fiber, this constraint yields measurements of the membrane response that are more accurate with respect to its absolute amplitude and wave-form than those obtained using external electrodes on the unconstrained fiber. Furthermore, with this constraint, the action potential can be measured when the membrane current is zero. In the experiment of Figure 1.4, the membrane potential was displaced by brief stimuli; thereafter the current was held at zero. The response to the smallest stimulus declined monotonically to the baseline demonstrating a subthreshold response by the very considerable deviation from the simple

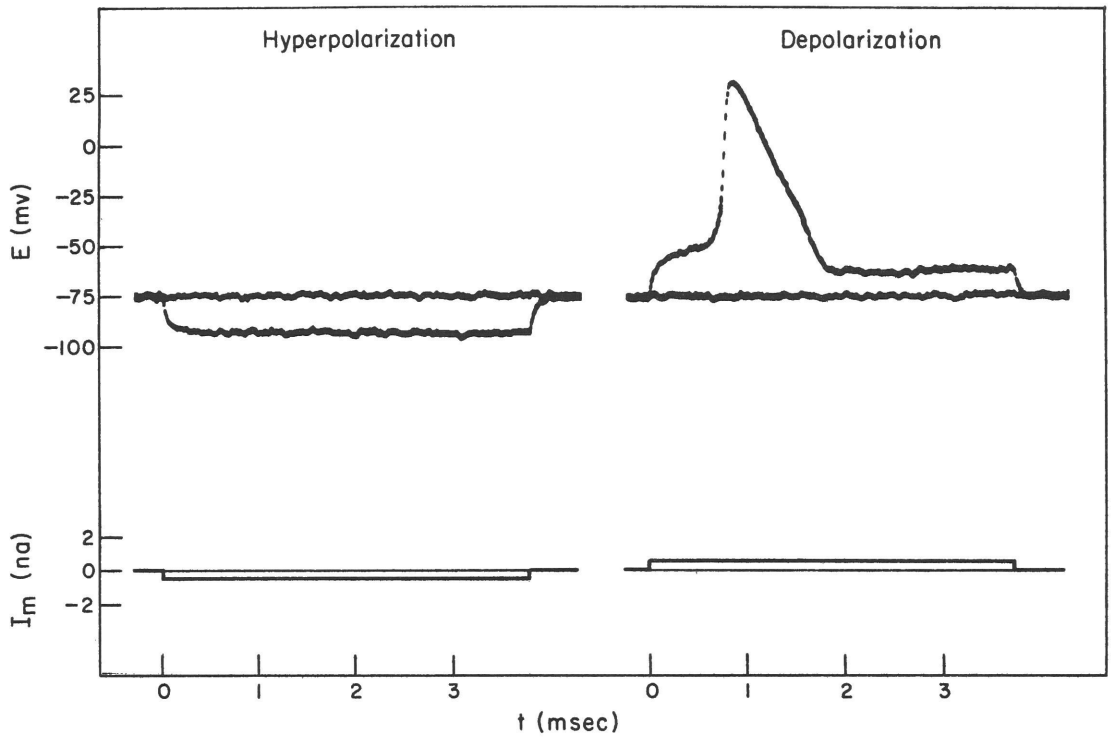


Figure 1.3: Time course of the membrane potential (E) during 3.8 msec long pulses of constant membrane current ($I_m$) of 0.5 na. At left, the current was inward (negative), hyperpolarizing the membrane. At right, the membrane current was outward, depolarizing the membrane sufficiently to evoke an action potential. Node 9; 20°C.

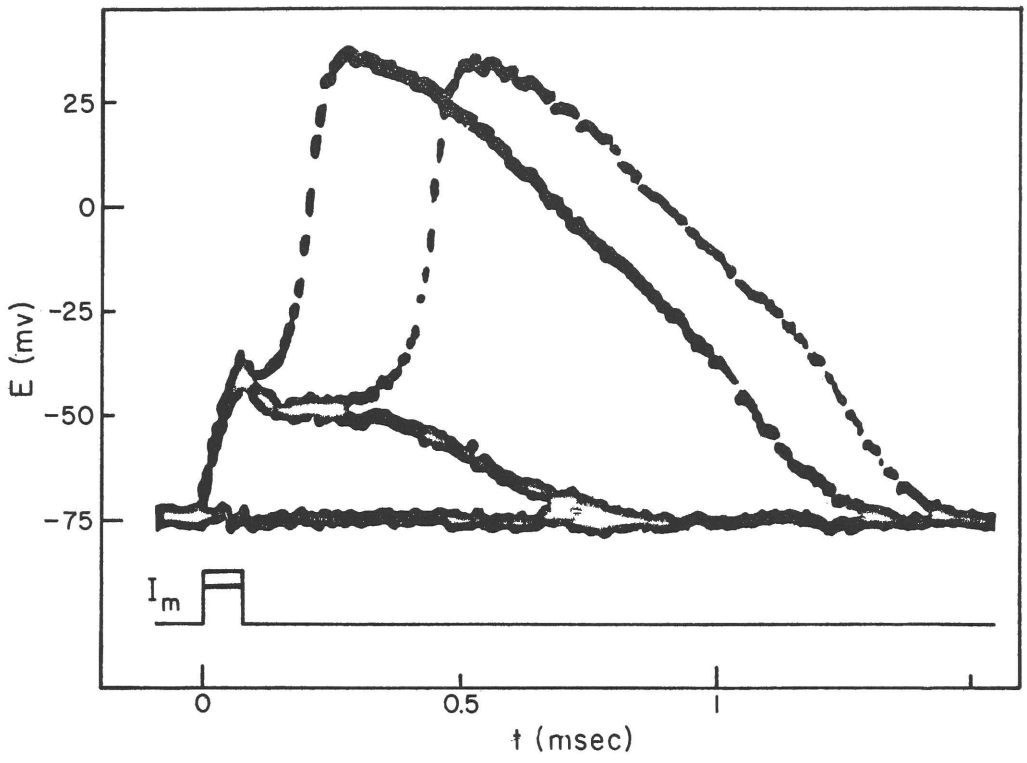


Figure 1.4: Time course of the membrane potential following brief (75 μsec) pulses of outward membrane current. After each pulse the membrane current was held to zero. Three records superimposed photographically. The subthreshold response and the just suprathreshold response (the action potential with long latency) were elicited by pulses of approximately 1.5 na. Node 8; 22°C.

exponential decay expected of a passive RC network. The response to an infinitesimally larger stimulus was the typical action potential, occurring after considerable latency. In response to a larger stimulus, the latency was reduced, but the wave-form of the action potential was virtually unaffected.

Applying Equation 1.1 to the conditions of this experiment, $I_m = 0$, after the stimulus, hence, $I_i = -C\dot{E}$. That is, the ionic current through the membrane can be calculated from the observed rate of change of the membrane potential. This relation shows that the necessary condition for the generation of the rising phase of the action potential when $\dot{E}$ is positive, is that the ionic current must be negative, or inward. This inward ionic current is opposite in direction to that expected in a passive electrical structure. However, the properties of the ionic current are examined more directly in voltage-clamp experiments.

B. Measurement of the membrane current under the voltage-clamp constraint

Characteristic features of the behavior of nodal membrane under the condition that the potential difference across the membrane is the controlled variable are illustrated in Figure 1.5. At the left, is a simultaneous recording of the membrane potential (E) and the membrane current ($I_m$) when the membrane potential is changed in a rectangular pulse hyperpolarizing the membrane by 60 mv. At the beginning and the end of the potential step, there were very brief, poorly resolved, surges of current required to charge the membrane capacitance quickly to the new level of membrane potential. Following the surge of capacity current (which will be neglected in most of the subsequent discussion) the ionic component of the membrane current was small and constant. This step of ionic current is simply that expected from the resistance of the membrane and the amplitude of the potential change. This result reflects the passive behavior of the hyperpolarized membrane revealed in the experiment of Figure 1.3.

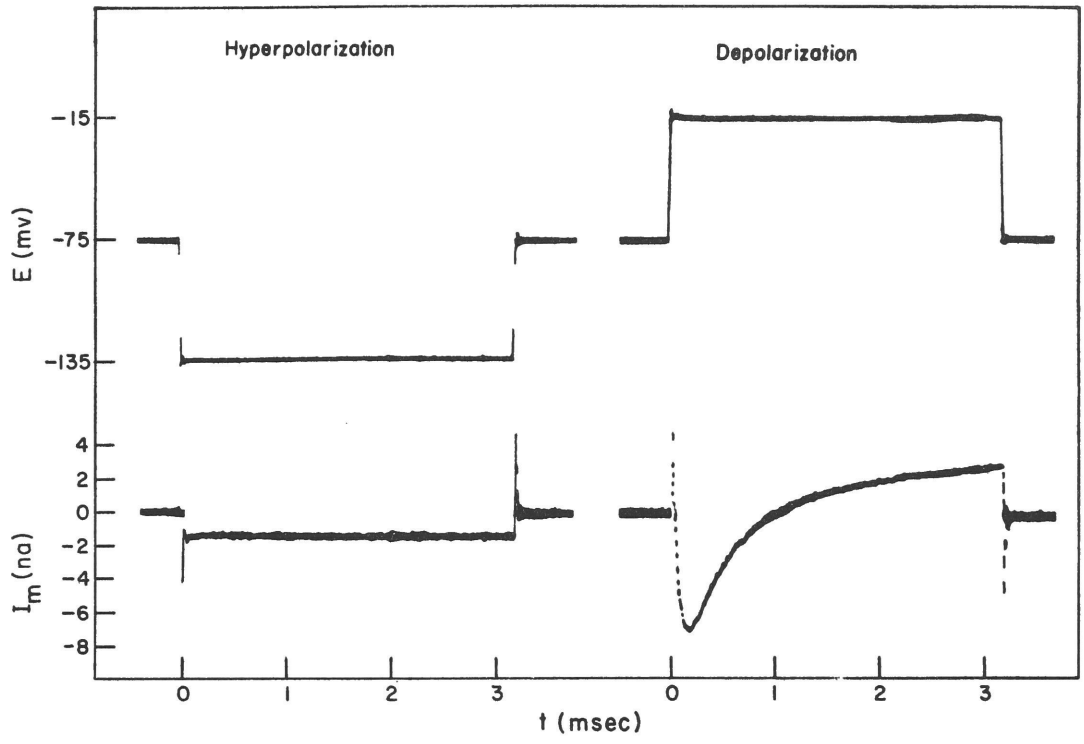


Figure 1.5: Time course of the membrane current ($I_m$) associated with rectangular step changes of the membrane potential (E). In both records of membrane current there is a brief, poorly resolved surge of capacity current at each transition of the potential. During the time that E is constant, $I_m$ is a direct measure of the ionic current of the nodal membrane. In response to a 60 mv hyperpolarization, left, the ionic current is a step of current in the same direction as the applied potential change. In response to a 60 mv depolarization, right, the ionic current shows a transient phase of inward current, opposite in direction to the applied potential change; the phase of inward current gradually gives way to a phase of outward current. Node 6; 20°C.

When the membrane underwent a step depolarization of 60 mv, a quite different pattern of membrane current is observed. In the first instant, there was the surge of capacity current, and the initial ionic current was, as expected, outward. Very rapidly, however, there followed a transient phase of inward current, which decayed at longer time to a steady level of outward current. The early phase of inward current is of particular interest because if the membrane potential were not constrained by the feedback amplifier, this inward current would act (according to the relation $I_i = - C \ddot{E}$) to depolarize the membrane further; indeed, at its peak, the amplitude of the inward current was about three times larger than that required to charge the membrane capacitance at its observed rate of charge during the rising phase of the action potential.

Ionic currents measured at different values of the membrane potential are shown in Figure 1.6. In this experiment, the membrane potential was abruptly changed from its resting value of -75 mv to various levels of test depolarization ($E_1$). For very small depolarizations ($E_1$ = - 60 mv) there was only a small step of outward current. At a somewhat larger depolarization ($E_1$ = - 45 mv) there was a small, slow, transient inward current. As the test depolarizations were made larger, the inward transient currents were larger and more rapid. The inward current was maximal at a depolarization to $E_1$ = - 15 mv. With a further increase in the level of depolarization the amplitude of the inward current decreased until, at $E_1$ = 30 mv, its peak value was nearly zero. For very much larger depolarizations, the early transient current was outwardly directed.

The steady-state values of outward currents at long times were larger the greater the depolarization, and the rate of approach to the steady level became continuously more rapid with membrane depolarization. The results of this experiment are conveniently summarized in Figure 1.7, where the peak values of the early transient currents ($I_{peak}$) and the steady-state values of the outward currents at long times ($I_\infty$) are plotted against

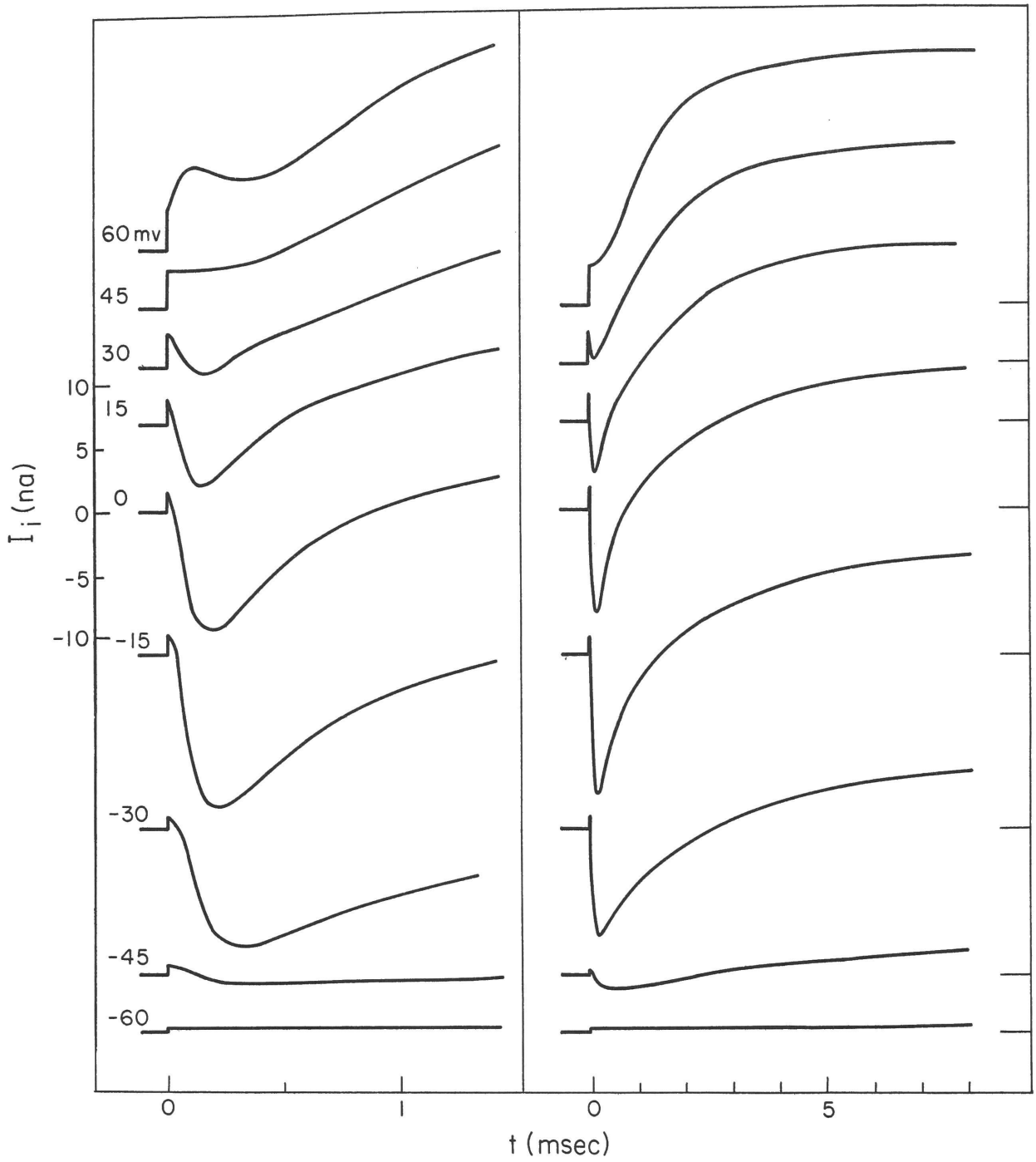


Figure 1.6: Curves of the time course of the ionic current, $I_i$ (capacity current subtracted from $I_m$), in response to stepwise depolarizations from the resting potential ($E_R$ = - 75 mv) to different values of membrane potential. The family of curves at the left from records on a fast sweep and the family at the right from records on a slower sweep, were measured at the same values of membrane potential. Each curve is identified by the value of membrane potential during the depolarization, i.e. by the number at the left. In each case, the short segment of curve for $t < 0$ marks the zero current baseline and corresponds to the zero on the ordinate scale. Node 8; 22°C.

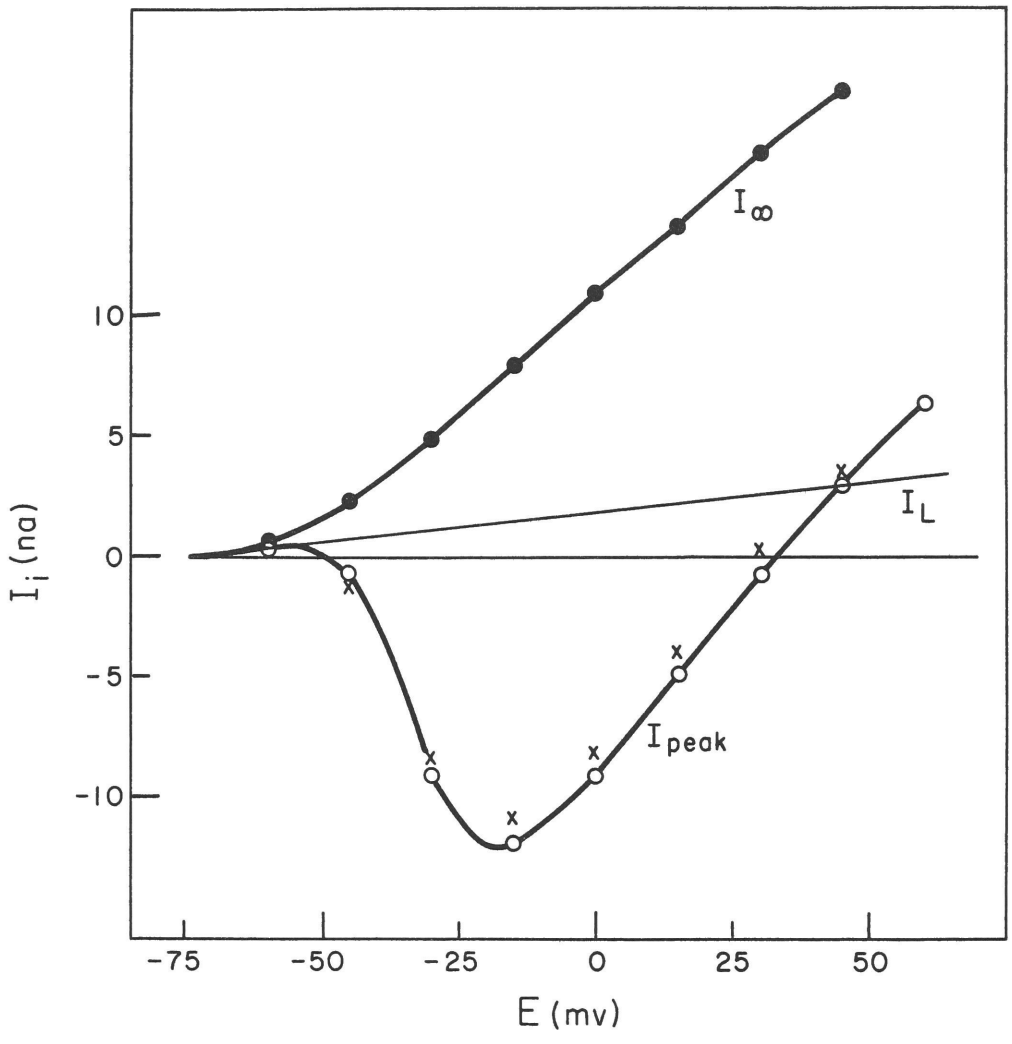


Figure 1.7: Three characteristic relations between the ionic current observed during step depolarizations and the membrane potential during the depolarizations. $I_{peak}$ was measured at its peak of the early transient phase of $I_i$ (open circles are measurements of the records of Figure 1.6 left and crosses are measurements of the records of Figure 1.6 right). $I_\infty$ is the steady-state value of outward current at long times. The straight line ($I_L$) corresponds to initial values of $I_i$ estimated from the resistance of the resting membrane. The discrepancy between the two measurements of $I_{peak}$ is due to inaccuracy in rebalancing the amplifier to $E_R$ before each run.

the membrane potential. The initial values of the ionic current estimated from the resistance of the resting membrane are shown as the dotted line ($I_L$).

C. Correlation of the current-voltage relations with excitation

The behavior of the excitable membrane of a node under conditions in which the membrane potential is controlled is thus seen to be different from that of an unconstrained node; completely absent are any indications of the threshold and "all-or-none" phenomena characteristic of nerve. At a constant membrane potential the ionic currents are smoothly continuous in time, and magnitudes and rates of change of the ionic current are smoothly graded with the membrane potential. That aspect of the observed ionic currents which is most significant with respect to the general behavior of the membrane is that, over the range of membrane potentials from about -50 mv to +33 mv, there is a period during which the ionic current is inward, opposite in direction to that expected of a passive system in response to the applied potential changes.

To examine the relations between the ionic current and membrane potential let us consider the membrane response under the current-clamp constraint, specifically, the response to a sudden displacement of the membrane potential by a very brief stimulus (Figure 1.8) with the total current through the membrane being held to zero thereafter. Under the latter condition, all the ionic current through the membrane goes to charge and discharge the membrane capacity. During the brief stimulus the externally imposed current quickly discharges the membrane capacity, displacing the membrane potential, initially at its resting value (E = -75 mv) to about E = -40 mv. In the first instant after the imposed potential change, the ionic current is outward, recharging the membrane capacitance toward the resting level ( $t_1$, Figure 1.8). Because the membrane is depolarized, however, the outward ionic current decreases toward zero, and hence the rate of change of the membrane potential approaches zero ( $t_2$). If, at this time,

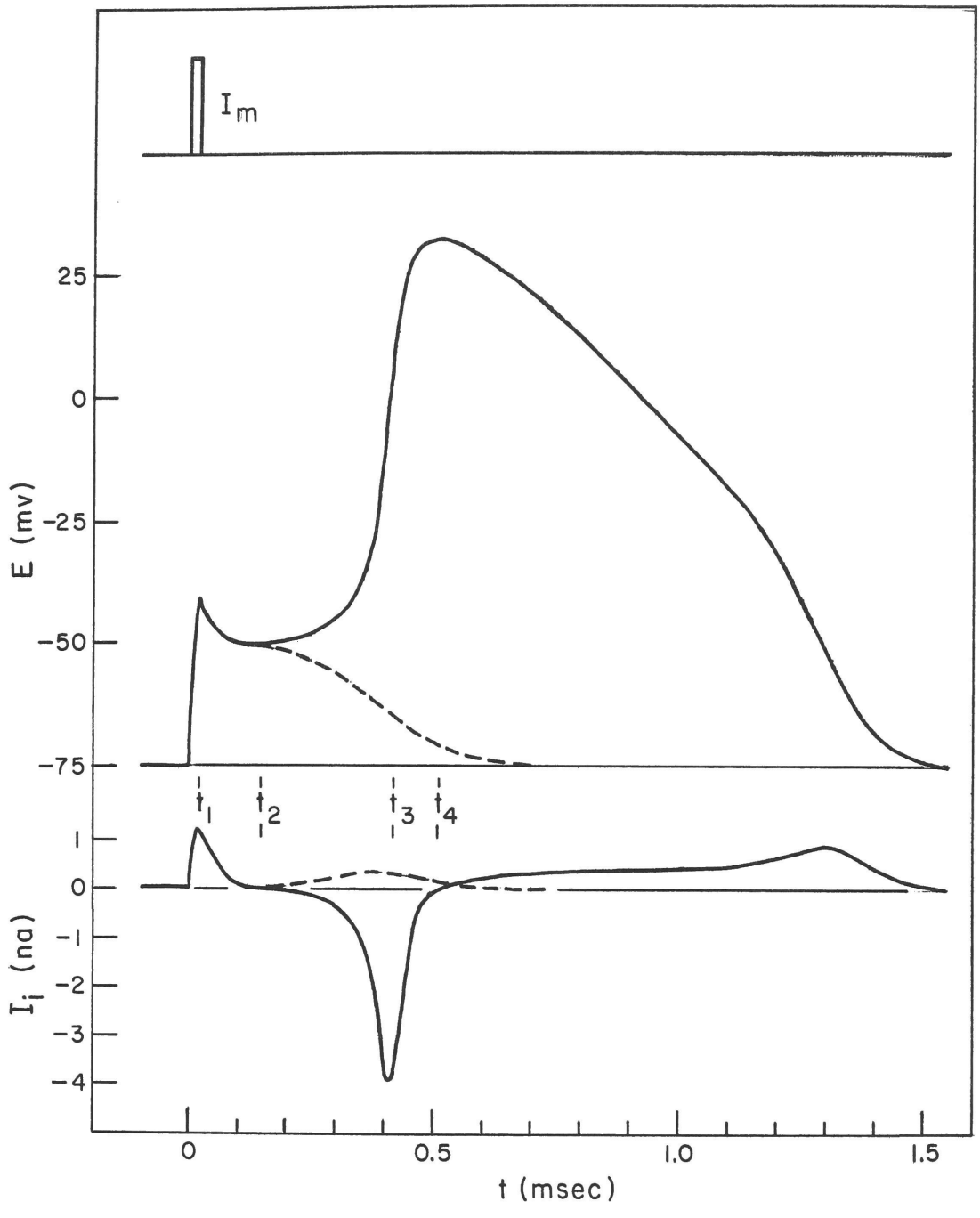


Figure 1.8: Time course of ionic current ($I_i$) during an action potential and during a subthreshold response. $I_i$ was calculated from $I_i = I_m - C\dot{E}$. The membrane current ($I_m$) was held to zero after the short stimulus. This figure is derived from theoretical computations (Chapter IV) with the empirical constants for node 8; cf. Figure 1.4.

the membrane potential is somewhat closer to the resting potential than to the critical value of -50 mv, the ionic current (as observed in the voltage-clamp experiment) remains outward at all times, continuing to charge the membrane capacitance back to the resting potential, and giving only a sub-threshold response. With a slightly larger stimulus one gets the same initial behavior except that when the rate of change of the membrane potential approaches zero, the membrane is slightly more depolarized than in the previous case. If at this time the membrane is more depolarized than -50 mv the ionic current becomes inward charging the membrane capacitance to a slightly more positive potential, that is, depolarizing the membrane further. In turn, the greater depolarization causes a larger inward current, and the depolarization becomes regenerative ( $t_3$ ). This rapid depolarization proceeds until the membrane potential approaches +33 mv, at which value there is no inward current, and the rate of change of the membrane potential goes to zero at the peak of the action potential ($t_4$ ). The subsequent transition to outward ionic current results in the slower repolarization of the membrane to the resting level. Clearly, if the stimulus produces a greater depolarization, the more rapid onset of the phase of inward current (observed at the intermediate levels of depolarization in the voltage-clamp experiment) would result in a very much shorter latency, but would not appreciably effect the amplitude of the action potential. Thus, qualitatively at least, the observed features of the ionic currents of the membrane, especially the characteristic dependence of the phase of inward current on the membrane potential, would appear to account for the threshold and the "all-or-none" nature of the action potential of a node.

This conclusion must be taken as somewhat tentative, however, because the slower time-dependent processes that cause the membrane current to become outward at long times were more or less neglected in the analysis presented in the preceding paragraph. Indeed, it will be possible to test whether the properties of the ionic currents of the nodal membrane are sufficient to account for electrical behavior of the node, only when it is possible

to describe the ionic current as a function of time for any variation of membrane potential. Although it would be possible to describe the system in purely formal terms by a generalized membrane electromotive force and a generalized membrane conductance (both of which would be functions of membrane potential and time!), simpler and physiologically more significant relations are obtained from the analysis of the specific ionic components of the membrane current.

# Chapter II

## IONIC BASIS OF THE MEMBRANE CURRENT

The dependence of the resting potential and action potential of the node on the ionic composition of the external medium has been investigated by Huxley and Stämpfli (1951). Their results strongly suggest that the ionic current of the nodal membrane results from changes of the permeability of the nodal membrane to sodium ions and to potassium ions. Consideration of the facts (1) that the regenerative nature of the action potential is the consequence of a transient phase of inward ionic current and (2) that the amplitude of the action potential varies with external sodium ion concentration as if, at the peak of the spike, the membrane were specifically permeable to sodium ions, tentatively identifies the early transient phase of the ionic current observed in the voltage-clamp experiment as a flux of soium ions. Similarly, the potassium electrode behavior of the node when the membrane is depolarized at high external potassium ion concentrations indicates that that ionic permeability of the depolarized node, in the steady state, is specific for potassium ions. This suggests the tentative identification of the steady-state outward current observed in the voltage-clamp experiment on the node in normal Ringer's solution as a flux of potassium ions.

The results of voltage-clamp experiments designed to test this ionic hypothesis will be described in two parts: the discussion in Part I, concerning the identification of the specific ionic components of the current and the quantitative measurement of the permeability, is based primarily upon previously published work: procedures for resolving the time courses of the specific sodium and potassium components are reported in Part II. The analyses of the experimental observations described in Part I were made with the tacit assumption that the specific permeability changes were reasonably well separated in time, i.e., first that the increase in potassium permeability did not begin until after the increase in sodium permeability had reached its

maximum, and, second, that the transient increase in sodium permeability during a maintained depolarization had declined to zero by the time the outward current approached its steady level. The results reported in Part II completely justify these assumptions, and a brief consideration of two representative examples will help to clarify subsequent discussion of the experimental observations. Figure 2.1 illustrates the resolution of the ionic current into three components: a step of "leakage" current ($I_L$), a transient sodium current ($I_{Na}$), and the delayed increase in potassium current ($I_K$). From these examples it is seen that $I_K$ is delayed beyond the peak of $I_{Na}$, hence, the peak amplitude of $I_{Na}$ is measured as the difference between the peak value of $I_i$ and $I_L$. Furthermore, $I_{Na}$ has declined before $I_K$ reaches its steady-state value ($I_{K\infty}$) hence, $I_{K\infty}$ can be measured as the difference between the steady-state value of $I_i$ and $I_L$. The "leakage" current ($I_L$), which is proportional to the displacement of the membrane potential from the resting potential, is probably carried mostly by potassium ions and represents a finite constant potassium permeability of the membrane to potassium ions.

Part I: Specific Sodium and Potassium Components of the Ionic Current.

The Sodium Current and Its Electrochemical Driving Force

The hypothesis that the early transient phase of the ionic current is a flux of sodium ions dependent upon the electrochemical potential difference for sodium across the membrane predicts that there is a definite value of membrane potential, the sodium equilibrium potential ($E_{Na}$), at which the electric force across the membrane just balances the diffusional force on the sodium ions arising from the difference of concentration on the two sides of the membrane. When these forces are equal in magnitude, the flux of sodium ions goes to zero. This value of membrane potential, $E_{Na}$, is the crossover point for the electrochemical driving force ($E-E_{Na}$) on sodium ions: the sodium current is inward when the membrane potential is more negative than $E_{Na}$, and outward when the membrane potential is more positive than $E_{Na}$.

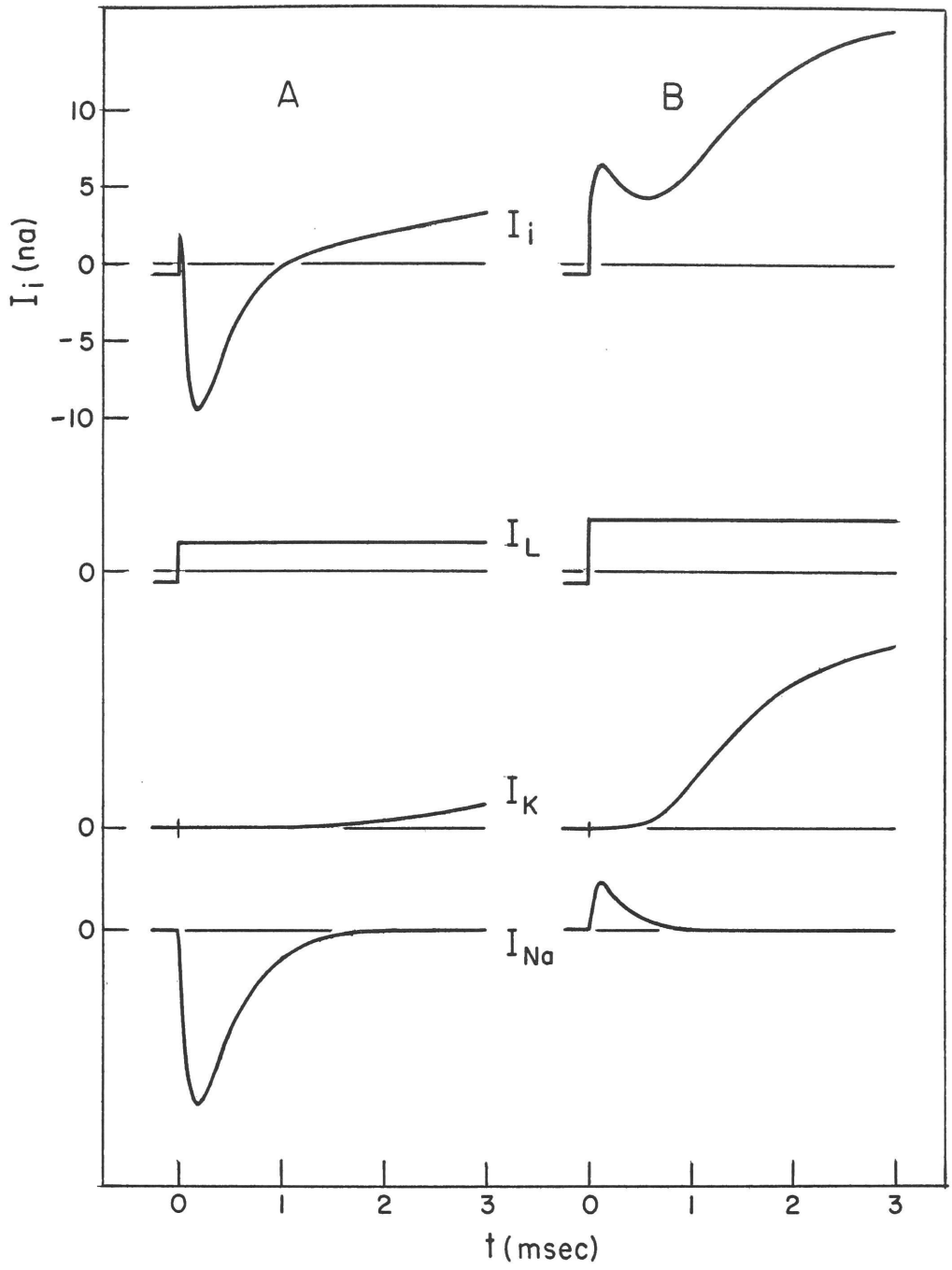


Figure 2.1: Representative examples of the resolution of the ionic current into three components: the step of outward leakage current ($I_L$), the delayed increase in outward potassium current ($I_K$), and the transient phase of sodium current ($I_{Na}$). In A, the membrane was initially hyperpolarized at E = - 105 mv, then at t = 0 depolarized to E = 0 mv. In B, the membrane was initially hyperpolarized at E = - 105 mv, then depolarized to E = 67.5 mv. Note that $I_{Na}$ is inward in A and outward in B. The components of $I_i$ were separated by the procedure described on page 56. The ordinate scale applies to all curves. Node 6; 20°C.

A. Determination of the sodium equilibrium potential

Measurements of the ionic currents at different values of membrane potential (Figure 1.6) clearly showed that the early transient current, which was inward at intermediate levels of depolarization, was outward at large depolarizations. An equilibrium potential for the early transient current may be defined operationally as that value of membrane potential at which this transient current is absent, marking the crossover from an inward flow of the initial ionic current to an outward flow (Hodgkin and Huxley, 1952 a).

The time course of the membrane current at several large depolarizations are shown in Figure 2.2. In this experiment, the test depolarization was preceded by an initial hyperpolarization of long duration, the initial condition that has the effect of increasing the amplitude of the early transient current, but does not otherwise alter the relation between the early transient current and the membrane potential (Dodge and Frankenhaeuser, 1958). Examination of the records for 60 mv and 52.5 mv (neglecting the first 50 μsec of the records during which time the ionic current is obscured by the decay of the capacity current) shows that the early ionic current appears as a definite hump of outward current; whereas, in the records for 37.5 mv and 30 mv it appears as a hump of inward current. For the record at 45 mv, the ionic current is essentially constant for about half of a millisecond. This value of membrane potential at which there is no hump of either inward or outward current is taken as the equilibrium potential for the early transient phase of the ionic current.

The magnitude of the step of outward current during the time that $\dot{I}_i$ is zero in this record is just the leakage current predicted from the resting resistance of the membrane and the amplitude of the membrane potential step. On the basis of this observation, the equilibrium potential is more easily determined graphically by the intersection of the curve of the peak value of the early current versus membrane potential ($I_{peak}$) with the extrapolation of current-voltage relation for the leakage current ($I_L$) as in

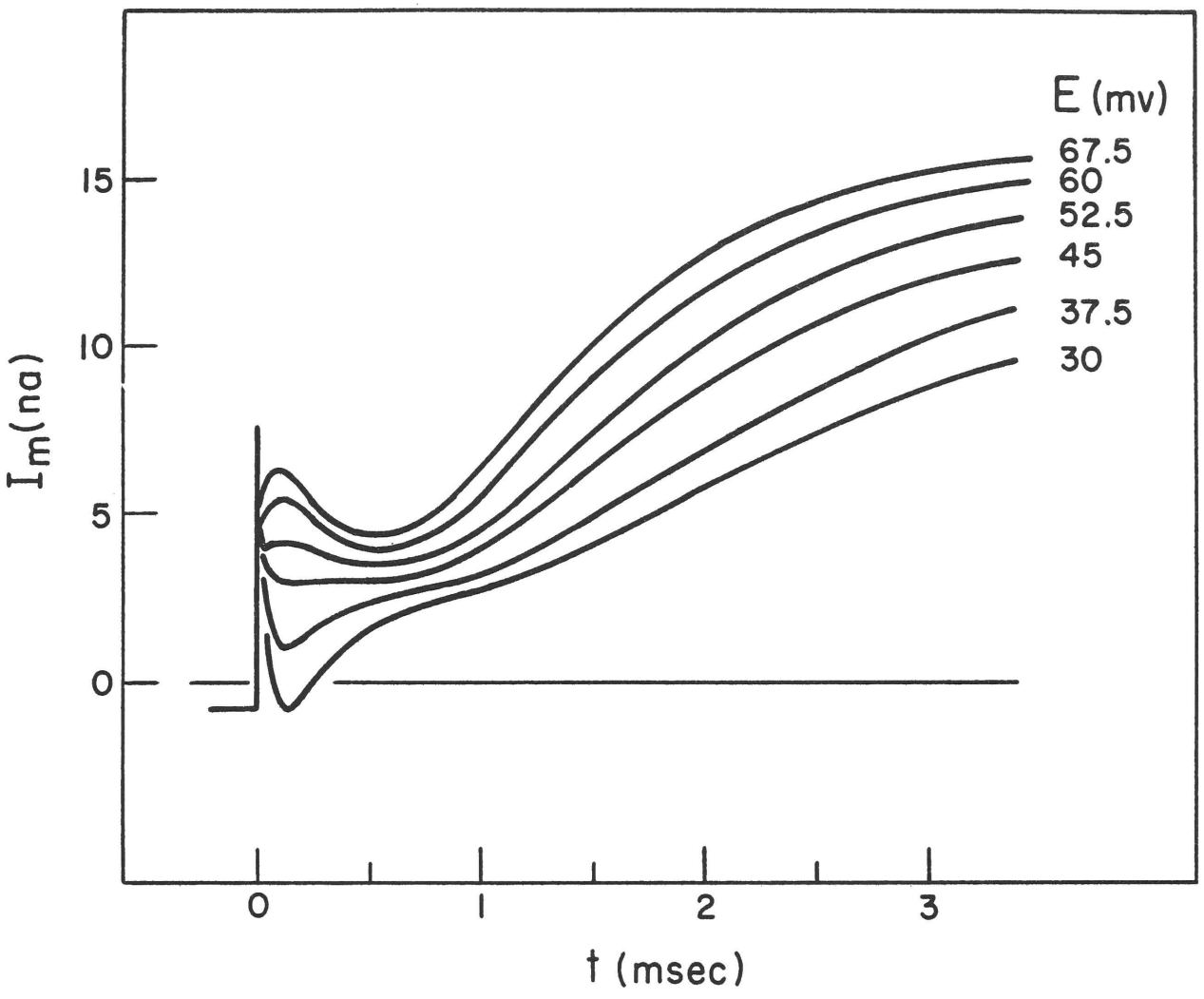


Figure 2.2: Tracings of records of the membrane currents ($I_m$) at several large depolarizations. The membrane was hyperpolarized at E = - 105 mv for 40 msec preceding each test depolarization. The curves are identified by the value of membrane potential (E) during the depolarization. Node 6; 20°C.

Figure 2.3.

Identification of this operationally-defined equilibrium potential as the sodium equilibrium potential requires that it satisfy two conditions defined by the fundamental equation

$$E_{Na} = \frac{RT}{F} \ln \frac{[Na]_o}{[Na]_i} \qquad (2.1)$$

namely: 1) The experimental value of $E_{Na}$ must be consistent with the distribution of sodium ions across the membrane and 2) it must vary in the predictable manner with changes in the external sodium concentration. The latter condition is subject to direct experimental test by voltage-clamp measurements.

B. Dependence of $E_{Na}$ on the external sodium ion concentration

In an experiment in which the external sodium concentration is changed from its normal value $[Na]_o$ to a lower value $[Na]'_o$ by substitution of an impermeant cation, then, with the reasonable assumption that there is no significant change in the internal sodium concentration during the experiment, Equation 2.1 predicts a change in the sodium equilibrium potential to be given by:

$$\Delta E_{Na} = E'_{Na} - E_{Na} = \frac{RT}{F}\left(\ln \frac{[Na]'_o}{[Na]_i} - \ln \frac{[Na]_o}{[Na]_i}\right) = \frac{RT}{F} \ln \frac{[Na]'_o}{[Na]_o} \qquad (2.2)$$

The dependence of the ionic currents of the nodal membrane on the external sodium ion concentration was investigated by Dodge and Frankenhaeser (1959) using myelinated fibers of the African toad, Xenopus laevis. In their experiments, the ionic currents measured on a node in normal Ringer's solution (100% Na) were compared with those measured in a solution in which the sodium concentration was reduced to 1/e of its normal value (37% Na); tonicity was maintained by choline chloride. The result of one experiment is summarized, Figure 2.3, by plots of the peak values of the transient current against membrane potential. Here it is seen that the shift

in the equilibrium potential associated with the early current was about - 24 mv, in good agreement with the theoretical value of -25 mv. In other experiments, the observed change tended to be somewhat less than the theoretical, the mean value of $\Delta E_{Na}$ being -22 ± 1 mv for the experiments in which choline replaced sodium. The small discrepancy was ascribed to known systematic errors. It was therefore concluded that the results of these experiments were fully consistent with the hypothesis that the early transient current is a sodium ion current dependent on the electrochemical potential difference for sodium ions across the membrane.

A few similar experiments, extending the range of variation of the external sodium ion concentration, were done in the course of the present investigation. The results of these experiments are reported in Table 2.1. Here again the observed values of $\Delta E_{Na}$ tended to be about 10% lower than the theoretical values. This discrepancy seems too large to be accounted for by errors in the measurements. In these experiments, attenuation in the membrane potential measuring system was judged to be less than 5%, and errors arising from rebalancing the amplifiers during the experiments would be expected to be random. On the other hand, observations that some ions, notably hydrazinium and ammonium ions, are more or less effective in substituting for sodium in maintaining excitability of frog nerves in sodium-free media (Lorente de Nó, et al, 1957; Cheng, 1962; Lüttgau, 1961) raise the question whether the assumption that the nodal membrane is impermeable to choline ions is completely valid. The effect of a small, but finite permeability to choline on the observed $\Delta E_{Na}$ can be predicted by the relation (Sollner, et al, 1955; Hodgkin, 1958)

$$\Delta E_{Na} = \frac{RT}{F} \ln \frac{[Na]'_o + b[choline]_o}{[Na]_o}$$

where b is a constant, measuring the permeability of the membrane to choline relative to that to sodium. In an experiment in which the sodium concentration is reduced to 10% of normal, the observed $\Delta E_{Na}$ would be 10% less than the theoretical value for an ideal sodium selective membrane

TABLE 2.1

Comparison of the observed and theoretical changes of the sodium equilibrium potential

| NODE | $\frac{[Na]'_o}{[Na]_o}$ | $\Delta E_{Na}$ OBSERVED (mv) | $\Delta E_{Na}$ THEORETICAL (mv) |
|---|---|---|---|
| 1 | 0.37 | - 23 | - 25 |
| 10 | 0.37 | - 24 | - 25 |
| | 0.37 | - 22 | - 25 |
| 13 | 0.10 | - 53 | - 58 |
| 14 | 0.10 | - 52 | - 58 |
| 19 | 0.10 | - 52 | - 58 |

if the permeability of the membrane to choline ions were only 2.5% of that to sodium.

C. The internal sodium concentration and $E_{Na}$

Comparison of the operationally defined equilibrium potential for the early transient current with the theoretical value predicted from the distribution of sodium ions across the membranes requires knowledge of the intracellular sodium concentration at the node. Chemical determination of this quantity is subject to many experimental uncertainties.

The first estimate of the intracellular sodium concentration was made by Fenn, et. al. (1934). They analyzed the sodium, potassium and chloride ion contents of freshly excised sciatic nerves of the frog. To correct for solution in the extracellular spaces they assumed that all the chloride was extracellular. With this assumption they estimated the intracellular concentration of sodium ions to be 37 mM (millimoles per Kg intracellular water) and of potassium ions to be 110 mM.

More recently Shanes and Berman (1955) analyzed the ion contents of nerve remaining after washing the nerve with a sodium-free solution. From their measurements the estimated ion contents are 40 mM sodium and 160 mM potassium. If these values represent the intracellular concentration of sodium at the node, Equation 2.1 predicts an equilibrium potential of only 33 mv. There would thus appear to be a considerable discrepancy between this prediction and the observed values, which are generally about 50 mv.

However, there are several unresolved questions concerning the interpretation of the chemical data. In particular, there is considerable uncertainty concerning the partitioning of the sodium ion content between the various structural components of the nerve in addition to the axoplasm such as connnective tissue, Schwan-cell cytoplasm, and the myelin sheath.

Another question that is yet to be resolved in comparison of the electrical and chemical data concerns the assumption implicit in Equation 2.1 that the ratio of the activity coefficients for the internal and external sodium

ion concentration is in fact unity (Hinke, 1961). Note, however, that this assumption is not necessary in deriving the relation for the change in sodium equilibrium potential. In this case, it is assumed only that the activity coefficient for sodium ions is the same in the normal and in the low sodium solutions.

D. Dependence of $I_{Na}$ on the external sodium concentration

Considering the general properties of membrane systems in which the flux of an ion species is passive, i.e. dependent upon its electrochemical potential difference across the membrane, Hodgkin and Huxley (1952 a) used the very general assumption that "the chance that any ion will cross the membrane in any specified interval of time is independent of the other ions which are present" to derive the following equation predicting the effect of a low sodium solution upon the amplitude of the sodium current:*

$$\frac{I'_{Na}}{I_{Na}} = \frac{([Na]'_o/[Na]_o)\exp\{(E_{Na} - E)F/RT\} - 1}{\exp\{(E_{Na} - E)F/RT\} - 1} \qquad (2.3)$$

Application of Equation 2.3, which has been called the independence principle, to the nerve membrane implicitly assumes that the state of the membrane structure controlling the flux of sodium is the same, at the same membrane potential and time, under the two different experimental conditions.

Equation 2.3 is compared with some available data (Dodge and Frankenhaeuser, 1959) in Figure 2.3 A. The amplitude of the sodium current at each value of membrane potential is measured as the difference between the peak value of the transient current and the step of leakage current

---

*Equation 2.3 can be derived also from specific membrane models, for example, the "constant field" theory of Goldman (1943) and the more general, "fixed-charge" membrane theory of Teorell (1953, Equation 9).

Figure 2.3: Test of the independence principle. Peak values of the early transient current, measured on a node of Xenopus laevis in standard Ringer's solution ($I_{peak}$) and in a low-sodium solution ($I'_{peak}$) in which the sodium concentration was reduced to 37% of the standard value by substitution of choline chloride, are plotted in A; the smooth curve of $I_{peak}$ was drawn by eye through the values measured before (crosses) and after (circles) the low-sodium measurements. The peak values of $I_{Na}$ at different membrane potentials were then estimated as the difference ($I_{peak} - I_L$); the intercept of the curves $I_{peak}$ and $I_L$ operationally defines the value of $E_{Na}$. The peak value of $I_{Na}$ was then used with Equation 2.5 to determine the peak value of the sodium permeability ($P_{Na}$) at the corresponding value of membrane potential. The peak $P_{Na}$ is plotted as the smooth curve in B. The curve of peak $P_{Na}$, together with the appropriate values of $[Na]'_o$ and $E'_{Na}$, were used in Equation 2.5 to predict the peak sodium current ($I'_{Na}$) in the low-sodium solution. The smooth curve $I'_{peak}$ is the predicted $I'_{Na}$ plotted with $I_L$ as the baseline. In effect, this procedure tests the conformity of the observed values of $I_{Na}$ and $I'_{Na}$ with the independence principle (Equation 2.3). This figure is replotted from Figures 5 and 6 of Dodge and Frankenhaeuser (1959). In their work, the ionic currents were normalized to the area of the nodal membrane; hence the units of $I_i$ are ma $cm^{-2}$ and units of $P_{Na}$ are cm $sec^{-1}$; $E_R$ = - 70 mv.

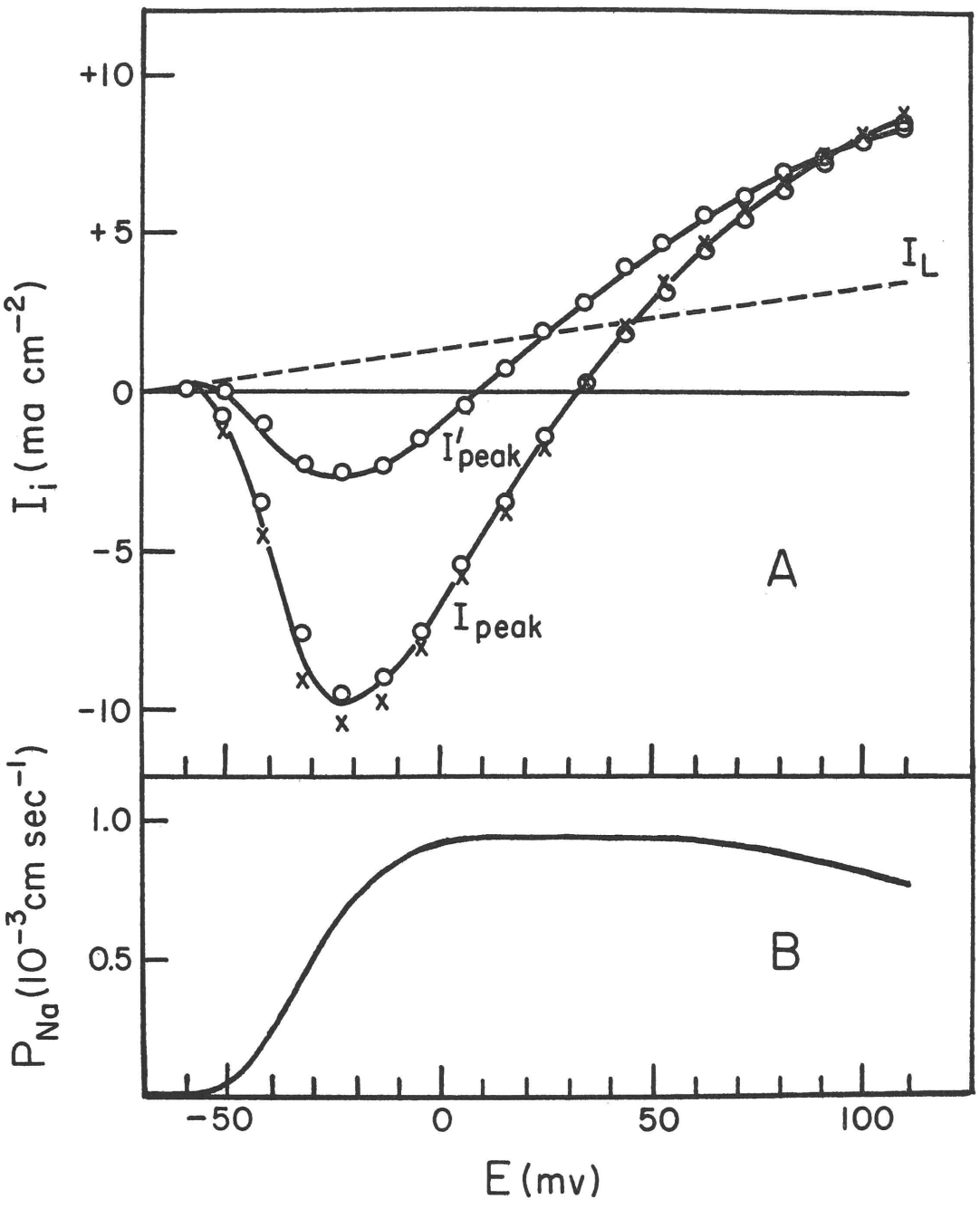
+10
+5
0
-5
-10
$I_i$ (ma cm$^{-2}$)
$I_L$
$I'_{peak}$
$I_{peak}$
A
1.0
0.5
$P_{Na}$ ($10^{-3}$cm sec$^{-1}$)
B
-50
0
50
100
E (mv)

(dotted line). The observed values of $I_{Na}$ measured in the normal solution were used together with Equation 2.3 to predict the smooth curve fitting the peak currents measured in the low-sodium solution. Here we see very close agreement between the experimental and the predicted values, confirming the hypothesis that the transient current is a sodium current.

The results of an experiment done in the course of the present investigation comparing the sodium currents measured in normal and in a 10% sodium solution are shown on Figure 2.4 A. The observed change in $E_{Na}$ was somewhat less than the theoretical value expected from Equation 2.2 which describes an ideal membrane that is selectively permeable to sodium ions. The small discrepancy may be attributed to a finite permeability for choline ions, as discussed previously (p. 34).

Combining Equations 2.1 and 2.3 yields an alternative form of 2.3 in which only the observed electrical quantities, $E'_{Na}$ and $E_{Na}$, are used, namely:

$$\frac{I'_{Na}}{I_{Na}} = \frac{\exp\left\{(E'_{Na} - E)\,F/RT\right\} - 1}{\exp\left\{(E_{Na} - E)\,F/RT\right\} - 1} \qquad (2.3a)$$

As is shown in Appendix III, Equation 2.3a is also applicable in the case that the membrane is not entirely selective against the substitute cation, that is, in the case that the change in $E_{Na}$ does not follow Equation 2.2 exactly. Here again (Figure 2.4 A) there is substantial agreement between the observed values of $I'_{Na}$ and the curve predicted with Equation 2.3a and the observed values of $I_{Na}$.

E. Measurement of the sodium permeability

The experimental evidence cited above is fully consistent with the idea that the early transient current is a flux of sodium ions diffusing through the membrane in accordance with a driving force resulting from the electrochemical potential difference for sodium ions across the membrane. The direction of the flux is determined solely by the driving force, but the

Figure 2.4: Test of independence principle on the frog node. Peak values of the early transient phase of the ionic current, measured in standard Ringer's ($I_{peak}$) and in a solution with 10% standard sodium ($I'_{peak}$), are plotted in A. Peak $P_{Na}$, determined as described in legend of Figure 2.3, is plotted against the corresponding value of membrane potential in B. In this experiment the observed shift of $E_{Na}$ was -52 mv, 6 mv less than the theoretical value of -58 mv predicted from Equation 2.2. According to Equation 2.2, the observed $\Delta E_{Na}$ = -52 mv corresponds to an effective $[Na]'_o$ of 12.5% of the standard $[Na]_o$, rather than 10%. With this effective $[Na]'_o$ and with the observed $E'_{Na}$ and the curve of peak $P_{Na}$ Equation 2.5 was used to predict the peak $I'_{Na}$. The smooth curve of $I'_{peak}$ is the predicted $I'_{Na}$ plotted with $I_L$ as the baseline. In effect, this procedure tests the conformity of the observed $I_{Na}$ and $I'_{Na}$ to the alternative form of the independence principle (Equation 2.3a). Node 13; 20°C.

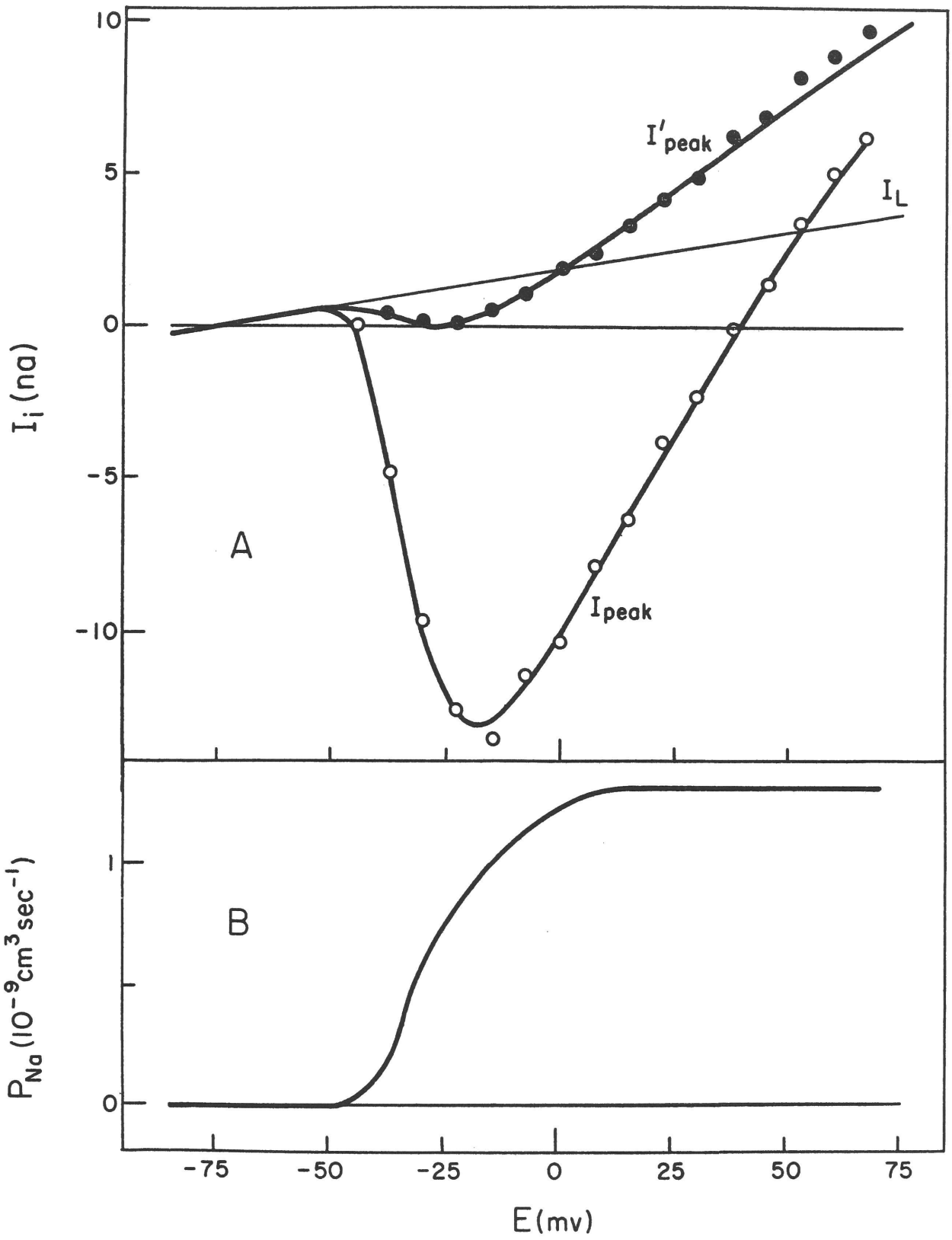
10
5
0
-5
-10
$I_i$ (na)
$I'_{peak}$
$I_L$
$I_{peak}$
A
B
1
0
$P_{Na}$ ($10^{-9}$ $cm^3$ $sec^{-1}$)
-75
-50
-25
0
25
50
75
E(mv)

magnitude of the flux is dependent both on the driving force and on the freedom with which the ions move through the membrane, that is, the permeability of the membrane to sodium ions. Expressed in terms of electrical quantities, the electro-chemical potential for sodium is measured as the departure of the membrane potential from the equilibrium potential, that is, $(E - E_{Na})$. It is then a matter for experimental investigation to determine the exact relation between the flux (current) and driving force in order to define an appropriate quantitative measure of the permeability of the membrane.

The simplest possible relation between current and driving force is direct proportionality, i.e.,

$$I_{Na} = g_{Na}(E - E_{Na}) \qquad (2.4)$$

which equation retains the form of Ohm's law for electrical circuits. A linear relation between $I_{Na}$ and $(E - E_{Na})$ was observed for the squid axon in its normal ionic environment, and the sodium permeability of the normal squid axon was measured in terms of the sodium conductance $(g_{Na})$.

On the basis of experimental observations on the nodal membrane a different equation relating $I_{Na}$ to its driving force has been found applicable. This equation, derived from the "constant-field" membrane theory (Goldman, 1943; Hodgkin and Katz, 1949) is

$$I_{Na} = P_{Na}[Na]_o \frac{F^2 E}{RT} \frac{\exp\{(E - E_{Na})F/RT\} - 1}{\exp\{EF/RT\} - 1} \qquad (2.5)$$

In this equation the specific permeability of the membrane to sodium ions is measured in terms of the permeability coefficient $(P_{Na})$.*

---

* If the membrane current were normalized to the area of the nodal membrane, i.e., if $I_{Na}$ were expressed in terms of the current density in amps $cm^{-2}$, $P_{Na}$ defined by Equation 2.5 would be expressed in terms of the usual units of a permeability coefficient, namely cm $sec^{-1}$. However, because the area of the nodal membrane is not reliably known, the membrane currents are reported here in terms of the total current per node. It is then convenient to include the unknown area factor (which is presumed to be constant during any finition of $P_{Na}$, hence $P_{Na}$ is reported in the units of

Equation 2.5 describes a non-linear relation between $I_{Na}$ and $(E - E_{Na})$ such that, for a fixed state of the membrane structure (constant $P_{Na}$), the sodium current is larger when it flows in the direction from the higher to the lower sodium concentration than it is for the same absolute value of driving force in the opposite direction. This non-linearity, or rectification, is presumed to arise from changes in the concentration profile for sodium within the membrane (Teorell, 1953). In theory, a change in the concentration profile is a time-dependent process; but considering the thinness of the cell membrane, it is reasonable to suppose that the relaxation time for changes in the concentration profile is very short (on the order of a fraction of a μsec) compared to the time resolution in any practical measurement. In other words, when we measure the sodium permeability in terms of $P_{Na}$ we assume that at all times the membrane is in a steady-state with respect to the concentration profile. Experiments designed to measure $g_{Na}$ for the squid axon and $P_{Na}$ for the node will now be described.

1. The squid axon: For the squid axon in sea water, Hodgkin and Huxley (1952b) observed that in response to a step change in membrane potential, the sodium current abruptly changed to a new value proportional to the new value of $(E - E_{Na})$; that is, the sodium conductance $(g_{Na})$ defined by Equation 2.4 had the same value immediately after a sudden change in membrane potential as before. Over the whole range of membrane potentials, this "instantaneous" relation between $I_{Na}$ and $(E - E_{Na})$ was found to be strictly linear.

In low sodium solutions, however, this instantaneous relation was not linear, but showed rectification such that for a fixed condition of the membrane, the measured sodium conductance was smaller when the driving force was inward. This rectification was reasonably well accounted for by applying the "independence principle" (Equation 2.3) to the linear instantaneous current-voltage relation observed when the axon was in sea water. Obviously, whenever a membrane shows such instantaneous rec-

tification, Equation 2.4 loses its usefulness, since $g_{Na}$ is no longer independent of the membrane potential at which it is measured.

2. The nodal membrane: Precise measurements of the instantaneous current-voltage relation of the node were not possible because of an inherent technical limitation on the voltage-clamp system. The type of experimental observation pertaining to the measurement of the instantaneous current-voltage relation is shown in Figure 2.5. Here the sodium permeability was turned on by a depolarizing pulse, then at the peak of the sodium current the reference potential was returned immediately to the resting level. In principle the membrane potential should immediately follow the reference potential, but the limitation on the high-frequency response of the clamping amplifier imposed by the cable properties of the myelinated fiber slowed the stabilization of the membrane potential to a time on the order of 30 μsec (Appendix II). If the membrane potential had stepped back to the resting value, the sodium current would have jumped to a new value because of the instantaneous increase in the driving force $(E - E_{Na})$. As is seen in Figure 2.5, however, the increase in sodium current indeed occurred, but not instantaneously. In response to the repolarization the sodium permeability was rapidly shut off; in fact, the time required to stabilize the membrane potential was not short in comparison with the time constant of the relaxation of the sodium permeability, with the result that there had been a significant change in sodium permeability before the membrane potential had been stabilized to the new value.

However, instantaneous rectification, i.e., non-linearity in the relation between $I_{Na}$ and $(E - E_{Na})$, was revealed by a somewhat indirect experiment (Dodge and Frankenhaeuser, 1959). In this experiment the sodium permeability was turned on by step depolarizations to different values of membrane potential, but at the peak of the sodium-current transient, the membrane was repolarized to the resting potential (as in Figure 2.5). It was observed that the "tail" of inward sodium current resulting from the repolarization was the same for all preceding depolarizations above $E = 0$.

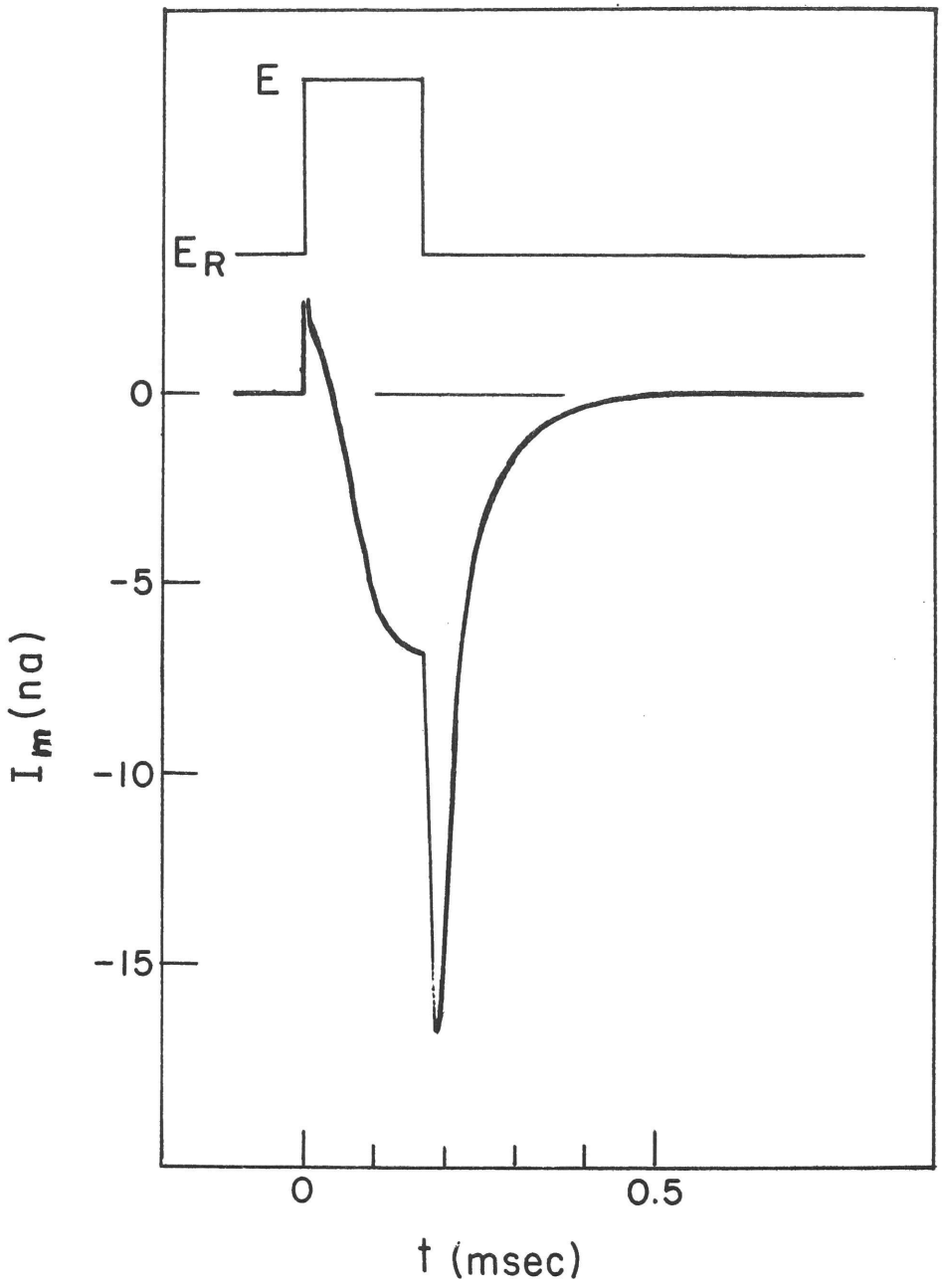


Figure 2.5: Membrane current associated with sudden repolarization of the membrane at the peak of the inward sodium current. At t = 0, the membrane was depolarized to E = 0 mv for 170 μsec, then repolarized to $E_R$ = 0; $E_{Na}$ was 45 mv. Note sudden large increase of inward current in response to repolarization consequent upon the sudden increase of the electrochemical driving force for sodium ($E - E_{Na}$). Subsequently, the "tail" of inward current declines rapidly to zero with a time course that is approximately an exponential decay with a time constant of about 50 μsec. Node 8; 22°C.

This result was taken to indicate that the state of the membrane was the same at corresponding peak sodium currents (in the range of membrane potentials above $E = 0$), hence, the curvature of the plot of peak (sodium) current against membrane potential reflected a non-linear relation between $I_{Na}$ and $(E - E_{Na})$. Consistent with this interpretation it was observed that the curve of peak current against membrane potential in low sodium solutions became linear as $E_{Na}$ approached 0 mv. Application of Equation 2.5, assuming a constant peak value of $P_{Na}$, yielded a good prediction of the degree of curvature observed in the peak current-voltage curve, and accounted for the rectification apparent in the "instantaneous" sodium currents. Thus, the sodium permeability of the nodal membrane as measured by $P_{Na}$ was independent of the instantaneous value of $E$ at which it was measured.

Furthermore, $P_{Na}$ was found to be independent of $[Na]_o$, since the same curve of peak $P_{Na}$ against membrane potential (Figures 2.3B and 2.4B) adequately described the peak $I_{Na}$ observed in both the standard Ringer's solution and in the low sodium solution. In regard to this result, it is easily shown that the independence principle (Equation 2.3) may be obtained directly by forming the ratio of $I'_{Na}$ to $I_{Na}$ using Equation 2.5 and assuming that $P_{Na}$ has the same value under the two experimental conditions.

Because the observations on the relation of $I_{Na}$ to membrane potential in the frog node are in essential agreement with those on Xenopus as described above, the sodium permeability of the frog node will be described in terms of $P_{Na}$ defined by Equation 2.5.

## The Potassium Current and Its Electrochemical Driving Force

During a maintained step depolarization, the early phase of sodium current gives way to an outward current which increases to a steady value. This steady-state current is generally much larger than the expected leakage current, and has been tentatively identified as an enhanced flux of potassium ions, consequent

upon an increase in the permeability of the membrane to potassium ions. This idea has been examined in voltage-clamp experiments in which the electro-chemical driving force for potassium $(E - E_K)$ was changed by changing the external potassium ion concentration.

A. Dependence of $I_K$ on $[K]_o$

Frankenaheuser (1962a) has investigated the dependence of the steady-state current of the node on the external potassium ion concentration. The results of one of his experiments is shown in Figure 2.6. Here the steady-state currents were measured at various membrane potentials in four different external potassium concentrations (NaCl in the standard Ringer's solution was replaced by KCl in various proportions). The amplitude of the steady-state potassium current was measured as the difference between the net current and the step of leakage current appropriate to that membrane potential. The relation between the steady-state value of $I_K$ $(I_{K\infty})$ and membrane potential observed for the standard potassium concentration (curve A) was used to predict $I_{K\infty}$ for the other $[K]_o$ on the basis of the appropriate form of the independence principle, namely,

$$\frac{I'_K}{I_K} = \frac{[K]'_o - [K]_i \exp\{EF/RT\}}{[K]_o - [K]_i \exp\{EF/RT\}} \tag{2.6}$$

where the primed quantities refer to the test solution, and $[K]_i$ is taken to be 120 mM. Implicit in this equation are the assumptions:

1) that the change in the potassium equilibrium potential is given by

$$\Delta E_K = E'_K - E_K = \frac{RT}{F} \ln \frac{[K]'_o}{[K]_o} \tag{2.7}$$

and

2) that the steady-state permeability of the membrane to potassium ions is the same at corresponding values of membrane potential in all cases. The substantial agreement between the observed potassium currents and the

Figure 2.6: Steady-state potassium current measured on a node of Xenopus laevis in several different external potassium concentrations ($[K]_o$); KCl was substituted for NaCl in the standard Ringer's solution, and the resting membrane potential maintained at normal value by the feedback amplifier. $[K]_o$ = 2.5 mM in A, 12.5 mM in B, 62.5 mM in C, and 114.5 mM in D. Zero current baseline displaced 10 ma $cm^{-2}$ for successive curves. The smooth curve (A), describing the steady-state $I_K$ measured in standard $[K]_o$, was used with the appropriate form of the independence principle (Equation 2.6) to predict the smooth curves B, C, and D. This figure is taken from Frankenhaeuser (1962a); the abscissa scale was changed to read absolute membrane potential assuming $E_R$ = - 70 mv. Membrane currents were normalized to area of nodal membrane.

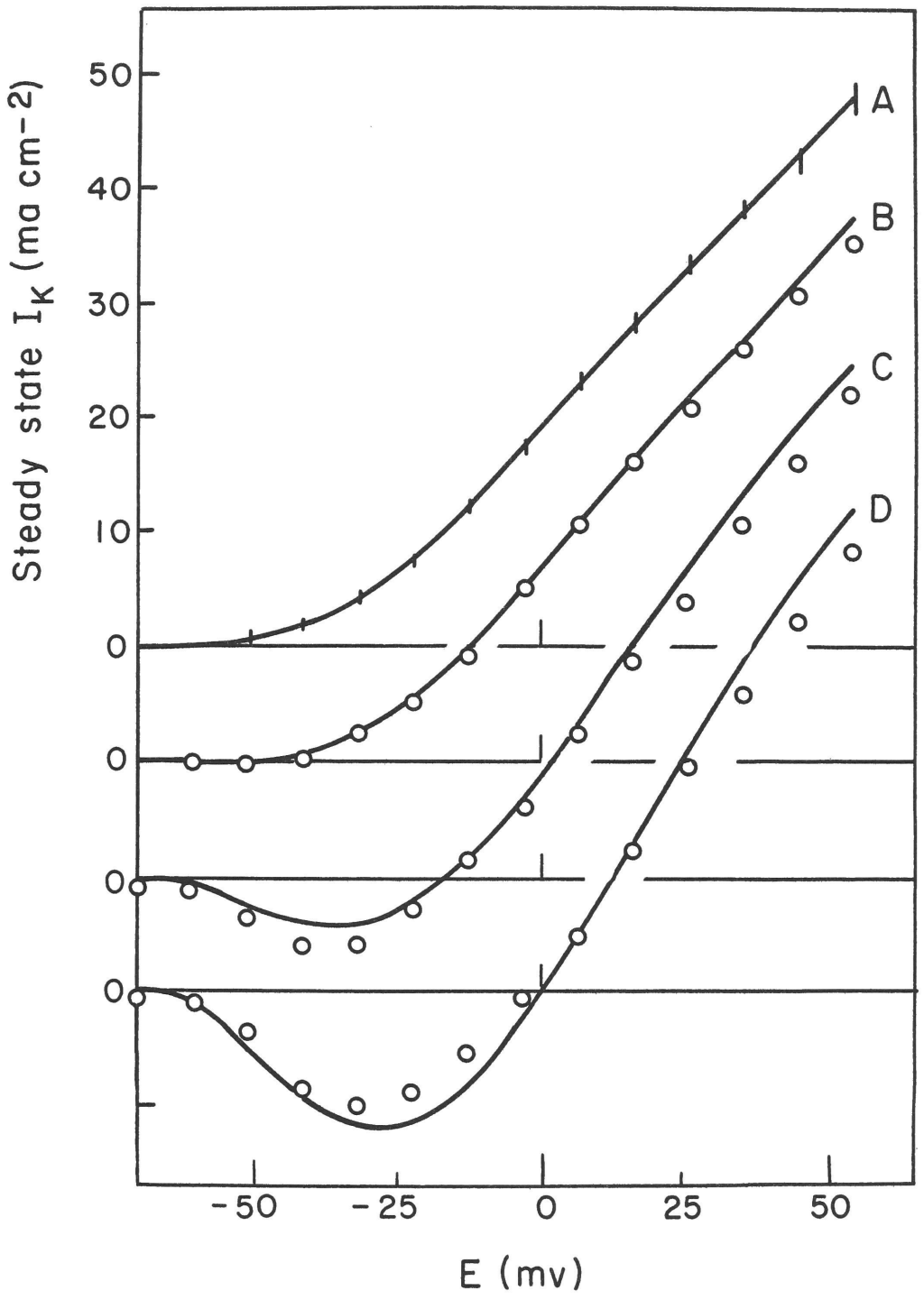
Steady state $I_K$ (ma cm-2)
50
40
30
20
10
0
0
0
0
A
B
C
D
-50
-25
0
25
50
E (mv)

predictions of equation clearly identifies this component of the membrane current with the flux of potassium ions through the membrane in accordance with the electrochemical potential difference for potassium ions across the membrane.

B. Measurement of the potassium permeability

1. The squid axon: For the squid axon in sea water or a low sodium solution containing the normal $[K]_o$, Hodgkin and Huxley (1952b) found that the instantaneous current-voltage relation of the membrane measured during a state of high potassium permeability was strictly linear. The zero current intercept of the instantaneous current-voltage relation (at about 12 mv negative of the resting potential) was taken as the potassium equilibrium potential ($E_K$).* On this basis, the potassium permeability of the membrane was measured in terms of the potassium conductance $g_K$ defined by the relation:

$$I_K = g_K(E - E_K) \tag{2.8}$$

2. The nodal membrane: Frankenhaeuser (1962 b, c) has further investiaged the potassium currents of the nodal membrane in an attempt to define the exact relation between $I_K$ and $(E - E_K)$. For the node in an

*In their experiments, however, the experimental value for $E_K$ was at least 10 mv smaller than the theoretical value predicted from the known values of $[I]_i$ and $[K]_o$, and the observed changes in $E_K$ with $[K]_o$ were smaller than the theoretical predictions. Nonetheless, the steady-state outward current was unambiguously identified as a flux of potassium ions in subsequent experiments (Hodgkin and Huxley, 1953) using radioactive potassium as a tracer. Moreover, the discrepancy in $E_K$ has been more-or-less accounted for by the demonstration of a diffusion barrier outside the membrane (Frankenhaeuser and Hodgkin, 1956) which would have the effect, under the conditions of the voltage-clamp experiments, of maintaining the potassium concentration just outside the membrane at a somewhat higher value than that in the external solution.

isotonic KCl solution the relation between the instantaneous values of $I_K$ and membrane potential was observed to be strictly linear, intersecting the zero current axis at the expected value of $E_K = 0$ mv. Measurements of the instantaneous currents for the node in Ringer's solution, however, were severely complicated by a small slow transient of inward current that was shown to be a sodium current.* The analysis of the records by Frankenhaeuser (1962 c) indicated that the relation of instantaneous $I_K$ and membrane potential for the node in the standard $[K]_o$, Figure 2.7, was non-linear in the manner predicted by applying Equation 2.6 to the linear relation observed in high $[K]_o$. On the basis of this analysis he concluded that the permeability of the nodal membrane to potassium ions is best measured in terms of a permeability coefficient ($P_K$) defined by:

$$I_K = P_K \frac{F^2 E}{RT} \cdot \frac{[K]_o - [K]_i \exp\{EF/RT\}}{1 - \exp\{EF/RT\}} \qquad (2.8)$$

The results of these experiments are summarized by the conclusion that the steady-state potassium permeability of the node, measured as $P_K$, is dependent on the membrane potential, but independent of the external potassium ion concentration.

Observations on the potassium currents of the frog node in the present experiments are in substantial agreement with those of Frankenhaeuser on the nodes of Xenopus nerve. There is, however, one important difference, the frog data strongly suggest that for the frog node in normal Ringer's solution the operationally defined $E_K$ is generally very close to the resting

---

*This unexpected sodium current is kinetically very different from the "tail" of sodium current associated with repolarization of the membrane during the early transient phase of the ionic current. Furthermore, this complication appears to be absent when the duration of the depolarization is only a msec, (see Figure 2.8) suggesting that it arises as a result of some secondary alteration of the membrane associated with large depolarizations of long duration.

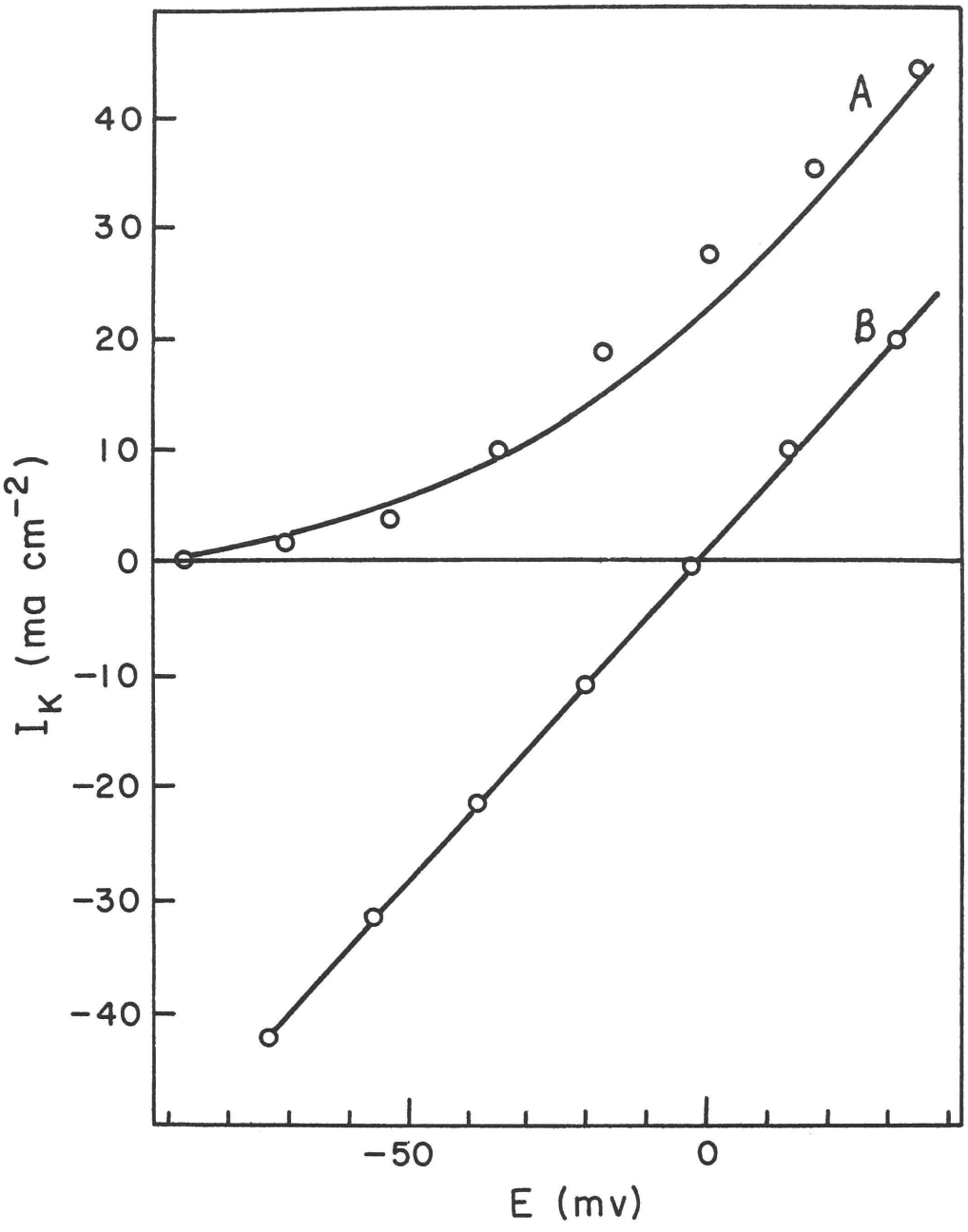


Figure 2.7: Instantaneous potassium currents measured on a node of Xenopus laevis in the standard Ringer's (A; $[K]_o$ = 2.5 mM) and in a high potassium solution (B; $[K]_o$ = 114.5 mM). Membrane currents were normalized to area of nodal membrane. Smooth curve A was calculated from Equation 2.9, assuming $P_K = 1.75 \times 10^{-3}$ cm sec$^{-1}$; straight line B was calculated from Equation 2.9, assuming $P_K = 1.36 \times 10^{-3}$ cm sec$^{-1}$. This figure is derived from Figures 2 and 3 of Frankenhaeuser (1962c) by replotting the data on an absolute potential scale assuming $E_R$ = - 70 mv for A and $E_K$ = 0 mv for B (conforming to Figure 2.6).

potential (E = -75 mv), and in some cases, even less than this value. Furthermore, the observed instantaneous $I_K$ versus E relation does not conform well to that predicted on the basis of a constant $P_K$, but shows a deviation at intermediate depolarizations similar to that observed in Frankenhaeuser's measurements. In view of these difficulties the potassium conductance $g_K$, defined by Equation 2.8, has been adopted as a reasonably good approximation for describing the potassium permeability of the frog node.

C. Approximate description of the potassium permeability

In principle, the potassium equilibrium potential ($E_K$) is determined experimentally by turning on the potassium permeability by a strong depolarization, then repolarizing the membrane to various membrane potentials in the neighborhood of the resting potential. $E_K$ would then be determined by measuring the variation in magnitude and direction of the transition of ionic current as $g_K$ slowly shuts off to its resting value. The records of ionic current obtained in such an experiment on the frog node are rather ambiguous and difficult to interpret; a sample is illustrated in Figure 2.8 A. Upon repolarization, the ionic current shows, first, a small transient phase of inward current that is followed by a very small, slow phase of outward current.

A likely interpretation of this record is that the transient of inward current is the unexpected sodium current described by Frankenhaeuser (1962 b) for the Xenopus node; and that the succeeding very small outward current is the later part of the expected potassium "tail" (extrapolated back by the dotted curve). If this interpretation were correct, $E_K$ would be estimated to be a few mv more negative than the resting potential. The transient phase of inward current appears to be absent following a much shorter pulse, as seen in a record from the same node (Figure 2.8 B); but in this case, $g_K$ has been turned on to only half its steady-state value with the consequent attenuation of the potassium "tail". In both records, the estimated potassium current is not much different from zero upon repolarization of the membrane to the resting level, hence, a value of $E_K$

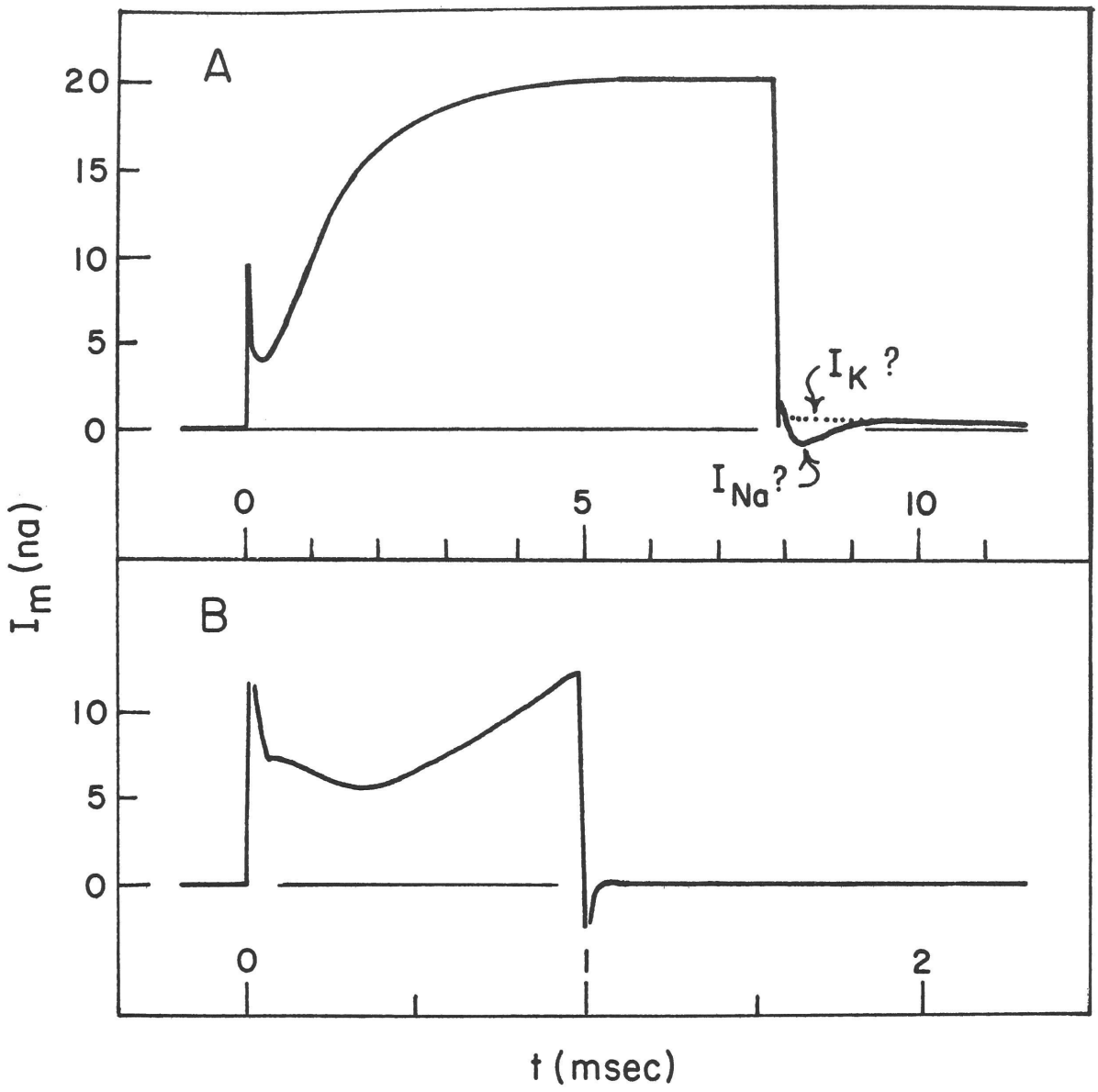


Figure 2.8: Complications apparent in measurements of the instantaneous potassium currents of a frog node in standard Ringer's solution. A: tracing of record of the membrane current associated with a 7.8 msec long depolarization to E = 45 mv. B: tracing of record of the membrane current associated with 1 msec long depolarization to E = 67.5 mv. Subsequent to the repolarization in A, there is observed a slow transient of inward current (probably carried by sodium ions) which gives way to a very small, slowly declining "tail" of outward (probably potassium) current (cf. Figure 3 of Frankenhaeuser, 1962b). This unexpected transient of inward current is not apparent after a shorter depolarization (B). Node 8; 22°C.

equal to -75 mv has been assumed for the approximate description of $I_K$.

In some experiments the experimental value of $E_K$ was less negative than the resting potential (arbitrarily established at -75 mv by the balance of Amplifier 1). This condition was invariably associated with a slowly declining after-depolarization (negative after-potential) following the spike of an action potential, Figure 4.4 D. The observed relation between steady-state potassium currents and membrane potential of such a node is illustrated in Figure 2.9 A together with the instantaneous $I_K$ versus $E$ relation measured when the potassium permeability was turned on maximally. The fit of the latter measurements to the dashed line shows the degree to which the approximate measure of the potassium permeability in terms of $g_K$ conforms to the experimental observations. The relation between the steady-state potassium conductance ($g_{K\infty}$) and membrane potential is shown in Figure 2.9 B.

## The Leakage Current and its Electrochemical Driving Force

When voltage-steps are applied to the node in the direction of hyperpolarizing the membrane, the ionic current is simply a step proportional to the displacement of the membrane potential from its resting value. This current results from the finite ionic permeability of the resting membrane. It has been convenient to assume that this step of leakage current is also a component of the ionic current during depolarizing voltage steps, since the initial ionic current is outward (Dodge and Frankenhaeuser, 1958) and the early current observed at the operationally defined $E_{Na}$ is the appropriate step of leakage current as $E_{Na}$ is changed by varying $[Na]_o$.

Three lines of evidence strongly suggest that the leakage current is carried predominantly by potassium ions. First, that a significant part of this current may be carried by anions seems unlikely from the observations that step of leakage current measured at $E_{Na}$ was unaffected by complete substitution of the external chloride ion by larger, and presumably less permeable, anions, such as isesthionate or methylsulphate (Frankenhaeuser,

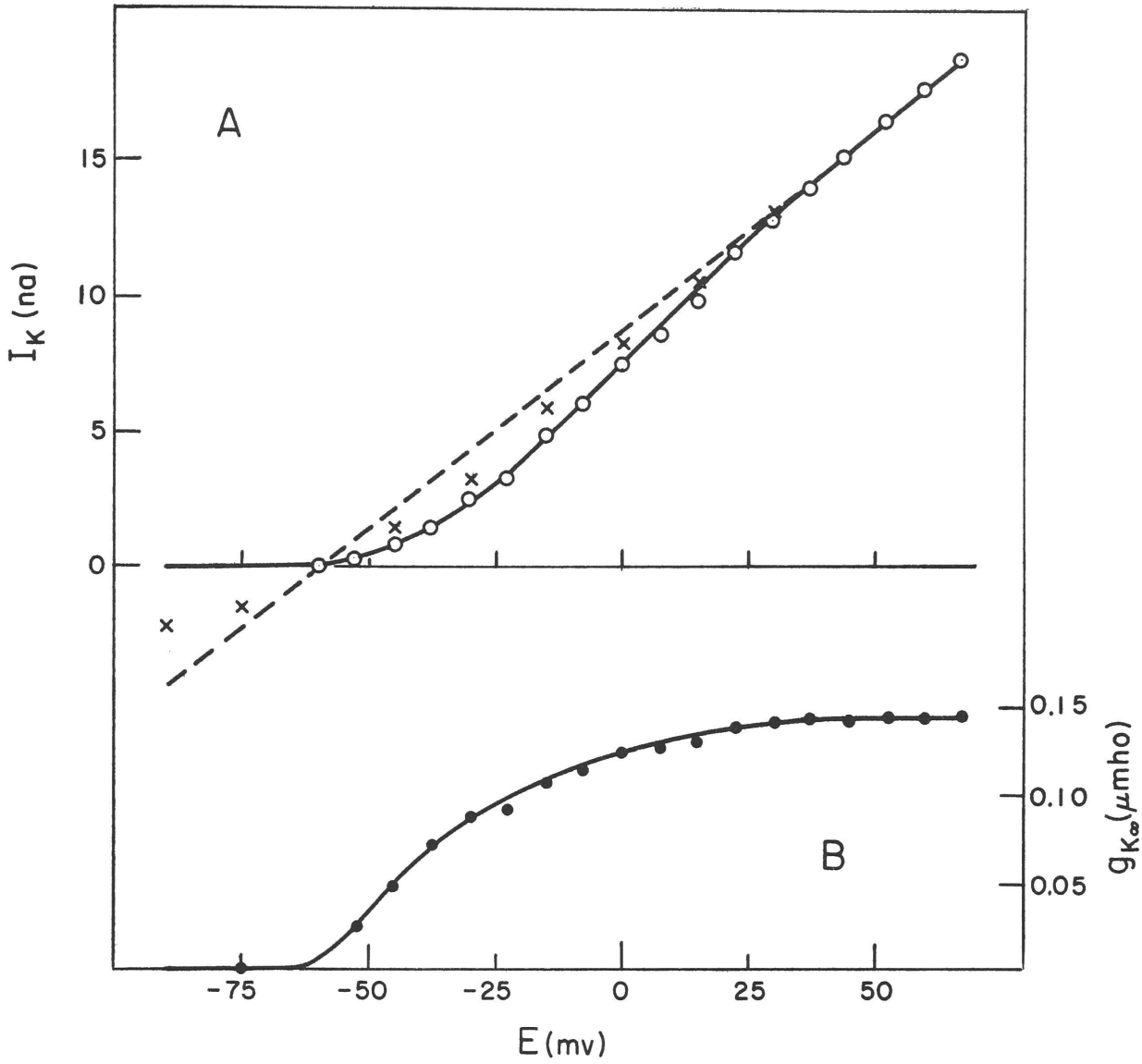


Figure 2.9: A: steady-state and instantaneous potassium currents of a frog node that had a low $E_K$. Steady-state $I_K$ (open circles) measured at 6.7 msec during the depolarization. Instantaneous $I_K$ (crosses) were measured by repolarizing the membrane to different levels following a preceding depolarization to E = 45 mv for 6.7 msec. There is considerable uncertainty in the instantaneous $I_K$ for E < - 25 mv due to the complications illustrated in Figure 2.8A. B: Steady-state potassium conductance ($g_{K\infty}$) determined from the steady-state $I_K$ and Equation 2.8. The relation between the instantaneous $I_K$ and membrane potential, expected from constant $g_K$, is shown as the dashed curve in A. Node 12; 20°C. These measurements were made late in the experiment and some deterioration of the node is apparent if these measurements are compared with those

1962 c). Secondly, chemical analyses of the electrolyte content of nerves have shown that the gain in intracellular sodium resulting from the conduction of action potentials is balanced by an equivalent loss of potassium (Asano and Hurlbut, 1958). But the mathematical synthesis of the nodal action potential (Figure 4.5) shows that the major part of the total outward current during an action potential must be attributed to the leakage current. Thirdly, the apparent equilibrium potential for the leakage current ($E_L$) was found to depend on the external potassium concentration, as shown in the following experiment. The node was bathed in a solution in which 90% of the NaCl in normal Ringer's solution was replaced by KCl, with the result that the resting potential, $E_{Na}$ and $E_K$ were all set at about $E = 0$ mv. A voltage step to $E = -135$ mv was applied for 40 msec in order to shut off the voltage-dependent specific sodium and potassium permeabilities; then the membrane potential was suddenly stepped to new values over the range to $E = +60$ mv. In Figure 2.10 are shown a plot of the ionic currents that were measured immediately after the potential step (filled circles) and corresponded to $I'_L$ in this solution, and a plot of the ionic currents that were measured 10 msec after the potential step (open circles) and corresponded to $I'_\infty$. (In the range of $E > -30$ mv, $I'_\infty$ was predominantly $I'_{K\infty}$ but included the step of $I'_L$.) The leakage current ($I_L$) and steady-state current ($I_\infty$) measured on the same node in the standard Ringer's solution are also shown for comparison. The results in the high $[K]_o$ clearly show that the relation between $I'_L$ and $E$ tended toward a zero current intercept, defining $E'_L$, at $E = 0$, which was the same as that for $I'_\infty$ which defined $E'_K$. This experiment also shows that the leakage conductance was increased by high $[K]_o$ although not nearly as much as would have been expected by applying the independence principle (Equation 2.6). Moreover, the observations on the steady-state current in this experiment essentially agreed with those of Frankenhaeuser cited previously.

Although the foregoing considerations consistently indicate that

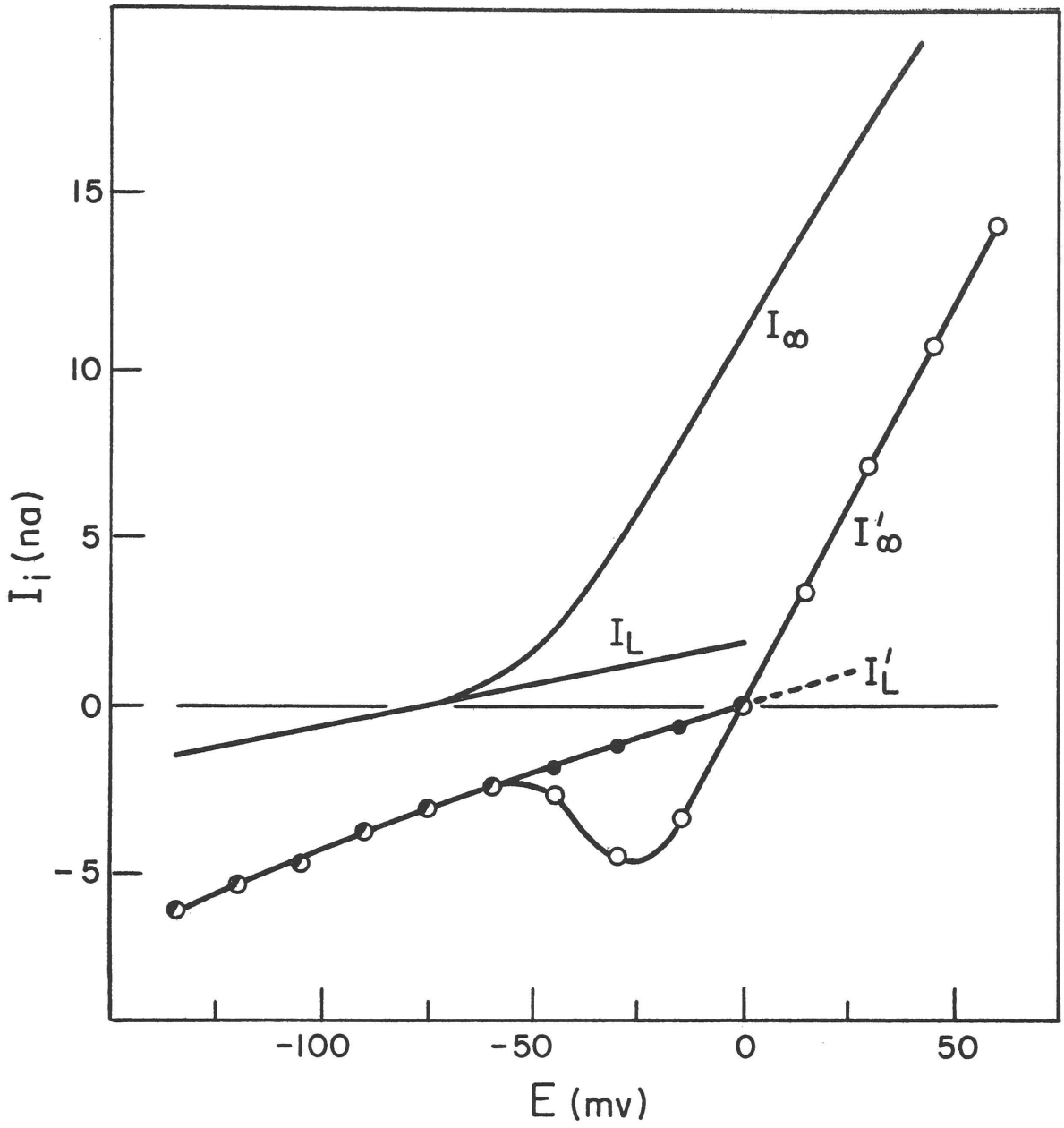


Figure 2.10: Shift of equilibrium potential of the leakage current ($E_L$) in a high potassium solution. Composition of the test solution: 10 mM NaCl, 112.5 mM KCl, 2.5 mM $NaHCO_3$, 2.0 mM $CaCl_2$, pH 7.5. Amplifiers balanced to the steady-state potential which is taken as 0 mv in the high $[K]_o$. A 40 msec long preceding hyperpolarization to E = - 135 mv was applied, then the membrane potential was stepped to a new value (E) and the ionic current measured immediately after the potential step ($I'_L$, filled circles) and 10 msec later ($I'_\infty$, open circles). Note that $I'_L$ and $I'_\infty$ have the same zero current intercept at E = 0 mv. Note further, the inward steady-state $I'_K$ ($I'_K = I'_\infty - I'_L$) in the range of membrane potentials between E = - 50 mv and E = 0 mv. $I_L$ and $I_\infty$ measured in the standard Ringer's solution are shown for comparison. Node 17; 22°C.

the leakage current is mainly potassium, a small but finite permeability of the resting membrane to sodium ions would contribute some sodium current, which would have the effect of making $E_L$ less than $E_K$ for a node in normal Ringer's solution. The expected difference, however, is small, and, at present, below the resolving power of the voltage-clamp technique. The sodium permeability of the resting node can be estimated from other experiments, as discussed in the following section, with the results 1) that the permeability of the resting node to sodium is negligibly small in comparison to increase in sodium permeability during a depolarization, and 2) that the contribution of sodium to the leakage current is also negligibly small.

On the basis of the preceding discussion, the following approximations have been made for the quantative description of the ionic currents of a frog node in its normal ionic environment: 1) $P_{Na}$ at the resting potential is assumed to be zero, and 2) the leakage current is described by

$$I_L = \bar{g}_L (E - E_L) \tag{2.10}$$

where $E_L = E_K$. In all but one of the nodes analyzed, $E_L$ and $E_K$ are assigned the value of -75 mv.* The leakage conductance ($\bar{g}_L$) is constant, i.e., voltage and time independent. Since the membrane currents of the node were calibrated on the assumption that the resistance of the resting node was 40 megohm (Chapter I), $\bar{g}_L$ is assigned the value of 0.025 μmho.

The Resting Potential and the Ionic Permeability of the Resting Membrane

In order to relate the resting potential of nerve to the ionic permeability of the resting membrane, it is generally assumed that the resting

---

* The exception is node No. 12 in which $E_L = E_K = -60$ mv and the resting potential was maintained at -75 mv assuming the imbalance of Amplifier 1 supplied a constant inward current through the node of 0.325 na.

potential is determined solely by the balance of passive ion fluxes, in other words, that there is no electrical signal associated with the operation of the metabolically-coupled mechanism which maintains the normal ion distributions. This assumption seems well justified for the squid axon under a variety of experimental conditions: thus a reasonably consistent set of values for the resting permeabilities were obtained by measuring the membrane potentials in external solutions of various compositions (Hodgkin and Katz, 1949), the electro-neutral operation of the metabolically-coupled ion-transport system was demonstrated (Hodgkin and Keynes 1955, 1956) and the maintenance of the steady-state ion distributions was accounted for (Hodgkin, 1958).

On the other hand, there is considerable experimental evidence that the resting potential of the node is not determined solely by the balance of passive ionic fluxes. Following a period of high-frequency (tetanic) stimulation (Gasser, 1935; Gerard, 1930) or following a long exposure to anoxia or metabolic poisons (Lorente de Nó, 1947), the nerve becomes hyperpolarized*, recovering slowly to the normal resting potential. Tetanic stimulation or interference with metabolism causes a gain in intracellular sodium and loss of potassium (Hurlbut, 1958), and the post-tetanic and post-anoxic hyperpolarization is highly correlated with the functioning of the metabolically-coupled mechanism that extrudes sodium ions and maintains the normal ionic distribution (Connelly, 1959). This mechanism is likely to be operative in maintaining the normal resting potential of the node (Böhm and Straub, 1962).

---

* It is often observed that an action potential evoked during such a hyperpolarization shows a slowly declining phase of depolarization following the spike. This observation is consistent with the idea that under this condition the membrane is hyperpolarized beyond $E_K$ and the after-depolarization results from the slow decline of $g_K$ turned on during the spike.

For want of sufficient information to completely specify the resting state of the node, we will tentatively assume that the resting potential of the node is determined by the balance of passive ion fluxes. On this basis we can estimate the sodium permeability of the resting membrane that is required for the quantitative description of the node. The simplest way to estimate the sodium permeability relative to the potassium permeability is the relation (from Hodgkin 1958)

$$E_R = \frac{RT}{F} \ln \frac{[K]_o + b[Na]_o}{[K]_i + b[Na]_i}$$

where b is the ratio $P_{Na}/P_K$. In order to determine b we can take $[K]_i$ as equivalent to 120 mM (since this concentration of potassium in the external solution makes $E_K = 0$, Stämpfli and Willi, 1957), $[K]_o$ is taken as 2.5 mM which is the potassium concentration of standard Ringer's solution, $[Na]_o$ is 115 mM and the term $b[Na]_i$ is negligibly small. With $E_R = -75$ mv, then $b = 0.03$, which would justify neglecting the contribution of the resting sodium permeability to the leakage conductance. Furthermore, this equation would tend to overestimate b, since the electrical measurments consistently suggest that $E_K$ in normal Ringer's solution is somewhat lower than that predicted from $[K]_o/[K]_i$.

There remains the further question of how large is the resting $P_{Na}$ compared to the maximum $P_{Na}$ turned on by a depolarization. The correct estimate of the resting $P_{Na}$ using the electrical measurements is critically dependent on the normal $E_K$, which is not accurately known from the voltage-clamp measurements. However, the membrane potential measurements of Huxley and Stämpfli (1951) can be used to estimate $E_K$. In their experiments they observed that complete substitution of the external sodium by choline resulted in hyperpolarization of the membrane to $E = -79$ mv (the normal resting potential $E_R = -71$ mv). With this complete removal of $[Na]_o$ we might assume that this membrane potential represents the normal $E_K$. Assuming that this value is applicable

to the present experiments in which $E_R$ = -75 mv would require that there be a passive leakage current of 4 mv/40 megohm = 1 x $10^{-10}$ amps. This leakage current would presumably be balanced by an inward $I_{Na}$ of the same magnitude. Using this value of current in Equation 2.5 shows that the resting $P_{Na}$ is less than 1/400th the maximum $P_{Na}$ turned on during a depolarization.

A check on the validity of these estimates of the resting sodium permeability is obtained on an entirely different basis that is independent of the assumptions concerning the resting potential and $E_K$. The influx of sodium in the resting nerve has been determined, using radio-active tracers (Shanes, 1957) and independently, by the initial rate of change of total sodium content during inhibition of the cellular metabolism (Hurlbut, 1958) to be about 20 μ moles of Na/gram dry weight per hour. If we then assume 1) that this sodium influx which was measured for all the nerve fibers is also representative of the influx in the large myelinated fibers, 2) that 1.0 gram dry weight of nerve is equivalent to 1.1 grams of fiber water, and 3) that the influx at each node is distributed to a volume of fiber water equal to the volume of an internode (10 μ inside diameter x 2 mm long is taken as representative of the fibers used in these experiments), then the resting flux for a node is calculated as

$$\frac{20\ \mu\ \text{moles Na}}{\text{gm dry x hr}} \cdot \frac{1\ \text{hr}}{3600\ \text{sec}} \cdot \frac{0.9\ \text{gm dry}}{\text{gm water}} \cdot \frac{1.6 \times 10^{-7}\ \text{gm water}}{\text{node}} =$$

$$= 7 \times 10^{-16}\ \text{moles Na/sec per node.}$$

Because the resting potential is at least 100 mv less than $E_{Na}$, the passive efflux of sodium is negligible (Ussing, 1949), and this influx can be considered a sodium current of 7 x $10^{-11}$ amps. Applying Equation 2.5 to this current shows that the resting sodium permeability is less than 1/500 of the maximum sodium permeability observed in a voltage-clamp experiment.

Part II. Separation of the Sodium and the Potassium Components of the Ionic Current

On the basis of a few simple assumptions Hodgkin and Huxley (1952 b) were able to achieve virtually complete resolution of the ionic current of the squid axon into a component carried by sodium ions and another carried by potassium ions. Comparing the ionic currents measured at the same membrane potential in sea water and in a low sodium solution, they assumed:

1) the time course of the potassium current was the same in both cases,

2) the time course of the sodium current was similar in the two cases, the amplitude and sometimes the direction being changed, but not the time scale or the form of the time course,

3) $\dot{I}_K = 0$ for a period about one-third of that taken by $I_{Na}$ to reach a maximum.

Assumption (1) was based on the observation that low sodium solutions had very little effect on the time course of the outward current at long times; assumption (2) was the simplest that could be made concerning this component of the ionic current; and assumption (3) was derived from observations of the early current near the sodium equilibrium potential and was used to estimate the relative amplitude of the sodium current in the two cases. Application of these assumptions to the experimental observations yielded a reasonably consistent separation of $I_{Na}$ and $I_K$. At all depolarizations, the $I_{Na}$ followed a characteristic time course, a relatively rapid S-shaped rise to a maximum, followed by a slow decline with an approximately exponential time course. Similarly, at all depolarizations $I_K$ increased to its steady-state value with a typical S-shaped time course. At large depolarizations, there was some slight ambiguity in the separation of $I_{Na}$ because assumption (1) was not completely valid: the steady-state outward currents in the low sodium solution tended to be somewhat smaller than those in sea water.

Direct application of these assumptions to the observations on the node, Figure 2.11 A, would not yield a reasonable separation of $I_K$ and $I_{Na}$, because over the whole range of depolarizations the amplitude of the outward currents at long times measured in low sodium solutions are only 75 to 85 percent of those observed in the standard Ringer's solution (Dodge and Frankenhaeuser, 1959). This reduction of the steady-state potassium current does not appear to be specific for low sodium solutions containing choline ions since a similar effect was observed when sucrose was used to partially replace sodium chloride (unpublished observations by Dodge and Frankenhaeuser). Nor is this effect simply related to reduction of the sodium ion concentration. The experimental evidence indicates that this effect cannot be explained on the basis of a change in the concentration of the permeant ions, but suggests that the effect is a depression of the maximum potassium permeability.

If it is assumed that the low sodium solution affects only the amplitude of the potassium current but not the form of its time course, the components of the ionic current of the nodal membrane can be resolved by a procedure similar to that employed by Hodgkin and Huxley. Comparing the ionic currents measured at the same value of membrane potential in normal Ringer's solution and in a low sodium solution, it is assumed that:

1) in both cases, the leakage current is a step of current proportional to the displacement of the membrane potential from its resting value,

2) the transitions of the potassium currents are similar in form and time scale in the two cases, but the amplitudes are different,

3) the transient changes of the sodium currents are similar in form and time scale in the two cases, but the amplitudes and sometimes the direction are different,

4) for the initial conditions employed in these experiments, $I_K \doteq 0$ until after the peak of the transient sodium current.

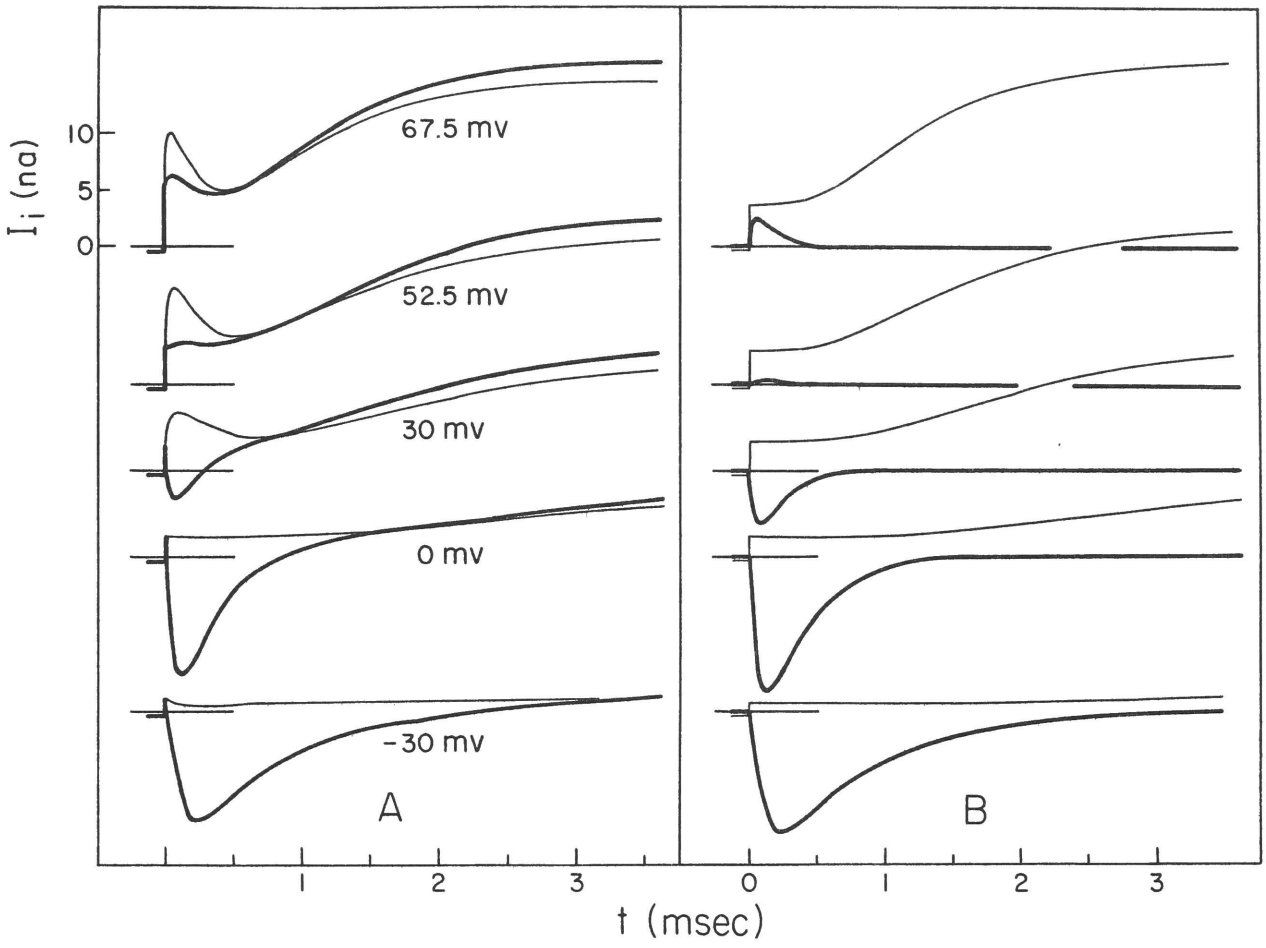


Figure 2.11: Sodium and potassium components of the ionic current resolved by comparing measurements in a standard Ringer's solution and in a low-sodium solution. A: Tracings of the pairs of records at the same membrane potential in Ringer's solution (heavy curves) and in 10% sodium solution (light curves). The membrane was hyperpolarized at E = - 90 mv for 40 msec preceding the depolarization. B: Time courses of the sodium component ($I_{Na}$, heavy curves) and potassium component ($I_K + I_L$, light curves) of the ionic current measured in Ringer's. The components were resolved by the procedure described on page 53. Node 13; 20°C.

In order to apply these assumptions to the experimental data, an interpolation formula for estimating $I_K$ was derived as follows: the components of the ionic currents measured in the two cases are denoted

$$\text{normal:} \quad I_i = I_{Na} + I_K + I_L$$
$$\text{low sodium:} \quad I'_i = I'_{Na} + I'_K + I'_L$$

subtracting the step of leakage current (assumption 1) for each case yields the derived curves

$$I_\delta = I_i - I_L = I_{Na} + I_K$$
$$I'_\delta = I'_i - I'_L = I'_{Na} + I'_K \ ;$$

but

$$\frac{I'_K}{I_K} = \xi \quad \text{(assumption 2)},$$

and

$$\frac{I'_{Na}}{I_{Na}} = \eta \quad \text{(assumption 3)};$$

hence, $I'_\delta = \eta I_{Na} + \xi I_K$ ; combining this with the relation for $I_\delta$ and simplifying yields

$$I_K = \frac{\eta}{\eta - \xi} I_\delta - \frac{1}{\eta - \xi} I'_\delta \ . \qquad (2.11)$$

The components of the ionic current were separated by the following procedure, illustrated in Figure 2.12.

(1) For each value of membrane potential the record of the membrane current measured in normal Ringer's solution and the corresponding record for the low sodium solution were traced on a common baseline, subtracting the appropriate step of leakage current (usually $I_L$ and $I'_L$ were the same; however, the limits of resolution of the measurements were such that a difference of 10% might not have been detected), yielding, respectively,

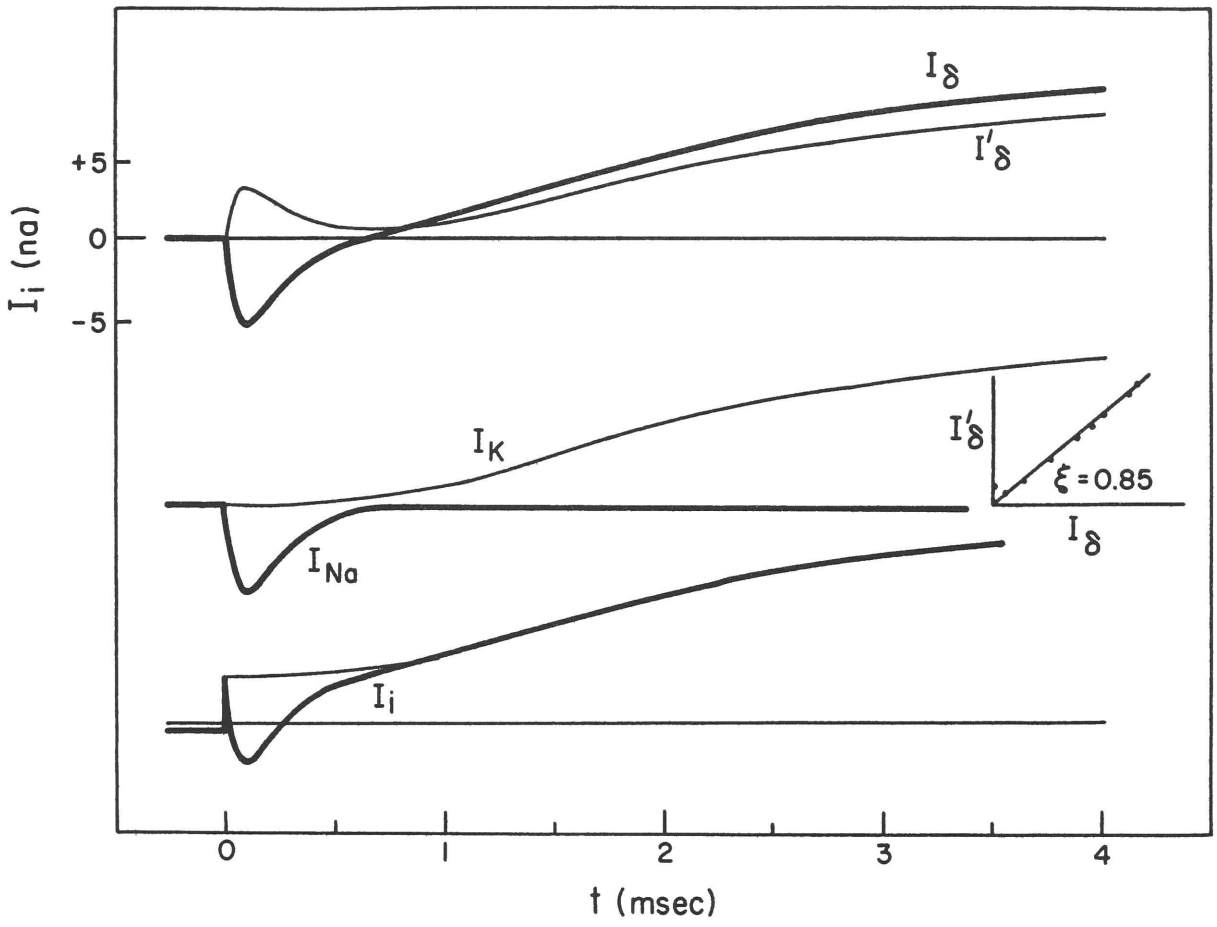


Figure 2.12: Details of the procedure of separating the components of the ionic current using low-sodium measurements. Data from the pair of records at E = 30 mv in Figure 2.11 A. Upper curves are plots of $I_\delta = I_i - I_L$ (Ringer's solution) and $I'_\delta = I'_i - I'_L$ (low-sodium solution). Inset at right: plot of $I'_\delta$ against $I_\delta$ to obtain proportionality constant $\xi$. Middle curves: plots of $I_K$ obtained by application of the interpolation formula (Equation 2.11) and of $I_{Na} = I_\delta - I_K$. Lower curve is a plot of $I_i = I_{Na} + I_K + I_L$.

the curves $I_\delta$ and $I'_\delta$.

(2) $I'_\delta$ was then plotted against $I_\delta$ for positive values of $I_\delta$. For large values of $I_\delta$ (corresponding to longer times) these points fell on a straight line through the origin from which the proportionality constant ($\xi$) was obtained as the slope of this line. The degree to which these points fall on a line serves as a check on the validity of the assumption 2.

(3) The proportionality constant ($\eta$) was obtained as the ratio of the peak values of the early transients of $I'_\delta$ and $I_\delta$ with assumption 3.

(4) Equation 2.10 was then applied to numerical values for $I_\delta$ and $I'_\delta$ determined at various times. The estimated values of $I_K$ were then plotted on the original curves, and fit by a smooth curve.

(5) $I_{Na}$ was estimated as $I_\delta - I_K$.

The results obtained by this procedure are illustrated in Figure 2.11 B. Here it is seen that the transient $I_{Na}$ is entirely inward at membrane potentials less than $E_{Na}$ and entirely outward at membrane potentials greater than $E_{Na}$, the form of the time course of $I_{Na}$ at all depolarizations is typically a relatively rapid rise to a maximum followed by a slower exponential decay. But the time scale and amplitude vary greatly. For all depolarizations $I_K$ is entirely outward, and its time course is typically a delayed S-shaped rise toward a steady level.

These results clearly show that the components of the ionic current of the nodal membrane can be resolved by operational procedures similar to those employed by Hodgkin and Huxley in their analysis of the squid axon. Frequent solution changes, required for the low sodium measurements, tended to accelerate deterioration of the node. The results of several low-sodium experiments, however, justified an alternative procedure for separating $I_K$ and $I_{Na}$, based on the similarity in the form of the time course of $I_K$, at all depolarizations. This procedure was suggested by the mathematical model developed by Hodgkin and Huxley (1952 d) to

describe the ionic current of the squid axon. For the initial condition of a preceding hyperpolarization their equations predict that $I_K$ for all depolarizations is described by a curve of the form

$$I_K = A(1 - \exp\{- t/\tau\})^4$$

in which the amplitude factor (A) and the time constant ($\tau$) depend on the membrane potential.

If $I_K$ in the node followed a similar kinetic equation, it should be possible to estimate $I_K$ at any membrane potential using the time course measured at $E_{Na}$. Figure 2.13 shows how the experimental values of $I_K$ (circles) measured at different membrane potentials are fit by curves obtained by an appropriate linear scaling of the record at $E_{Na}$. These results demonstrate that the time course of $I_K$ is similar in form, but different in time scale and amplitude, at different membrane potentials.

This result justifies the following procedure for estimating $I_K$. In this procedure (illustrated in Figure 2.14):

(1) curves of $I_\delta$ (= $I_i - I_L$) were plotted on log-log paper,

(2) the log-log curve of $I_\delta$ at $E_{Na}$, together with the coordinate axes, was traced to give a master curve,

(3) the log-log plot for another membrane potential was then superimposed on the master curve, maintaining parallel alignment of the coordinate axes, to give the best fit to $I_\delta$ at long times,

(4) $I_K$ at this membrane potential was estimated at shorter times by extrapolation along the master curve, and $I_{Na}$ was estimated as $I_\delta - I_K$.

The results obtained using this procedure (Figure 2.15) are entirely consistent with those obtained previously using measurements in low sodium solutions. This method of separating the components of the ionic current was routinely employed in the subsequent experiments for the determination of the kinetics of the permeability changes. At constant membrane potential

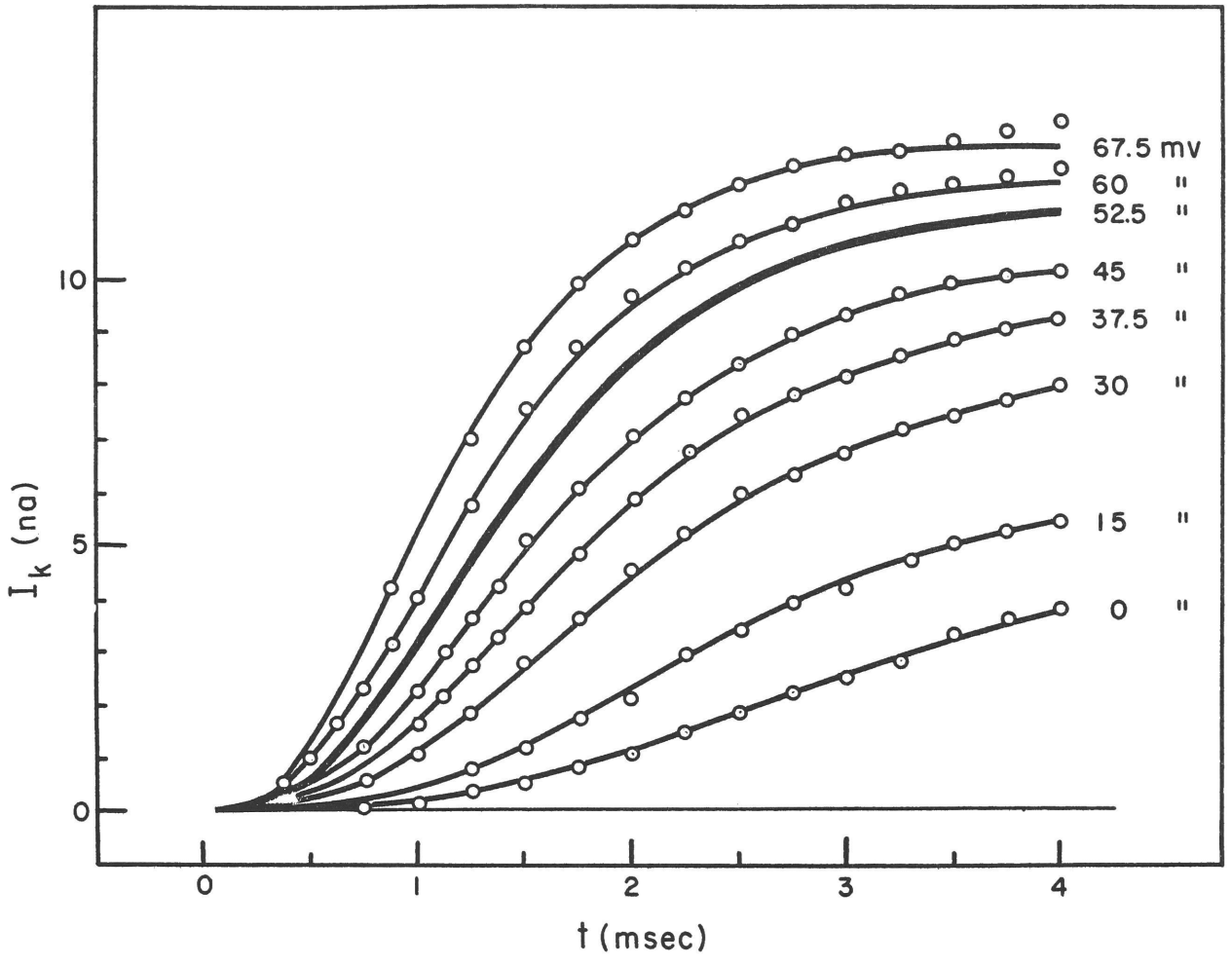


Figure 2.13: Comparison of time courses of the potassium current ($I_K$) at several different membrane potentials, estimated by separating the components of the ionic current by the low-sodium procedure (circles), with the smooth curve obtained by appropriate linear scaling (both amplitude and time) of $I_K$ measured at $E = E_{Na}$ (heavy curve). Data from the experiment illustrated in Figure 2.11.

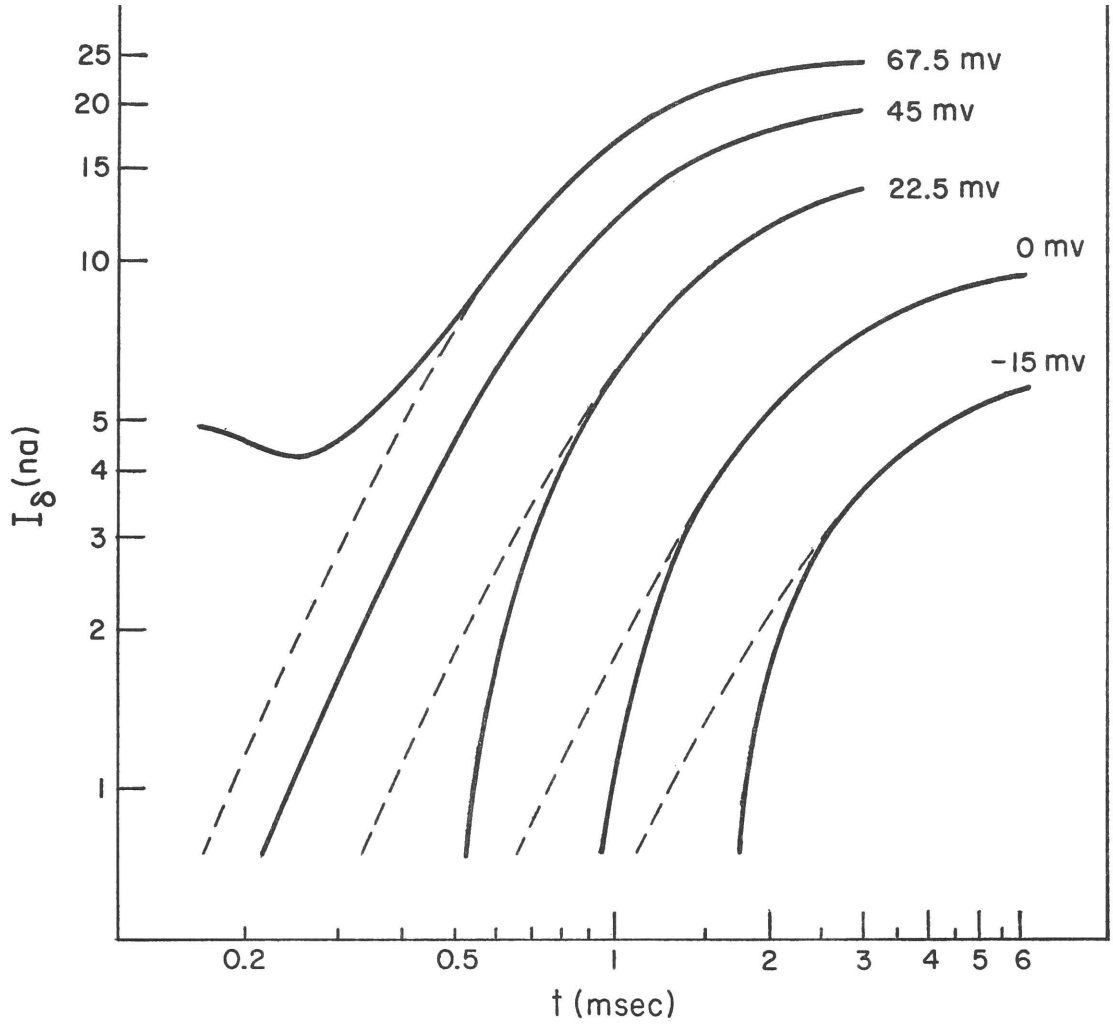


Figure 2.14: Details of procedure for estimating $I_K$ by linear scaling of the curve of $I_K$ measured at $E = E_{Na}$. The solid curves are log-log plots of the time courses of $I_\delta = I_i - I_L$ at several different values of membrane potential. The curve of $I_\delta$ at $E_{Na}$ = 45 mv is taken as the master curve. The other curves are superimposed on the master curve so as to give the best fit at long times. The extrapolation along the master curve at short times (dashed curves) is then taken as the estimate of the time course of $I_K$ at that value of membrane potential. Data of Figure 2.15 and other records at lower sweep speed.

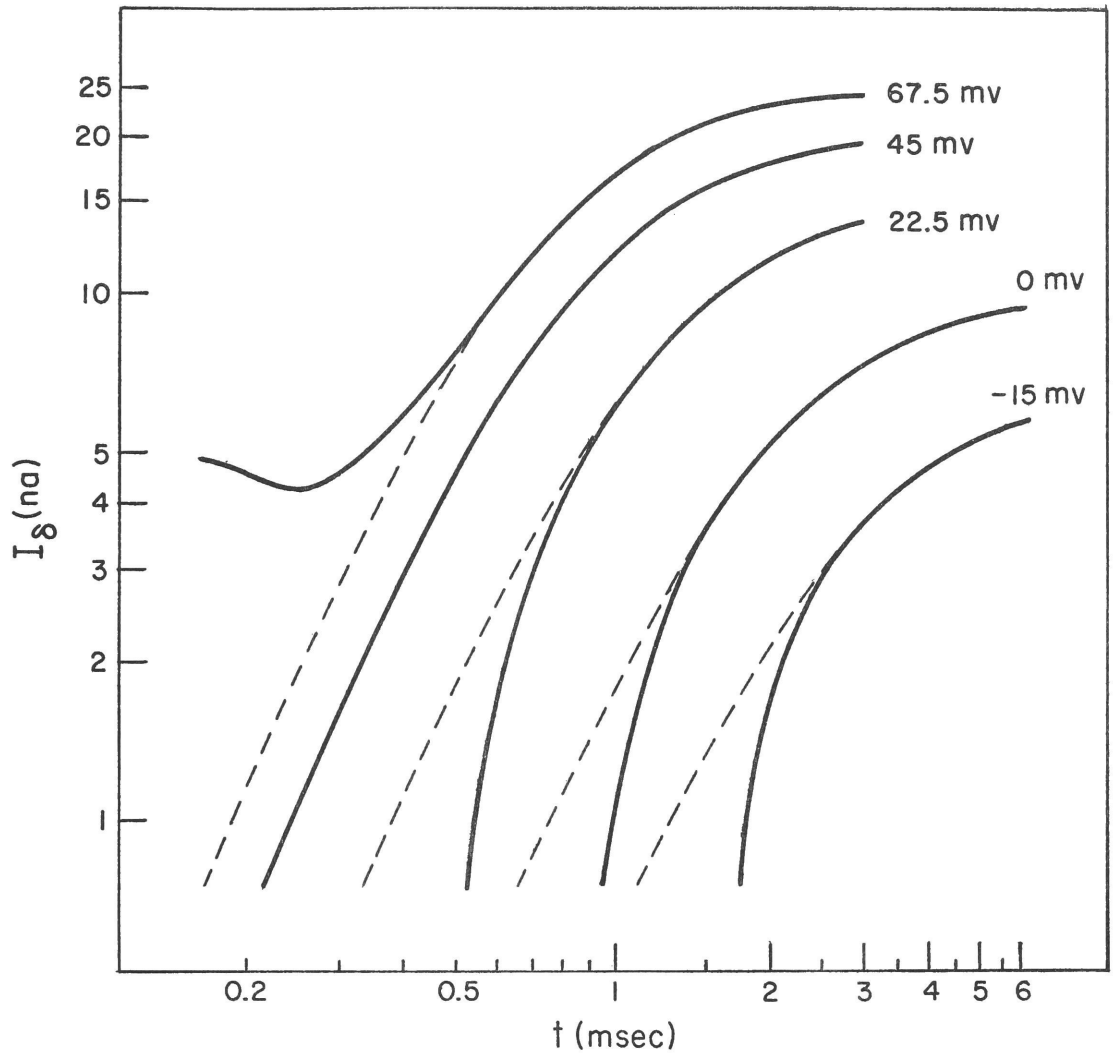


Figure 2.14: Details of procedure for estimating $I_K$ by linear scaling of the curve of $I_K$ measured at $E = E_{Na}$. The solid curves are log-log plots of the time courses of $I_\delta = I_i - I_L$ at several different values of membrane potential. The curve of $I_\delta$ at $E_{Na}$ = 45 mv is taken as the master curve. The other curves are superimposed on the master curve so as to give the best fit at long times. The extrapolation along the master curve at short times (dashed curves) is then taken as the estimate of the time course of $I_K$ at that value of membrane potential. Data of Figure 2.15 and other records at lower sweep speed.

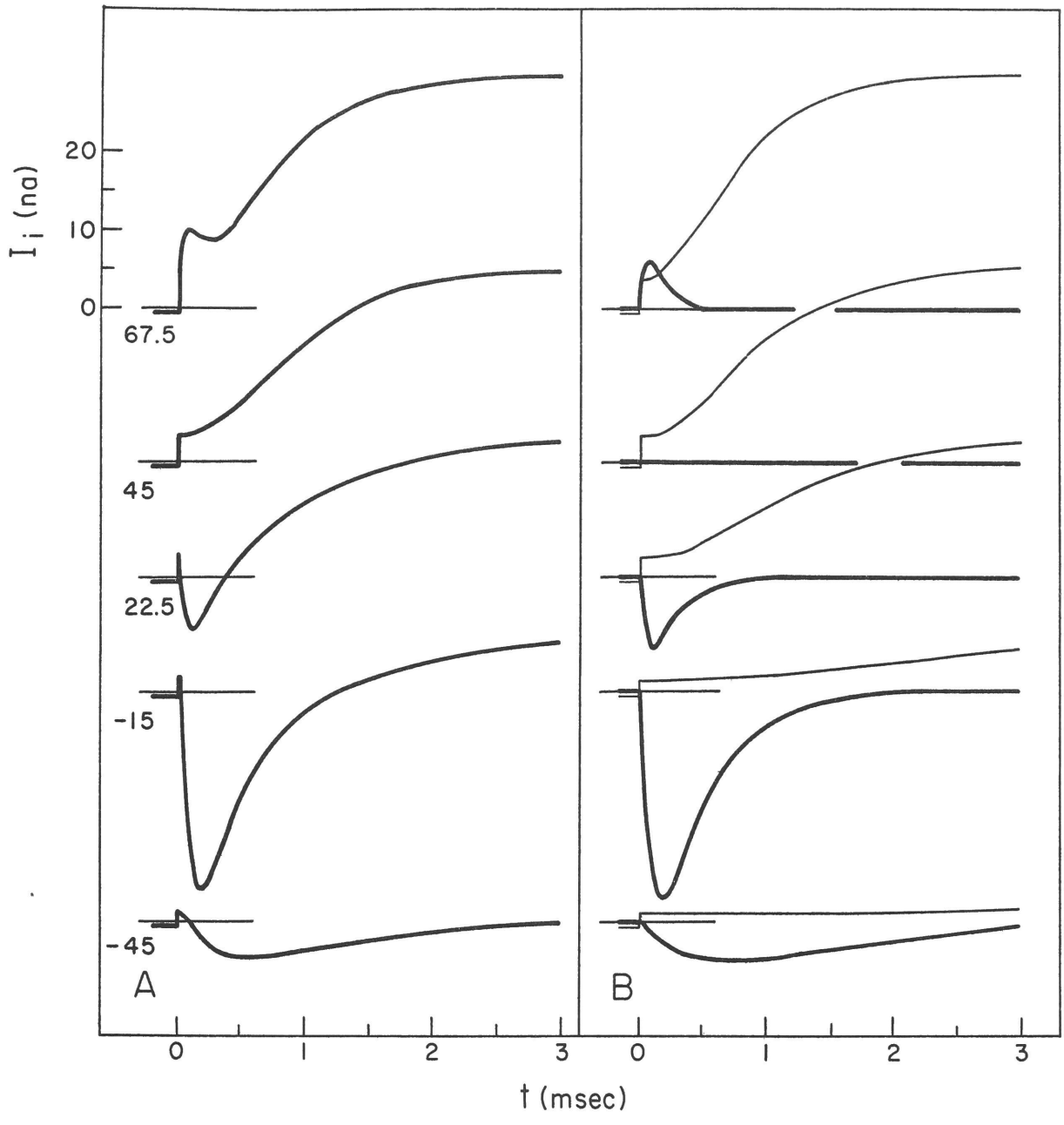


Figure 2.15: Sodium and potassium components of the ionic current separated by the procedure of estimating $I_K$ by linear scaling of the curve of $I_K$ measured at $E = E_{Na}$. A: time courses of the ionic current measured at several different membrane potentials. The membrane was hyperpolarized at $E = -105$ mv for 40 msec preceding the depolarization. $E_{Na}$ was 45 mv. B: time courses of $I_{Na}$ (heavy curves) and of $I_K + I_L$ (light curves). Details of the separation of the components are illustrated in Figure 2.14. Node 12; 20°C.

$P_{Na}$ and $g_K$ are simply proportional to the respective sodium and potassium components of the ionic current, the proportionality constant depending on E, as indicated by Equations 2.5 and 2.8. The time courses of $P_{Na}$ and $g_K$ are shown in Figure 2.16.

An alternative method of measuring the time course of $P_{Na}$ during a maintained depolarization makes use of the fact that $P_{Na}$ does not change instantaneously when the membrane potential is stepped to a new value (Hodgkin and Huxley, 1952 b; Dodge and Frankenhaeuser, 1959; Frankenhaeuser, 1960). In this method the step depolarization is interrupted at various times by repolarization to the resting potential, and the value of $P_{Na}$ is determined at each time from the instantaneous value of the ionic current, since at resting potential $I_K$ is negligibly small. In the present experiments, the instantaneous currents were not accurately resolved because of the finite response time of the measuring systems, but a reasonably accurate estimate of the instantaneous value of $I_{Na}$ was obtained by extrapolation of the exponential "tail" of ionic current to the time of potential change. An experiment examining the instantaneous $P_{Na}$ during a maintained depolarization is shown in Figure 2.17. Within the limits of resolution of the method, there is good agreement between the time course of $P_{Na}$ determined from the instantaneous currents and that obtained by separating $I_K$ and $I_{Na}$.

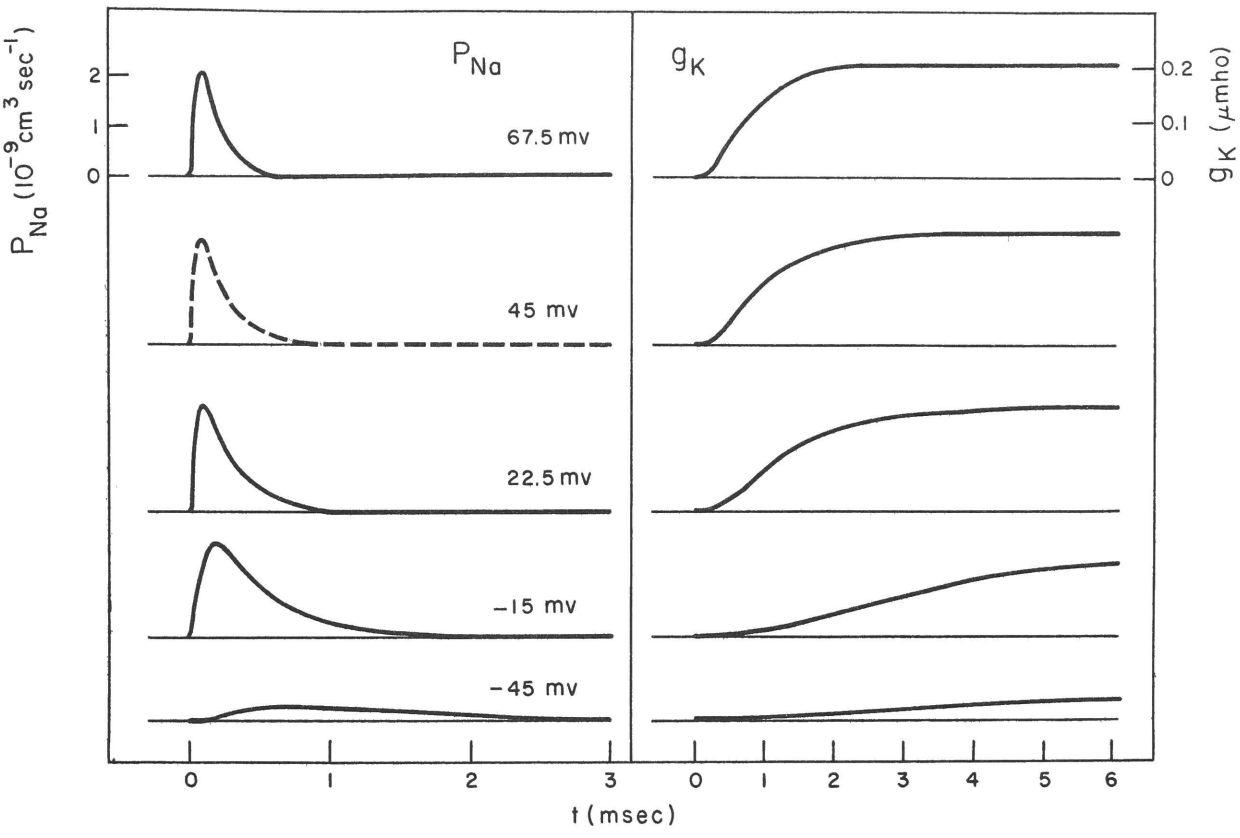


Figure 2.16: Time courses of the sodium permeability ($P_{Na}$) and of the potassium conductance ($g_K$) at several different membrane potentials. Note difference in time scales. Data are from the experiment illustrated in Figure 2.15. The curve of $P_{Na}$ at $E = E_{Na} = 45$ mv is determined by procedure illustrated in Figure 2.17B.

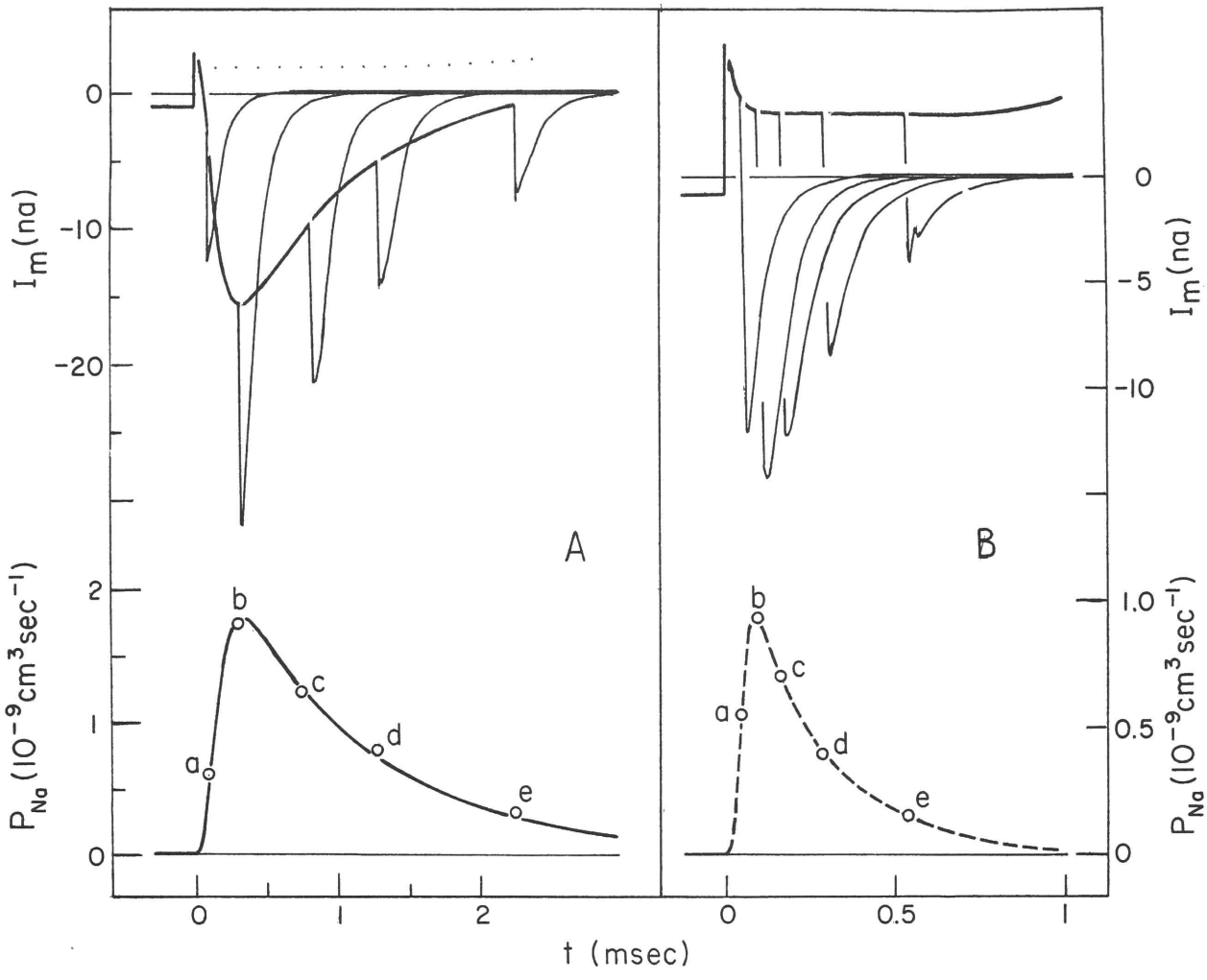


Figure 2.17: A: Comparison of measurements of $P_{Na}$ by instantaneous sodium currents with the time course of $P_{Na}$ determined by separation of the components of $I_i$. In the upper figure are tracings of five records of $I_m$. The membrane was initially hyperpolarized at E = - 105 mv; at t = 0 it was depolarized to E = 0 mv for varying lengths of time, then repolarized to E = - 60 mv (the decline of the "tails" is slower and more reliably measured at E = - 60 mv than at $E_R$). The declining phase of the tail of inward current was plotted on semi-log paper, and fitted by the best straight line. This line was exrapolated to the time of the repolarization to estimate the instantaneous $I_{Na}$. The value of $P_{Na}$ at that time was calculated and plotted in the lower figure for comparison with the smooth curve of $P_{Na}$ determined from the time course of $I_{Na}$ separated by the scaling procedure

(page 56); the estimated variation of $I_L + I_K$ is shown as the series of dots in the upper figure. $E_{Na}$ was +47 mv. The observed agreement between the two measurements must be considered somewhat fortuitous because the determination of the instantaneous $I_{Na}$ required considerable extrapolation, cf. Figure 3.15. The estimated values of the instantaneous $I_{Na}$ and of the time constants ($\tau$) of decay of the sodium "tails" are:

| POINT | $I_{Na}$(na) | $\tau$(μ sec) |
|---|---|---|
| a | - 17 | 90 |
| b | - 53 | 110 |
| c | - 37 | 135 |
| d | - 24 | 125 |
| e | - 10 | 145 |

Node 3; 15°C.

B: Determination of the time course of $P_{Na}$ at $E = E_{Na}$ using measurements of the instantaneous sodium currents. In the upper figure are tracings of five records of $I_m$. The membrane was initially hyperpolarized at $E = -105$ mv for 40 msec; at $t = 0$ it was depolarized to $E = E_{Na} = 45$ mv for varying lengths of time, then repolarized to $E = -60$ mv. The instantaneous values of $I_{Na}$ were estimated as described above, yielding the following values of the instantaneous $I_{Na}$ and of the time constants ($\tau$) of the decay of the sodium "tails".

| POINT | $I_{Na}$ (na) | $\tau$(μ sec) |
|---|---|---|
| a | - 16 | 58 |
| b | - 28 | 66 |
| c | - 21 | 76 |
| d | - 12 | 84 |
| e | - 4.4 | 84 |

The values of $P_{Na}$ determined from these values were plotted in the lower figure and the dashed curve was drawn to fit the points. The peak $P_{Na}$ (point b) found by this procedure was about 10% less than the peak $P_{Na}$ determined by separating the components of $I_i$ at other large depolarizations.

Node 6; 20°C.

# Chapter III

## A QUANTITATIVE DESCRIPTION OF THE IONIC CURRENT OF THE NODAL MEMBRANE - ANALYSIS OF THE VOLTAGE-CLAMP DATA

The investigations reviewed in the preceding chapter have shown that the ionic current of the nodal membrane results from a sequence of changes in the ionic permeability of the membrane: a rapid transient increase in sodium permeability and a slower, delayed increase in potassium permeability. In this chapter we will examine the kinetics of these permeability changes in order to represent the electrical behavior of the membrane by a quantitative mathematical model that will predict the ionic current during any variation of the membrane potential.

The striking similarity between the ionic currents of the node and those of squid axon suggests that the temporal variation of the specific ion permeabilities of the nodal membrane may follow kinetic laws similar to those deduced for the squid axon by Hodgkin and Huxley (1952 d). Since their mathematical model has served as a guide in the analysis of the nodal membrane, it is worthwhile to briefly consider the elements of the squid model.

The mathematical model of the squid axon is shown in Figure 3.1. Here, Equation 1 is the fundamental theoretical equation for the distribution of current within the axon in terms of the variables which are the distance along the axon (x), time (t) and the membrane potential (E). Equation 2 is basically a statement of the ionic hypothesis which says that the current carried by the movement of ions through the membrane is the sum of components carried by sodium ions and by potassium ions, moving in accordance with their respective electro-chemical driving forces and the state of ionic permeability of the membrane measured in terms of $g_{Na}$ and $g_K$. In addition, there is a small leakage current carried by other ions. The time and voltage dependence of the specific ion permeabilities,

Figure 3.1: Quantitative model of the squid axon, taken from Hodgkin and Huxley (1952d) and modified by expressing the membrane potential on the absolute scale (E) with the assumption that $E_R$ = - 60 mv. The rate constants were recalculated to correspond to a temperature of 20°C using the measured $Q_{10}$ of 3 (Hodgkin and Huxley, 1952d).

$$\frac{a}{2R_2} \cdot \frac{\partial^2 E}{\partial x^2} = I_m = C\frac{\partial E}{\partial t} + I_i \qquad (1)$$

$$I_i = \bar{g}_{Na}\, m^3 h (E - E_{Na}) + \bar{g}_K\, n^4 (E - E_K) + \bar{g}_L (E - E_L) \qquad (2)$$

$$\frac{dm}{dt} = \alpha_m (1-m) - \beta_m m \qquad (3)$$

$$\frac{dh}{dt} = \alpha_h (1-h) - \beta_h h \qquad (4)$$

$$\frac{dn}{dt} = \alpha_n (1-n) - \beta_n n \qquad (5)$$

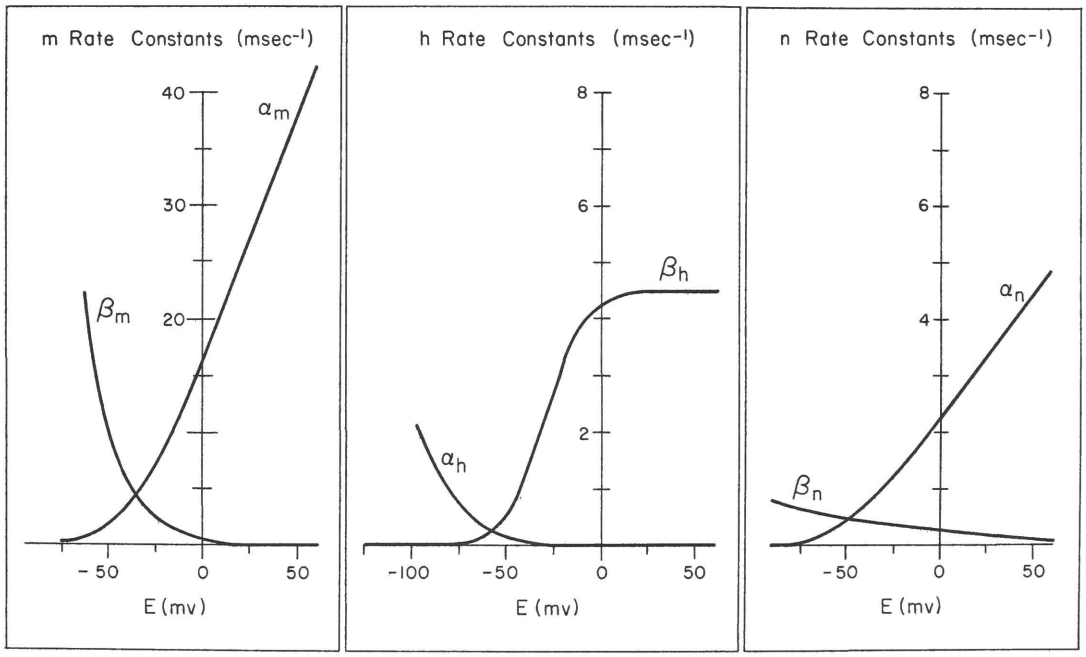


$C = 1.0 \frac{\mu f}{cm^2}$ $\quad \bar{g}_{Na} = 120 \frac{mmho}{cm^2}$ $\quad \bar{g}_K = 36 \frac{mmho}{cm^2}$ $\quad \bar{g}_L = 0.3 \frac{mmho}{cm^2}$

$E_{Na} = +55\,mv$ $\quad E_K = -72\,mv$ $\quad E_L = -50\,mv$

$g_{Na}$ and $g_K$ are described in terms of empirical kinetic parameters m, h, and n, which follow first order rate equations (3, 4 and 5) in which the empirical rate constants are functions only of the membrane potential. This model, derived solely from the analysis of voltage-clamp experiments, provides a complete specification of the electrical properties of the squid axon, predicting all the characteristic electrical behavior associated with excitation and conduction of the action potential (Hodgkin and Huxley, 1952 d; Huxley, 1959; FitzHugh and Antosiewicz, 1959).

In the following sections we develop a model of very similar form to describe the nodal membrane.

## Kinetics of the Variation of Sodium Permeability

The transient variation of the sodium permeability during depolarization at constant membrane potential is conveniently described in terms of the simultaneous operation of two independent, reversible processes - one process that rapidly turns on or activates the sodium permeability, and a second process that more slowly shuts off or inactivates the sodium permeability. The kinetics of these operationally-defined processes are examined qualitatively in the following experiments.

### A. Preliminary experiments

The recovery of the sodium permeability from inactivation is demonstrated by an experiment, Figure 3.2, in which the current was measured in response to two successive identical depolarizing pulses with various intervals between the pulses. The amplitude of the pulses was adjusted to give the maximum inward (sodium) current, and the duration of the pulses was sufficient for the sodium permeability to be completely inactivated by the end of the first, or conditioning pulse. The amplitude of the sodium current during the second, or test pulse, relative to the amplitude of the sodium current during the first pulse, is taken as a

Figure 3.2: Recovery from inactivation of the sodium permeability. Two depolarizing pulses (to $E_1$ = - 15 mv) were applied in succession and the interval between the pulses was varied. Tracings of four representative records of $I_i$ are shown. Estimated variation of $I_L + I_K$ is shown as a series of dots. The first pulse was of sufficient duration to inactivate completely the sodium permeability. The ratio of the peak $I_{Na}$ during the second (test) pulse relative to the peak $I_{Na}$ during the first pulse was taken as a measure of the extent to which the sodium permeability had recovered from inactivation during the interval between the pulses. These ratios were plotted against the duration of the interval in the lower figure and the experimental points fitted by a smooth curve of the form $(1 - \exp\{-t/\tau\})$ where the time constant ($\tau$) was 4.6 msec. Node 24; 19°C.

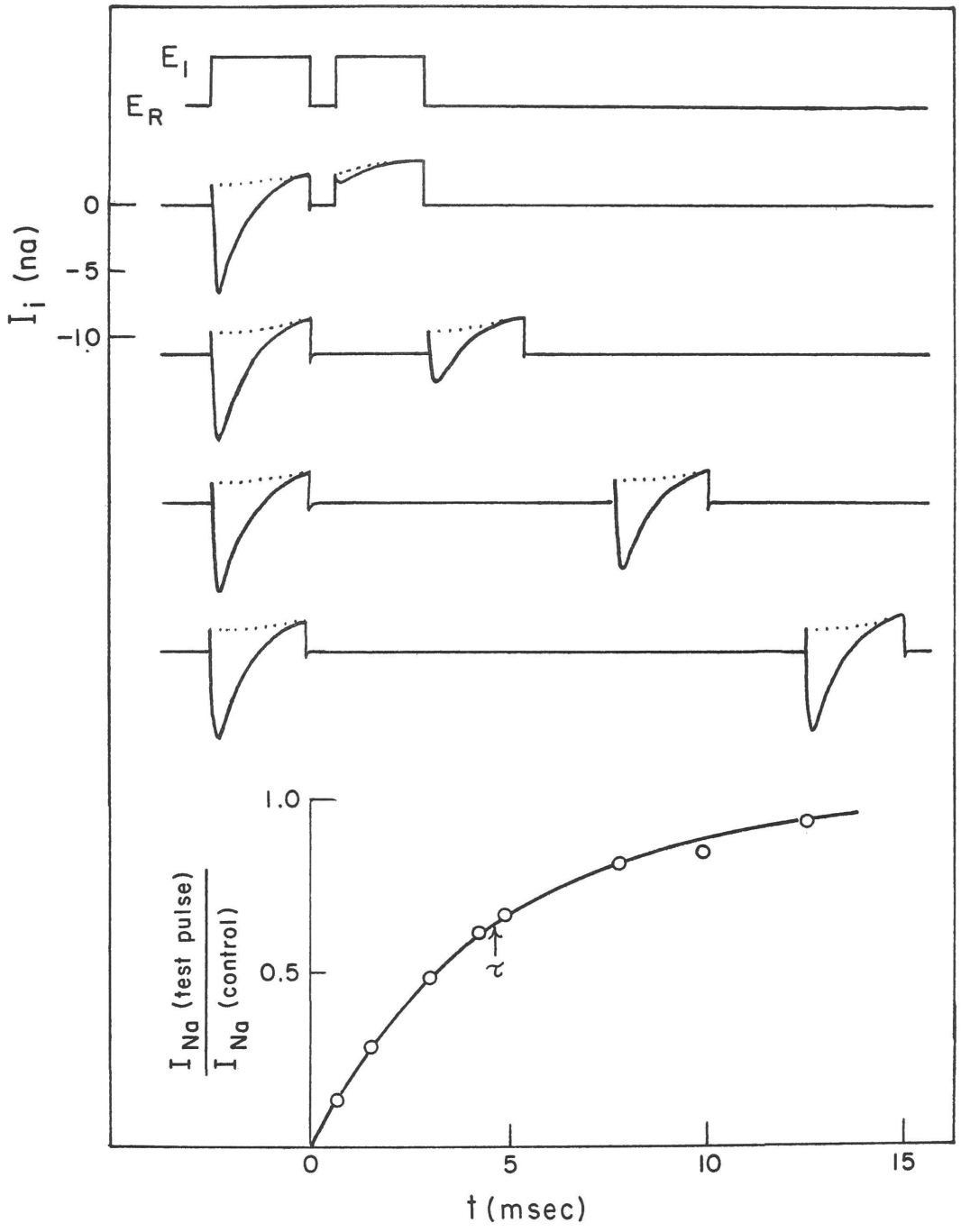
E1
ER
0
-5
-10
Ii (na)
1.0
0.5
INa (test pulse) / INa (control)
τ
0
5
10
15
t (msec)

measure of the extent to which the sodium permeability had recovered from inactivation by the time of the second pulse. For the shortest interval between the pulses, it is seen that the sodium current during the test pulse was so small that the total ionic current remained outward. But, as the interval was lengthened, the sodium current during the test pulse increased and approached the amplitude characteristic of the node in the resting state. The results of this experiment are summarized in the lower figure where the relative amplitude of sodium current during the test pulse is plotted against the time of the beginning of that pulse. The experimental points were fitted by a smooth curve of the form $\exp\{-t/\tau\}$, which suggests that, at the resting potential, recovery from inactivation of the sodium permeability is a first-order process with a time constant ($\tau$) of about 5 msec.

The reversible nature of the activation process is demonstrated by an experiment, Figure 3.3, in which the temporal variations of the sodium permeability during a maintained depolarization are compared with those during a depolarization that is interrupted by a step-wise repolarization to resting potential. In Figure 3.3, the sequence of membrane potential changes is shown in the upper curve; the corresponding records of the ionic current are shown in the middle curves. The membrane current was resolved into its ionic components, and $P_{Na}$ was determined from $I_{Na}$ and Equation 2.5. The time courses of $P_{Na}$ are plotted in the lower curves. In response to the maintained step-depolarization, Figure 3.3 A, $P_{Na}$ at first increased rapidly along a smooth S-shaped curve to a maximum, then more slowly declined to zero along an approximately exponential curve, as the sodium permeability became inactivated during the maintained depolarization. When the membrane was suddenly repolarized at the time of the maximum sodium permeability, Figure 3.3. B, there was a sudden increase of inward sodium current, because the permeability of the membrane to sodium ions did not change instantaneously. However, the sodium current decreased quickly to zero thereafter, reflecting a rapid

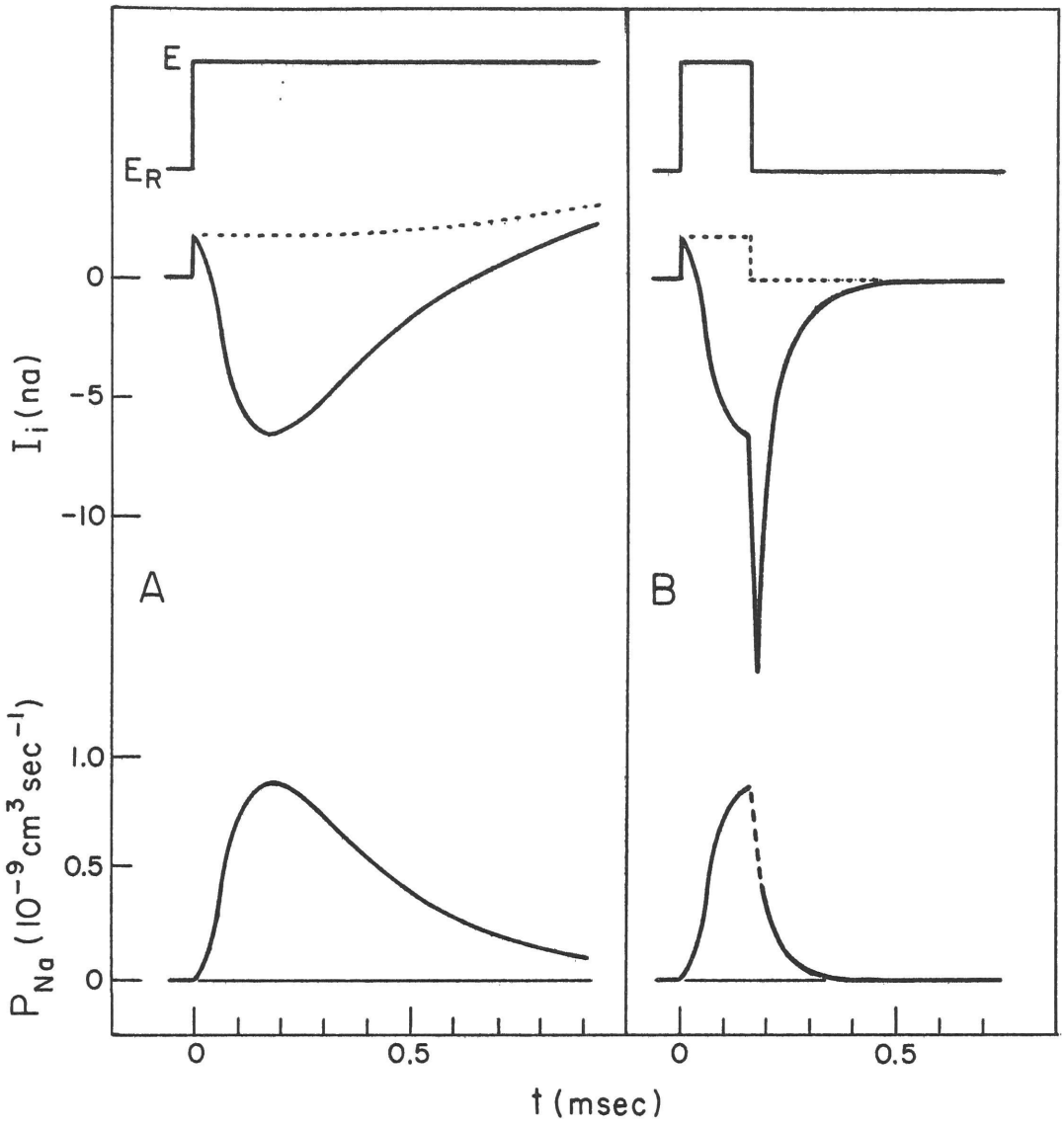


Figure 3.3: Reversible nature of the activation of the sodium permeability. A: curves of the ionic current ($I_i$) and of the sodium permeability ($P_{Na}$) during a maintained depolarization to E = 0 mv. B: curves of $I_i$ and $P_{Na}$ associated with sudden repolarization at the peak of the sodium permeability change. Estimated values of $I_L + I_K$ are shown as the series of dots on curves of $I_i$. Note the rapid shutting off of $P_{Na}$ consequent upon repolarization. The dashed portion of the curve of $P_{Na}$ in B represents the time during which the measurements of $P_{Na}$ are unreliable because of the finite time required for the amplifier to stabilize the membrane potential at the new value (page 23). Node 8; 22°C.

shutting off of the sodium permeability. This effect of repolarizing the membrane is ascribed to a rapid reversal of the activation process, returning the membrane to the state of low permeability to sodium ions characteristic of the resting condition; this effect cannot be ascribed to operation of the inactivation process since the node will respond to an immediate test depolarization with large inward sodium current.

The simultaneous, independent operation of the activation and inactivation processes is demonstrated by an experiment in which the time course of inactivation is compared with the variation of the sodium permeability at the same membrane potential. In this experiment, Figure 3.4, the membrane was depolarized to potential $E_1$, which gave a small and relatively slowly changing phase of inward sodium current, from which the time course of $P_{Na}$ was determined; in addition, the extent to which the sodium permeability had been inactivated was measured at various times during the depolarization to $E_1$ by a test pulse ($E_2$). In Figure 3.4, the sequence of changes of the membrane potential is shown in the upper curve, and curves a - d are samples of a series of records of the ionic current in which the duration of the initial depolarization to $E_1$ was successively shortened. For Record d, the membrane was depolarized immediately from the initial level to $E_2$ in order to record a control value for the sodium current during the test pulse before there was any inactivation of the sodium permeability of the membrane at potential $E_1$. The time course of inactivation at $E_1$ was determined by plotting the relative amplitude of $I_{Na}$ during the test pulse against the time of the onset of the test pulse, and a smooth curve of the form $\exp\{-t/\tau\}$ was fitted to the experimental points. The time course of $P_{Na}$ at $E_1$ was determined from $I_{Na}$ in Record a. Comparison of these two curves clearly shows that inactivation of the sodium permeability began as soon as the membrane potential changed to $E_1$, before there was appreciable activation of the sodium permeability. This result justifies the assumption that the two processes are kinetically independent.

Figure 3.4: Simultaneous and independent operation of the activation and the inactivation processes. The membrane was hyperpolarized at $E_o$ = -105 mv for 40 msec preceding each measurement; at t = 0 the membrane was depolarized to $E_1$ = -45 mv for varying lengths of time, whereupon the membrane was further depolarized to $E_2$ = -15 mv for 1.6 msec. Curves a, b, and c are tracings of representative records of $I_i$ as the duration of the depolarization to $E_1$ was progressively shortened. Curve d is $I_i$ measured when the membrane potential was stepped directly from $E_o$ to $E_2$. Estimated values of $I_L + I_K$ are shown as the dotted curves. The ratio of the peak $I_{Na}$ during the test depolarization ($E_2$) to the peak $I_{Na}$ in record d was taken as a measure of the extent to which the sodium permeability had been inactivated during the depolarization at $E_1$. These ratios were plotted against the duration of $E_1$ (lower figure) and fitted by a smooth curve of the form $(\exp\{-t/\tau\})$ whose time constant ($\tau$) was 2.7 msec. A semi-log plot of the time course of $I_{Na}$ in record a during the depolarization to $E_1$ showed that the declining phase was accurately described by an exponential decay with the same time constant (2.7 msec) as determined for the inactivation process. The time course of $I_{Na}$ at $E_1$, suitably scaled so that the declining phase coincides with the inactivation curve, is plotted in the lower figure (heavy curve). This comparison clearly shows that inactivation of the sodium permeability began immediately upon the depolarization to $E_1$, before there had been any significant activation of $P_{Na}$. Node 2; 18°C.

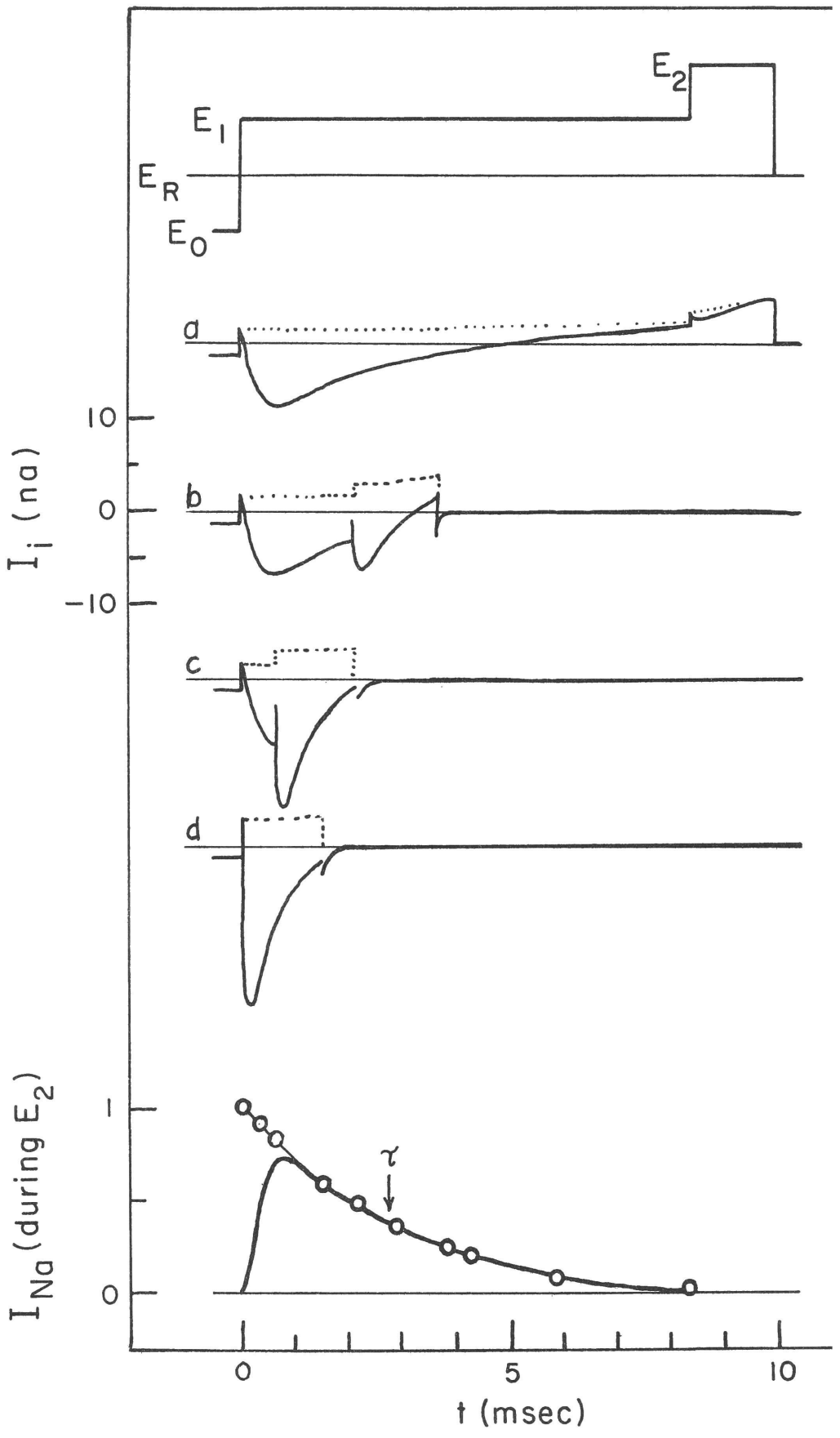
E2
E1
ER
E0
a
b
c
d
10
0
-10
Ii (na)
1
0
INa (during E2)
τ
0
5
10
t (msec)

These experiments, describing transitions in the state of the membrane that take place following an imposed change of potential difference, are interpreted in terms of two independent simultaneous processes, activation and inactivation of the permeability for sodium. This interpretation, in terms of states of the membrane, can be diagrammatically presented by a mechanical analog that has similar macroscopic properties. In the analog, Figure 3.5, the sodium permeability is represented by a channel which can be blocked by two independent gates - the fast-acting A gate which is identified kinetically with the activation process, and the slow-acting I gate which is identified kinetically with the inactivation process.

As a function of membrane potential each gate assumes a definite steady-state position. The A gate is completely closed near the resting potential, progressively more open as the membrane is depolarized beyond threshold, and wide open in the steady state, for depolarization exceeding zero membrane potential. On the other hand, the I gate is almost wide open in the resting state, but is completely closed, in the steady-state, for depolarization exceeding threshold potentials. The diagram also represents the transitions in sodium permeability during a voltage-clamp experiment. State (1) represents the resting state in which the channel is blocked by the A gate. In response to a maintained depolarization the channel relaxes to the steady-state (3), blocked then by the I gate, through a transition state (2) in which the fast A gate has opened before the slower I gate has closed very much. The channel is open in state (2) and there is an observable sodium current which is transient because of the slow closing of the I gate, as in the experiments of Figures 3.3 and 3.4 A. Sudden repolarization of the membrane when it is in state (2) would cause the A gate to close rapidly, cutting off the sodium permeability as the system rapidly reverted to a state approximating the resting state. Such an effect was observed in the experiment of Figure 3.4 B. If, however, the depolarization of the membrane is main-

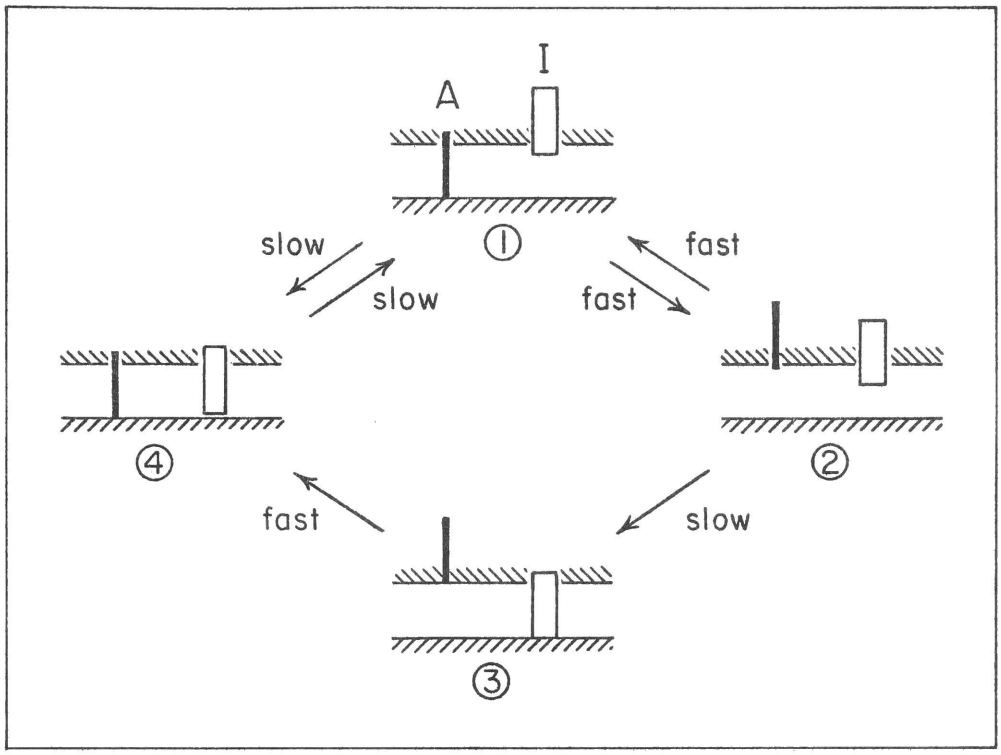


Figure 3.5: Mechanical analog describing general features of the kinetics of the sodium permeability change. It is supposed that sodium ions cross the membrane through channels controlled by two independent gates, the fast-acting A gate (activation process) and the slow-acting I gate (inactivation process). The steady-state positions and rate constants governing the opening and closing of the gates are dependent solely upon the membrane potential. For discussion see text.

tained, the steady state (3) is achieved. Now, repolarization of the membrane to the resting level restores the system to the resting state (1) through the transition state (4) in which the fast-acting A gate closes before the slower I gate has opened very much. Thus, no sodium current is measured during the transition from state (3) to state (1) at the resting potential; but by applying a test depolarization at various times after the repolarization, we can test the extent to which the I gate is open, as in the experiment of Figure 3.2. The independence of the A and I gates is further demonstrated by the fact that the sodium permeability can be completely inactivated by a small depolarization during which one observes no sodium current. This is represented in the diagram by a slow transition between states (1) and (4). This mechanistic interpretation in terms of two independent processes controlling the sodium permeability is formulated more precisely by the mathematical description developed in the next section.

B. Formal description of the temporal variation of $P_{Na}$

The results of these preliminary experiments indicate the typical features of the kinetics of the sodium permeability changes. At constant membrane potential the sodium permeability is inactivated, Figure 3.4, or recovers from inactivation, Figure 3.2, with an exponential time course, suggesting that the inactivation process may be described by a variable (h) that obeys a first order rate equation. At constant membrane potential after a step depolarization the sodium permeability is activated with a time course that is an S-shaped curve, but the time course of the reversal of activation (Figure 3.3 B) follows an approximately exponential decay starting immediately upon repolarization of the membrane. Whereas the reversal of activation could be described by a variable following a first order rate equation, the S-shaped curve of the rising phase of the sodium permeability would require a higher order rate equation. This dfficulty is avoided, however, with the simplification employed by Hodgkin and Huxley, in which it is assumed that the activation of the sodium permeability

is described by the third power of a variable (m) that obeys a first order rate equation.

These ideas are expressed by the following equations:

$$P_{Na} = \overline{P}_{Na} m^3 h \tag{3.1}$$

$$\dot{m} = \alpha_m (1 - m) - \beta_m m \tag{3.2}$$

$$\dot{h} = \alpha_h (1 - h) - \beta_h h \tag{3.3}$$

in which $\overline{P}_{Na}$ is a constant, the maximum possible sodium permeability; h is the fraction of sodium permeability that is available for activation [the quantity (1 - h) therefore being the direct measure of the extent of inactivation]; and $m^3$ is the fraction of the available sodium permeability that is activated. The parameters m and h are dimensionless quantities varying between zero and one. They obey first order rate equations (3.2 and 3.3) in which the rate constants ($\alpha$'s and $\beta$'s) depend only upon the membrane potential.

Following Hodgkin and Huxley, the rate equations 3.2 and 3.3 are written in a form which describes a reversible first order reaction. The rate constants are related to empirical measurements of the steady-state values of the parameters ($m_\infty$ and $h_\infty$) and the time constants ($\tau_m$ and $\tau_h$) through the following equations:

$$m_\infty = \frac{\alpha_m}{\alpha_m + \beta_m} \tag{3.4}$$

$$\tau_m = \frac{\alpha_m}{\alpha_m + \beta_m} \tag{3.5}$$

$$h_\infty = \frac{\alpha_h}{\alpha_h + \beta_h} \tag{3.6}$$

$$\tau_h = \frac{1}{\alpha_h + \beta_h} \tag{3.7}$$

(These definitions may be obtained by comparison of the first order rate equations with the canonical form of a first order differential equation, e.g., compare $\dot{m} = \alpha_m(1 - m) - \beta_m m$ with $\tau_m \dot{m} + m = m_\infty$.)

Application of this mathematical model to the transient change in sodium permeability following a step change of the membrane potential is illustrated in Figure 3.6 A in which the time course of $P_{Na}$ in the experiment of Figure 3.4 is described in terms of the parameters m and h. From an initial potential, at which the parameters have initial values $m_o$ and $h_o$, the membrane potential is suddenly changed to a new value, and the rate constants (the $\alpha$'s and $\beta$'s) instantly assume new constant values appropriate to the new value of membrane potential. The solutions of the rate equations for constant membrane potential are:

$$m = m_\infty - (m_\infty - m_o) \exp\{ - t/\tau_m \} \tag{3.8}$$

$$h = h_\infty - (h_\infty - h_o) \exp\{ - t/\tau_h \} \tag{3.9}$$

These solutions describe the exponential relaxations of the parameters, m and h, from their initial values to their steady-state values. The time course of $P_{Na}$ is proportional to $m^3 h$ (Equation 3.1).

The effect of a sudden repolarization from $E_1$ to $E_R$ is illustrated in Figure 3.6 B. With the time of repolarization taken as zero time, $h_o$ and $m_o$ are the values of the parameters at the end of the preceding depolarizing pulse; equations 3.8 and 3.9 are solved with values of the rate constants appropriate to the resting potential $E_R$. The rapid relaxation of m to its steady-state value at $E_R$ describes the rapid reversal of the activation process, and the slower recovery of h toward its resting value describes the relatively slow recovery of the membrane from the effect of inactivation that accumulated during the depolarizing pulse.

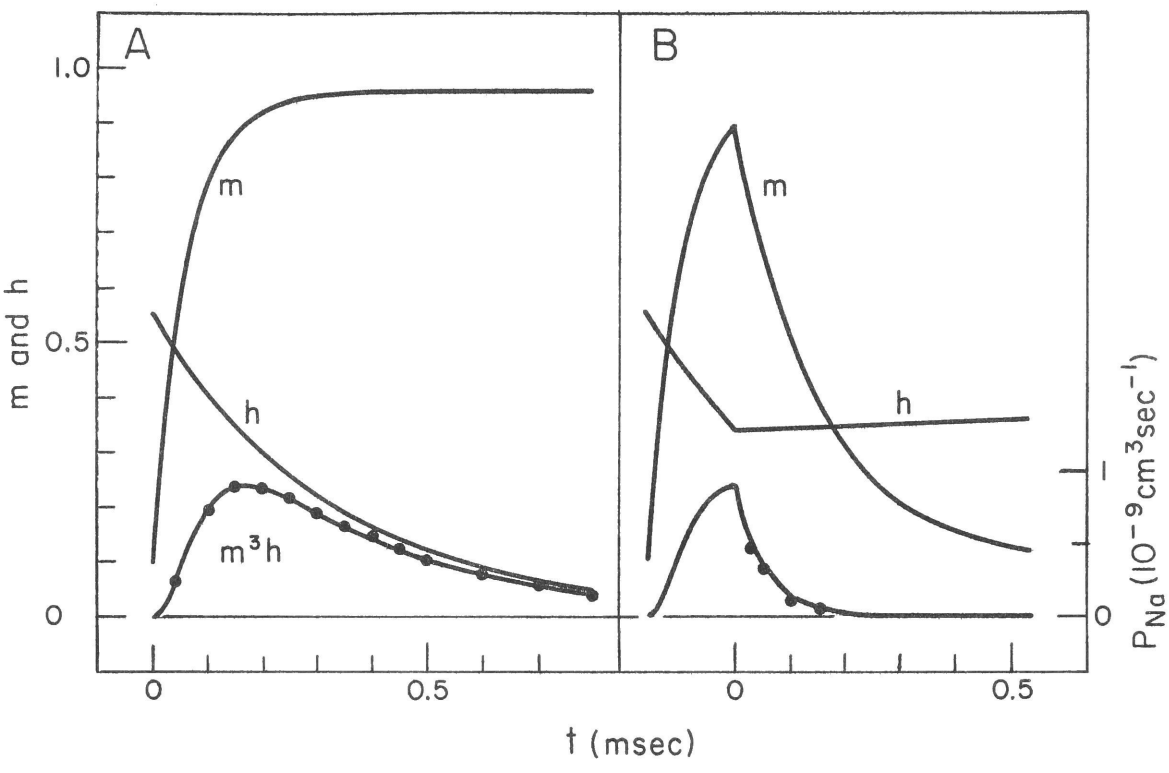


Figure 3.6: Quantitative description of the temporal variation in sodium permeability observed in the experiment of Figure 3.4 in terms of the mathematical model of $P_{Na}$, i.e., $P_{Na} = \bar{P}_{Na}\, m^3 h$. The time courses of the parameters m and h were calculated from Equations 3.8 and 3.9 using the following empirical steady-state values and time constants:

| E(mv) | $m_\infty$ | $\tau_m$ (msec) | $h_\infty$ | $\tau_h$ (msec) |
|---|---|---|---|---|
| - 75 | 0.10 | 0.15 | 0.55 | 5.0 |
| 0 | 0.95 | 0.062 | 0.00 | 0.32 |

$\bar{P}_{Na}$ was $3.9 \times 10^{-9}$ cm$^3$ sec$^{-1}$. Experimental values of $P_{Na}$ are shown as filled circles.

C. Experimental evaluation of the parameters of the nodal model

In the following sections, voltage-clamp data are systematically analyzed for the steady-state values and the time constants of the parameters m and h in the formal model for $P_{Na}$. In this analysis, particular attention is given to those experiments which demonstrate that all of these quantities are single-valued functions of the membrane potential.

1. The relation between $h_\infty$ and membrane potential: The parameter h is defined formally as the fraction of the sodium permeability that is immediately available for activation by a depolarization. This definition is made operational in the experiment of Figure 3.7, in which the membrane potential was held at an initial level ($E_o$) for 40 msec (which is long enough to insure that the membrane is in a steady state), whereupon the condition of the membrane is tested by a depolarizing pulse to a standard membrane potential ($E_1$), chosen to give the maximum inward (sodium) current. The series of records of the ionic current during the test pulse for the different initial membrane potentials ($E_o$) clearly shows the profound influence of the initial conditions on the amplitude of the sodium currents, which are increased by a preceding hyperpolarization, and decreased by a preceding depolarization. The effect of the hyperpolarization saturates for initial membrane potentials exceeding 35 mv negative of the resting potential ($E_R$ = - 75); whereas, if the membrane is initially more than 25 mv depolarized from the resting level, the inward component of the ionic current is completely suppressed.

The records of Figure 3.7 do not clearly show whether there is any effect of these initial conditions on the potassium component of membrane current. This point is examined in a similar experiment (Figure 3.8) in which the test depolarization is made to the sodium equilibrium potential in order to eliminate the sodium component of the current. These records show that the steady level and later part of the time course of $I_K$ are unaffected by the initial level of membrane potential, but that the delay in the

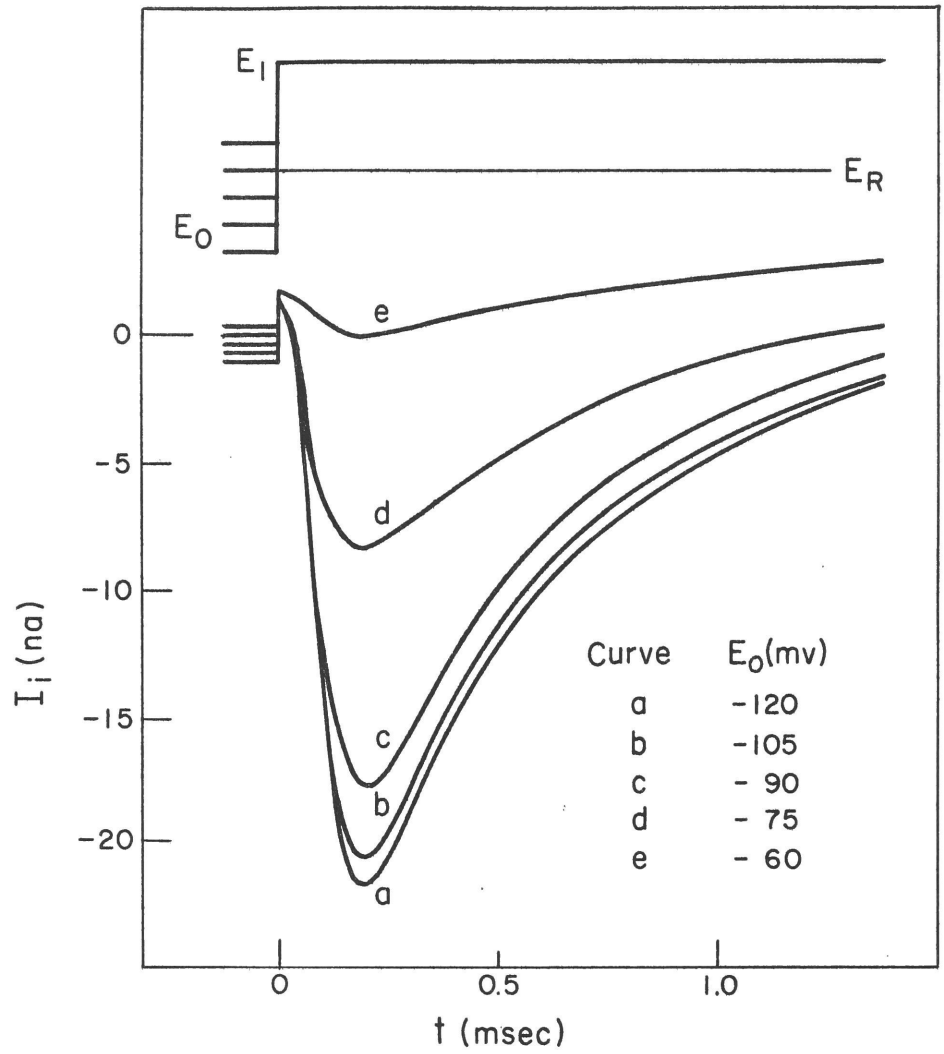


Figure 3.7: Curves of the ionic current ($I_i$) measured during a standard depolarization to $E_1$ = - 15 mv after a 40 msec long preceding polarization ($E_o$) at each of several different membrane potentials. Note strong effect of the initial conditions on the amplitude of $I_{Na}$. Node 7; 22°C.

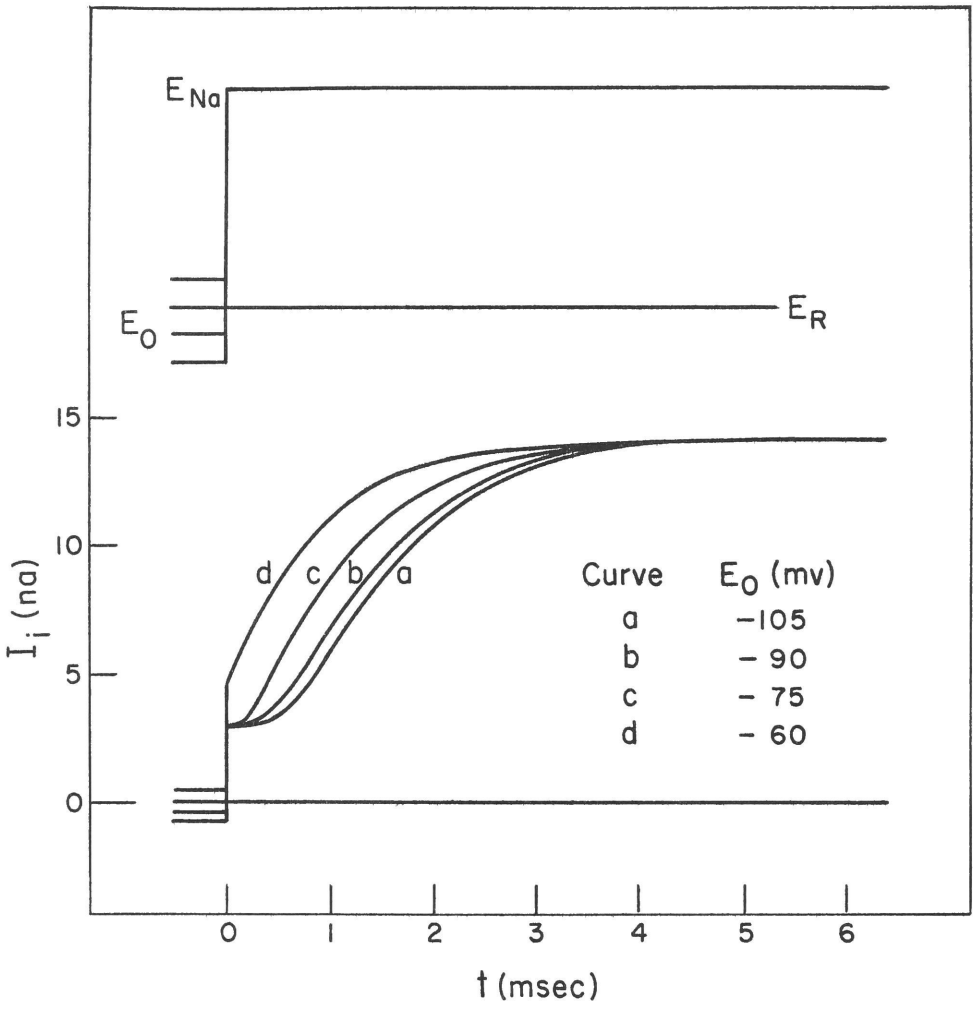


Figure 3.8: Curves of the ionic current ($I_i$) measured at $E = E_{Na}$ after a 40 msec long polarization ($E_o$) at each of several different membrane potentials. Note that the initial conditions affect the delay in the onset of $I_K$, but do not significantly affect the rate of the subsequent approach to the steady-state level. Node 16.

onset of $I_K$ is increased by a preceding hyperpolarization and decreased by depolarization.

Taking account of this effect in estimating $I_K$, the ionic currents from records of Figure 3.7 were resolved into their components $I_{Na}$, $I_K$, and $I_L$. The time course of $P_{Na}$ (proportional to $I_{Na}$) was then calculated by Equation 2.5. Values of $P_{Na}$ at various times for each of the initial conditions are plotted in Figure 3.9 for comparison with a family of theoretical curves. Significantly, these curves differ only in relative amplitude by the factor designated $h_o$. The equation for these curves is

$$P_{Na} = \overline{P}_{Na} m_\infty^3 h_o (1 - \exp\{-t/\tau_m\})^3 \exp\{-t/\tau_h\} \qquad (3.10)$$

in which all coefficients except $h_o$ depend only on the membrane potential during the test pulse. This equation is derived from the formal model by combining Equation 3.1, 3.8, and 3.9 with two additional assumptions: (1) $h_\infty = 0$, corresponding to complete inactivation of $P_{Na}$ during the test pulse and (2) $m_o = 0$, consistent with the observation that no appreciable sodium permeability was activated during the preceding polarizations $E_o$.

Since the initial potential $E_o$ was held for a long time, the values of $h_o$, determined in these experiments, are the steady-state values $h_\infty$ at the corresponding membrane potential $E_o$. These are plotted in Figure 3.10. Zero value is assigned to $h_\infty$ for membrane potentials more positive than $E = -50$ mv since it is observed that $P_{Na}$ is completely inactivated during maintained depolarizations exceeding this potential. The relation between $h_\infty$ and the membrane potential is seen to be a steep S-shaped curve, centered near the resting potential. For this node $h_\infty$ at the resting potential is 0.4, indicating that 60% of the maximum possible sodium permeability is inactivated. Most freshly mounted nodes have $h_\infty$ at the resting potential in the range 0.4 to 0.6.

The detailed analysis of this experiment has established that only

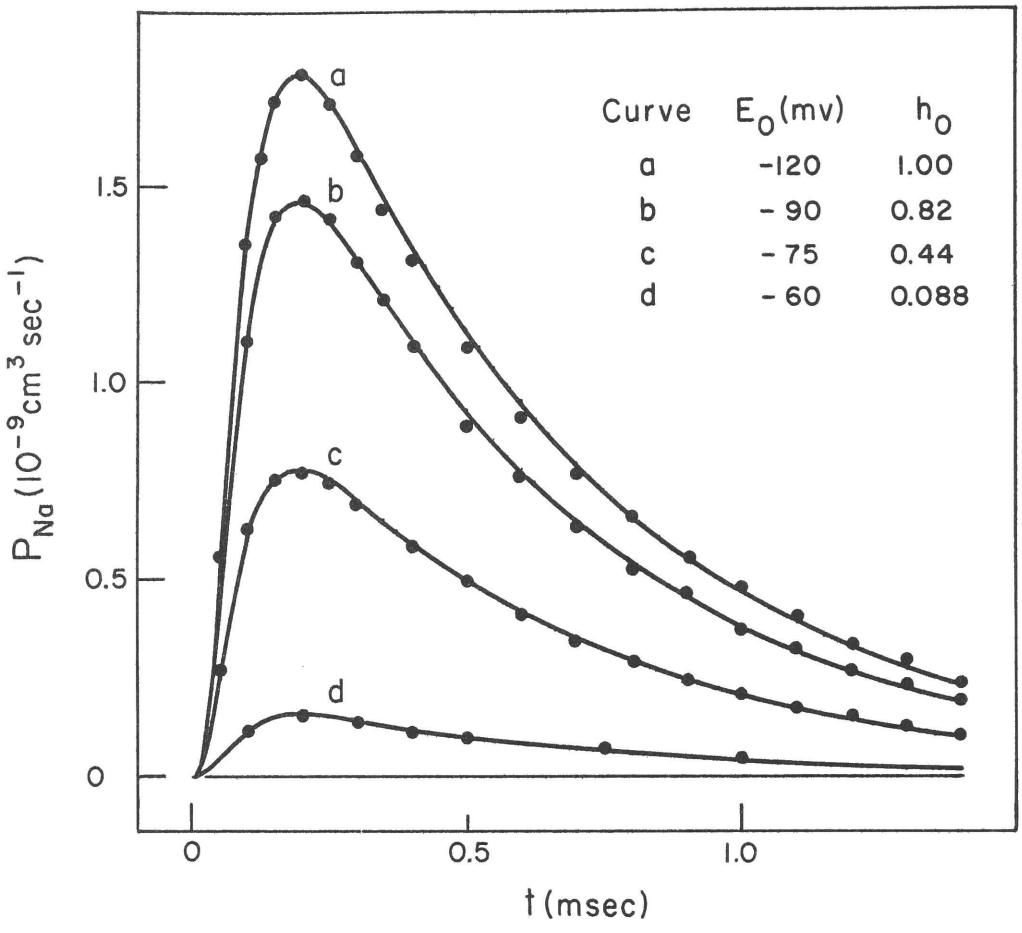


Figure 3.9: Determination of $h_\infty$. For each of the curves in Figure 3.7 the components of $I_i$ were separated by the scaling procedure (page 56) taking into account the effect of $E_o$ on the delay of $I_K$ (Figure 3.8). The curves of the time course of $I_{Na}$ were transformed into curves of $P_{Na}$ by application of Equation 2.5. Values of $P_{Na}$ at various times are plotted here (fillled circles) for comparison with a family of smooth curves calculated from Equation 3.10. These curves differ only by the amplitude factor $h_o$, the initial value of the parameter h. Under the conditions of the experiment the other terms in Equation 3.10 are constant, and their empirical values are: $\overline{P}_{Na} = 3.9 \times 10^{-9}$ $cm^3$ $sec^{-1}$, $m_\infty = 0.90$, $\tau_m = 56$ μsec and $\tau_h = 560$ μsec. (The curve for $E_o = -105$, for which $h_o = 0.95$, was omitted in order to simplify this figure.) The empirical values of $h_o$ determined here are the steady-state values ($h_\infty$) at the preceding value of membrane potential, since for all $E_o$ the duration of the preceding polarization was long with respect to the time constant of the relaxation of h, cf. Figures 3.10 and 3.11. Node 7; 22°C.

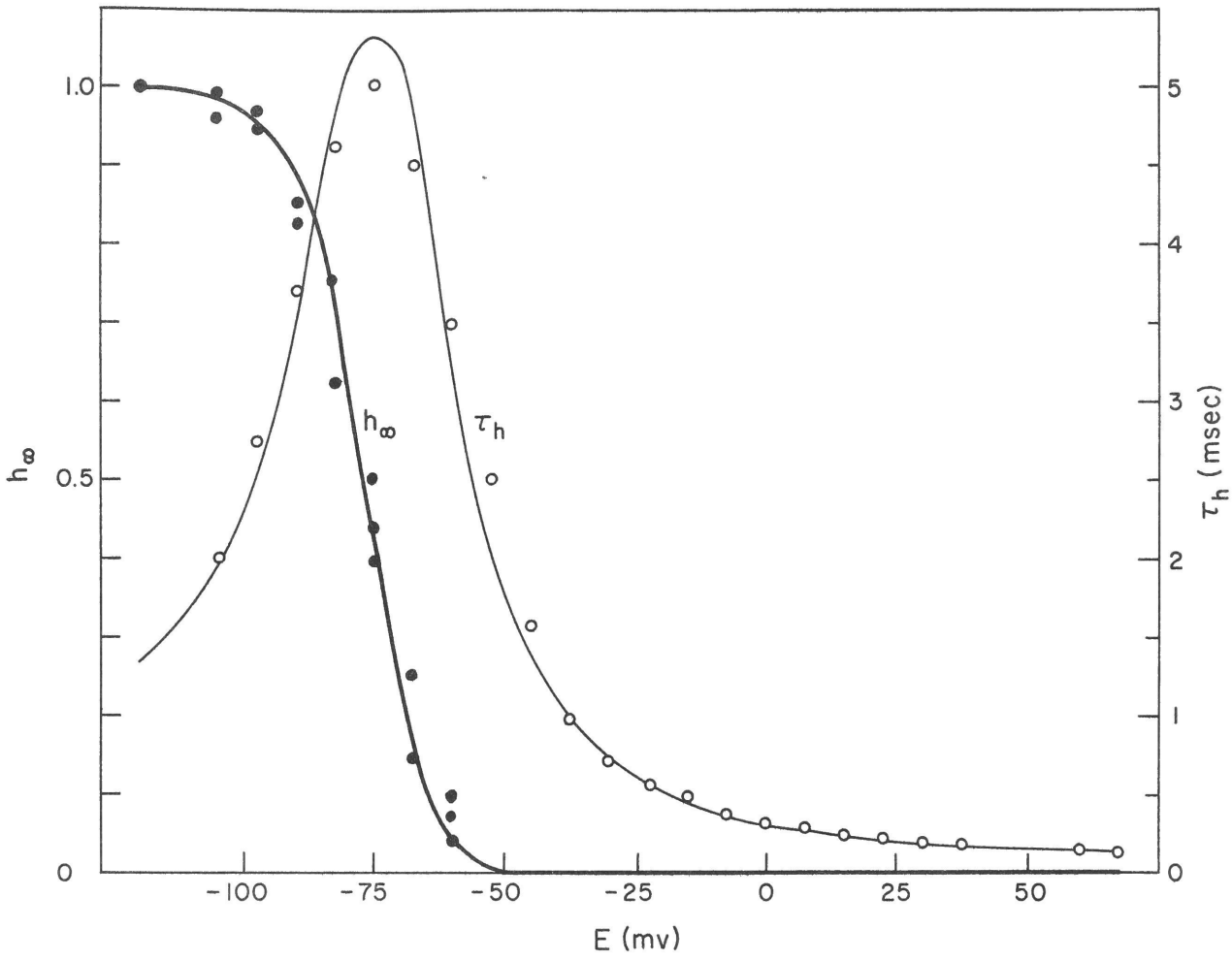


Figure 3.10: Steady-state values ($h_\infty$) and time constants ($\tau_h$) as a function of membrane potential. The empirical values are represented in theoretical computations by the smooth curves which are solutions of Equations 3.6 and 3.7 using the approximating functions for the rate constants $\alpha_h$ and $\beta_h$ (Figure 3.19). The scatter of points around the curve of $h_\infty$ represents an uncertainty of about ± 3 mv in re-balancing the amplifiers to $E_R$ = - 75 mv. Node 7; 22°C.

the amplitude of the sodium permeability change during a standard test pulse is affected by the initial conditions in the range of membrane potentials more negative than $E = -50$ mv. On this basis, the value of $h_\infty$ is routinely measured (in this restricted range of initial conditions) as the ratio of the amplitude of $I_{Na}$ observed in a test pulse to the amplitude of $I_{Na}$ when the test pulse was preceded by a saturating hyperpolarization.

2. The relation between $\tau_h$ and membrane potential: The time course of the relaxation of $h$ at constant membrane potential (for membrane potentials below which there is no significant activation of $P_{Na}$) is measured by an experiment in which an arbitrary initial value is established by a long polarization ($E_o$), then the membrane potential is stepped to the experimental value ($E_1$), and, at various times after the onset of $E_1$, $h$ is measured by the relative amplitude of $I_{Na}$ during a standard test pulse ($E_2$). The results of four such experiments are summarized in Figure 3.11, in which the measured values of $h$ are plotted against time. The value of $\tau_h$ at $E_1$ is obtained by fitting a curve of Equation 3.9 to the observed points. In Figure 3.11 the two curves in which $E_1 = -82.5$ mv are most significant, in that $h$ approaches the same steady-state value along curves with the same time constant, but from opposite directions, that is, when values of $h_o$ are the extremes. That $\tau_h$ is independent of the initial value of $h$ was already indicated by the results of the previous experiment, Figure 3.9, where the family of theoretical curves was calculated on the basis of the same value of $\tau_h$, but different values of $h_o$.

For the range of membrane potentials more positive than $E = -50$ mv $\tau_h$ is determined from the time course of the decay of $P_{Na}$ during a maintained depolarization. Figure 3.12 illustrates semi-log plots of the time course of $P_{Na}$ at several values of membrane potential. The latter parts of the curves are fit well by a straight line indicating that the falling phase of $P_{Na}$ is described by a single exponential whose time constant ($\tau_h$) is obtained from the slope of the line.

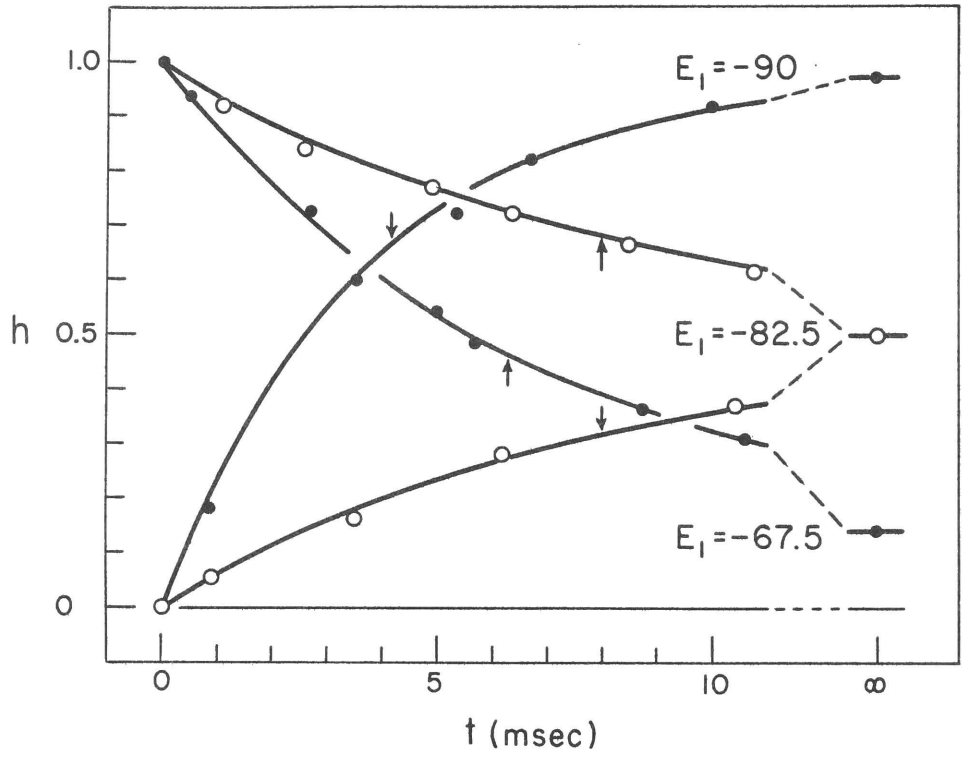


Figure 3.11: Determination of time constant ($\tau_h$) at membrane potentials near $E_R$. One or the other of two arbitrary initial conditions was established by a 40 msec polarization $E_o$ ($h_\infty$ was 1.0 for $E_o$ = - 105 mv, $h_\infty$ was 0 for $E_o$ = - 60 mv); the membrane potential was then stepped to a new value $E_1$ for varying lengths of time, whereupon the ionic current was measured during a standard test depolarization ($E_2$ = - 15 mv). The value of the parameter h at the time of application of $E_2$ was measured as the ratio of peak $I_{Na}$ during the test pulse to the peak $I_{Na}$ observed when the test pulse was preceded by a 40 msec long hyperpolarization at E = - 105 mv. Experimental values of h are plotted against the duration of $E_1$ and fitted by smooth curves which are solutions of Equation 3.9 yielding the following empirical values of the parameters:

| $E_1$ (mv) | $h_\infty$ | $\tau_h$ (msec) |
|---|---|---|
| - 90 | 0.98 | 4.1 |
| - 82.5 | 0.50 | 8.0 |
| - 67.5 | 0.13 | 6.4 |

The small arrows mark the appropriate $\tau_h$. Node 4; 19°C.

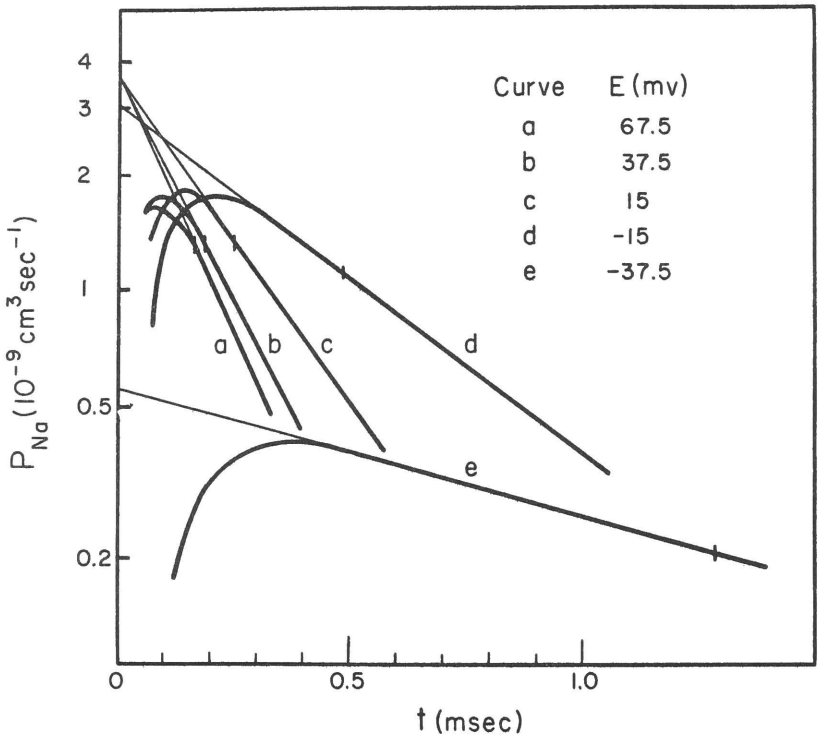


Figure 3.12: Determination of $\tau_h$, $\overline{P}_{Na}$, and $m_\infty^3$. The heavy curves are semi-log plots of the time courses of $P_{Na}$ at different membrane potentials. $\tau_h$ was determined from the slope of the straight line fitted to the curves at long times; these lines were extrapolated to zero time to estimate the value of $P_{Na}$ that would have been attained if m turned on to $m_\infty$ instantaneously ($P'_{Na}$). The curves at large depolarizations (curves a, b, and c) have a common intercept which is also the maximum ($P'_{Na\,max}$) for which the value 1 is assigned to $m_\infty^3$. With the previously determined value of $h_o = 0.95$ (a 40 msec long hyperpolarization at $E_o = -105$ mv preceded each depolarization), $\overline{P}_{Na}$ was determined from the relation $P'_{Na} = \overline{P}_{Na} m_\infty^3 h_o$ to be $3.9 \times 10^{-9}$ $cm^3 sec^{-1}$. At other depolarizations (curves d and c) $m_\infty^3$ was determined as the ratio of $P'_{Na}$ to $P'_{Na\,max}$. The graphical analysis of these curves yielded the following values of the parameters:

| E (mv) | Curve | $m_\infty$ | $\tau_h$ (msec) |
|---|---|---|---|
| 67.5 | a | 1 | 0.16 |
| 37.5 | b | 1 | 0.19 |
| 15 | c | 1 | 0.25 |
| - 15 | d | 0.94 | 0.49 |
| - 37.5 | e | 0.55 | 1.30 |

Node 7; 22°C.

For a few values of membrane potential near $E = -50$ mv, at which the degree of activation of $P_{Na}$ is small compared to that during a larger test pulse, it is possible to determine $\tau_h$ simultaneously by both methods as in Figure 3.4. The results of such a comparison give the same value of $\tau_h$ within the limits of reliability of estimating $I_{Na}$ during a small depolarization.

The characteristic relation between $\tau_h$ and membrane potential (Figure 3.10) is a sharply peaked curve showing that h changes most slowly near the resting potential.

3. The relation between $m_\infty$ and membrane potential: The formal definition of the parameter m is that the third power of m is the fraction of the available sodium permeability that is activated at any instant. According to Equation 3.10, the zero time intercept (P') of the extrapolated straight lines in Figure 3.12 is given by $P' = \overline{P}_{Na} m_\infty^3 h_o$ in which $\overline{P}_{Na}$ and $h_o$ have the same values for all the curves. For large depolarizations, the extrapolated lines have a common intercept which is also the maximum, hence the value one is assigned to $m_\infty$ for these values of membrane potential. For intermediate depolarizations, $m_\infty = (P'/P'_{max})^{1/3}$. The sodium permeability of the resting node is so small in comparison to the maximally activated sodium permeability (page 50) that the value zero is assigned to $m_\infty$ for membrane potentials more negative than $E_R$. Experimental values of $m_\infty$ are plotted against membrane potential in Figure 3.13.

The value of the constant $\overline{P}_{Na}$ is obtained from the maximum intercept and the previously determined value of $h_o$.

4. The relation between $\tau_m$ and membrane potential: In a semi-log plot of the time course of $P_{Na}$ (Figure 3.12), the deviation of the actual curve from the straight-line extrapolation at short times is due to the finite rate at which m approaches $m_\infty$. In determining the time course by which m approaches $m_\infty$, the effect of inactivation was factored out by plotting, against time, the ratio of the observed value of $P_{Na}$ at some short time

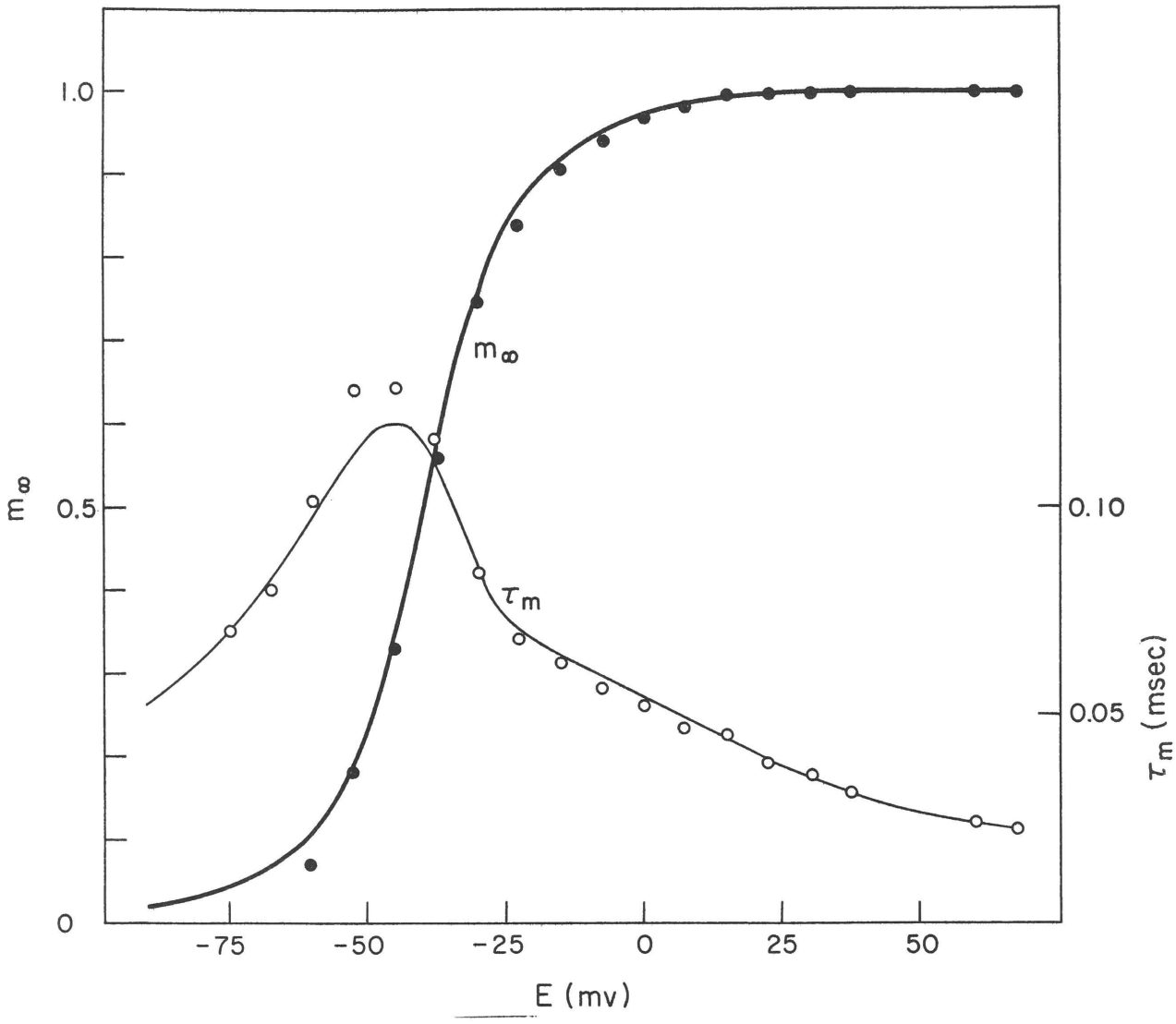


Figure 3.13: Steady-state values ($m_\infty$) and time constants ($\tau_m$) as a function of membrane potential. The empirical values are represented in theoretical computations by the smooth curves which are solutions of Equations 3.4 and 3.5 using the approximating functions for the rate constants $\alpha_m$ and $\beta_m$ (Figure 3.19).

to the value of $P_{Na}$ at the same time on the extrapolated straight line. The resulting S-shaped curve was then compared to theoretical curves of the form $(1 - \exp\{-t/\tau_m\})^3$, from which the value of $\tau_m$ was determined from the curve that gave the best fit (Figure 3.14). In the range of membrane potentials near the resting potential where $m_\infty = 0$, $\tau_m$ is obtained from the approximately exponential shutting off of $P_{Na}$ on repolarization of the membrane as in the experiment of Figure 3.6B.*

Empirical values of $\tau_m$ are plotted in Figure 4.11.

D. Relaxation of $P_{Na}$ at different membrane potentials

The analytical complexity of the determination of the time course of m does not permit a simple experimental demonstration that $m_\infty$ and $\tau_m$ are single-valued functions of the membrane potential, as is presumed by the formal model for $P_{Na}$. However, the validity of these assumptions is tested in a straight-forward manner by comparing the predictions of the complete model of $I_{Na}$ (Equations 3.1, 3.8, and 3.9) with experimental observations of the ionic current in a double-step experiment as, in Figure 3.15. In this experiment $h_\infty$, $m_\infty$, $\tau_h$, and $\tau_m$ were determined for various membrane potentials by the graphical analysis of single-step records as described above. These empirical values were then used to predict the relaxation of the sodium current during a second step change of the membrane potential superimposed upon the initial step depolarization. Neglecting the first 50 microseconds following the potential change, during which time the records are complicated by the capacitative current and the slow stabilization of the amplifiers, there is very satisfactory agreement between the predicted and observed ionic current. This agreement strengthens a confidence that this model will accurately predict $P_{Na}$ for any variation of the membrane potential.

---

* A systematic variation in the time constant of the shutting off of $P_{Na}$ observed in the experiments of Fig. 2.17 is not expected from the model, and it is an open question whether this effect indicates an error in the control of the membrane potential, or a deficiency of the model.

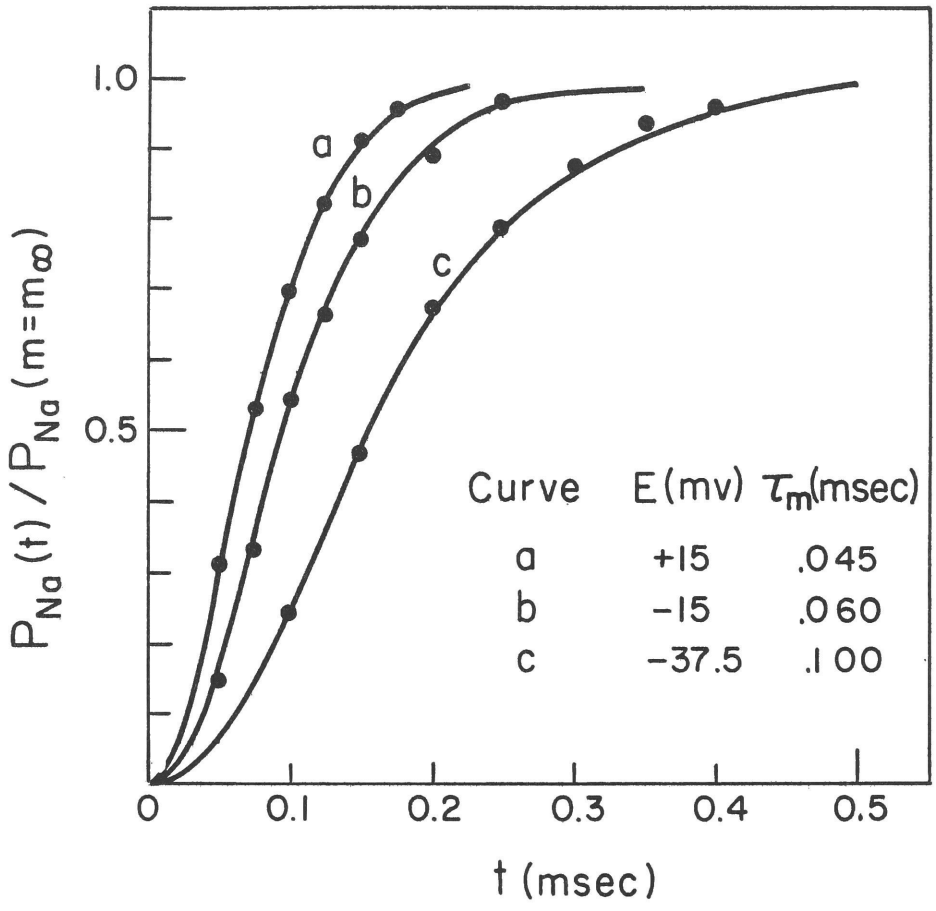


Figure 3.14: Determination of $\tau_m$. Data from curves c, d, and e of Figure 3.12. Here is plotted the ratio of the $P_{Na}$ observed at some early time to the value of $P_{Na}$ expected at that time if m were $m_\infty$ (i.e., the value of $P_{Na}$ along the extrapolated straight lines in Figure 3.12). The value of $\tau_m$ was then determined by fitting a smooth curve of the form $(1 - \exp\{-t/\tau_m\})^3$ to the experimental points, yielding the values cited in the figure.

Figure 3.15: Comparison of the observed ionic current with that predicted from the formal model of $P_{Na}$ in a double-step experiment. This comparison constitutes a test of the assumption that $m_\infty$ and $\tau_m$ are single-valued functions of $E$ by examining the relaxation of $m$ from an initially large value to its steady-state value during the second step. Graphical analysis of the records of $I_i$ during single-step depolarizations yielded the following empirical values for the parameters describing the variation of $P_{Na}$:

| E(mv) | $m_\infty$ | $\tau_m$(msec) | $h_\infty$ | $\tau_h$(msec) |
|---|---|---|---|---|
| -15 | .90 | .075 | 0 | 0.57 |
| -37.5 | .57 | .135 | 0 | 1.40 |
| -45 | .37 | .180 | 0 | 2.58 |

$P_{Na}$ was $2.3 \times 10^{-9}$ cm$^3$ sec$^{-1}$ and $E_{Na}$ was 45 mv. Equations 3.8, 3.9, 3.1, and 2.5 were then solved to predict $I_{Na}$ during the two double-step experiments. The membrane was initially hyperpolarized at $E_o$ = -105 mv for 40 msec; then at $t = 0$ the membrane was depolarized to -15 mv for .27 msec, and then repolarized to -45 mv (left) or to -37.5 mv (right). At the end of the step depolarization to -15 mv, $m$ was .88 and $h$ was .60. Under the conditions of the experiment, the variation of $I_K$ was negligibly small, and the predicted values of $I_{Na}$ were plotted (points) with respect to the appropriate step of $I_L$ as a baseline. Tracings of the experimental records are shown as the heavy curves. The severe attenuation of the observed instantaneous currents is qualitatively accounted for by the failure of the control system to stabilize the membrane potential to a new value instantaneously (Appendix II). Node 6; 20°C.

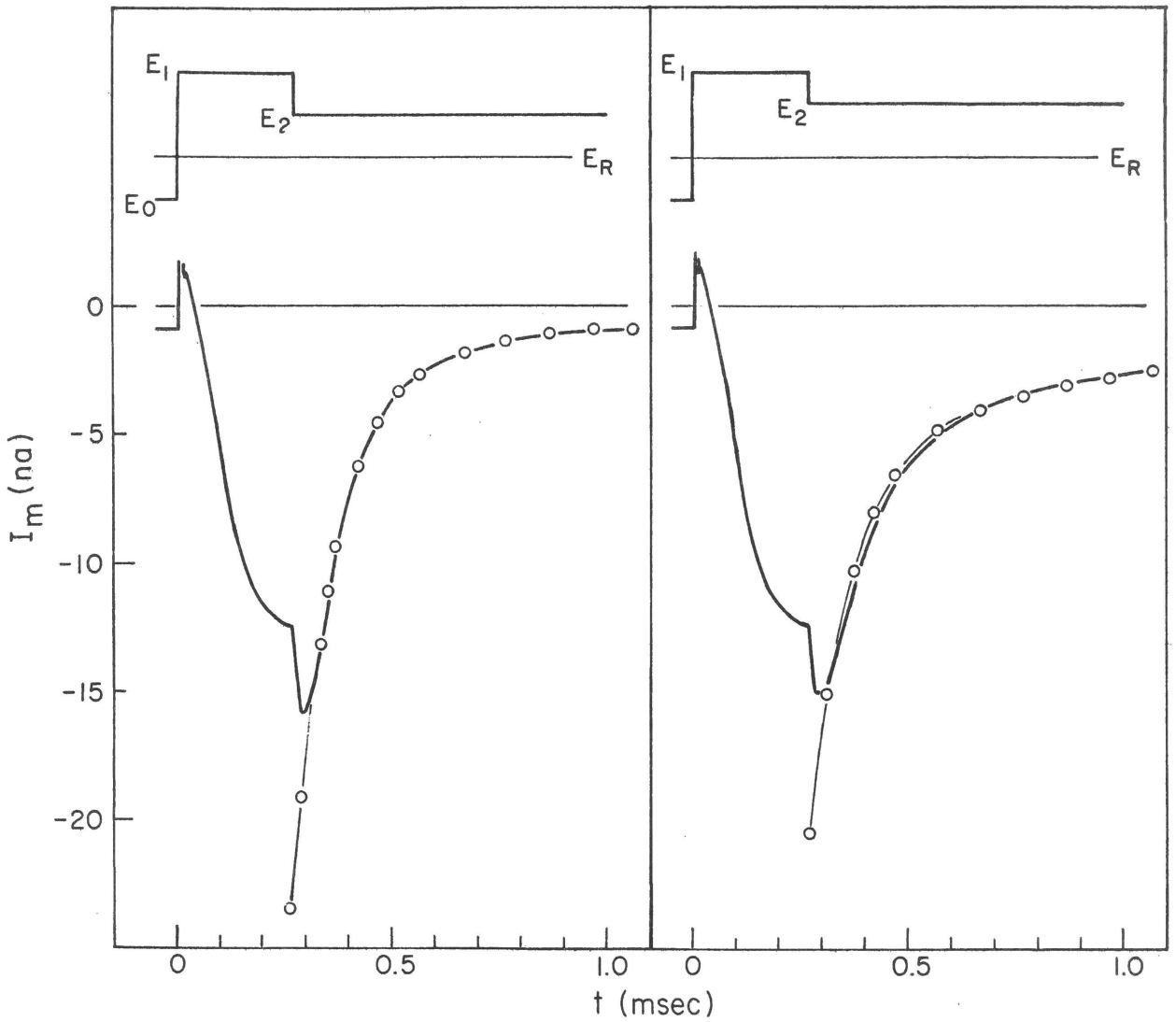
E1
E2
ER
E0
E1
E2
ER
0
-5
-10
-15
-20
Im (na)
0
0.5
1.0
0
0.5
1.0
t (msec)

## Kinetics of the Potassium Conductance Change

### A. General description

The time course of the increase in potassium conductance during a step depolarization is a smooth S-shaped curve approaching a steady value ($g_{k\infty}$) that is maintained for the duration of the depolarization. As a function of membrane potential, $g_{k\infty}$ increases with depolarization to a maximum value, $\bar{g}_K$ (Figure 2.9 B). However, the rate at which $g_K$ approaches $g_{K\infty}$ does not approach a maximum value at large depolarization, but continues to be more rapid the greater the depolarization.

The time course of the recovery of $g_K$ to its resting value upon repolarization is best demonstrated by an experiment like that devised by Frankenhaeuser (1962) to avoid the complications associated with the potassium "tail" discussed on page 45 . In this experiment, (Figure 3.16 A) the membrane was depolarized to $E = E_{Na}$ and held at this potential until $I_K$ reached its steady value, then the membrane potential was stepped back to the resting potential for various lengths of time, whereupon the membrane was again depolarized to $E = E_{Na}$. The initial value of $I_K$ for the second depolarization was then used to calculate $g_K$ at that instant (Figure 3.16 B). These values then effectively map out the time course of the recovery of $g_K$ at $E = E_R$. An exponential curve accurately describes the experimental points, indicating that the recovery of $g_K$ begins without any delay upon repolarization.

### B. Formal description of the temporal variations of the potassium conductance

Whereas the exponential recovery of $g_K$ could be described by a variable obeying a first order rate equation, the very significant delay in the turning on of $g_K$ in response to depolarization would require a higher order equation. This difficulty is again avoided by employing the formal model for $g_K$ developed for the squid axon (Hodgkin and Huxley, 1952 d), in which it is assumed that $g_K$ is proportional to the fourth power of a variable (n) that follows a first order rate equation: that is,

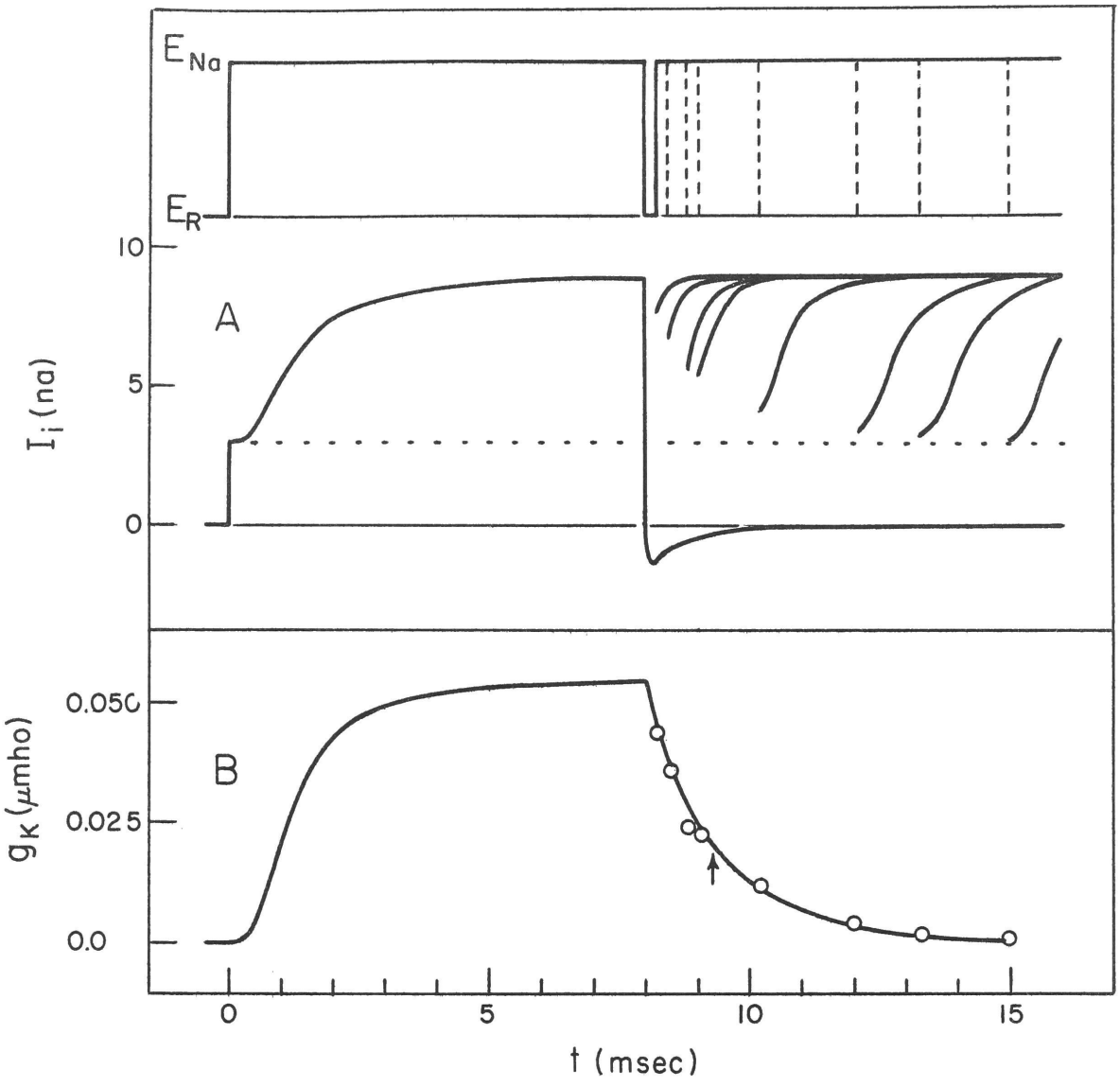


Figure 3.16: Recovery of the potassium conductance change. Two 8 msec long depolarizing pulses to $E = E_{Na} = 45$ mv were applied in succession and the interval between the pulses was varied. Tracings of several records are shown in the center figure; the step of $I_L$ is shown as a series of dots. The initial value of $I_K$ ($I_K = I_i - I_L$) at the onset of the second pulse was used to calculate the instantaneous value of $g_K$ at that time according to Equation 2.8, with the assumption that $E_K$ was - 75 mv. These values of $g_K$ are plotted in the lower figure together with the time course of $g_K$ during the first pulse. A smooth curve of the form $(\exp\{-t/\tau\})$, where $\tau = 1.3$ msec (indicated by small arrow), was fitted to the points describing the recovery of $g_K$. This preparation showed a large transient of inward (presumably sodium) current when the membrane was repolarized after the first pulse, cf. Figure 2.8 A. Node 15; 23°C.

$$g_K = \bar{g}_K n^4 \tag{3.11}$$

$$\dot{n} = \alpha_n(1 - n) - \beta_n n \tag{3.12}$$

where the constant $\bar{g}_K$ is the maximum possible potassium conductance and $n^4$ is the fraction of $\bar{g}_K$ that is turned on at any instant. The variable $n$ is a dimensionless parameter, varying between zero and one, which obeys the first order rate equation (3.12) in which the rate constants are single-valued functions of the membrane potential.

The solution of Equation 3.12 at constant membrane potential is

$$n = n_\infty - (n_\infty - n_o) \exp\left\{ - t/\tau_n \right\} \tag{3.13}$$

where

$$n_\infty = \frac{\alpha_n}{\alpha_n + \beta_n} \tag{3.14}$$

and

$$\tau_n = \frac{1}{\alpha_n + \beta_n} \tag{3.15}$$

Application of the formal model for $g_K$ to the experimental observations is illustrated in Figure 3.17 where the time course of $g_K$ measured in the experiment of Figure 3.16 is described in terms of the variation of the parameter $n$.

1. The relation between $n_\infty$ and membrane potential: In the preceding chapter, it was observed (Figure 2.9 B) that the steady-state value of $g_K$ increases with the membrane depolarization to a limiting value. The constant $\bar{g}_K$ was taken as this limiting value of $g_K$, and the value one was assigned to $n$, for those levels of membrane potential at which this limiting value was attained. At intermediate levels of depolarization, $n_\infty$ was determined by the relation $n_\infty = (g_{K\infty} / \bar{g}_K)^{1/4}$. In the range of membrane potentials near the resting potential $n_\infty$ was determined from experimental observations such as those illustrated in Figure 3.8, by comparing log-log plots of the time course of $I_K$ (proportional to $g_K$) at

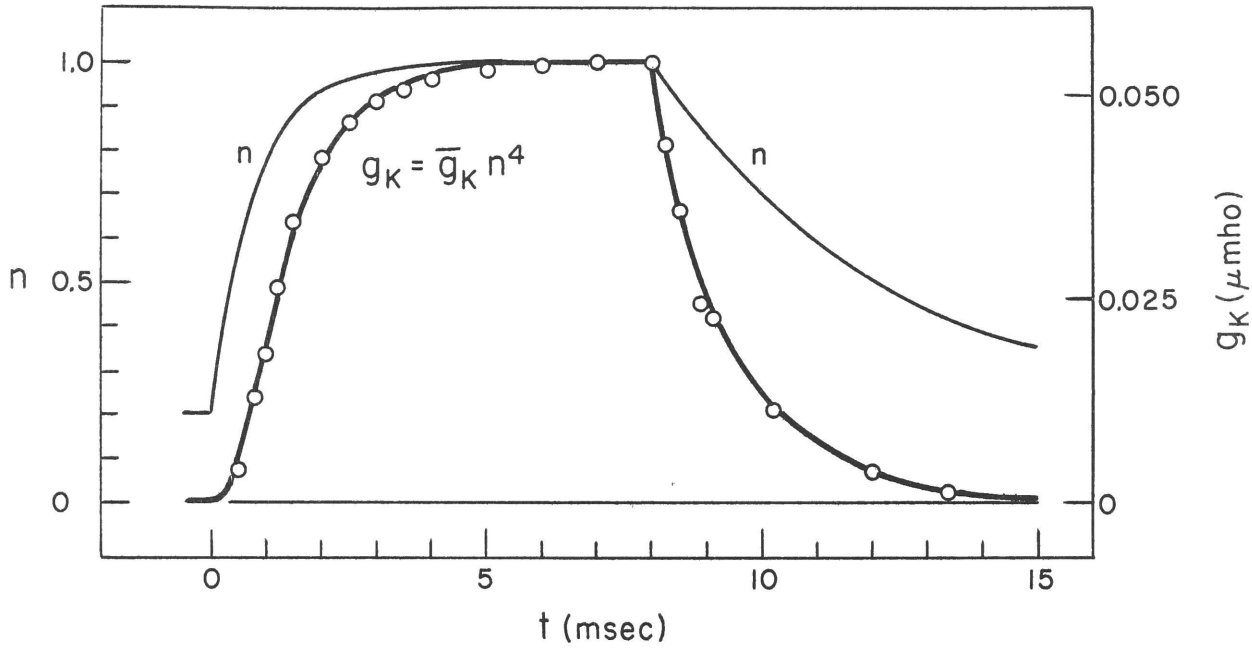


Figure 3.17: Quantitative description of the temporal variation of $g_K$ observed in the experiment of Figure 3.16 in terms of the mathematical model of $g_K$, i.e. $g_K = \bar{g}_K n^4$. The time course of the parameter n was calculated from Equation 3.13 using the following empirical steady-state values and time constants:

| E (mv) | $n_\infty$ | $\tau_n$ (msec) |
|---|---|---|
| 45 | 1 | 1.1 |
| - 75 | 0.2 | 4.1 |

$\bar{g}_K$ was .053 $\mu$mho. Experimental values of $g_K$ are shown as circles.

$E = E_{Na}$ for each of the initial conditions with a family of log-log plots of Equation 3.13 for different values of $n_o$, $n_\infty$ being 1 at $E_{Na}$. In this case, the value of $n_o$ was determined by the best fit, and was taken as the value of $n_\infty$ at the preceding level of membrane potential.

Empirical values of $n_\infty$ are plotted against membrane potential in Figure 3.18.

2. The relation between $\tau_n$ and membrane potential: The values of $\tau_n$ at various depolarizations were obtained by the best fit of the log-log plot of $I_K$ (proportional to $g_K$) employed in the estimation of $I_K$ by the scaling procedure (page 56) to the appropriate master curve of the log-log plot of the Equation 3.13. The master curve was calculated from previously determined values of $n_o$ and $n_\infty$. Generally, $I_K$ was determined by the scaling procedure in experiments where the initial condition was strong preceding hyperpolarization; for this initial condition $n_o$ was zero.

In a few experiments in which the pertinent data were available, values of $\tau_n$ at membrane potentials near the resting level were obtained by application of Equation 3.11 and 3.13 to the observed recovery of $g_K$ upon repolarization of the membrane. More often, however, these data were not available. When required for computations, values for $\tau_n$ were estimated from interpolation of the $\alpha_n$ and $\beta_n$ curves on the assumption that these functions behaved like $\alpha_n$ and $\beta_n$ in the mathematical model for the squid axon (Hodgkin and Huxley, 1952 d). Any errors resulting from this interpolation will have little effect on any of the subsequent computations, since at these membrane potentials $I_K$ is very small.

Empirical values of $\tau_n$ are plotted against membrane potential in Figure 3.18 and the interpolated values are indicated by the broken curve.

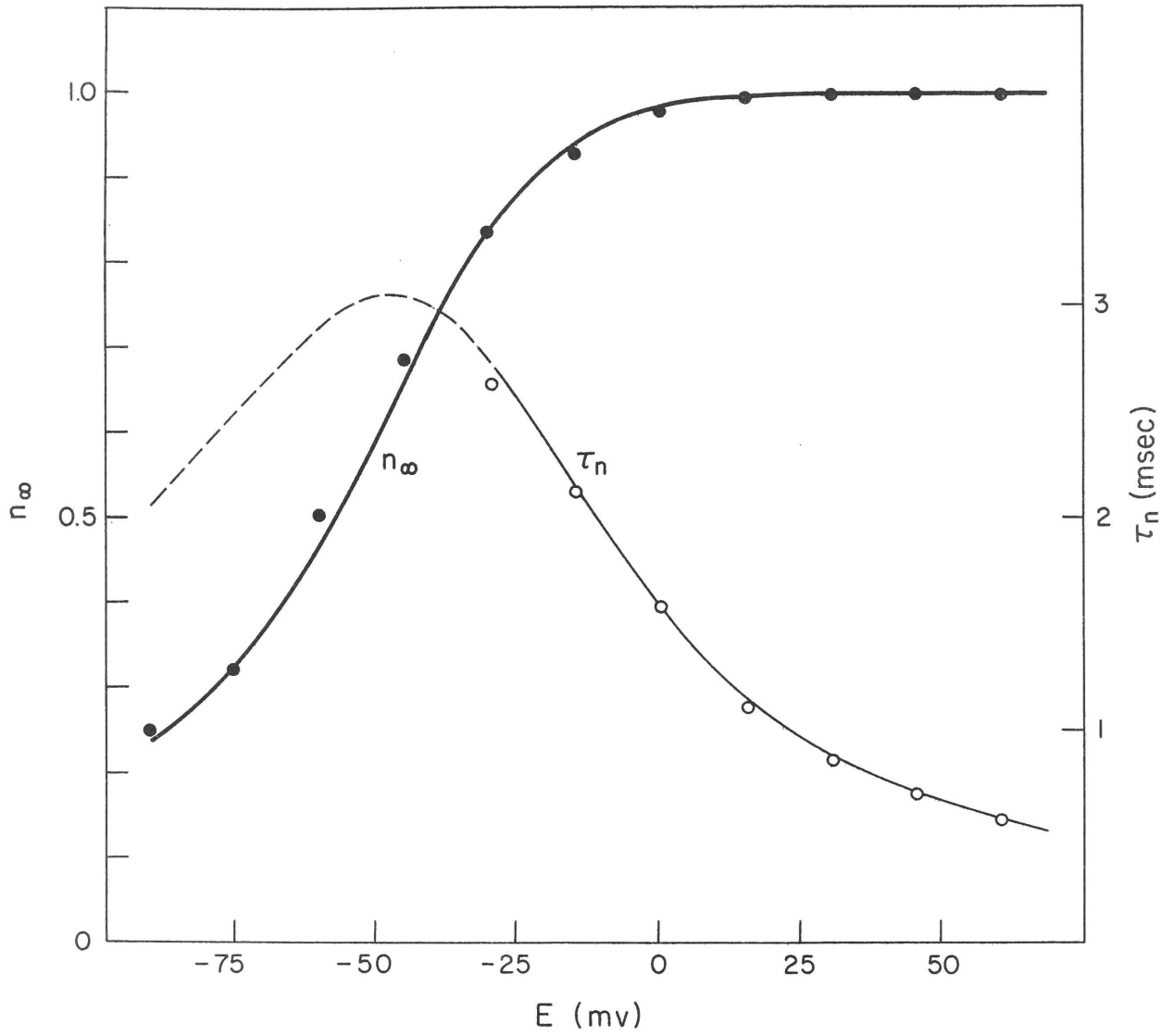


Figure 3.18: Steady-state values ($n_\infty$) and time constants ($\tau_n$) as a function of membrane potential. The empirical values are represented in theoretical computations by the smooth curves which are solutions of Equations 3.14 and 3.15 using the approximating functions for $\alpha_n$ and $\beta_n$ (Figure 3.19). No data were obtained on this preparation to determine $\tau_n$ over the range of membrane potentials indicated by the dashed curve.

## Summary

A. The Mathematical Model of the Nodal Membrane

The following equations predict the total membrane current of a node as a function of membrane potential and time. These are:

$$I_m = C\dot{E} + I_i \tag{1.1}$$

$$I_i = \bar{P}_{Na} m^3 h [N_a]_o \frac{F^2 E}{RT} \cdot \frac{\exp\{(E - E_{Na})F/RT\} - 1}{\exp\{EF/RT\} - 1} + \bar{g}_K n^4 (E - E_K) + \bar{g}_L (E - E_L) \tag{3.16}$$

$$\dot{m} = \alpha_m (1 - m) - \beta_m m \tag{3.2}$$

$$\dot{h} = \alpha_h (1 - h) - \beta_h h \tag{3.3}$$

$$\dot{n} = \alpha_n (1 - n) - \beta_n n \tag{3.12}$$

Equation 1.1 expresses the fundamental assumption concerning the electrical properties of the nerve membrane, namely that the total membrane current is the sum of the displacement current associated with the membrane capacity and the current carried by the movement of ions through the membrane. Equation 3.16 is a quantitative formulation of the ionic hypothesis as applicable to the nodal membrane, in which the ionic current is the sum of three components, a sodium current, a potassium current, and a leakage current. This equation relates each component of the ionic current to the permeability of the membrane to that ion and its electro-chemical driving force. The sodium permeability is described by the constant $\bar{P}_{Na}$ and the dimensionless variables m and h which obey the subsidiary rate equations 3.2 and 3.3. The potassium permeability is approximated in terms of the potassium conductance described by the constant $\bar{g}_K$ and the dimensionless variable n which obeys the rate equation 3.12. The empirical rate constants in these equations depend only on the instantaneous value of the membrane potential and are relatively simple functions of the membrane potential (Figure 3.19).

TABLE 3.1

Empirical constants derived from the voltage-clamp data of node 7

| CONSTANT | VALUE PER NODE | PAGE REFERENCE |
|---|---|---|
| $C$ | 2.2 μμf | 23 |
| $\bar{P}_{Na}$ | $3.9 \times 10^{-9}$ cm$^3$ sec$^{-1}$ | 69 |
| $\bar{P}_{Na}[Na]_o F^2/RT$ | 1.68 μ mho | |
| $E_{Na}$ | 47 mv | 32 |
| $\bar{g}_K$ | 0.130 μ mho | 71 |
| $E_K$ | -75 mv | 45 |
| $\bar{g}_L$ | 0.025 μ mho | 48 |
| $E_L$ | -75 mv | 48 |

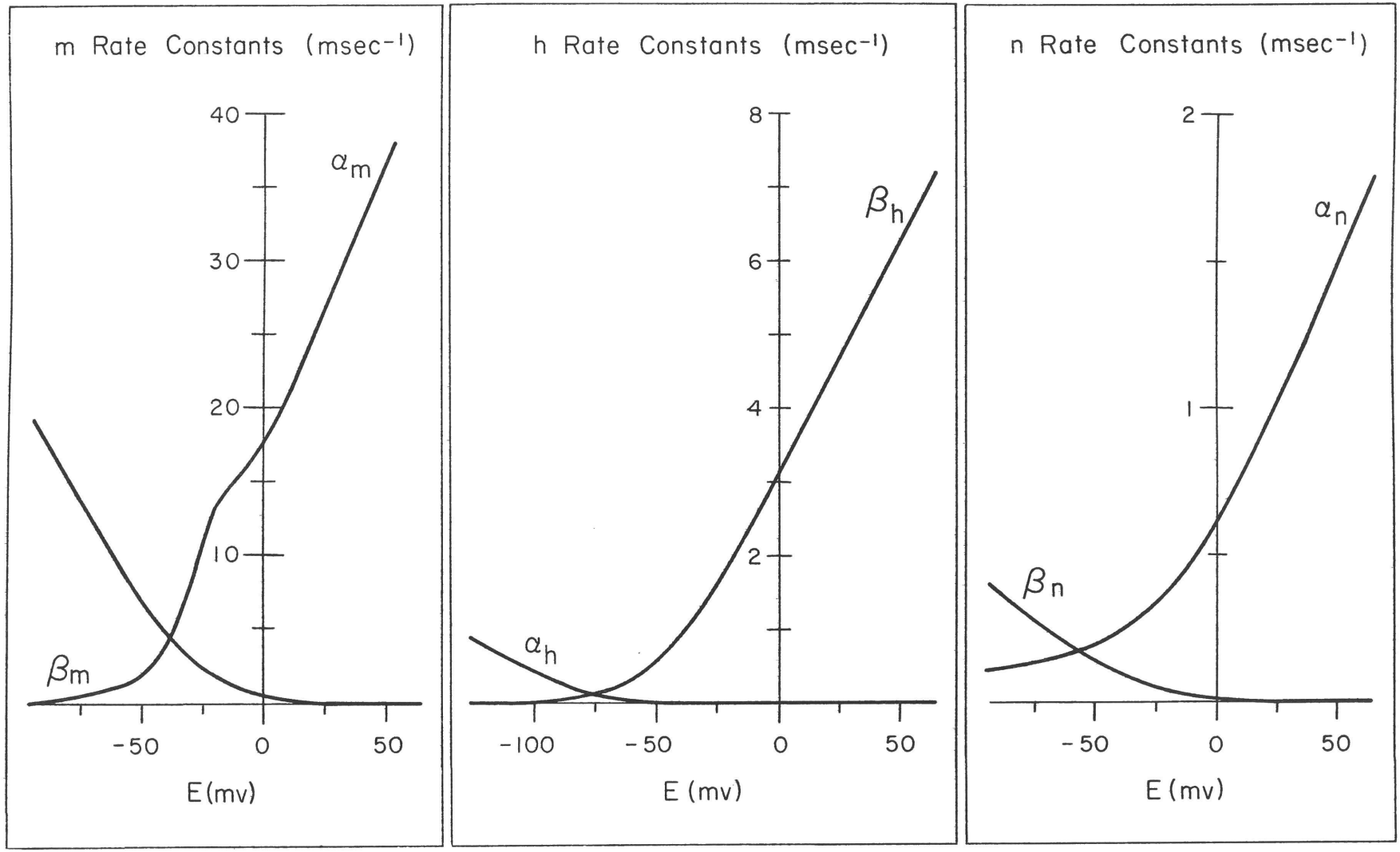


Figure 3.19: Graphs showing the voltage dependence of the rate constants of the parameters m, h, and n. These curves, the equations for which are tabulated in Appendix I, are based on and are the equivalent representation of the empirically determined steady-state values and time constants of the parameters. Node 7; 22°C.

# Chapter IV

## MATHEMATICAL SYNTHESIS OF THE ELECTRICAL BEHAVIOR OF THE NODE

The relations between the ionic currents of the nodal membrane and the membrane potential are represented by the quantiative mathematical model described in the previous chapter. Although the model was developed entirely from voltage-clamp measurements, nonetheless it can be applied to other experimental conditions by computing solutions of the equations for boundary conditions appropriate to the experimental constraints. The results of such computations then provide the basis for interpreting the normal excitation and response of the node in terms of the properties of the permeability changes as revealed by the analysis of the voltage-clamp data.

### Membrane Currents During a Voltage Clamp

In order to check the accuracy with which the empirical constants had been determined the equations were solved to regenerate the original voltage clamp data. The boundary conditions appropriate to the voltage clamp constraint are simply that $E$ is a step-wise change to a maintained value, hence $I_m = I_i$ (neglecting the brief surge of capacity current at the beginning of the step). When $E$ is constant, the $\alpha$'s and $\beta$'s are also constant, hence the rate equations for $m$, $h$, and $n$ are solved directly as previously described (Equations 3.8, 3.9 and 3.13). The total ionic current is then calculated according to Equation 3.16.

Comparison of the computed ionic currents with those observed experimentally provided a very sensitive test of the empirical functions approximating the dependence of the rate constants upon membrane potential. Whenever sufficient computer time was available, these functions were adjusted for a better fit of the computed $I_i$ than was obtained with the rate

constants estimated by graphical analysis of the voltage clamp records. This extra step of refining the approximating functions for the rate constants was done for nodes 4, 7, and 11C. Figures 4.1 and 4.2 illustrate the degree of fit that was achieved after two cycles of refinement. In every case, however, the small discrepancies between the computed ionic currents and those observed experimentally on the same node produced no significant distortion of the predicted action potential and only minor error in the predicted threshold.

## The Action Potential of the Node

Accurate measurements of the action potential of the node are obtained only when the longitudinal current within the fiber is under experimental control by the current-clamp constraint (page 23). The boundary condition on Equation 1.1 appropriate to this constraint is that $I_m$ is equal to the stimulating current applied from an external source, and the equations are solved for the time course of the membrane potential. With this boundary condition the nerve model becomes a system of four simultaneous, first-order, nonlinear differential equations. Such a system cannot be solved in terms of elementary functions, but requires a point by point numerical integration. Numerical solution of these equations was programmed for the IBM 650 digital computer. The numerical method is described in Appendix I.

An action potential predicted by the model using empirical constants derived from voltage-clamp measurements on a single node is compared with the experimentally observed action potential of the same node in Figure 4.3 For both the experimental and computed action potential, the membrane was hyperpolarized preceding the stimuli. In the experimental case the stimuli were short (80 μsec) pulses of constant current; whereas in the computed case the stimuli were instantaneous displacements of the membrane potential, which were equivalent to very much shorter and

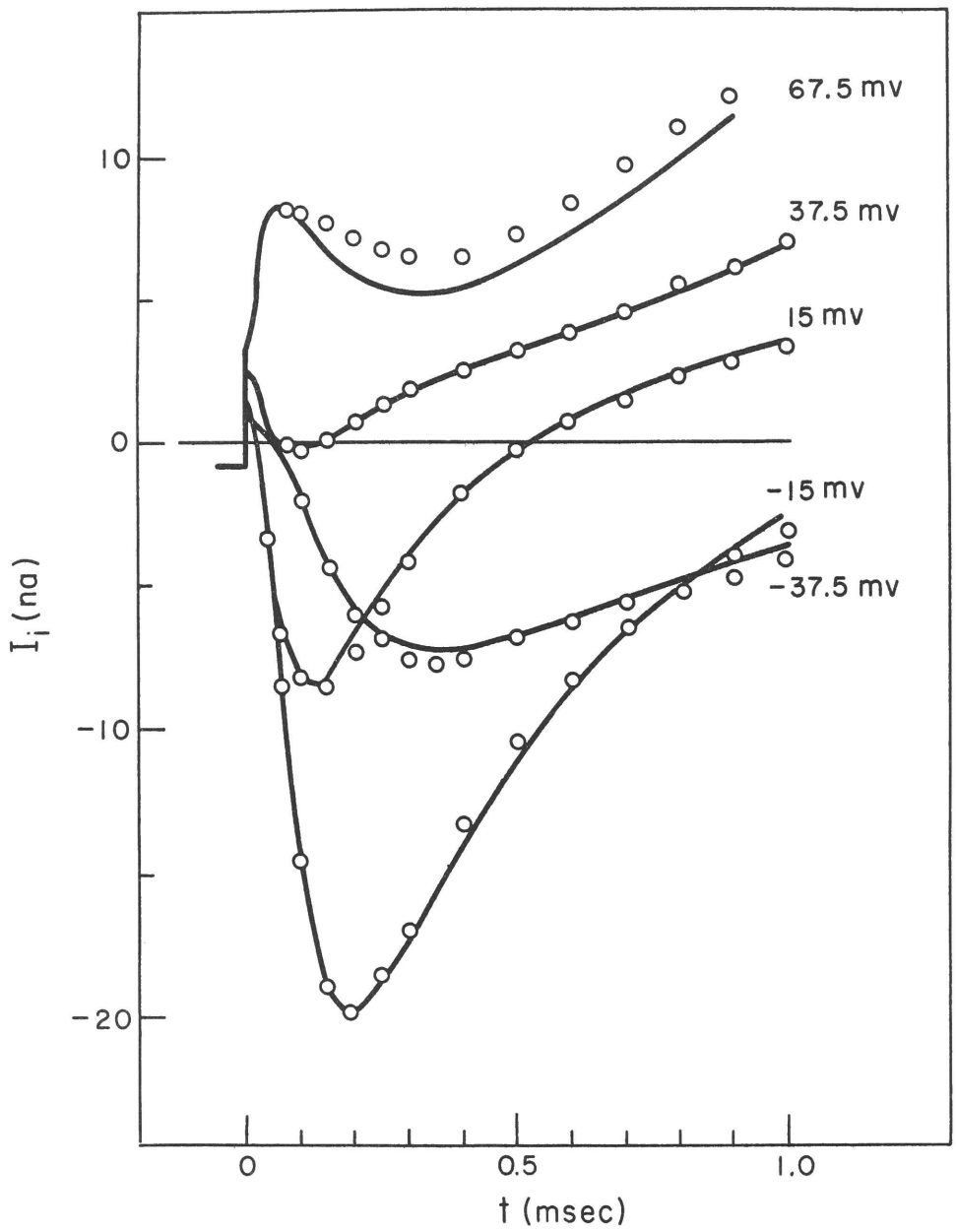


Figure 4.1: Comparison of the ionic currents calculated from the mathematical model with those with those measured in the voltage-clamp experiment. Smooth curves were calculated from Equations 3.16, 3.8, 3.9, and 3.13 using empirical constants for Node 7 (Table 3.1 and Figure 3.19). Experimental values of $I_i$ (circles) are from the same node. An initial hyperpolarization at E = - 105 mv ($h_o$ = 0.95) for 40 msec preceded each depolarization.

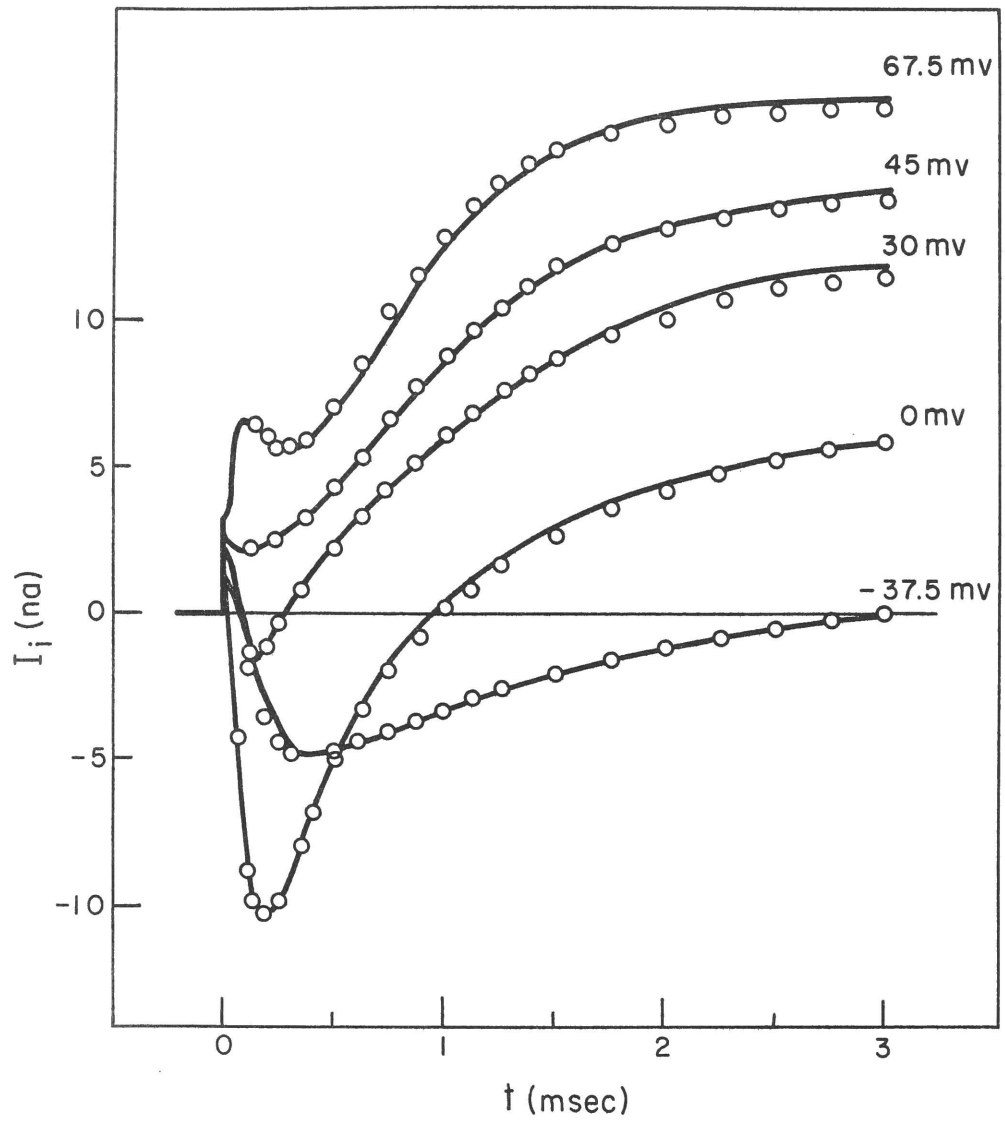


Figure 4.2: Comparison of calculated ionic currents with experimental observations. Smooth curves were calculated from Equations 3.16, 3.8, 3.9, and 3.13 using empirical constants for Node 11 C (Appendix IV). Experimental values of $I_i$ (circles) are from the same node. The membrane was in the steady state at $E_R$ preceding each depolarization ($h_o = 0.51$).

stronger current stimuli. (This instantaneous displacement was used only because it is more conservative of computer time than a pulse of finite duration.) In each case $I_m$ was held to zero after the stimulus.

This comparison (Figure 4.3) shows that the mathematical model gives a fairly accurate prediction of the amplitude and wave form of the action potential, the threshold as measured by the membrane potential during the latency of the spike, and the sub-threshold response. Similar comparisons for other nodes are shown in Figure 4.4. The generally good agreement between the predicted and observed action potentials demonstrates the resolving power of the analysis of the voltage-clamp measurements when sufficient data is obtained on an individual node.

A. The sequence of events during an action potential

When the equations are solved for the action potential, solutions for the time courses of the permeability changes and of the components of the ionic current are obtained simultaneously. These results (Figure 4.5) precisely describe the sequence of events that generate the action potential.

At each instant during the action potential, the membrane potential tends toward that value (dependent on $P_{Na}$, $g_K$, and $\bar{g}_L$) at which the inward sodium current ($I_{Na}$) and the outward potassium currents ($I_K + I_L$) would be in balance. But the actual membrane potential cannot achieve that value instantaneously because of the membrane capacitance, with the result that there is an imbalance of the components of the ionic current which determines the instantaneous rate of change of the membrane potential; i.e., $I_i = - C\dot{E}$. In effect, the charging of the membrane capacity causes the membrane potential to lag behind the instantaneous value of the intrinsic electromotive force of the membrane. During the action potential of the frog node the lag is always less than 100 μsec, and even in a hypothetical node with no capacity the action potential would not be appreciably different from the normal one, since the time course of the action potential is determined primarily by the kinetics of the permeability changes.

Figure 4.3: Comparison of the nodal action potential and subthreshold response observed experimentally (upper curves) with those predicted by the mathematical model of the node (lower curves). The theoretical curves are numerical solutions of the system of Equations 1.1, 3.16, 3.2, 3.3, and 3.12 (numerical method described in Appendix I) using empirical constants for Node 7 (Table 3.1 and Figure 3.19). Initial condition was a preceding hyperpolarization at $E = -105$ mv for 40 msec ($h_o = 0.95$). In the experimental case the stimuli were pulses of constant current ($I_m$) of approximately 1.6 na for 75 μsec. In the computations the stimuli were instantaneous displacement to $E = -33.8$ mv (suprathreshold) and $E = -34.2$ mv (subthreshold). The interruptions on the fast rising phases in the experimental records result from the chopping of the oscilloscope beam.

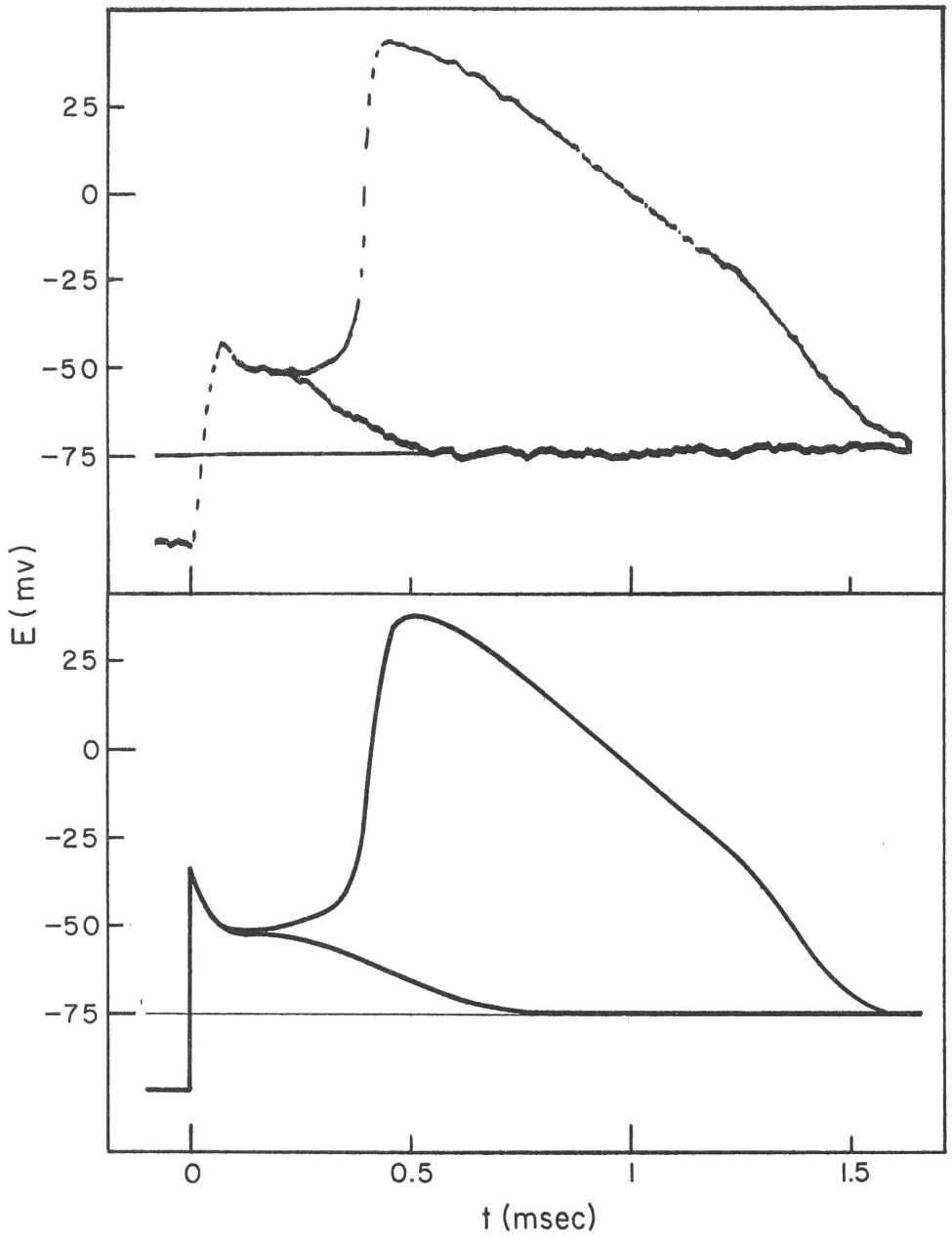
25
0
-25
-50
-75
E (mv)
25
0
-25
-50
-75
0
0.5
1
1.5
t (msec)

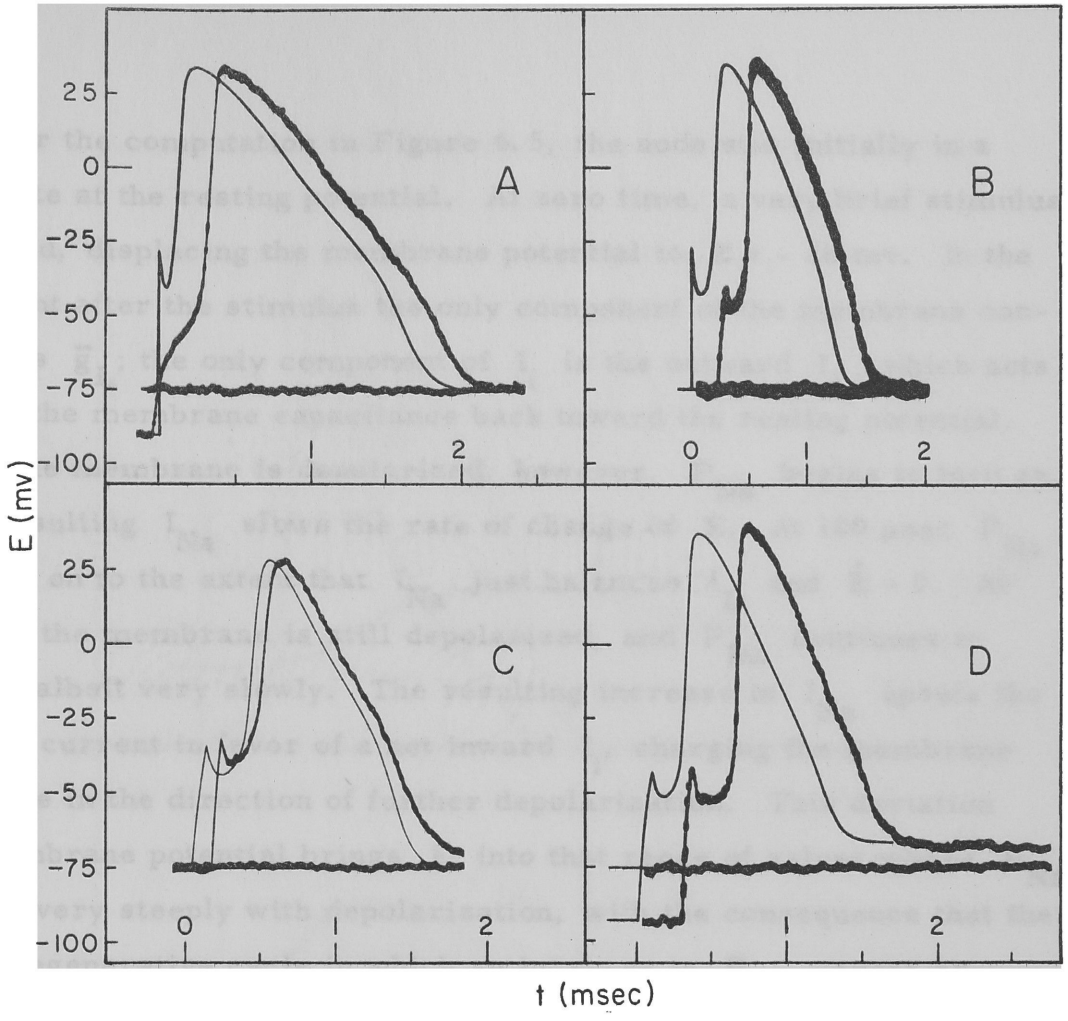


Figure 4.4: Comparison of experimentally observed action potentials (noisy records) with those predicted from the mathematical model (smooth curves) using the empricial constants (Appendix IV) derived from the voltage-clamp data from the same node.

| Figure | | Initial condition | Stimulus |
|---|---|---|---|
| A: Node 4 | experimental: | $E_o$ = - 90 mv | $I_m$ = 0.5 na for 350 μsec |
| | theoretical: | $h_o$ = .80 | displacement to E = -28 mv |
| B: Node 8 | experimental: | resting potential | $I_m$ = 1.5 na for 80 μsec |
| | theoretical: | $h_o$ = .57 | displacement to E = -28 mv |
| C: Node 11C | experimental: | resting potential | $I_m$ = 1.9 na for 75 μsec |
| | theoretical: | $h_o$ = .51 | $I_m$ = 1.53 na for 100 μsec |
| D: Node 12 | experimental: | $E_o$ = - 90 mv | $I_m$ = 1.6 na for 75 μsec |
| | theoretical: | $h_o$ = .86 | $I_m$ = 1.25 na for 100 μsec |

Rising phases of the experimental records were retouched.

For the computation in Figure 4.5, the node was initially in a steady state at the resting potential. At zero time, a very brief stimulus was applied, displacing the membrane potential to $E = -28$ mv. In the first instant after the stimulus the only component of the membrane conductance is $\bar{g}_L$; the only component of $I_i$ is the outward $I_L$, which acts to charge the membrane capacitance back toward the resting potential. Because the membrane is depolarized, however, $P_{Na}$ begins to turn on, and the resulting $I_{Na}$ slows the rate of change of $E$. At 100 μsec $P_{Na}$ has turned on to the extent that $I_{Na}$ just balances $I_L$ and $\dot{E} = 0$. At this time, the membrane is still depolarized, and $P_{Na}$ continues to increase, albeit very slowly. The resulting increase in $I_{Na}$ upsets the balance of current in favor of a net inward $I_i$, charging the membrane capacitance in the direction of further depolarization. This deviation of the membrane potential brings $E$ into that range of values where $P_{Na}$ increases very steeply with depolarization, with the consequence that there begins a regenerative cycle in which an increase in $P_{Na}$ causes an increase in $I_{Na}$, which causes further depolarization, which in turn causes an increase in $P_{Na}$, etc. As the depolarization continues, however, $I_{Na}$ decreases because the driving force on sodium decreases as $E$ approaches $E_{Na}$, concurrently the outward current increases, until, at the peak of the action potential, the inward and outward components of $I_i$ are balanced. By this time, the outward current is slightly enhanced by an increase of $g_K$. The state of high sodium permeability is transient, however, as a consequence of the inactivation process. As $P_{Na}$ decreases the balance of currents is upset in favor of the outward current $(I_K + I_L)$, and the membrane potential begins to fall back toward the resting potential. Throughout the major part of the falling phase $P_{Na}$ is being shut off by inactivation but, at the knee of the action potential, the decline in $P_{Na}$ is speeded up by the reversible shutting off of the activation process, and the membrane potential is quickly restored to the resting level. The membrane is not yet in a steady state, however, because of the inactivation of $P_{Na}$ accumulated

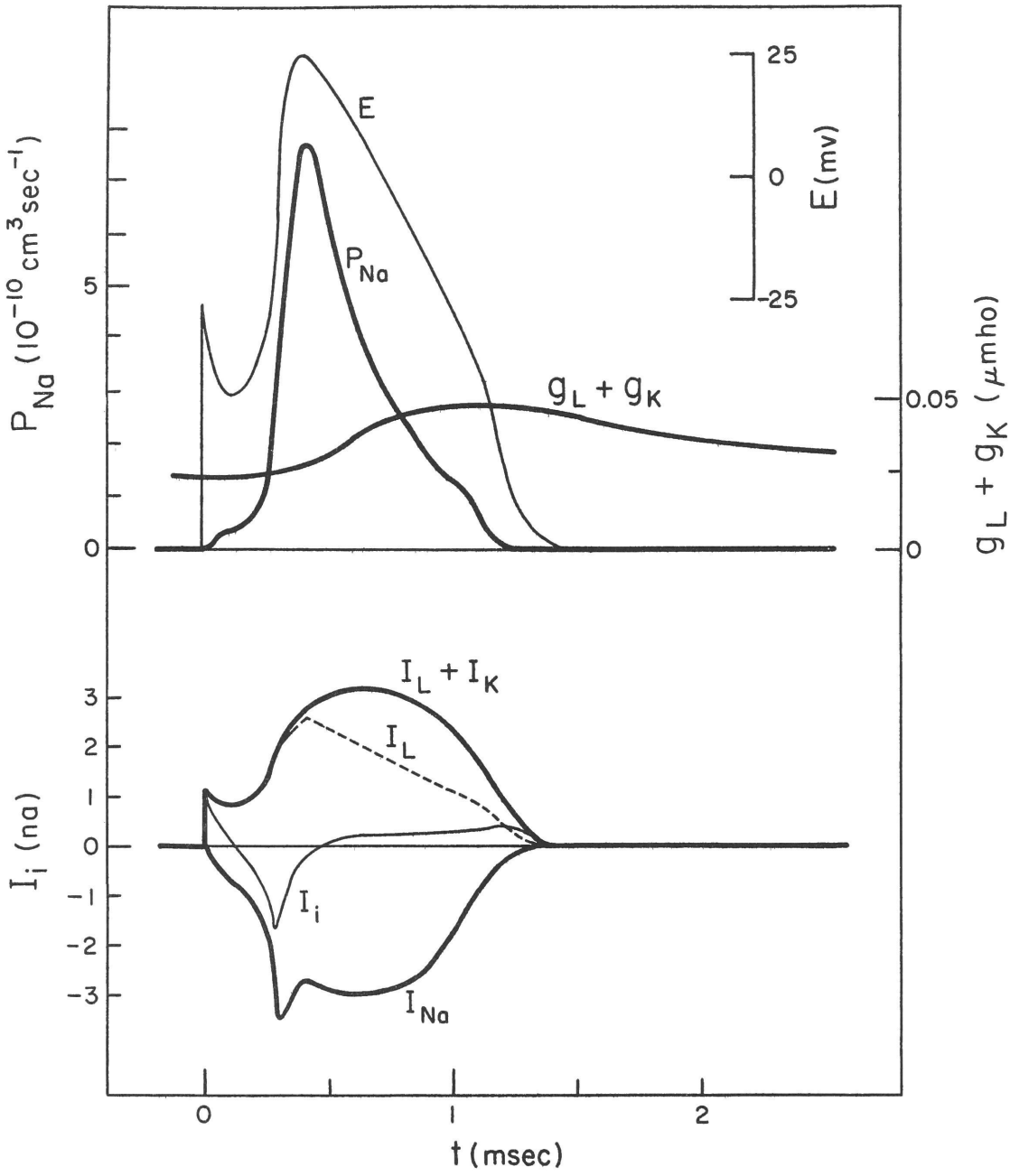


Figure 4.5: Theoretical computations of the sodium permeability change, of the potassium conductance change, and of the components of the ionic current during an action potential. Node 11C; the stimulus was an instantaneous displacement of the membrane potential to E = - 25 mv.

during the spike and because of the increase in $g_K$. Both of these recover to their steady-state values with time constants of a few milliseconds; during this recovery, the membrane is in the condition of relative refractoriness (see below).

Associated with the sequence of permeability changes during the action potential, there is a variation of the electrical impedance of the membrane. Measurements of the impendance change are compared with the predictions of the model in the next section.

The net result of the ionic currents during an action potential is that the fiber gains a small quantity of sodium ions and loses an equal quantity of potassium ions. Chemical measurements of the exchange of ions are compared with the predictions of the model in a later section.

B. Impedance change during the action potential

The time course of the impedance change of the action potential of a node has been measured by Tasaki and Mizuguchi (1949) and later by Tasaki and Freygang (1955), using a Wheatstone bridge driven by moderately high frequency alternating current. Analysis of the experimental results showed that the capacitance of the membrane remained essentially constant, but that the resistance of the membrane had dropped to less than a tenth of its resting value by the peak of the action potential, recovering to the resting value with a time course similar in form to that of the action potential.

To obtain a theoretical prediction of the resistance change from the model of the nodal membrane, we must define the sodium conductance of the membrane in a manner appropriate to this type of measurement taking into account the nonlinear relation between the instantaneous sodium current and the membrane potential. If the amplitude of the alternating current driving the bridge is sufficiently small and the frequency is sufficiently high that this current has no effect on the time course of $P_{Na}$, the

appropriate sodium conductance is then the slope conductance ($G_{Na}$) defined by

$$G_{Na} = \frac{\partial I_{Na}}{\partial E}$$

at constant $P_{Na}$. The slope conductance for sodium is different from the chord sodium conductance

$$g_{Na} = \frac{I_{Na}}{E - E_{Na}}$$

because of the nonlinear relation between sodium current and its driving force in the definition of $P_{Na}$.

The time course of $G_{Na}$ during an action potential can be determined from the computed time course of $P_{Na}$ by the relation

$$G_{Na} = P_{Na}[Na]_o \frac{F^2}{RT}\left(\frac{xy - z[y - z]}{y^2}\right)$$

where,

$$x \equiv \exp\left\{(E - E_{Na})F/RT\right\} - 1, \quad y \equiv \exp\left\{EF/RT\right\} - 1, \quad \text{and } z \equiv \frac{EF}{RT}.$$

Since the potassium and leakage currents are adequately described by a linear relation between current and driving force, the corresponding slope conductances are identical with the chord conductances, $g_K$ and $\bar{g}_L$, respectively.

The membrane resistance ($R_m$) is then calculated by the equation

$$R_m = G_m^{-1} = (G_{Na} + g_K + \bar{g}_L)^{-1}.$$

The time course of the variation in membrane resistance predicted by the model (Figure 4.6) is in general agreement with the results of Tasaki and Freygang, demonstrating that the resistance at the peak of the action potential was less than a tenth of the resting value, and that the time course of the recovery was approximately similar to that of the action potential.

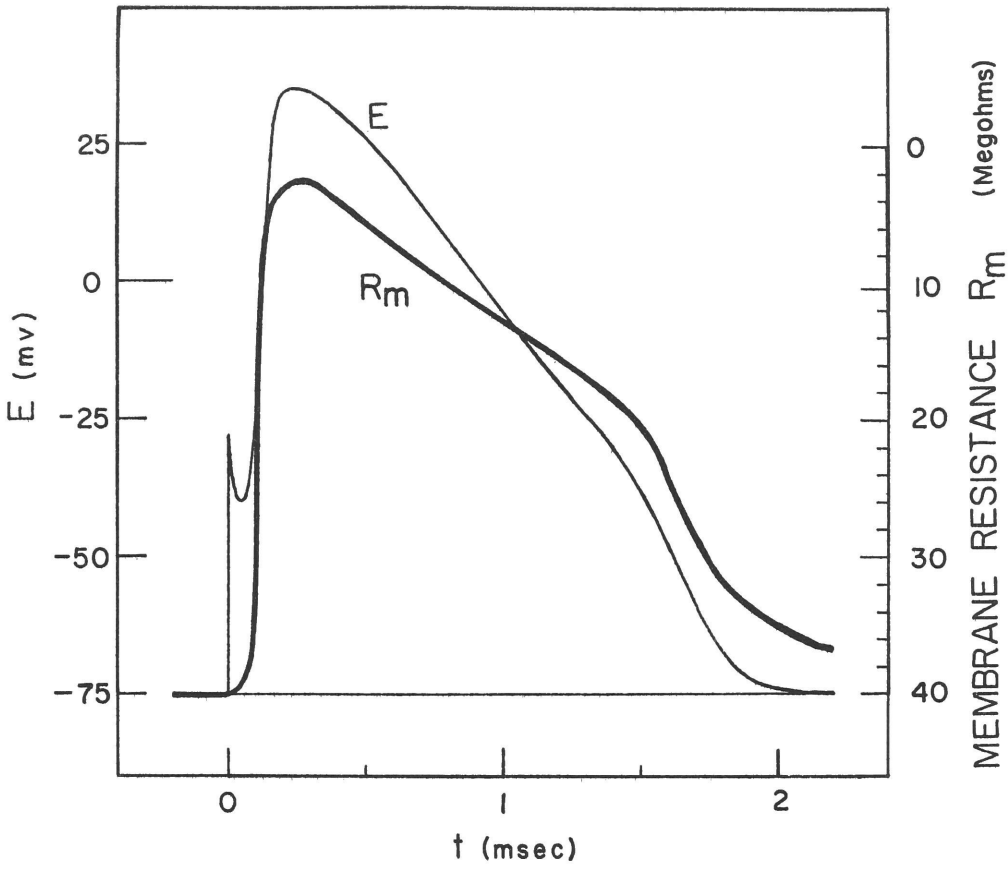


Figure 4.6: Theoretical computation of the time course of the membrane resistance ($R_m$) during an action potential (E). Node 4.

However, there is one point of substantial disagreement. In their experiments, Tasaki and Freygang were unable to detect a phase of low resistance following the spike. Such a phase is predicted by the model and corresponds to the slow recovery of $g_K$ turned on during the spike. Two possibel explanations for this discrepancy are:

1) The bridge method becomes very insensitive when the resistance approaches its resting value, because most of the a.c. current is shunted through the membrane capacitance;

2) Some nodes, in particular those showing prolonged action potentials, undergo only a very small change of $g_K$ in the voltage-clamp measurements. The predicted resistance change during the action potential of such a node follows the time course of the action potential very closely.

A phase of low resistance following the nodal action potential was detected in a very simple experiment (Figure 4.7), in which the action potential was measured (and computed) for a maintained constant current stimulus. It is observed that the membrane potential, after the spike, is only about half of the IR drop expected if the membrane resistance had returned to its resting value.

C. Refractoriness

The gradual recovery from refractoriness following an action potential, as measured by the amplitude of a second action potential, is adequantely predicted by the equations (Figure 4.8). The equations predict further that, although the action potentials initiated in a resting node are essentially all-or-none, the amplitude of the response initiated during the relative refractory period appears to be graded with the strength of the stimulus; more accurately, the response is smaller the longer the latency. The computations show that refractoriness in the node results primarily from inactivation of the sodium permeability during the spike, and that the gradual recovery from refractoriness reflects the slow recovery of $h$ at the resting potential, as

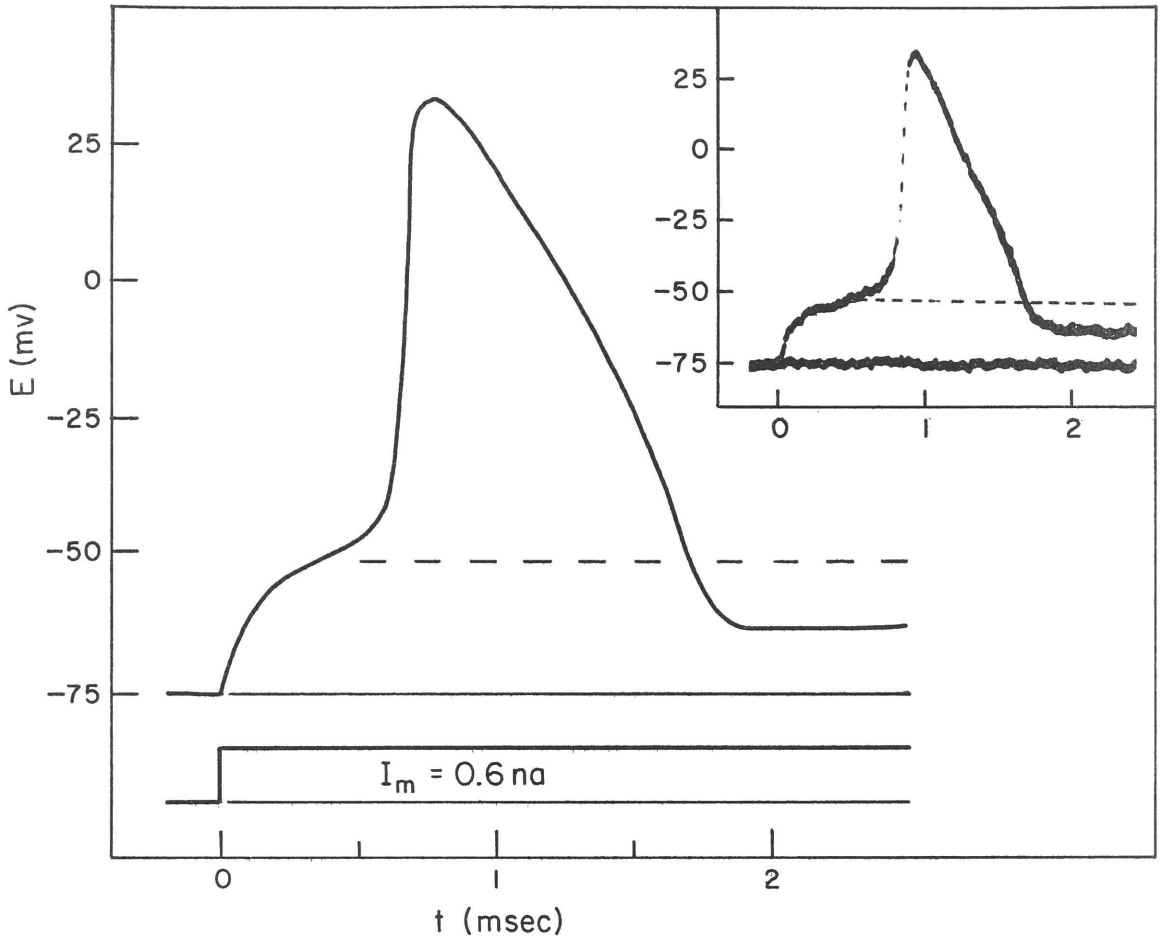


Figure 4.7: Computation of the time course of the membrane potential during a maintained constant current stimulus. The dashed line shows the displacement of the membrane potential expected if the membrane resistance remained constant at the resting value. Node 8. Inset: record of the membrane potential during a constant outward current of .5 na; the dashed line is the membrane potential expected if the resistance had remained constant. Node 9.

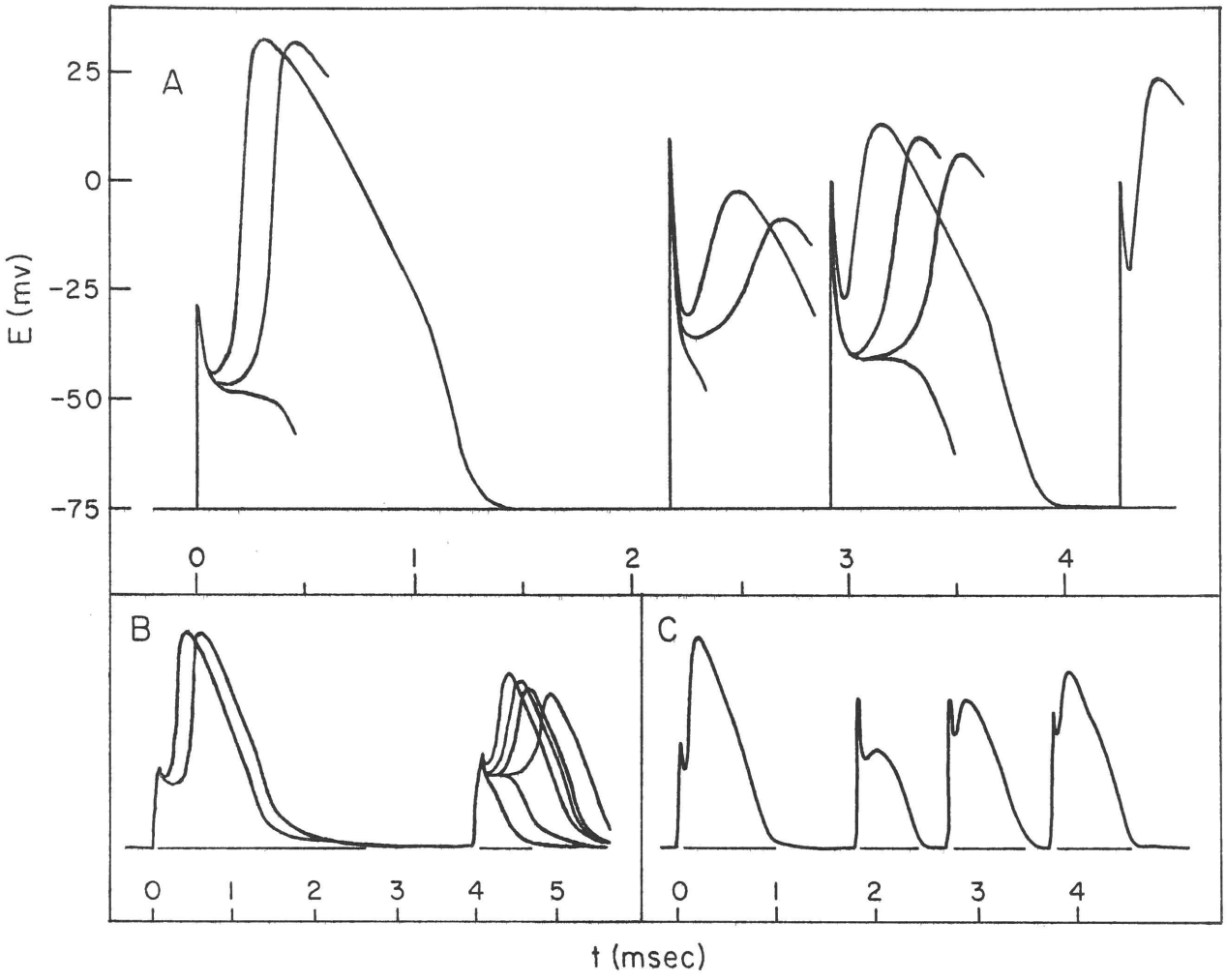


Figure 4.8: A: Theoretical computations of responses evoked by brief stimuli during the period of refractoriness following an action potential; Node 8.

B and C: Tracings of experimental records in a similar experiment; Node 21.

observed in the voltage-clamp experiments. The slow recovery of $g_K$ to its resting value also contributes to refractoriness, but this is of minor importance in the node.

D. Ionic Movements

Using the equations, it is possible to separate the ionic current ($I_i$) during the action potential into the components carried by sodium ions ($I_{Na}$) and the components carried by potassium ions ($I_K + I_L$), as illustrated in Figure 4.5. The total amount of charge carried by either ion is measured by integrating its respective current over the duration of the action potential. For this node, the equations predicted that $2.4 \times 10^{-17}$ moles of sodium entered the fiber during each impulse and that there was an equal loss of potassium. The results obtained on other nodes are shown in Table 4.1.

The changes in ion content of frog nerves resulting from the conduction of impulses have been measured by Asano and Hurlbut (1958) for two different conditions in which the mechanism maintaining the ion distributions were inhibited. These were: 1) that potassium was absent from the external medium, and 2) that 0.2 mM sodium azide was added to the Ringer's solution in order to inhibit the increase in oxygen consumption associated with activity. The results obtained in the two kinds of experiment were consistent, and showed that, as a result of an hour's stimulation at 50 per sec (i.e., 180,000 impulses), the experimental nerves accumulated $32 \pm 6$ $\mu$ moles of sodium per gram dry weight and lost an equivalent amount of potassium, compared with unstimulated controls otherwise treated in the same way.

The changes in ion content were measured on nerves in which the action potentials were propagated, whereas the equations were solved for the condition that there was no current flow in the internodes. To assess the importance of this difference, an action potential was computed in which the membrane capacitance was increased to twice its normal value,

TABLE 4.1

Theoretical predictions of the quantity of sodium ions which enter the fiber at each node during an action potential

| NODE NUMBER | INITIAL CONDITION | $[h_o]$ | SODIUM GAIN ($10^{-17}$ moles/impulse) |
|---|---|---|---|
| 4 | hyperpolarized | [0.80] | 3.2 |
| 7 | resting potential | [0.40] | 2.0 |
| | hyperpolarized | [0.95] | 2.3 |
| 8 | resting potential | [0.57] | 2.9 |
| 11 | resting potential | [0.51] | 2.4 |

to represent the charging of the capacitance of the internode during propagation of the impulse. Doubling the capacitance resulted in a slight distortion of the action potential and very considerable distortion of the time course of $I_{Na}$, but there was no significant effect on the amount of charge carried by sodium ions. This result seems to justify comparison of the chemical and electrical data.

Such a comparison can be made, making the following assumptions: 1) that the amount of fiber water in frog nerve is nearly equivalent to the dry weight (1 gram dry weight = 1.1 gram fiber water, Hurlbut, 1958); 2) that the amount of fiber water associated with each node is equivalent to the volume of an internode (10 μ inside diameter by 2 mm long is representative of the fibers used in the voltage-clamp experiments); and 3) that the exchange of ions determined for the whole population of fibers in the nerve trunk is representative of the changes in the large fibers. The quantity of sodium entering a representative node during an impulse is then estimated from the chemical measurements as:

$$32 \pm 6 \frac{\mu \text{ moles Na}}{\text{gram dry}} \times \frac{1}{180,000 \text{ impulses}} \times \frac{0.9 \text{ gram dry}}{\text{gram fiber water}} \times$$

$$1.6 \times 10^{-17} \frac{\text{gram fiber water}}{\text{node}} = 2.6 \pm 0.5 \times 10^{-17} \text{ moles/node per impulse.}$$

This estimate agrees very well with the values predicted by the mathematical model using voltage-clamp data for normal nodes (Table 4.1). However, this agreement must be considered somewhat fortuitous in view of some quantitative uncertainty in assumptions 2 and 3 above, and in the calibration of the membrane current (± 20%).

E. The abolition phenomenon

If, at any time during the action potential, one applies a brief pulse of inward current sufficiently strong to restore the membrane potential to the neighborhood of the resting potential, it is possible to prevent the membrane from completing the remaining part of its normal action potential

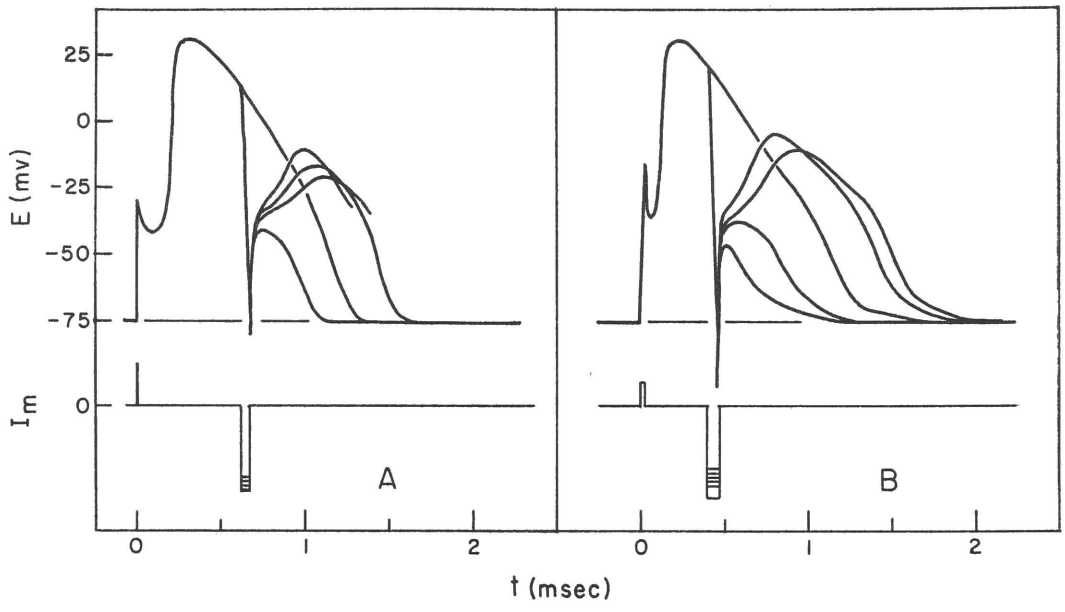


Figure 4.9: A. Theoretical computations of the effect of brief strong pulses of inward current applied during the falling phase of an action potential; Node 8.

B: Tracing of experimental records in a similar experiment; Node 23.

(Hodgkin, Huxley, and Katz, 1949; Weidmann, 1951; Tasaki, 1956; Lüttgau, 1956). Usually this shutting off, or abolition, of the action potential behaves in an all-or-none manner with the strength of the current pulse.

The behavior is predicted by the equations (Figure 4.9) which show that it is accounted for by the reversible nature of the activation process which turns off $P_{Na}$ very rapidly whenever the membrane potential approaches the resting level (Figure 3.3).

F. Repetitive firing

For most of the nodes observed during the present investigation, a superthreshold constant current stimulus of long duration elicited only one action potential. Theoretical predictions of the nerve model, with empirical constants determined on such nodes, agree with this experimental observation.

In a very few cases, however, an isolated node was observed to fire a finite train of action potentials in response to a constant stimulating current. A striking example of this is shown in Figure 4.10. Examination of the voltage clamp records obtained on this node revealed only one obvious difference between this and the usual node; the curves of $h_\infty$ and $\tau_h$ were shifted along the voltage axis by about 10 mv such that there was less inactivation of the sodium permeability at the resting potential.

When the rate constants derived from a normal node were modified to introduce this difference, the equations predicted repetitive firing (Figure 4.11). It is not yet possible to define precisely the necessary and sufficient conditions required for repetitive firing, but theoretical analysis of the equations by the methods of non-linear mechanics (FitzHugh, 1961) may give new insight into this problem.

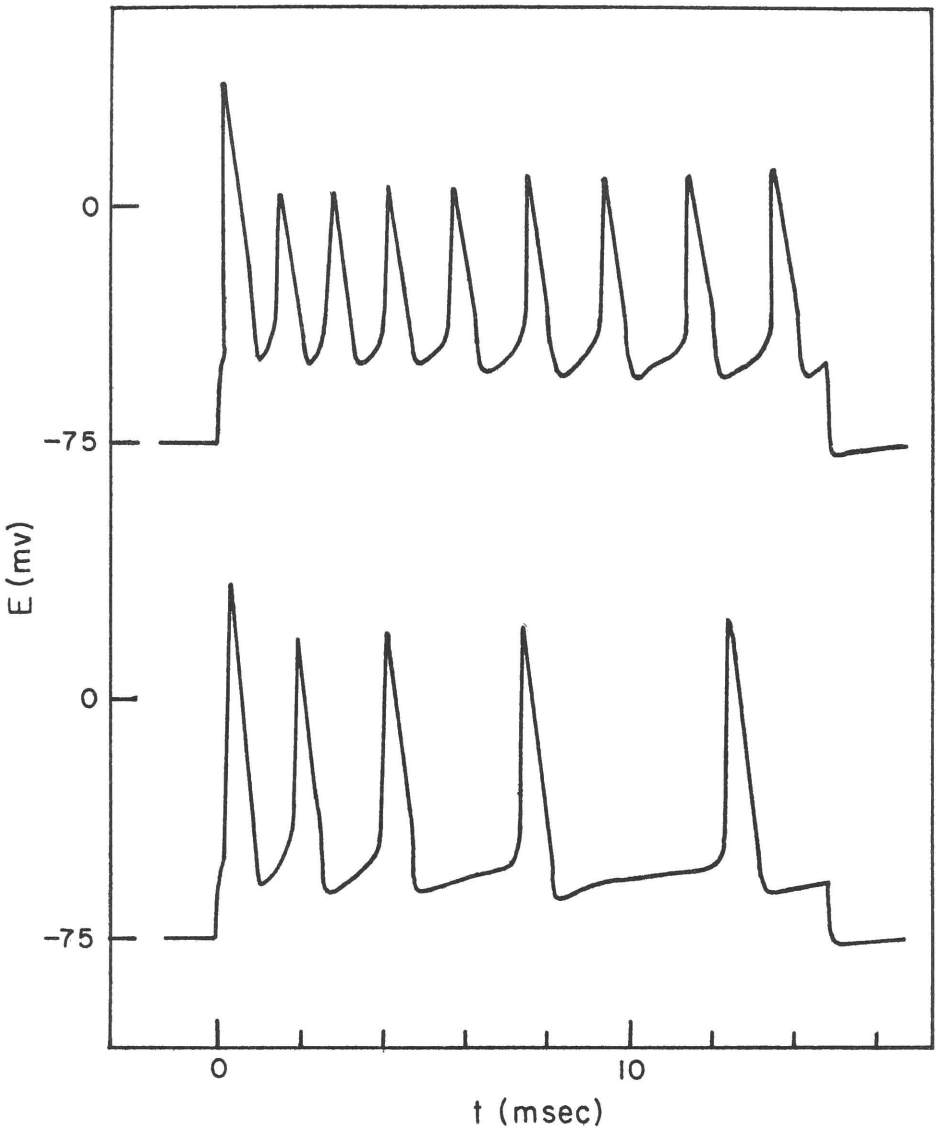


Figure 4.10: An example of a node which fired repetitively in response to long constant current stimuli. The figures are tracings of records in which the stimulus ($I_m$) was .9 na (upper) and .7 na (lower).

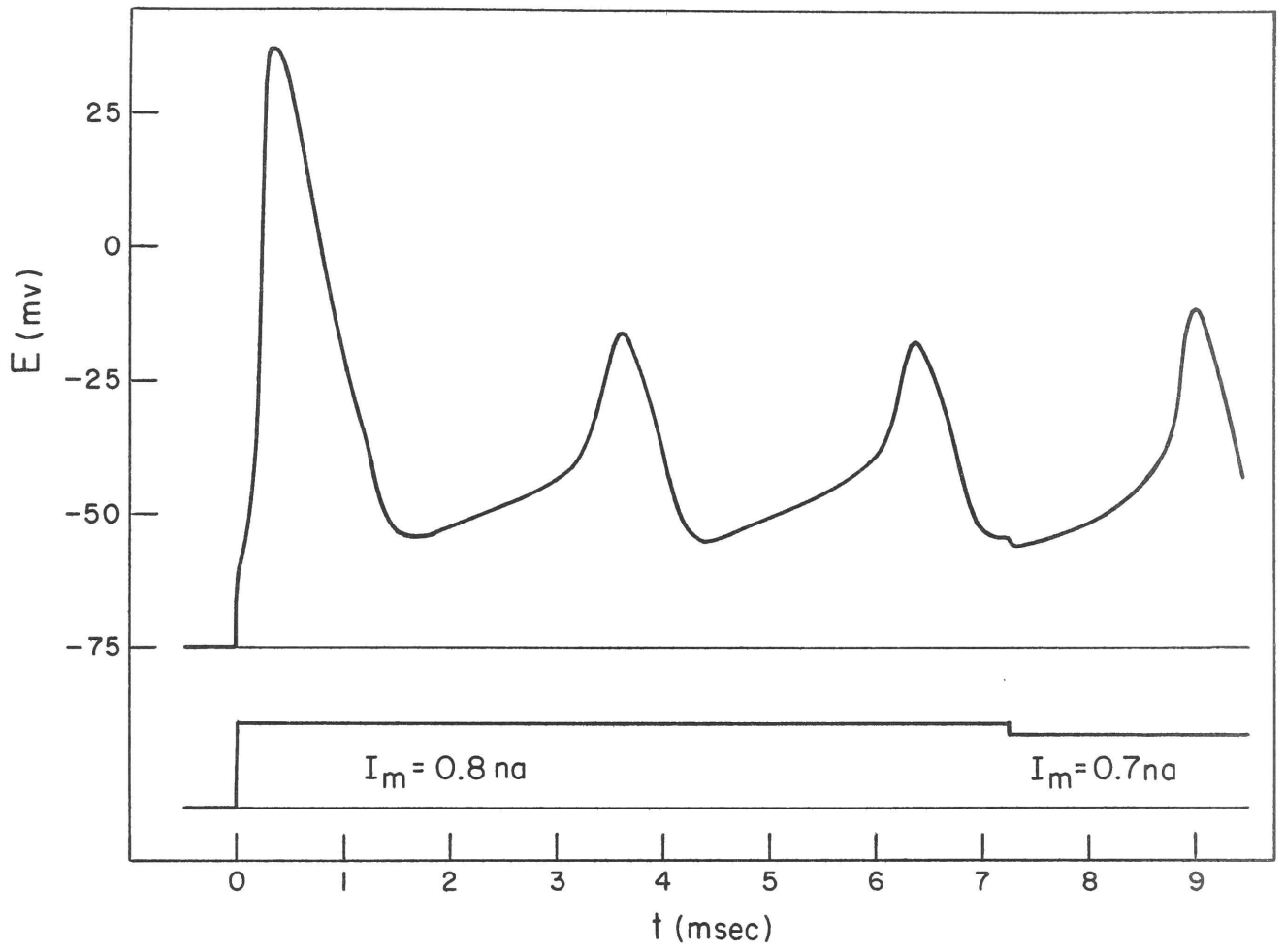


Figure 4.11: Theoretical computations of repetitive firing obtained by modifying the voltage-dependence of the rate constants $\alpha_h$ and $\beta_h$ for Node 7.

# DISCUSSION

## On the Theoretical Computations

The quantitative formulation of the ionic hypothesis, embodied in the mathematical model for the current-voltage relations of the node, has been found to predict the action potentials of the node in excellent agreement with the experimental observations. This agreement is evidence that:

(1) the fundamental assumption that the total membrane current of a node is the sum of the capacitative displacement current and the current carried by the movement of ions through the membrane is valid;

(2) the current-voltage relations of the nodal membrane are reliably measured in the voltage-clamp experiment,

(3) the observed current-voltage relations are accurately represented by the equations, and

(4) the current-voltage measurements alone are sufficient to predict all of the electrical phenomena at a node that are associated with excitation of the action potential.

The agreement between the theoretical and observed action potentials, by itself, is not direct proof of validity of the ionic hypothesis, since any formal model which reproduces, in detail, the observed dependence of the ionic current upon the membrane potential and time would predict the action potential equally well.

Analysis of the ionic currents of the nodal membrane has demonstrated that the ionic hypothesis provides a simple and coherent interpretation of the observed current-voltage relations. The evidence for this conclusion is provided by the observations that the ionic currents of the node vary with changes in the electrochemical driving forces for sodium and potassium ions in the manner predicted by the ionic hypothesis and that the temporal

variation of the ionic permeability of the membrane measured by resolution of the specific sodium and potassium components of the membrane current is in essential agreement with electrical measurements based on the instantaneous current-voltage relations.

The substantial quantitative agreement between the theoretical prediction of the exchange of extracellular sodium ions for intracellular potassium ions resulting from conduction of impulses with that measured by chemical analyses of nerve is further evidence for the validity of the ionic hypothesis.

The foregoing considerations permit the conclusion that, under normal conditions, excitation of the action potential of a node results from reversible alterations of the sodium and potassium permeability of the nodal membrane.

## Propagation of the Action Potential

Quantitative prediction of the excitation and propagation of the action potential in an unconstrained meyelinated fiber requires solution of a very complex partial differential equation in which the nodes are considered point sources of current connected by short lengths of passive cable. Since the wave length of the propagating action potential (duration times velocity) includes about twenty nodes, in order to predict the propagation of only the rising phase of the action potential requires the simultaneous computation of E at several nodes (each described by the complete system of four nonlinear differential equations) and at several points along their connecting cables. A point-by-point integration in both (variables, x and t) was beyond the capability by the computer used in the present work, hence no attempt was made to compute the propagated action potential.

However, FitzHugh (1962) has solved the equation for a model of the myelinated fiber in which the ionic currents of the nodes were represented by the eqautions for the squid axon (scaled to the resting resistance of the frog node) and in which the cable constants were those determined from

frog myelinated fibers. These computations predicted a constant conduction velocity and a spatial variation of the membrane potential during the action potential in good agreement with experimental observations. An interesting theoretical result with regard to the propagated action potential was that, although the action potential at each node had a smooth rising phase, the time course of the variation in membrane potential near the middle of the internode had pronounced hump on the rising phase, this hump resulting from the successive excitation of the two nodes at either end of the internode. Action potentials measured with a micro-pipette in a frog nerve (Woodbury, 1951) were typically of this form.

In view of the great similarity of the equations describing the ionic current of the squid axon and the node, substantially the same results would be expected from computations using the equations for the nodal membrane.

## On the Limitations of the Model

The quantitative formulation of the ionic hypothesis involves empirical description of the kinetics of the permeability changes derived from voltage-clamp measurements. The applicability of the model is thereby limited to such general conditions as the ionic composition of the extracellular medium for which voltage-clamp data are available.

There is a further limitation, also in the normal case, resulting from the fact that it is presently impossible to specify, quantitatively, all of the ionic processes involved in maintaining the resting potential. Consequently, the model does not account for the slow after-potentials observed in intact nerves under special experimental conditions; a particularly significant example is the cumulative hyperpolarization which follows either a period of tetanic stimulation or a period of anoxia. Nonetheless, the effect of these experimental conditions on the excitability of nerve (threshold, refractory period, conduction velocity and the like) are predicted by the model with

the additional ad hoc assumption of an appropriate value for the membrane hyperpolarization.

## Comparison of the Membrane Properties of the Node and Squid Axon

Voltage-clamp experiments have shown that the relations between the ionic current and membrane potential are qualitatively similar in the node and the squid axon. In fact, they are so nearly alike that the permeability changes of the nodal membrane are described by kinetic equations of the same form as those developed for the squid axon by Hodgkin and Huxley. Consequently, the major features of excitation, such as the threshold phenomenon and refractoriness, which are common to both nerves, are shown to have a common basis in the similar dependence of their ionic currents on membrane potential difference. However, these experiments have revealed several significant differences in the properties of the membranes of these two kinds of nerve. Consideration of these details will serve to sharpen the interpretation of nerve excitability in terms of the ionic permeability changes.

The relation between the transient sodium permeability change and membrane potential is strikingly similar in the two nerves. Comparison of the peak current-voltage relation of the two nerves shows that, in both cases, there is a transient phase of net inward current over the range of membrane potentials from -50 mv to +40 mv. Consequently, in both nerves the regenerative phase of the action potential begins at the same value of membrane potential (-50 mv), and the action potential has the same overshoot (+40 mv). The normal resting potentials differ somewhat, being -75 mv for the node and -60 mv for the squid axon. Two direct consequences of this difference are that the node has a higher threshold measured as the minimum displacement of the membrane potential from the resting potential, and that the node does not normally show anode-break excitation (Frankenhaeuser and Widén, 1956). In both nerves, the relation between the steady-state inactivation of sodium permeability and membrane potential

is a steep, S-shaped curve symmetrical about the resting potential. Thus, in the node this curve is shifted to more negative values of membrane potential relative to the threshold potential. This fact is likely related to the absence of repetitive firing of the node in response to a constant current stimulus.

The wave form of the nodal action potential differs significantly from that of the squid axon as a consequence of the quantitative differences in the kinetics of the permeability changes. These differences are clearly resolved by voltage-clamp measurements at intermediate levels of depolarization where it is observed that the sodium permeability is turned on at about the same rate in both nerves but the sodium permeability of the nodal membrane is inactivated at about half the rate, and the potassium conductance is turned on at only one-fifth the rate, seen in the squid axon. As a direct consequence of this difference, the duration of the nodal action potential is about twice that of the squid axon. Because the variation of $g_K$ in the node is slower than in the squid, there is a relatively much smaller increase in $g_K$ during the nodal action potential; as a result, the total conductance of the nodal membrane immediately following the spike is less than twice the resting conductance, in contrast to the ten-fold difference of conductance in the case of the squid axon (Cole and Curtis, 1939). As a further consequence of the relatively smaller increase in $g_K$ during the nodal action potential, and the fact that the resting potential of the node appears to be quite close to the potassium equilibrium potential, there is no undershoot following the nodal action potential, such as is characteristic of the action potential of the isolated squid axon (Hodgkin and Huxley, 1952d).

The most significant differences in the properties of the potassium permeability are revealed at membrane potentials near the resting potential. The resting state of the node is dominated by the large, constant leakage conductance which appears to be a voltage-independent component of the

potassium permeability. In the squid axon the constant leakage conductance is very small and probably reflects permeability of the membrane to ions other than sodium and potassium (Adelman and Taylor, 1961). The resting state of the squid axon is determined partly by the leakage conductance and partly by the finite value of the voltage-dependent potassium conductance. Whereas hyperpolarization has virtually no effect on the conductance of the nodal membrane, it has the effect of greatly decreasing the conductance of the squid axon. This difference between the two nerves is clearly seen by comparing the steady-state current-voltage relations. Both nerves show qualitatively similar rectifying properties, but in the node the ratio of forward conductance (depolarized) to back conductance (hyperpolarized) is only about 7:1, but in the squid axon it is larger, better than 100:1 (Cole and Moore, 1960). The fact that the conductance of the nodal membrane is constant near the resting potential accounts for the absence of sub-threshold oscillations which are prominent in the behavior of the squid axon (Hodgkin and Huxley, 1952 d).

The significance of these differences may be assessed from a theoretical point of view by comparing the results of computation of an "action potential" for the condition that $g_K$ is held constant at its resting value. The theoretical computation for the squid membrane shows that after the spike the membrane potential recovers only to an infinitely long plateau, at a value of membrane potential 50 mv depolarized from the resting potential (FitzHugh, 1960). For the node, however, holding $g_K$ constant only increases the duration of an otherwise normal action potential by about 50 percent. The results of such computations are of more than academic interest, however, as they provide a partial explanation for effects observed under special experimental conditions.*

* These include: prolongation of the squid action potential by injection of tetraethylammonium chloride (Tasaki and Hagiwara, 1957), has been accounted for by theoretical computations (FitzHugh, 1960); prolongation of nodal action potential by nickel ions (Spyropoulos and Brady, 1959) and the abolition of prolonged action potentials by temperature shock or by a sudden increase of the external calcium ion concentration (Spyropoulos, 1961) have been considered in theoretical computations (George and Johnson, 1962); also, there are theoretical computations of the long action potentials of normal heart muscle fibers (Noble, '62).

# CONCLUSIONS

1) The quantitative formulation of the ionic hypothesis has been found to be applicable to the node of Ranvier.

2) The membrane currents responsible for the propagation of the impulse in myelinated nerve fibers are passive manifestations of diffusional fluxes of sodium and potassium ions.

3) The ionic currents in the nodal membrane are generated by a sequence of permeability changes of the membrane which are highly specific for sodium and potassium ions.

4) In the normal case, the kinetics of the permeability changes are dependent solely on the membrane potential.

5) These kinetics have been described by an empirical mathematical model similar to that developed for the squid axon by Hodgkin and Huxley.

6) The empirical model, the definitions of the specific ionic permeabilities which relate the ionic currents to the electrochemical driving forces for the specific ions, and the equations for the distribution of membrane current within the cable-like structure of the myelinated nerve fiber, all taken together, constitute a quantitative mathematical model which predicts the electrical phenomena associated with excitation and propagation of the nerve impulse.

7) The equations account for the time course of the resistance change of the node, and for the exchange of ions associated with the propagation of the impulses. (Conclusion 7 depends upon some reasonable ad hoc assumptions.)

## Appendix I

## COMPUTATION OF THE NODAL ACTION POTENTIALS

In order to predict the action potential the equations of the model node are solved for the boundary condition that the net membrane current is zero, except during the stimulus. This condition corresponds exactly to the experimental measurement of the action potential by a system that prevents current from flowing through the adjacent internode, thereby preventing propagation of the impulse.

For this boundary condition the model node is a system of four simultaneous, first order, non-linear differential equations. These are

(1) $$C\dot{E} = I_m - I_i$$

where $I_m$ is the stimulus which is an arbitrary function of time, and

$$I_i = \bar{P}_{Na} m^3 h [Na]_o \frac{F^2 E}{RT} \frac{\exp\{(E - E_{Na})F/RT\} - 1}{\exp\{EF/RT\} - 1} + \bar{g}_K n^4 (E - E_K) + \bar{g}_L (E - E_L)$$

(2) $$\dot{m} = \alpha_m (1 - m) - \beta_m m$$

(3) $$\dot{h} = \alpha_h (1 - h) - \beta_h h$$

(4) $$\dot{n} = \alpha_n (1 - n) - \beta_n n$$

where the empricial rate constants (the $\alpha$'s and $\beta$'s) depend only on the instantaneous value of the membrane potential (E).

This system of differential equations cannot be solved analytically, but requires a step by step numerical integration of the four variables (E, m, h, and n) over small increments in time. For this purpose the iterative integration method of Adams (See e.g. Scarborough, 1955, p. 245)

has been used. In this method the next value of the variable ($x_1^*$) is predicted for the new time ($t_1 = t_0 + \delta t$) by the prediction formula:

$$(P) \qquad x_1^* = x_0 + \delta t(\dot{x}_0 + \frac{1}{2}\Delta_1 \dot{x}_0 + \frac{5}{12}\Delta_2 \dot{x}_0 + \frac{3}{8}\Delta_3 \dot{x}_0 + \frac{251}{720}\Delta_1 \dot{x}_0)$$

which uses the last confirmed values of the variable ($x_0$), its derivative at that time ($\dot{x}_0$) and the backward differences of the derivative defined as $\Delta_1 \dot{x}_0 = \dot{x}_0 - \dot{x}_{-1}$, $\Delta_2 \dot{x}_0 = \Delta_1 \dot{x}_0 - \Delta_1 \dot{x}_{-1}$, etc. The value of the derivative at $t_1$ is then calculated from its appropriate equation using the predicted value of the variable ($x_1^*$). The predicted value of the variable is then checked by applying the confirmation formula:

$$(C) \qquad x_1 = x_0 + \delta t(\dot{x}_1 - \frac{1}{2}\Delta_1 \dot{x}_1 - \frac{1}{12}\Delta_2 \dot{x}_1 - \frac{1}{24}\Delta_3 \dot{x}_1 - \frac{19}{720}\Delta_4 \dot{x}_1).$$

If the confirmed value ($x_1$) agrees with the predicted value ($x_1^*$), the computation is continued for the next increment of time. If they do not agree, $x_1$ is taken as the predicted value ($x_1^*$), the derivative at $t_1$ is recalculated, and the confirmation formula (C) applied again. This process is iterated until $x_1$ and $x_1^*$ do agree. If a number of iterations are required, this is a sign that the interval of integration ($\delta t$) is too large, and this is then cut in half. On the other hand, if the computation is going smoothly (no iterations required) and the increment in the variable is small, then the computation can be speeded up by doubling the integration interval.

This integration method was applied to systems of equations of the model node by the following procedure.

General computation: Assuming that the solution has been started so that there are previously confirmed values of the variables, derivatives and backward differences of the derivatives, at the time $t_0$, then

1) $E_1^*$, $m_1^*$, $h_1^*$ and $n_1^*$ are predicted for $t_1$ using formula (P),

2) the rate constants are evaluated for $E_1^*$,

3) $\dot{m}_1$ is calculated from Equation 2 using $m_1^*$,

4) $m_1$ is calculated according to formula (C),

5) if $|m_1 - m_1^*|$ is less than $10^{-7}$, $m_1$ is taken as the confirmed value, and the computation continues at step 6; if not, $m_1$ is taken as $m_1^*$ and the process iterated from step 3.

6) The confirmed value $h_1$ is obtained in a manner similar to steps 3-5.

7) The confirmed value $n_1$ is obtained in a manner similar to steps 3-5.

8) $\dot{E}_1$ is calculated from Equation 1 using $E_1^*$, $m_1$, $h_1$ and $n_1$.

9) $E_1$ is calculated according to formula (C).

10) If $|E_1 - E_1^*|$ is less than 1 μv then $E_1$ is taken as the confirmed value, and the computation continues at step 11; if not, $E_1$ is taken as $E_1^*$ and the computation is repeated from step 2.

11) $E_1 - E_0$ is tested for justifying a change in integration interval - if $|E_1 - E_0|$ is less than 0.3 mv and at least ten values of E have been computed with the previous value of $\delta t$, then $\delta t$ is doubled; if $|E_1 - E_0|$ is greater than 1.0 mv, $\delta t$ is halved.

12) Computation for the next interval is started at step 1, taking $t_1$ as $t_0$, $E_1$ as $E_0$, etc.

Starting the computation: At the beginning of the computation the backward differences of the derivatives are not known, hence, a special starting procedure is required. In this case, the integration interval ($\delta t$) is chosen so small (1 μsec) that the high order differences have negligible effect, and the initial values of the derivatives and the first difference of the derivatives are estimated, assuming an exponential decay of the variables with the steady-state values and time constants appropriate to the initial value of the membrane potential.

Change of integration interval: The integration interval is changed on the basis of step 11 in the general procedure. In addition, the interval is halved if, during the computation for any interval, the total number of

iterations (for all variables) exceeds ten. The change of interval is accomplished by modification of the table of differences of the derivatives in accordance with their definitions; for doubling the interval, the appropriate new value for $\Delta_1 x_1$ is given in terms of the old interval by $x_1 - x_{-1} = \Delta x_1 + \Delta x_0$, etc; for halving the interval, analogous expressions are derived using a standard interpolation procedure (Scarborough, 1955, p. 65).

Approximating functions for the empirical rate constants: For computational purposes the empirical rate constants are represented by approximating functions of the membrane potential. A convenient form for the approximating function is

$$\text{rate constant} = \frac{a\phi}{\exp \phi - 1} \quad \text{where} \quad \phi = \frac{E - b}{c},$$ in which $E$ is the membrane potential, and a, b, and c are constants which are empirically determined for each rate constant. An additional correction term is added to the approximating function when necessary.

As a specific example, the rate constants for node 7, illustrated in Text figure 3.19, were represented by the following functions:

$$\alpha_m = \frac{1.6\left(\frac{37.5 - E}{3.8}\right)}{\exp\left\{\frac{37.5 - E}{3.8}\right\} - 1} + \frac{6}{1 + \left(\frac{E - 23}{17.5}\right)^2}$$

$$\beta_m = \frac{4.05\left(\frac{E - 37.5}{13.2}\right)}{\exp\left\{\frac{E - 37.5}{13.2}\right\} - 1}$$

$$\alpha_h = \frac{0.08\left(\frac{E - 75}{4.9}\right)}{\exp\left\{\frac{E - 75}{4.9}\right\} - 1}$$

$$\beta_h = \frac{0.6\left(\frac{49 - E}{9.7}\right)}{\exp\left\{\frac{49 - E}{9.7}\right\} - 1}$$

$$\alpha_n = \frac{0.34\left(\frac{15 - E}{15.9}\right)}{\exp\left\{\frac{15 - E}{15.9}\right\} - 1} + 0.1$$

$$\beta_n = \frac{0.085\left(\frac{E - 37.5}{12.2}\right)}{\exp\left\{\frac{E - 37.5}{12.2}\right\} - 1}$$

In order to avoid difficulties in evaluating the approximating function at (or near) the value of $\phi = 0$, where the function takes the form 0/0, the function is computed from its power series expansion for $|\phi| < 1$, namely:

$$\frac{a\phi}{\exp \phi - 1} = \frac{a}{1 + \sum_{n=2}^{\infty} \frac{\phi^{n-1}}{n!}}$$

For the same reason, the exponential terms in the relation between $I_{Na}$ and its driving force (in Equation 1) are evaluated in a similar manner.

## Appendix II

## NOTES ON SOME SOURCES OF ERROR IN THE VOLTAGE-CLAMP MEASUREMENTS

Here we shall consider limitations on the control of the nodal membrane potential imposed by the structure of the myelinated nerve fiber. Clearly, an estimate of the errors introduced by these limitations is of importance in assessing the validity of the measurements. This discussion will show that, except for measurement of the instantaneous sodium currents, instrumental errors have been minimized to the extent that they do not seriously affect the observed current-voltage relations of the node.

Before discussing instrumental errors, let us first consider two questions concerning current flow at the node: 1) to what extent is the potential difference uniform over the surface of the nodal membrane, and 2) how large is the resistance in series with the nodal membrane arising from convergence of current to the limited area of the nodal membrane

1. Uniformity of the membrane potential. Even in its most conductive state, the membrane is still a formidable barrier to ion movements (Frankenhaeuser 1959, p. 675). On this basis, it is reasonable to presume that voltage drops in the axoplasm in the vicinity of the node are small in comparison to those across the membrane, so that the distribution of current may be described by the one-dimensional cable equation (e.g. Hodgkin and Rushton , 1946). If we then assume 1) that the properties of the nodal membrane are uniform over its surface and 2) that the current through the myelin sheath is negligible, we can solve the cable equation for the steady-state distribution of membrane potential along the node under the boundary conditions that current is injected through left-hand internode and there is neglible longitudinal current through the right-hand internode, the conditions that were imposed by the operation of the membrane potential measuring system. For these boundary conditions, the solution of the cable equation

is given (Weidmann, 1952) by:

$$V(x) = V_0 \frac{\cosh\{(L-x)/\lambda\}}{\cosh\{L/\lambda\}} \qquad (1)$$

where $x$ is the distance along the node with the origin at the left-hand boundary of the node, $L$ is the length of the nodal gap, and $\lambda$ is the characteristic length of the cable. For this question we are interested in $\lambda$ for the node in its most conductive state; i.e., when the resistance of total nodal membrane is 3 megohms. Taking the nodal gap as 1 $\mu$ and the radius of the axis cylinder at the node as 4 $\mu$ (as in Figure 1) the specific transverse resistance ($R_m$) of the equivalent membrane conforming to the geometrical area is .75 ohm cm$^2$. Since the fiber is in a large volume of solution, we may neglect the resistance of the extracellular medium whence, $\lambda$ is given by $\lambda = \sqrt{aR_m/2R_i}$, where $a$ is the radius of the axis cylinder, $R_m$ is the specific transverse resistance of the membrane, and $R_i$ is the specific resistance of the axoplasm. $R_i$ is about 100 ohm cm (Tasaki and Frank, 1955). Therefore, $\lambda$ is about 12 $\mu$ for the active node. With this value Equation 1 predicts that the membrane potential at $x = L$ is .997 $V_0$. If the nodal gap were taken as 2 $\mu$, which appears to be more nearly the case when the isolated fibers are examined under the microscope, then $\lambda$ is 17 $\mu$ and Equation 1 predicts that $V$ at $L$ is .993 $V_0$. In either case, this predicts that the membrane potential deviates less than 1% along the nodal gap.

2. Convergence of current to the nodal membrane. In the voltage-clamp experiments, the peak inward current may be as large as $3 \times 10^{-8}$ amps. Considering the very small effective area of the node (1 $\mu$ gap x 4 $\mu$ radius of axis cylinder), this is a current density of 120 ma/cm$^2$. The existence of such high current densities raises the question whether there is a significant IR drop between the bulk of extracellular solution and the surface of nodal membrane. This is a crucial point for the voltage-clamp technique, since any IR drop here would cause a deviation of the true membrane potential

from the measured value. The following presents an approximate calculation of the resistance between the surface of the node and the extracellular solution.

On the basis of the previous discussion, we may assume that the current flow through the nodal membrane is essentially radial, Figure 1. In the immediate vicinity of the node, we may consider the current flow bounded by the segment of the sphere enclosed by the dotted lines, which subtends a solid angle of $\pi/2$ steradian about the origin. This is a reasonably good approximation out to a radius of about 7 $\mu$, but thereafter the current diverges rapidly, such that beyond a radius of about 10 $\mu$ the current may be approximated as radial, subtending a solid angle greater than $2\pi$. The resistance between the surface of two concentric spheres limited to a zone of solid angle ($\psi$) in a medium of specific resistance ($\rho$ = 100 $\Omega$ cm for Ringer's solution) is given by the formula

$$R = \frac{\rho}{\psi}\left[\frac{1}{r_1} - \frac{1}{r_2}\right]$$

where $r_1$ is the smaller radius. According to the formula, the resistance between the surface of the node and the surface at 7 $\mu$ (Figure 1) is about 70 k$\Omega$, and for the approximation above the resistance from the surface at 10 $\mu$ to infinity is about 16 k$\Omega$. In the space between 7 $\mu$ and 10 $\mu$, where the current flow departs greatly from radial, the resistance cannot be calculated on such a simple basis; however, we can estimate reasonable bounds: the resistance between 7 $\mu$ and 10 $\mu$ is certainly less than if its current flow were radial in the zone of $\psi = \pi/2$ (dotted lines) which would predict 25 k$\Omega$, and it is certainly greater than if the current flow were radial in the zone $\psi = 2\pi$, which would predict 6k$\Omega$. Taking 9 k$\Omega$ as a rough estimate of the resistance between 7 $\mu$ and 10 $\mu$, 75 k$\Omega$ between 4 $\mu$ and 7 $\mu$, and 16 k$\Omega$ beyond 10 $\mu$, the total resistance in series with the node is in the order of 100 k$\Omega$ for this idealized geometry. The real situation is complicated by the processes of the Schwann cells projecting into the nodal gap (Robertson, 1960) which would tend to increase this resistance. On the other hand, the nodal gap appears to be longer in an isolated fiber than the dimensions used

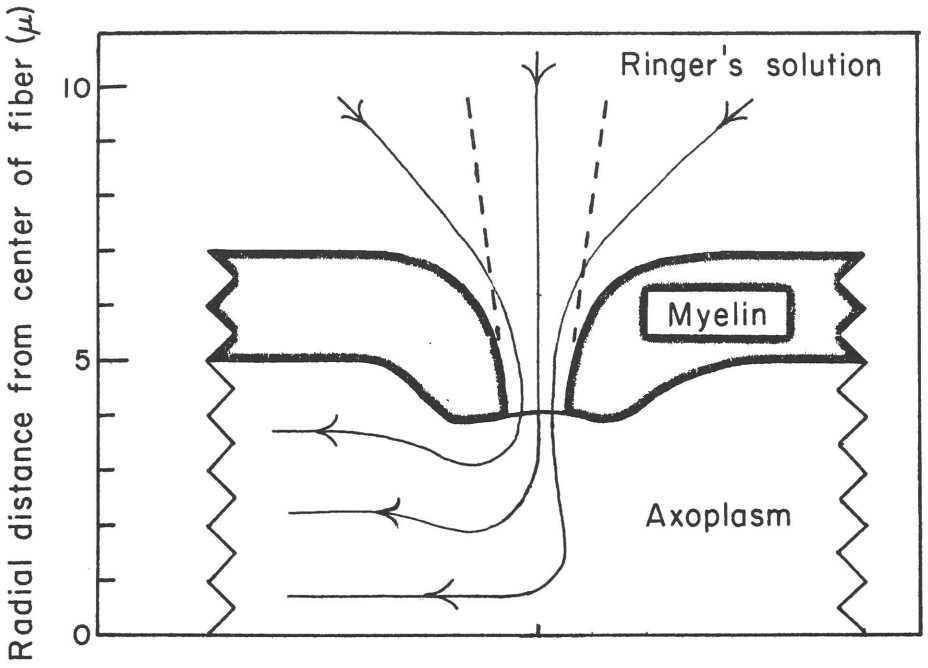


Figure 1: Diagram illustrating the geometrical relations of the current flow at a node used to estimate the resistance of the external solution in series with the membrane. The light lines with arrows represent the assumed lines of current flow. The angle between the two radii (dashed lines) is $\pi/8$ radians. Immediately outside the membrane the current flow is assumed to be radial, subtending a solid angle of $\pi/2$ steradians with respect to a point in the center of the axon.

in this calculation; this would tend to reduce the series resistance.

If the series resistance is as large as 100 kΩ, then, during an inward current of $3 \times 10^{-8}$ amps, the true membrane potential would be 3 mv more depolarized than the measured potential. The deviation of the membrane potential of course follows the time course of the membrane current. The effect of such an error is discussed in the section below.

3. Instrumental limitations on control of the membrane potential. Here we shall examine how well the voltage-clamp system holds the membrane potential to the desired value ($E_{ref}$). It is convenient to divide this discussion into two parts: a) deviations of the measured membrane potential from $E_{ref}$ resulting from the characteristics of the feedback amplifier and b) deviation of the true membrane potential from the measured membrane potential.

a) In order for a feedback amplifier system to be stable, it is necessary that the gain be less than one at that frequency at which the phase lag is 180°. Because of the distributed resistance and capacitance of the internodal cable (and the response characteristics of the membrane potential measuring system), the phase lag of this system goes to 180° at some frequency around 100 kc. It is therefore necessary to limit the high-frequency gain of the voltage-clamp amplifier(2); this may be accomplished simply by attenuating the output with a single-time-constant, low-pass, filter. The response of the amplifier is then approximately described by the simple differential equation,

$$\tau_f \dot{V}_{out} + V_{out} = a_2 V_{in}$$

where $\tau_f$ is the time constant of the filter and $a_2$ is the gain of the wide band amplifier. In the voltage-clamp application $V_{in}$ is $(E_{ref} - E)$ and $V_{out} = I_m R_{ED}$, yielding the following equation for the control of the measured membrane potential

$$(E_{ref} - E) = \frac{R_{ED}}{a_2} I_m + \frac{\gamma_f R_{ED}}{a_2} \dot{I}_m$$

This equation identifies two sources of error; the control error proportional to $I_m$ and a dynamic error proportional to $\dot{I}_m$. The control error was discussed in Chapter I where it was shown to be always less than a millivolt under the conditions of these experiments. In each experiment, the gain ($a_2$) and frequency response ($\gamma_f$) of the amplifier must be adjusted to that the system does not oscillate. When the high-frequency response is cut as described above, nominal values are $a_2 = 400$ and $\gamma_f = 0.5$ msec. Since the rate of change of inward current may be as large as $R_{ED} \dot{I}_m = 5000$ v/sec, the dynamic error is then equivalent to 6 mv depolarization. The effect of such an error is shown in Figure 4. In the present experiments, however, the necessary high-frequency cut is achieved in a more complicated manner which permits the higher gain over most of the frequency range, with the result that the error from this source is not apparent as a deviation of the measured membrane potential.

b) Two other sources of error have been identified which have the effect of causing a deviation of the true membrane potential from the measured potential.

One error, proportional to $I_m$, arising from a resistance in series with the membrane, has been discussed in section 2 above.

The other error, proportional to $\dot{I}_m$, is introduced by stray capacitance between the signal $R_{ED} I_m$ and the input of the membrane potential system. As it is probably this error which prevents air-gap systems from achieving adequate control, let us briefly consider the error in relation to this simple system. In the typical air-gap system, Figure 2, the solution outside the node is grounded, the membrane potential is measured through the series resistances of the left-hand internode ($R_{CD}$) by a high impedance preamplifier (i.e. $V_C$ is taken as a measure of $V_N$), and the measured membrane potential ($V_C$) is then compared with the reference pulse ($V_{ref}$) by the feedback amplifier whose output is applied through the right-hand

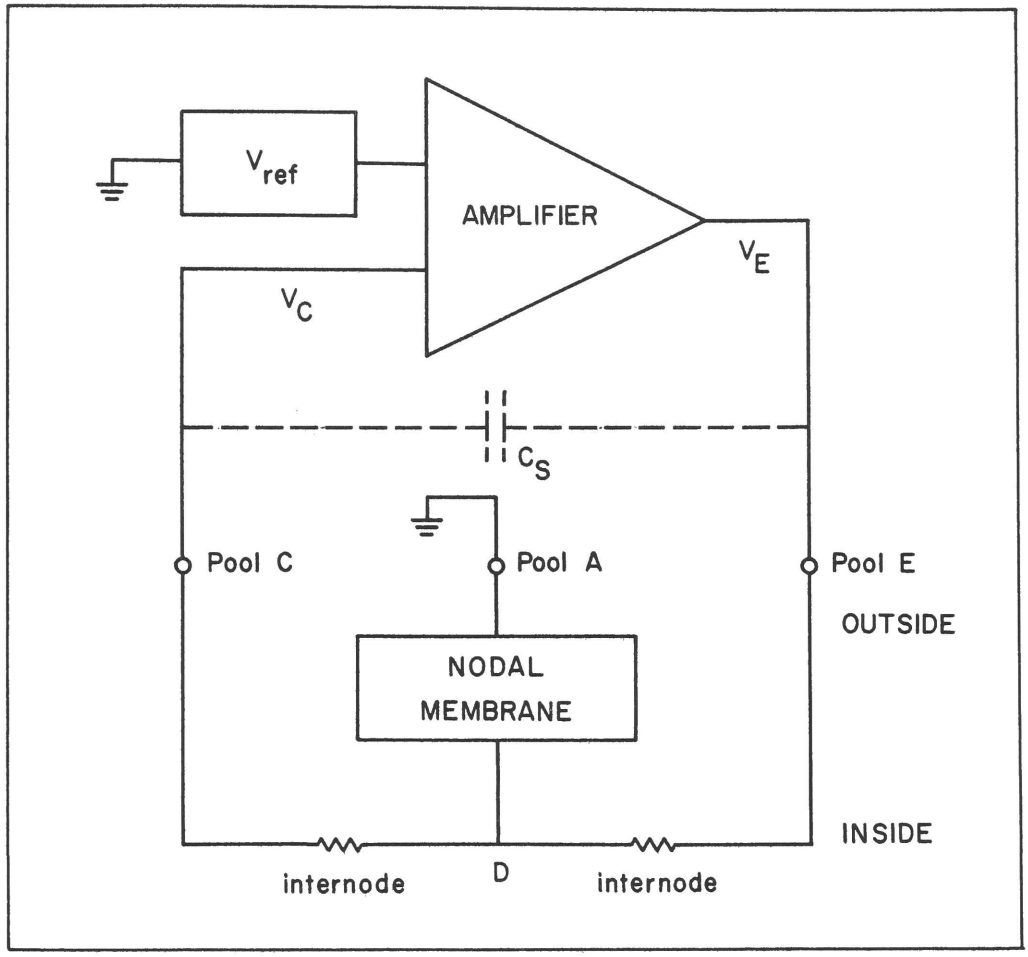


Figure 2: Equivalent circuit of a voltage-clamp system employing air-gaps to increase the resistance of the current paths external to the fiber. Electrical contact to the fiber is made through pools of solution which are designated such as to conform as closely as possible to Figure 1.1 with respect to the functional significance of the electrical signals. In this sytem the membrane potential is measured as the potential difference between pools C and A. Other details are described in the text.

internode. We are interested in the error $(V_C - V_N)$ introduced by a stray capacitance $(C_s)$ between pools E and C. By the operation of the clamping amplifier, the variation in the potential $V_C$ is negligibly small compared to $V_E$, which again is approximately $I_m R_{ED}$. The stray capacitance thus injects a current $C_s \dot{V}_E$ which develops as a potential difference between $V_C$ and $V_N$ which is $R_{CD} C_s \dot{V}_E$. Thus, if $C_s$ is as small as 0.1 μμf, then, since $R_{CD}$ is about 40 megohms and $\dot{V}_E$ as large as -5000 v/sec, there would be an error such that $V_N$ deviates 20 mv depolarized of the measured potential $V_C$.

Stray capacitance between pools E and C in the Frankenhaeuser system has a similar qualitative effect, but is quantitatively quite different. Because his potential measuring system is relatively insensitive to stray capacitance to ground, pool C can be shielded so that the coupling time constant $(\tau_c)$ which is analogous to the term $R_{CD} C_s$ above, can be made vanishing by small, i.e. $\tau_c < 0.1$ μsec, determined by direct measurement (for method, see Dodge and Frankenhaeuser, 1958, p. 79). It has been found empirically that the introduction of a very small capacitance between pools E and C, $\tau_c$ approximately 0.4 μsec, results in cutting the high-frequency response of the clamping amplifier in such a manner that the gain can be set significantly higher than in the case of using a simple low-pass filter. In addition, this method markedly reduces the high-frequency noise of the system. However, because the resulting error does not appear as a deviation of the measured membrane potential, this method must be used with the utmost caution. If $\tau_c$ becomes too large ($\approx$ 1 μsec), the error in control of the membrane potential results in peaking of the inward currents like that illustrated in Figure 4.

4. Consequences of error in control of the membrane potential. Measurements of the current-voltage relations are most sensitive to these errors, particularly the dynamic error, in the range of membrane potentials where the curve of peak current against membrane potential has negative

slope. In this range both the amplitude and the rate of change of the inward current increase rapidly with depolarization. Since all of these errors result in a depolarizing deviation of the membrane potential during the initial phase of inward current, this characteristic of the membrane results in this tendency toward regeneration of the error.

When these errors are excessive, Figure 3, the membrane potential is very poorly controlled and the phase of inward current shows large oscillations. The records of Figure 3A were obtained by severely limiting the high-frequency response of the clamping amplifier by means of a low-pass filter

$$(\frac{\tau_f}{a_2} > 3\ \mu\text{sec})$$

with the result that the voltage record quite accurately shows the true deviation of the membrane potential. The records of Figure 3B were obtained by introducing a large stray capacity between pools E and C ( $\tau_c > 3\ \mu$sec). In this case, the error is generated as a deviation between the true membrane potential and the measured value, hence the oscillations of the membrane potential do not appear significant on the voltage record. These records (Figure 3B) are typical of those obtained for voltage-clamp systems using air-gaps (Tasaki and Bak, 1958). The records of Figure 3C were obtained on the same node with optimum trim of the clamping amplifier ( $\tau_c \approx 0.4\ \mu$sec).

Less severe error causes an appreciable distortion or "peaking" of the inward currents, Figure 4. In this case, the high-frequency response of the clamping amplifier was cut by the filter

$$(\frac{\tau_f}{a_2} \approx 1\ \mu\text{sec})$$

so the resulting deviation of the membrane potential (about 6 mv) is observed on the voltage record. Peaking of the inward currents of about this magnitude was reported by Dodge and Frankenhaeuser (1958).

The residual error for the case of optimum trim of the amplifier (Figure 4) is not observed directly. On the basis of measurements of $\tau_c$,

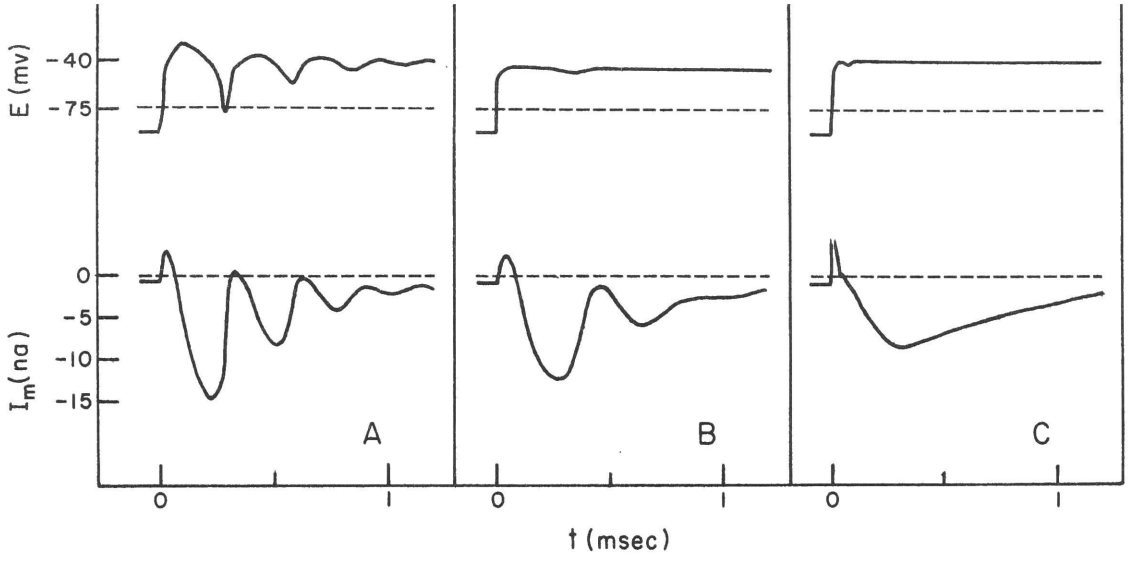


Figure 3: Oscillatory membrane currents associated with errors in control of the membrane potential. Tracings of experimental records of $I_m$ and E. A: error generated by severe attenuation of the high-frequency response of the clamping amplifier; failure of control is apparent on record of the membrane potential. B: error generated as a deviation of the true membrane potential from the measured membrane potential; failure of control is not apparent in record of the membrane potential. C: membrane current associated with adquate control of the membrane potential. Node 2; 18°C.

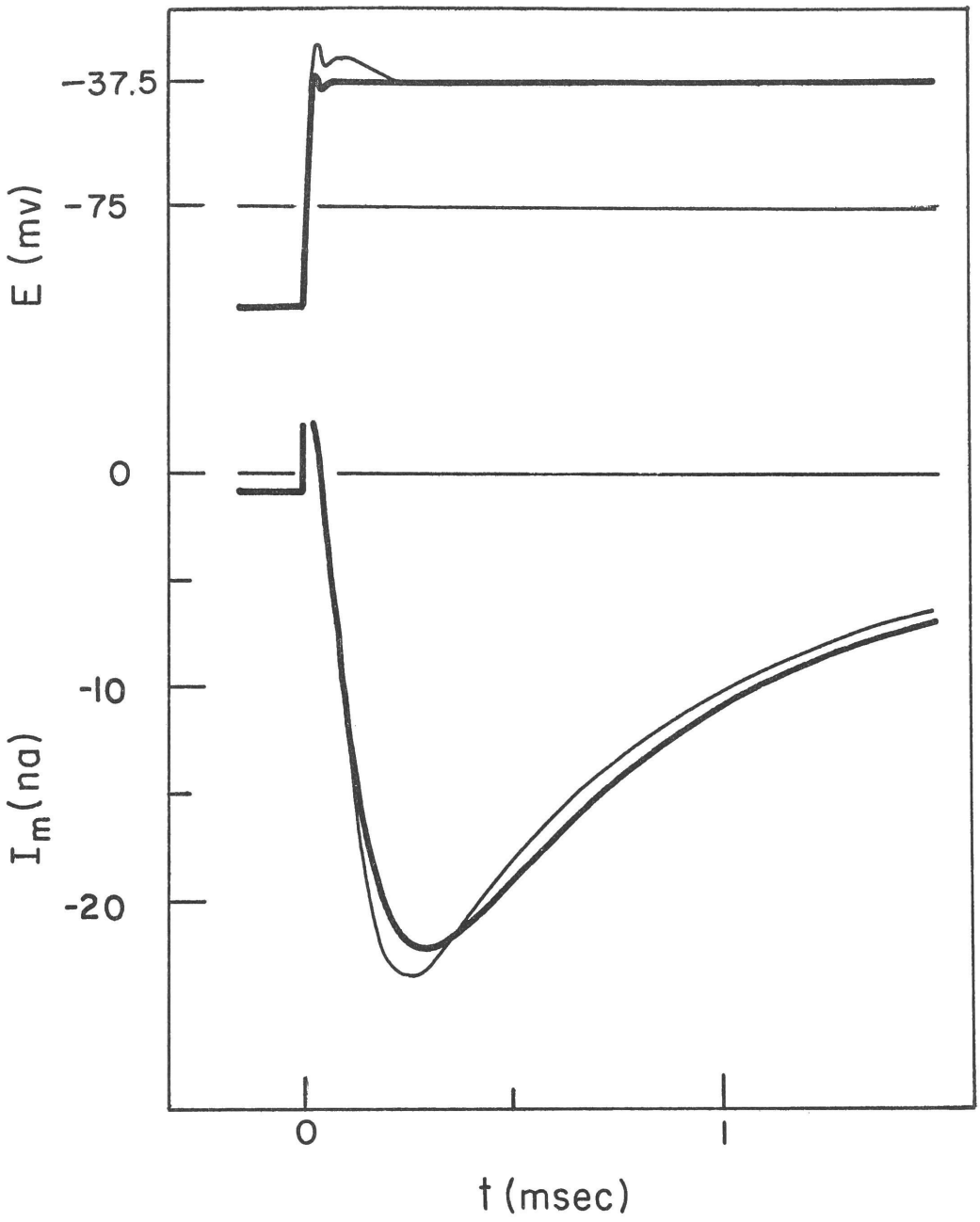


Figure 4: "Peaking" of the inward current associated with moderate error in control of the membrane potential. Heavy curves: tracings of records of the membrane current and membrane potential obtained under optimum conditions. Light curves: tracings of records obtained with excessive attenuation of the high-frequency response of the clamping amplifier. Note deviation of the membrane potential at short times. Node 22.

the calculated error is about 2 mv. The observation that the time constants describing the sodium currents are independent of the values of $h_0$ (text Figure 3.9) provides indirect evidence that this residual error does not seriously affect the measurement during maintained depolarization.

During the rapid changes of membrane current associated with the instantaneous sodium currents (text Figure 2.5), even this small error ($\tau_c \approx 0.4$ μsec) is very significant. Furthermore, in this case we must also include the surge of capacity current as well as the rapid change of the ionic current. Indeed, for this condition the interaction between the node and the electronic system is so complicated as to defy exact analysis, and the question whether the known sources of error explain why the apparent stabilization time is as long as 50 μsec remains open.

## Appendix III

## NON-IDEAL SELECTIVITY OF THE SODIUM PERMEABILITY

Theory: Here we shall develop a generalization of the "independence principle" to relate the ratio of the "sodium" current observed in a low-sodium test solution to that observed in the normal Ringer's solution if, during the state of high sodium permeability, the membrane were also permeable to the cation (S) which was substituted for sodium in the test solution.

In this treatment we shall use the integrated form of the flux equations obtained from the "constant field" membrane theory of Goldman (Hodgkin and Katz, 1949), namely

$$I_x = P_x \frac{F^2 E}{RT} \frac{[X]_o - [X]_i \exp\{EF/RT\}}{1 - \exp\{EF/RT\}} \qquad (1)$$

For our special case we assume the permeability to the substitute ion is at all times proportional to the permeability to sodium, i.e., $P_S = b P_{Na}$. We will also introduce the reasonable assumption that $[S]_i = 0$.

The "sodium" current observed in the test solution is then the sum of that carried by sodium and by the substitute ion, i.e.,

$$I^* = I'_{Na} + I_S \ .$$

That value of membrane potential at which $I^*$ is zero, defining the apparent equilibrium potential $(E_*)$, is found as follows:

$$I^* = I'_{Na} + I_S = P_{Na} \frac{F^2 E}{RT} \cdot \frac{[Na]'_o - [Na]_i \exp\{EF/RT\}}{1 - \exp EF/RT} + P_S \frac{F^2 E}{RT} \cdot$$

$$\cdot \frac{[S]_o}{1 - \exp\{EF/RT\}} = P_{Na} \frac{F^2 E}{RT} \cdot \frac{[Na]'_o + b[S]_o - [Na]_i \exp\{EF/RT\}}{1 - \exp\{EF/RT\}} \qquad (2)$$

Setting $I^* = 0$ at the definite membrane potential $E_*$, we see that the right hand side of Equation (2) goes to zero only if

$$[Na]'_o + b[S]_o - [Na]_i \exp \{ E_* F/RT \} = 0 \qquad (3)$$

or

$$E_* = \frac{RT}{F} \ln \frac{[Na]'_o + b[S]_o}{[Na]_i} \qquad (4)$$

Equations of the form (4) have been developed previously for discussing the case of non-ideal selectivity of membrane (Hodgkin, 1958; Sollner, Dray, Grim and Niehof, 1955).

However, here we are interested in comparing the ratio of the currents (measured at the same value of membrane potential) observed in the test solution and in the normal $[Na]_o$, i.e.

$$\frac{I^*}{I_{Na}} = \frac{I'_{Na} + I_S}{I_{Na}}$$

Forming the ratio of Equation 2 to $I_{Na}$ given by Equation 1 we obtain

$$\frac{I^*}{I_{Na}} = \frac{[Na]'_o + b[S]_o - [Na]_i \exp \{ EF/RT \}}{[Na]_o - [Na]_i \exp \{ EF/RT \}}$$

and upon substituting in the definitions of the appropriate equilibrium potentials we obtain

$$\frac{I^*}{I_{Na}} = \frac{\exp \{ E_* F/RT \} - \exp \{ EF/RT \}}{\exp \{ E_{Na} F/RT \} - \exp \{ EF/RT \}}$$

which simplifies to

$$\frac{I^*}{I_{Na}} = \frac{\exp \{ (E_* - E) F/RT \} - 1}{\exp \{ (E_{Na} - E) F/RT \} - 1} \qquad (5)$$

An experimental case: Ammonium as a substitute for sodium.

In an investigation of the effect of quaternary ammonium compounds on the excitability of nerve, it was discovered that a solution of ammonium ions would temporarily restore excitability to a nerve that had been pre-treated with a sodium-free solution (Lorente de Nó, et al, 1957). The excitability in the ammonium solution was temporary because of the depolarizing action of the ammonium ions (Lorente de Nó, 1947, p. 31); however, the excitability could be maintained by applying an external current to repolarize the membrane.

Lüttgau (1961) has shown that an isolated node bathed in an ammonium Ringer's solution will respond to a short stimulus with an action potential that is somewhat smaller than normal (if the membrane potential is maintained by external current). In these experiments, the action potential was followed by a long-lasting after-depolarization, suggesting that $NH_4$ also acts to some extent as a substitute for potassium.

The ionic currents of a node bathed by ammonium solution have been measured with the voltage-clamp technique. Sample records of the ionic currents and of the observed action potential are compared with controls in Figure 1. Here we see that the primary effect of $NH_4$ is to reduce the amplitude of the early transient current, and to decrease the equilibrium potential for the early current. The outward currents at long times are somewhat larger in the $NH_4$ solution than in standard Ringer's. Except for this, these records appear similar to those expected from an experiment in which the sodium concentration was reduced to about 20 percent of the normal value. This result suggests that during the state of high sodium permeability, the membrane is also somewhat permeable to $NH_4$.

This idea is tested quantitatively in terms of Equation 5 above. In Figure 2 a smooth curve ($I_{peak}$) was drawn to approximate the mean between the values of peak current observed in the standard Ringer's solution before (crosses) and after (open circles) the measurements in an $NH_4$ solution (filled circles). Equation 5 was then applied to the values of ($I_{peak} - I_L$), assuming the value of $b = 0.23$, to predict the smooth curve of peak currents in the $NH_4$ solution ($I'_{peak}$). The result of this comparison indicates that the observed change in equilibrium potential and the observed relation between peak current and membrane potential are quantitatively accounted for by the idea that the membrane is not completely selective against $NH_4$ ions; but that during the state of high sodium permeability, the membrane is also permeable to $NH_4$ to the extent that $P_{NH_4}$ is about $0.23\ P_{Na}$.

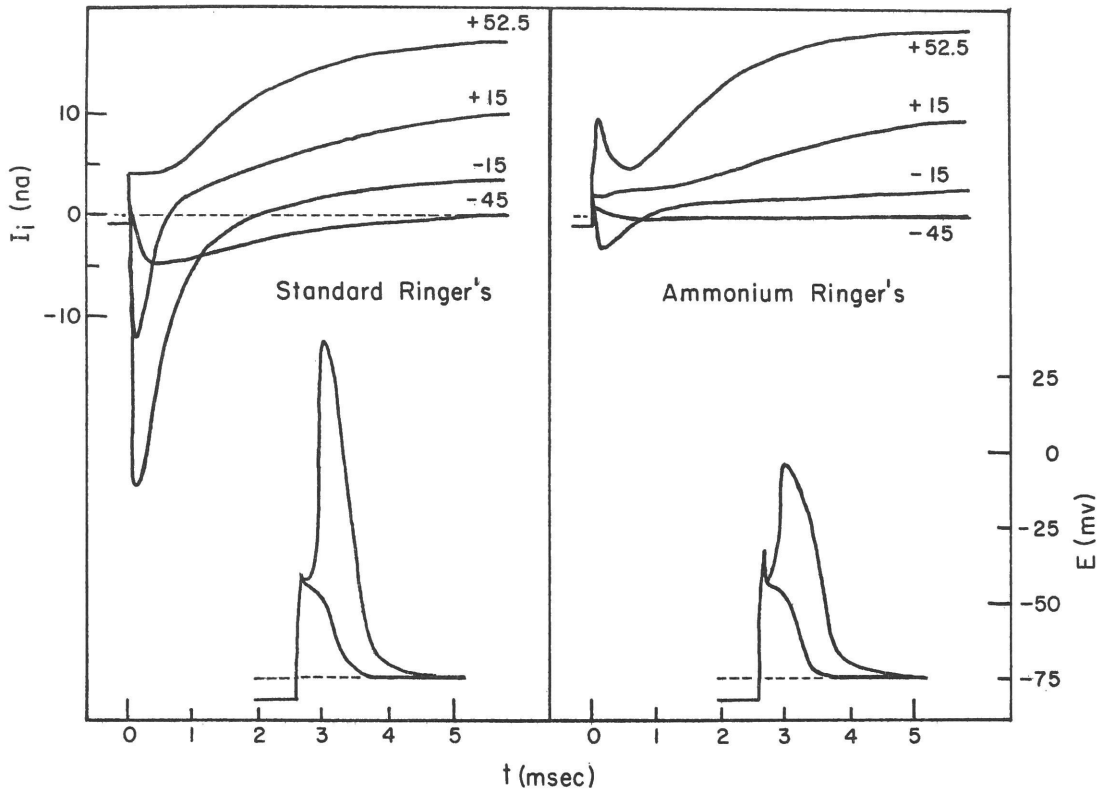


Figure 1: Tracings of selected records of the ionic current measured in voltage-clamp experiments and of the action potentials from a node in standard Ringer's solution (left) and in an ammonium Ringer's solution (right). The composition of the ammonium solution is cited in Table 1. An initial hyperpolarization at E = - 105 mv for 40 msec preceded each depolarization. Node A:1; 20°C.

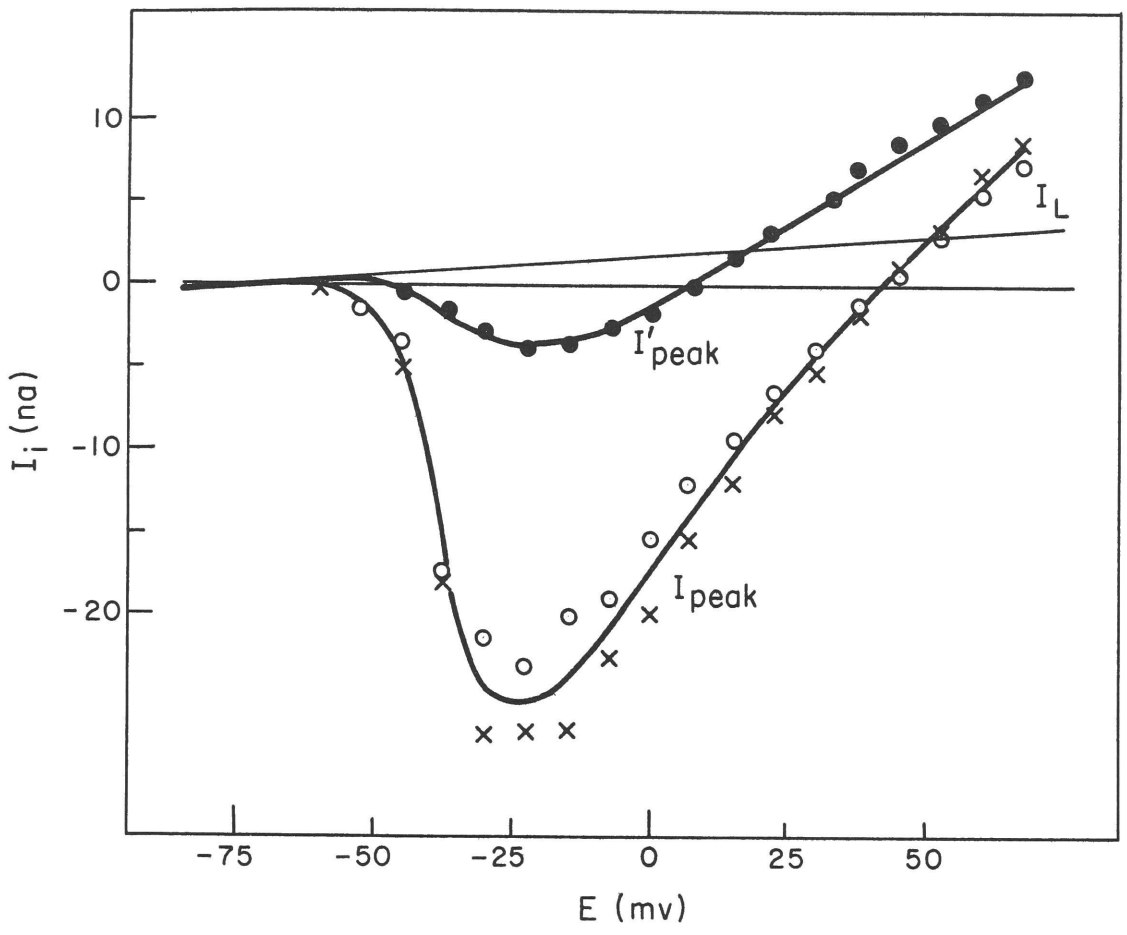


Figure 2: Comparison of the observed peak values of the early current with the theoretical predictions of the generalized independence principle. A smooth curve ($I_{peak}$) was drawn by eye to approximate the mean of measurements of the peak currents before (crosses) and after (open circles) the measurements in the ammonium Ringer's solution (filled circles). Peak $I_{Na}$ was estimated as the difference ($I_{peak} - I_L$); $I^*$ was then calculated from Equation 5, predicting the smooth curve $I'_{peak} = I^* + I_L$. Data from experiment illustrated in Figure 1.

The results of other experiments are summarized in Table 1 in terms of the parameter b calculated from the observed change in equilibrium potential according Equation 4, above.

In these experiments it was consistently observed that there was no "tail" of after-depolarization in the observed action potential, and that the potassium currents at long times were usually slightly larger in the $NH_4$ solutions, than in the controls. These observations are clearly inconsistent with the suggestion that the membrane is also permeable to $NH_4$ during the state of high potassium permeability. Unless the externally applied current in Lüttgau's experiments overcompensated the depolarizing action of the $NH_4$ solution, there is no simple explanation for the discrepancy between his observations and those reported here. Further experiments are required to see if this discrepancy arises from the slight difference in experimental procedures.

The voltage-clamp experiments have not revealed how the $NH_4$ exerts its depolarizing effect on the resting membrane, and other experiments are required to elucidate this point.

TABLE 1

Determination of the permeability to ammonium relatative to that to sodium (b) from measurements of the equilibrium potential for the early current measured in the standard Ringer's solution ($E_{Na}$) and in an ammonium solution ($E_*$)

| Expt. | $E_*$ (mv) | $E_{Na}$ (mv) | b |
|---|---|---|---|
| A:1 | 16 | 51 | .23 |
| A:2 | 13 | 52 | .19 |
| A:3 | 16 | 53 | .21 |
| A:4* | 15 ± 3 | 52 ± 2 | .21 ± 0.3 |

* Mean and standard deviation for 5 trials in an experiment in which 5 minutes were allowed after each solution change in order for the temperature to equilibrate at 13°C. In other experiments the temperature was 20°C. Composition of the ammonium solution was: 122 mM $NH_4Cl$, 2.5 mM KCl, 2.5 mM $NaHCO_3$, 2.0 mM $CaCl_2$, pH 7.4.

## Appendix IV

## SUMMARY OF EMPIRICAL CONSTANTS

In this investigation a set of empirical constants for the mathematical model was determined from the voltage-clamp measurements on several different nodes. The constants for node 7 were reported in Table 3.1 and Fig. 3.19. The constants for the other nodes are tabulated below, together with plots of the rate constants as a function of membrane potential.

### Constants for Node 4

| Constant | Value per node |
|---|---|
| $C$ | 2.5 μμf |
| $\bar{P}_{Na}$ | $2.4 \times 10^{-9}$ cm$^3$ sec$^{-1}$ |
| $\bar{P}_{Na}[Na]_o F^2/RT$ | 1.95 μ mho |
| $E_{Na}$ | 44 mv |
| $\bar{g}_K$ | 0.093 μ mho |
| $E_K$ | -75 mv |
| $\bar{g}_L$ | 0.025 μ mho |
| $E_L$ | -75 mv |
| Temp. | 19 °C |

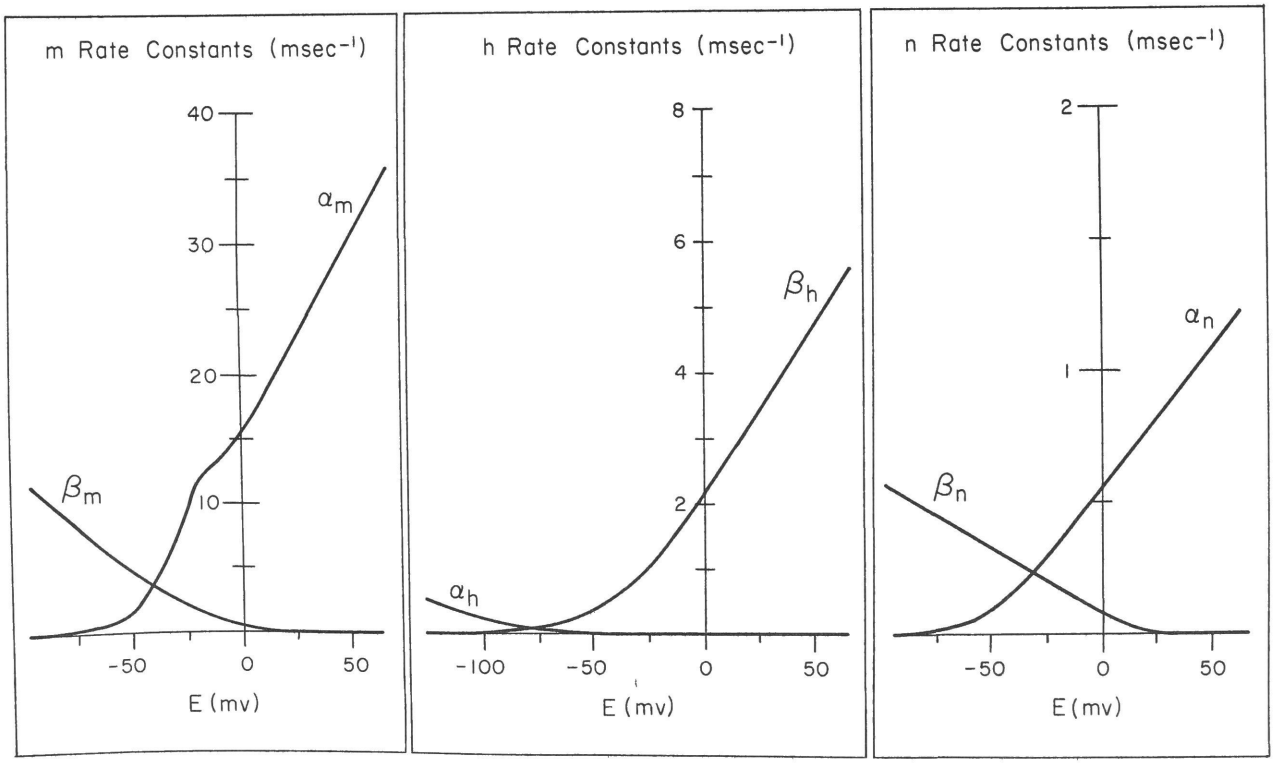

Constants for Node 8

| Constant | Value per node |
|---|---|
| C | 2.5 μμf |
| $\overline{P}_{Na}$ | 5.2 x $10^{-9}$ $cm^3$ $sec^{-1}$ |
| $\overline{P}_{Na}[Na]_o F^2/RT$ | 2.3 μ mho |
| $E_{Na}$ | +45 mv |
| $\overline{g}_K$ | 0.150 μ mho |
| $E_K$ | -75 mv |
| $\overline{g}_L$ | 0.025 μ mho |
| $E_L$ | -75 mv |
| Temp. | 22 °C |

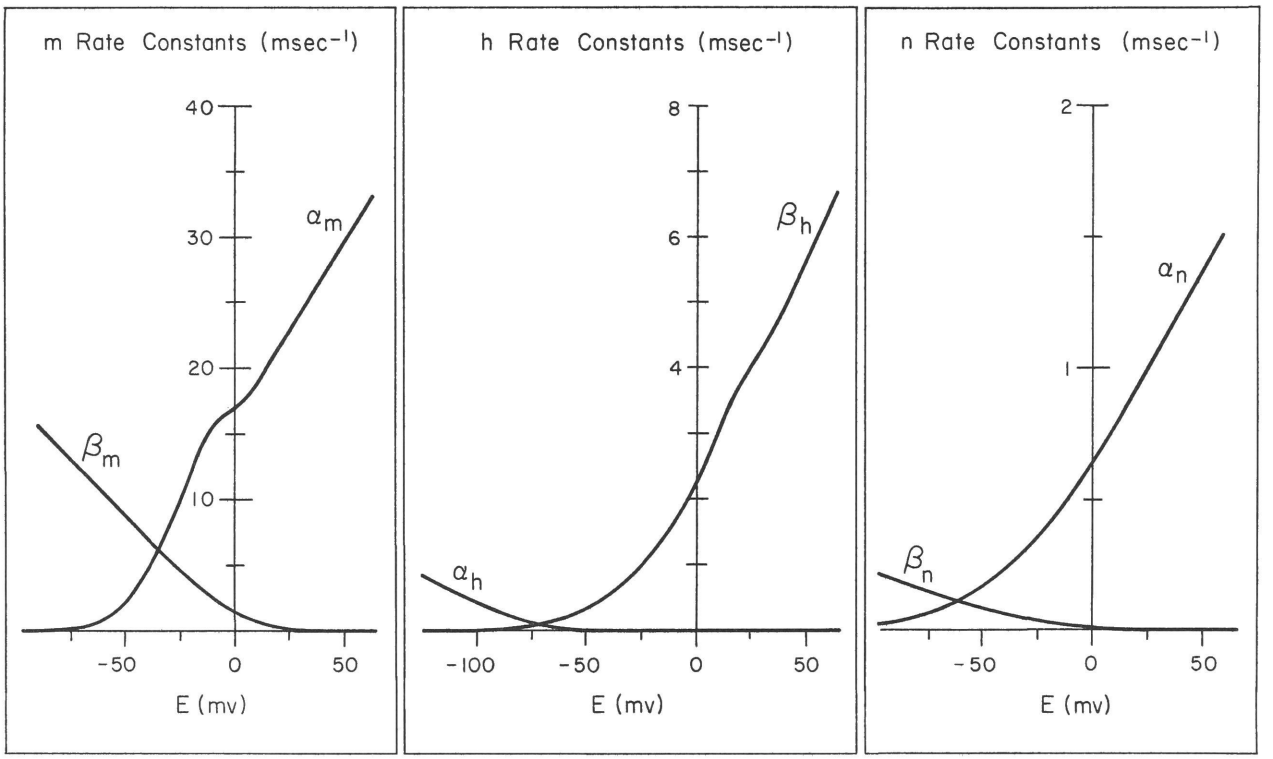

## Constants for Node 11C

| Constant | Value per node |
|---|---|
| $C$ | 2.5 μμf |
| $\bar{P}_{Na}$ | $3.04 \times 10^{-9}$ cm$^3$ sec$^{-1}$ |
| $\bar{P}_{Na}[Na]_o F^2/RT$ | 1.34 μ mho |
| $E_{Na}$ | +48 mv |
| $\bar{g}_K$ | 0.104 μ mho |
| $E_K$ | -75 mv |
| $\bar{g}_L$ | 0.025 μ mho |
| $E_L$ | -75 mv |
| Temp. | 22 °C |

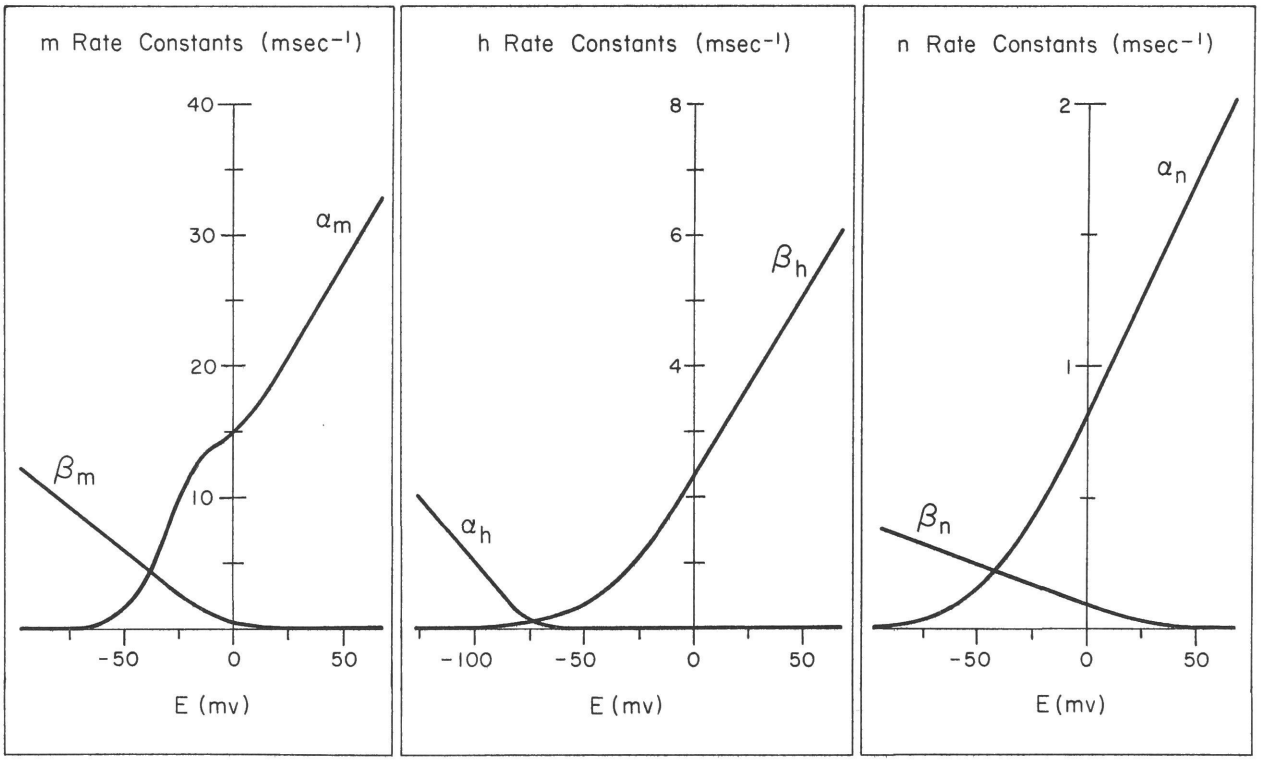

## Constants for Node 12

| Constant | Value per node |
|---|---|
| $C$ | 2.5 μμf |
| $\bar{P}_{Na}$ | $5.35 \times 10^{-9}$ cm$^3$ sec$^{-1}$ |
| $\bar{P}_{Na}[Na]_o F^2/RT$ | 2.36 μ mho |
| $E_{Na}$ | +45 mv |
| $\bar{g}_K$ | 0.20 μ mho |
| $E_K$ | -60 mv |
| $\bar{g}_L$ | 0.025 μ mho |
| $E_L$ | -60 mv |
| Temp. | 20 °C |

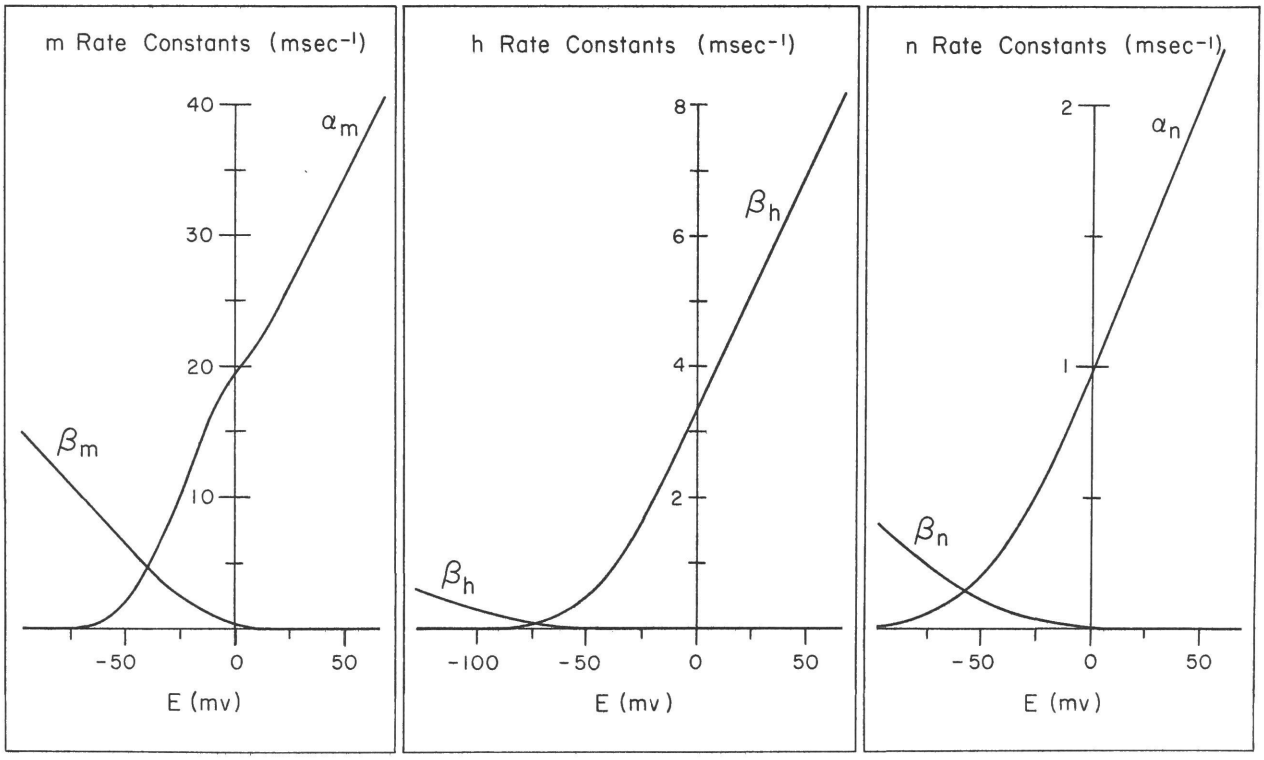

# BIBLIOGRAPHY

Adelman, W. J. and Taylor, R. E. (1961). Leakage current rectification in the squid giant axon. Nature, 190, 883-885.

Asano, T. and Hurlbut, W. P. (1958). Effects of potassium, sodium, and azide on the ionic movements that accompany activity in frog nerves. J. Gen. Physiol. 41, 1187-1203.

Bernstein, J. (1902). Untersuchungen zur Thermodynamik der bioelektrischen Ströme. Erster Theil. Arch. ges. Physiol. 92, 521-562.

Baker, P. F., Hodgkin, A. L. and Shaw, T. I. (1962). Replacement of the axoplasm of giant nerve fibres with artificial solutions. J. Physiol. 164, 330-354.

Böhm, H. W. and Straub, R. W. (1962). Der Effekt von Lithium-Ionen auf das Ruhepotential von markhaltigen Nervenfasern. Arch. Ges. Physiol. 274, 468-479.

del Castillo, J., Lettvin, J. Y., McCulloch, W. S. and Pitts, W. (1957). Membrane currents in clamped vertebrate nerve. Nature, 180, 1290-1291.

Cheng, S. C. (1962). Functional uptake of hydrazine by frog nerve in sodium-deficient Ringer's solution. Nature, 193, 691-692.

Cole, K. S. (1949). Dynamic electrical characteristics of the squid axon membrane. Arch. Sci. Physiol. 3, 253-258.

Cole, K. S. and Curtis, H. J. (1939). Electric impedance of the squid giant axon during activity. J. Gen. Physiol. 22, 649-670.

Cole, K. S. and Moore, J. W. (1960). Ionic current measurements in the squid giant axon membrane. J. Gen. Physiol. 44, 123-167.

Connelly, C. M. (1959). Recovery processes and metabolism of nerve. Rev. Mod. Phys. 31, 475-484.

Curtis, H. J. and Cole, K. S. (1940). Membrane action potentials from the squid giant axon. J. Cell. and Comp. Physiol. 15, 147-157.

Curtis, H. J. and Cole, K. S. (1942). Membrane resting and action potentials from the squid giant axon. J. Cell. and Comp. Physiol. 19, 135-144.

Dodge, F. A. and Frankenhaeuser, B. (1958). Membrane currents in isolated frog nerve fibre under voltage clamp conditions. J. Physiol. 143, 76-90.

Dodge, F. A. and Frankenhaeuser, B. (1959). Sodium currents in the myelinated nerve fibre of Xenopus laevis investigated by the voltage clamp technique. J. Physiol. 148, 188-200.

Fenn, W. O., Cobb, D. M., Hegnauer, A. H. and Marsh, B. S. (1934). Electrolytes in nerve. Am. J. Physiol. 110, 74-96.

FitzHugh, R. (1960). Thresholds and plateaus in the Hodgkin-Huxley nerve equations. J. Gen. Physiol. 43, 867-896.

FitzHugh, R. (1961). Impulses and physiological states in theoretical models of nerve membrane. Biophys. J. 1, 445-466.

FitzHugh, R. (1962). Computation of impulse initiation and saltatory conduction in a myelinated nerve fiber. Biophys. J. 2, 11-21.

FitzHugh, R. and Antosiewicz, H. A. (1959). Automatic computation of nerve excitation - detailed corrections and additions. J. Soc. Indust. Appl. Math. 7, 447-458.

Frankenhaeuser, B. (1957). A method for recording resting and action potentials in the isolated myelinated nerve fibre of the frog. J. Physiol. 135, 550-559.

Frankenhaeuser, B. (1959). Steady state inactivation of sodium permeability in myelinated nerve fibres of Xenopus laevis. J. Physiol. 141, 671-676.

Frankenhaeuser, B. (1960). Quantitative description of sodium currents in myelinated nerve fibres of Xenopus laevis. J. Physiol. 151, 491-501.

Frankenhaeuser, B. (1962 a). Delayed currents in myelinated nerve fibres of Xenopus laevis investigated with voltage clamp technique. J. Physiol. 160, 40-45.

Frankenhaeuser, B. (1962 b). Instantaneous potassium currents in myelinated nerve fibres of Xenopus laevis. J. Physiol. 160, 46-53.

Frankenhaeuser, B. (1962 c). Potassium permeability in myelinated nerve fibres of Xenopus laevis. J. Physiol. 160, 54-61.

Frankenhaeuser, B. and Hodgkin, A. L. (1956). The after-effects of impulses in the giant nerve fibres of Loligo. J. Physiol. 131, 341-376.

Frankenhaeuser, B. and Persson, A. (1957). Voltage clamp experiments on the myelinated nerve fibre. Acta Physiol. Scand. Suppl. 145, 45.

Frankenaheuser, B. and Widén, L. (1956). Anode break excitation in desheathed frog nerve. J. Physiol. 131, 243-247.

Gasser, H. S. (1935). Changes in nerve-potentials produced by rapidly repeated stimuli and their relation to the responsiveness of nerve to stimulation. Am. J. Physiol. 111, 35-50.

George, E. P. and Johnson, E. A. (1962). Response of the Hodgkin-Huxley model to temperature and chemical impulses. Nature, 194, 874-875.

Gerard, R. W. (1930). Delayed action potentials in nerve. Am. J. Physiol. 93, 337-341.

Geren, B. B. (1954). The formation from the Schwan cell surface of myelin in the peripheral nerves of chick embryos. Exp. Cell Res. 7, 558-562.

Goldman, D. E. (1943). Potential, impedance, and rectification in membranes. J. Gen. Physiol. 27, 37-60.

Hinke, J. A. M. (1961). The measurement of sodium and potassium activities in the squid axon by means of cation-selective glass micro-electrodes. J. Physiol. 156, 314-335.

Hodgkin, A. L. (1951). The ionic basis of electrical activity in nerve and muscle. Biol. Rev. 26, 339-409.

Hodgkin, A. L. (1958). Ionic movements and electrical activity in giant nerve fibres. Proc. Roy. Soc. London, Ser. B, 148, 1-37.

Hodgkin, A. L. and Huxley, A. F. (1939). Action potentials recorded from inside a nerve fibre. Nature, 144, 710-711.

Hodgkin, A. L. and Huxley, A. F. (1952 a). Currents carried by sodium and potassium ions through the membrane of the giant axon of Loligo. J. Physiol. 116, 449-472.

Hodgkin, A. L. and Huxley, A. F. (1952 b). The components of membrane conductance in the giant axon of Loligo. J. Physiol. 116, 473-496.

Hodgkin, A. L. and Huxley, A. F. (1952 c). The dual effect of membrane potential on sodium conductance in the giant axon of Loligo. J. Physiol. 116, 497-506.

Hodgkin, A. L. and Huxley, A. F. (1952 d). A quantitative description of membrane current and its application to conduction and excitation in nerve. J. Physiol. 117, 500-544.

Hodgkin, A. L. and Huxley, A. F. (1953). Movement of radioactive potassium and membrane current in a giant axon. J. Physiol. 121, 403-414.

Hodgkin, A. L., Huxley, A. F. and Katz, B. (1949). Ionic currents underlying activity in the giant axon of the squid. Arch. Sci. Physiol. 3, 129-150.

Hodgkin, A. L., Huxley, A. F. and Katz, B. (1952). Measurement of current voltage relations in the membrane of the giant axon of Loligo. J. Physiol. 116, 424-448.

Hodgkin, A. L. and Katz, B. (1949). The effect of sodium ions on the electrical activity of the giant axon of the squid. J. Physiol. 108, 37-77.

Hodgkin, A. L. and Keynes, R. D. (1955). Active transport of cations in giant axons from Sepia and Loligo. J. Physiol. 128, 28-60.

Hodgkin, A. L. and Keynes, R. D. (1956). Experiments on the injection of substances into squid giant axons by means of a microsyringe. J. Physiol. 131, 592-616.

Hodgkin, A. L. and Rushton, W. A. H. (1946). The electrical constants of a crustacean nerve fibre. Proc. Roy. Soc. London, Ser. B, 133, 444-479.

Hurlbut, W. P. (1958). Effects of azide and chloretone on the sodium and potassium contents and the respiration of frog sciatic nerves. J. Gen. Physiol. 41, 959-988.

Huxley, A. F. (1959). Ion movements during nerve activity. Ann. New York Acad. Sci. 81, 221-246.

Huxley, A. F. and Stämpfli, R. (1949). Evidence for saltatory conduction in peripheral myelinated nerve fibres. J. Physiol. 108, 315-339.

Huxley, A. F. and Stämpfli, R. (1951). Effect of potassium and sodium on resting and action potentials of single myelinated nerve fibres. J. Physiol. 112, 496-508.

Katz, B. (1939). Electric excitation of nerve. London, Oxford University Press.

Keynes, R. D. and Lewis, P. R. (1951). The sodium and potassium content of cephalopod nerve fibres. J. Physiol. 114, 151-182.

Lorente de Nó, R. (1947). A study of nerve physiology. Studies Rockefeller Inst. Med. Res. 131 and 132.

Lorente de Nó, R., Vidal, F. and Larramendi, L. M. H. (1957). Restoration of sodium-deficient frog nerve fibres by onium ions. Nature, 179, 737-738.

Lüttgau, H.-C. (1956). Das Na-Transportsystem während der Erregungsprozesse am Ranvier-Knoten isolierter markhaltiger Nervenfasern. Experientia, 12: 482-486.

Lüttgau, H.-C. (1961). Weitere Untersuchungen über den passiven Ionen transport durch die erregbare Membran des Ranvierknotens. Arch. Ges. Physiol. 273, 302-310.

Marmont, G. (1949). Studies on the axon membrane. J. Cell. and Comp. Physiol. 34, 351-383.

Noble, D. (1962). A modification of the Hodgkin-Huxley equations applicable to Purkinje fibre action potential and pace-maker potentials. J. Physiol. 160, 317-353.

Ooyama, H. and Wright, E. B. (1962). Activity of potassium mechanism in single Ranvier node during excitation. J. Neurophysiol. 25, 67-93.

Robertson, J. D. (1960). The molecular structure and contact relationships of cell membranes. Prog. Biophys. and Biophys. Chem. 10, 344-418.

Scarborough, J. B. (1955). Numerical mathematical analysis, ed. 3, Baltimore. Johns Hopkins Press.

Shanes, A. M. (1957). Ionic transfer in a vertebrate nerve. In Murphy, Q. R., ed., Metabolic aspects of transport across cell membranes, Madison, University of Wisconsin Press, p. 127-150.

Shanes, A. M. and Berman, M. D. (1955). Penetration of the desheathed toad sciatic nerve by ions and molecules. II. Kinetics. J. Cell. and Comp. Physiol. 45, 199-240.

Sollner, K., Dray, S., Grim, E. and Neihof, R. (1955). Membranes of high electrochemical activity in studies of biological interest. In Shedlovsky, T., ed., Electrochemistry in biology and medicine, New York, John Wiley, p. 65-90.

Spyropoulos, C. S. (1961). Initiation and abolition of electric response of nerve fiber by thermal and chemical means. Am. J. Physiol. 200, 203-208.

Spyropoulos, C. S. and Brady, R. O. (1959). Prolongation of response of node of Ranvier by metal ions. Science, 129, 1366-1367.

Stämpfli, R. and Willi, M. (1957). Membrane potential of a Ranvier node measured after electrical destruction of its membrane. Experientia 13, 297-298.

Tasaki, I. (1953). Nervous transmission. Springfield, Ill., C. C. Thomas.

Tasaki, I. (1955). New measurements of the capacity and the resistance of the myelin sheath and the nodal membrane of the isolated frog nerve fiber. Am. J. Physiol. 181, 639-650.

Tasaki, I. (1956). Initiation and abolition of the action potential of a single node of Ranvier. J. Gen. Physiol. 39, 377-395.

Tasaki, I. and Bak, A. F. (1958). Current-voltage relations of single nodes of Ranvier as examined by voltage-clamp technique. J. Neurophysiol. 21, 124-137.

Tasaki, I. and Frank, K. (1955). Measurement of the action potential of myelinated nerve fiber. Am. J. Physiol. 182, 572-578.

Tasaki, I. and Freygang, W. H., Jr. (1955). The parallelism between the action potential, action current, and membrane resistance at a node of Ranvier. J. Gen. Physiol. 39, 211-223.

Tasaki, I. and Hagiwara, S. (1957). Demonstration of two stable potential states in the squid giant axon under tetraethylammonium chloride. J. Gen. Physiol. 40, 859-885.

Tasaki, I. and Mizuguchi, K. (1949). The changes in the electric impedance during activity and the effect of alkaloids and polarization upon the bioelectric processes in the myelinated nerve fiber. Biochim. et Biophys. Acta 3, 484-493.

Teorell, T. (1953). Transport processes and electrical phenomena in ionic membranes. Progr. Biophys. and Biophys. Chem., 3 305-369.

Ussing, H. H. (1949). The distinction by means of traces between active transport and diffusion; the transfer of iodide across the isolated frog skin. Acta Physiol. Scand. 19, 43-56.

Weidmann, S. (1951). Effect of current flow on the membrane potential of cardiac muscle. J. Physiol. 115, 227-236.

Weidmann, S. (1952). The electrical constants of Purkinje fibres. J. Physiol. 118, 348-360.

Woodbury, J. W. (1952). Direct membrane resting and action potentials from single myelinated nerve fibers. J. Cell. and Comp. Physiol. 39, 323-339.

Young, J. Z. (1936). Structure of nerve fibres and synapses in some invertebrates. Cold Spring Harbor Symp. Quant. Biol. 4, 1-6.

End